Projects, Progress and Special Accomplishments

in the

Mechanical Sciences

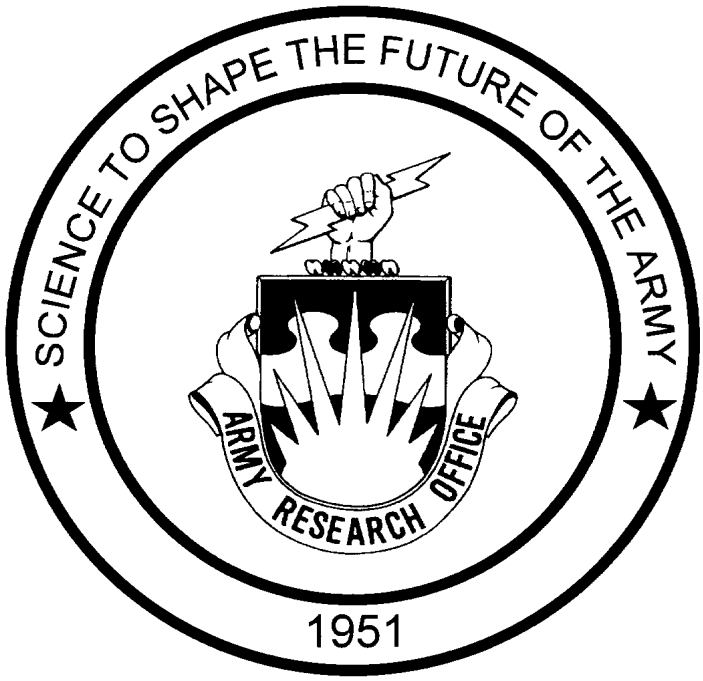

Mechanical and Environmental Sciences Division
Engineering Sciences Directorate

U.S. Army Research Office
PO Box 12211
Research Triangle Park, NC 27709-2211

June 2000

U.S. Army Research Office
P.O. Box 12211
Research Triangle Park, NC 27709-2211

This book contains short summaries of activities, programs, and accomplishments on those research projects supported within the Mechanical Sciences which were active as of January 1. Projects supported within the Multidisciplinary University Research Initiative (MURI) program will be reported separately and are not included in this booklet.

These project descriptions are disseminated to the interested public and serve the purpose of illustrating examples of research areas of current interest to the Army in the Mechanical Sciences field. Hopefully, this information will also serve to simulate other innovative research areas and projects within the Division purview.

Mechanical Sciences Staff

Dr. David M. Mann, Acting Director, Engineering Sciences Directorate
Phone: 919/549-4249; DSN: 832-4249; E-Mail: dmann@arl.aro.army.mil

Dr. Thomas L. Doligalski, Acting Associate Director
Phone: 919/549-4251; DSN: 832-4251; E-Mail: tom@arl.aro.army.mil

Dr. Gary L. Anderson, Chief, Structures and Mechanics
Phone: 919/549-4317; DSN: 832-4317; E-Mail: anderson@arl.aro.army.mil

Dr. Mohammed Zikry, Acting Chief, Solid Mechanics
Phone: 919/549-4246; DSN: 832-4246; E-Mail: zikry@arl.aro.army.mil

Mrs. Pamela Robinson, Secretary
Phone: 919/549-4362; DSN: 832-4362; E-Mail: robinson@arl.aro.army.mil

FAX: 919/549-4310
Web Site: http://www.aro.army.mil

(Intentionally left blank)

U.S. ARMY RESEARCH OFFICE

PROJECTS, PROGRESS, AND SPECIAL ACCOMPLISHMENTS IN THE MECHANICAL SCIENCES

Table of Contents

FLUID DYNAMICS

PROPULSION & ENERGY CONVERSION

SOLID MECHANICS

STRUCTURAL DYNAMICS & VIBRATIONS

FLUID DYNAMICS

36425-EG "Experimental Studies of High-Speed Separated Flows"

J.C. Dutton, University of Illinois at Urbana-Champaign

The objective of this experimental research program is to investigate the fundamental fluid dynamic mechanisms and interactions within high-speed separated flows in order to develop a better understanding of projectile and missile base flow phenomena. Detailed experiments are conducted using non-intrusive laser-based diagnostic techniques. During the past year significant progress has been made on three projects within this research program.

Planar Visualizations of Supersonic Base Flows. In 1999, the emphasis of this investigation shifted from studying the turbulent structure in the near wake of blunt-based afterbodies to boattailed afterbodies. Introducing a solid angle of 5º to the final 1.25 inches (1 base radius) of the afterbody significantly decreases the turbulent energy in the wake region, and significantly reduces the base drag. This work has demonstrated that there are significant differences in the behavior of the turbulent structures and turbulent motions present in boattailed and blunt-based axisymmetric base flows close to the base. In the end views, approximately 20% more structures are visible in the boattailed case than in the blunt-based case, and the structures appear to be larger and more inclined toward the streamwise axis in the side view, indicating lower entrainment rates. Secondly, the overall magnitude of pulsing and flapping motions is significantly smaller than in the blunt-based case. Finally, the large-scale turbulent structures appear less oriented toward the circumferential direction due to boattailing, indicating that ejection-type motions are less prevalent. Despite these differences seen upstream, the reattachment process seems to produce remarkably similar mean turbulent structure statistics for the two cases, indicating that adverse pressure gradients cause similar large-scale structure behavior regardless of upstream conditions.

Three-Dimensional Supersonic Base Flows. After completion of flow visualization and surface pressure measurements in 1998, efforts were shifted in the past year to experimentally measure velocity statistics in a three-dimensional supersonic base flow. A two-component laser Doppler velocimeter system was set up to measure axial and radial components of velocity throughout this three-dimensional flowfield. In addition, the LDV traverse system was updated to function in a 32-bit operating system, a necessary improvement to allow for computer-controlled positioning with current LDV data-acquisition software. For all velocity measurements, a nominal Mach 2.5 flow passed over a cylindrical afterbody with an L/D ratio of 1.5 inclined at a 10° angle-of-attack. Velocity measurements were completed in the incoming flow to compare approach boundary layer profiles to those measured about a similar cylindrical afterbody at zero angle-of-attack. The incoming freestream Mach number and boundary layer thickness were measured as M =

2.45 and δ/R = 0.103, respectively. Excellent agreement was observed between the 0° and 10° angle-of-attack boundary layer velocity profiles, suggesting that differences in the downstream velocity field between these two cases are driven by the flow three-dimensionality rather than differing initial conditions.

CARS Measurements of Pressure, Temperature, Density, and Velocity. In 1999, high-resolution N_2 CARS measurements were performed in the flowfield of an underexpanded sonic jet. By resolving the rotational structure of the $\nu=0 \rightarrow 1$ N_2 Q-branch to $\Delta\omega=0.10$ cm^{-1}, this laser-based technique was used to obtain spatially well resolved, non-intrusive measurements of pressure, temperature, and density in this high-speed gas flow. The experimental $P/T/\rho$ measurements were compared to similar quantities extracted from a RANS CFD simulation of the jet flowfield. The agreement between the mean CARS measurements and CFD predictions along the centerline (**Figure 1**) and radial traverses in the jet flowfield was generally excellent. This CARS technique is able to capture the low-pressure and low-temperature conditions of the M=3.2 flow entering the Mach disk, as well as the conditions immediately downstream of it. Further, in the downstream region, both the CARS and CFD temperature distributions corroborate the existence of concentric inner and outer shear layers. Slight deviations of the CARS pressure measurements from the CFD pressure distribution in the outer compressible shear layer suggest the existence of streamwise-oriented vortices.

A high resolution N_2 CARS method for simultaneous measurement of pressure, temperature, and velocity in high-speed flows was also investigated. Pressure and temperature are resolved by the lineshapes and relative intensities of the rotational and vibrational transitions of the nitrogen molecule. Initial attempts to resolve velocity involved the use of counter-propagating pump beams, which generate a Doppler shift between the resulting CARS signals from each. This Doppler shift is determined by the phase-matching geometry used. Efforts were made to detect a vibrational and a pure rotational CARS signal. Due to the complex nature of the CARS system, several modifications were tested. Using a homenergetic flow assumption, the velocity magnitude can be obtained through knowledge of the temperature. This allows use of the high-resolution N_2 CARS system described above for the simultaneous measurement of pressure, temperature, and density to be extended to measure the velocity magnitude as well.

36435-EG "The Origin and Structure of Trailing Vortices Aerodynamics"

A.T. Conlisk and O.R. Burgraff, The Ohio State University, and N.M. Komerath, Georgia Institute of Technology

The helicopter rotor wake is among the most complex flowfields in aerodynamics. Despite the fact that a large amount of computational and experimental work on the rotor wake has been published, little of a quantitative nature is known about the origin of the main component of the rotor wake, the tip-vortex as a function of the rotor speed, rotor blade geometry, and the angle of attack. The major objective of this project is to delineate the major features of the origin of the tip-vortex and the rotor wake both experimentally and computationally, resulting in the ability to

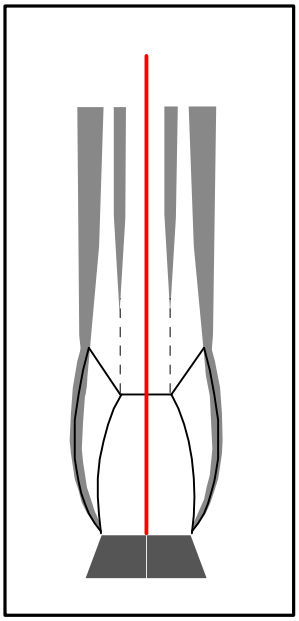

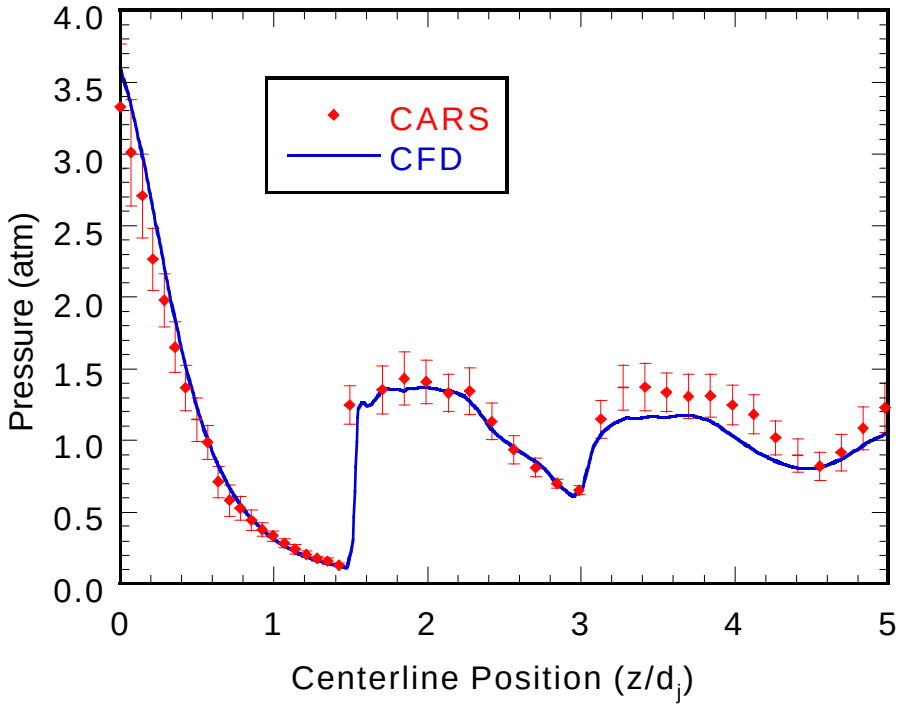

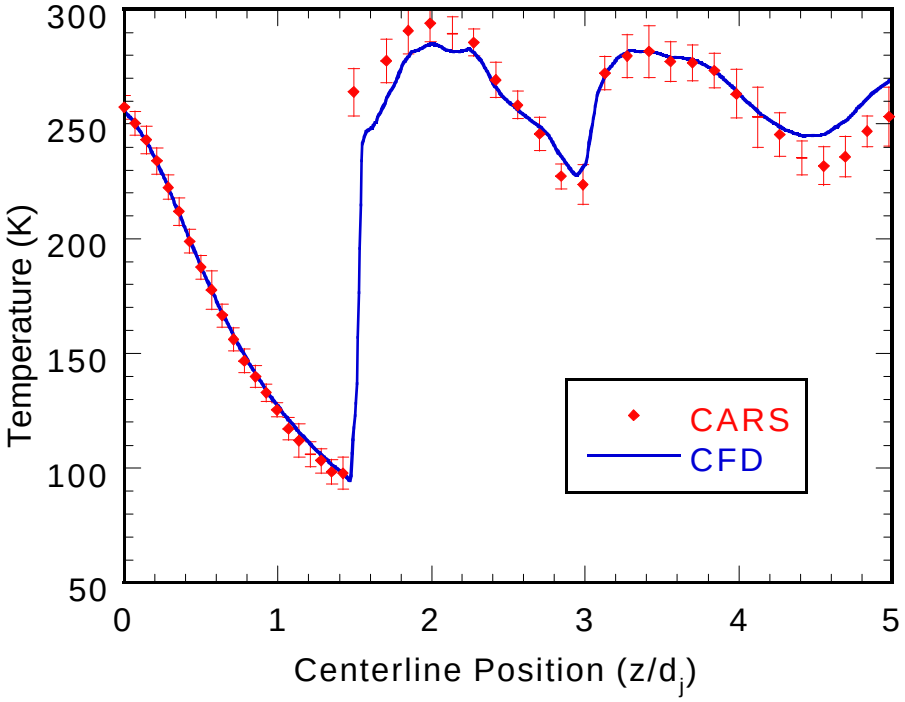

Figure 1 Comparison of CARS measurements and RANS CFD predictions of pressure and temperature along the centerline of an underexpanded jet

predict accurately circulation, asymptotic core radius, initial tip-vortex position, axial flow speed within the vortex, and local blade loads. While the rotor-blade tip-vortex is of primary interest, the techniques developed would be applicable to fixed wings as well.

On the computational side, classical inviscid lifting line and lifting surface methods were applied locally near the wing tip to describe the origin of the tip vortex. It may seem odd to describe the formation of the tip-vortex in this manner when viscous flow methods have been used. However, correlation of experimental data has revealed little dependence on the Reynolds number. Of course, this lack of dependence on Reynolds number will hold only if the flow remains substantially unseparated, though it may be noted that drag coefficients of bluff bodies are remarkably constant over wide range of Reynolds number.

The tip region for a large aspect ratio fixed wing can be viewed as a semi-infinite wing and the leading order inner problem has an analytical solution given by Stewartson. A similar analysis was performed for the lifting surface. The comparison of the computed bound circulation with the experimental data indicates good agreement. Next, the formation of the tip-vortex was considered. In a steady flowfield, vortex lines are also streamlines. Therefore, we solve the three dimensional streamline equations to describe the process whereby individual vortex filaments roll around each other to form the trailing vortex.

Next the rotary wing case was considered. It is shown that in the tip region, an analytical solution for the bound circulation on the rotary wing may be obtained whose form is similar to the fixed wing except that there is a parameter which is dependent on the induced angle of attack, the aspect ratio and the number of blades. The experiments on the rotor near wake show that the wake geometry is not a perfect helix, a simple vortex cylinder model was used to represent the rotor wake contraction and its results compare well with experimental data. The formation of the tip-vortex on a rotating rectangular blade is illustrated on **Figure 2**.

On the experimental side, Laser Doppler velocimetry (LDV) measurements were conducted on a two-bladed model rotor in forward flight. Measurements at the blade tip on the advancing blade side (ABS) in forward flight show that there is significant spanwise velocity, approaching 40 percent of tip speed, on both the upper and lower surfaces. The peak core axial velocity appears to tend to the tip speed. Secondary effects were also seen in several core circulatory velocities profiles. However, higher resolution measurements are required to determine the causes of these secondary effects. During formation the vortex moves slightly inboard and upward as indicated in the computational results on Figure 2. Measurements were also made in the wake of the rotor to gain further insight on the vortex structure. The evolution of the core circumferential velocities shows a periodic pattern. The Strouhal number based on this period, tip speed and blade tip thickness is 0.16. This suggests that the periodicity is caused by a shedding phenomenon. Comparison with a turbulent Lamb vortex shows that the expected decay of the circumferential velocity is significantly faster than the measured decay rate. Furthermore, measurements of the core axial velocity

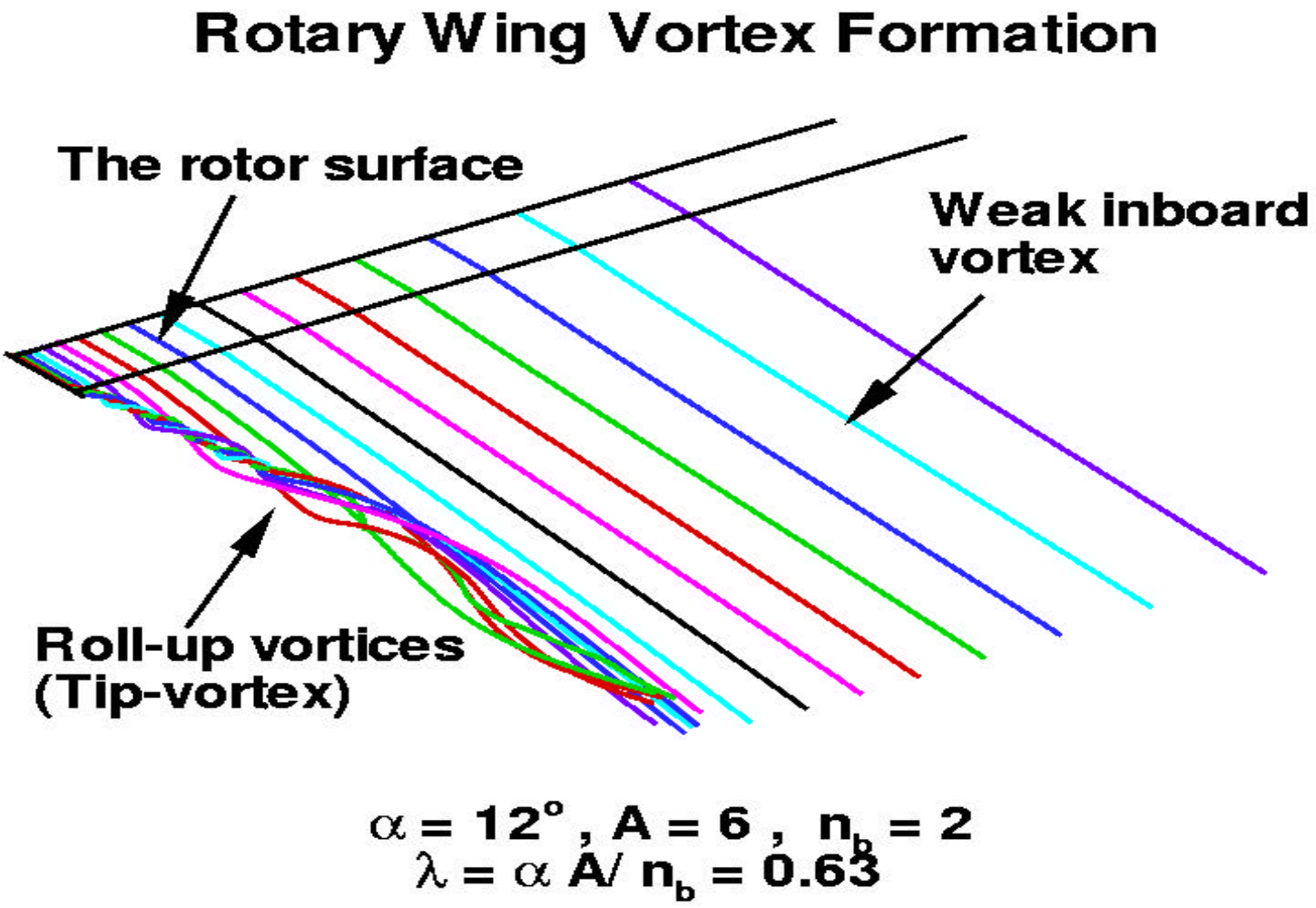

Figure 2 Rotary Wing Vortex Formation

also show no evidence of turbulent flow within the core.

Rotary wing circulation measurements from several researchers have been correlated. An expression for the core circulation has been obtained in terms of aspect ratio, Reynolds number and angle of attack. The experimental core circulation values match the prediction well. A significant fact is that data taken in a particular test always clump together and are not scattered around the theoretical value.

36477-EG "Fluid Mechanics of Compressible Dynamic Stall Control Using Dynamically Deforming Airfoils"

M. S. Chandrasekhara, Naval Postgraduate School, Monterey, CA

During 1999, two different dynamic stall control approaches were compared. One was the slatted airfoil (research conducted for the Army Aviation and Missile Command's Aeroflightdynamics Directorate) and the other was the ARO supported Dynamically Deforming Leading Edge (DDLE) airfoil. Both were successful in controlling the dynamic stall behavior at M=0.3 and $\alpha = 10^O + 10^O \sin \omega t$. The required vorticity distribution for this was achieved through very different mechanisms. The potential flow changes arising from even small changes in the airfoil leading edge geometry was the cause for the DDLE airfoil and the bleed flow through the slot produced the benefit in case of the slatted airfoil. Similar changes in the flow were noted at M=0.4, but a weak dynamic stall vortex was still present. More detailed and complete studies need to be conducted for establishing the preference of one method over the other, but the ability to adapt the blade shape continuously through its rotational cycle might offer measurable benefit at a lower drag. An invited paper on the comparison was presented at the AIAA 17th Applied Aerodynamics Conference in Norfolk.

The DDLE data was supplied to Georgia Tech. and University of New Mexico researchers for validating their computations.

Another major component of the research was the study of the surface flow behavior using heat-flux gages. A 6-inch chord NACA 0012 airfoil was fully instrumented with 148 hot film gages starting from x/c = 0.1 on the lower surface to x/c = 0.95 on the upper surface. From the lower surface to x/c = 0.25 on the upper surface, 40 gages/in were mounted. From there on, four sensors were mounted for each x/c increment of 0.05. The sensors were 0.005 in wide and were operated by TSI 1750/1755 hot wire anemometers (provided by the Air Force Frank J Seiler Laboratories). A custom data acquisition software package was developed (using LabVIEW™) for the high-speed data acquisition boards (32 channels at 768 kHz total rate). Both digital and analog data were acquired as the airfoil was oscillated as $\alpha = 10^O + 10^O \sin \omega t$ at M = 0.3. These preliminary tests were intended to prove the instrumentation. The results demonstrated some significant features of the flow.

At the Reynolds number of the experiment (1.1×10^6), transition first occurred at $\alpha \approx 3^O$ at x/c ≈ 0.7 and rapidly moved upstream to x/c ≈ 0.03 at $\alpha \approx 7^O$. At just about this angle of attack, a separation bubble formed and as has been shown earlier in the point diffraction interferometry studies, eventually burst

around $\alpha = 14°$ to produce a dynamic stall vortex. The vortex propagated on the upper surface rapidly and deep dynamic stall ensued. The hot film gage studies verified the PDI studies, but the new fundamental information gathered was the fact the transition point moved dramatically over the airfoil. This new knowledge can now be included in the computational modeling of compressible dynamic stall flow. The additional physical insight should enable a more complete representation of the flow and lead to more realistic results.

37032-EG "Experimental Investigation of Tip Clearance Flow Fields and Methods of Desensitizing Tip Clearance Effects in Turbines"

B. Lakshminarayana, Pennsylvania State University

The main focus of the research program is to carry out a systematic study of the tip clearance flow fields and methods of desensitizing their effects in turbines. The objective is to understand the flow physics, origin, nature, and effects of leakage flow and their dependency on blade and flow geometry and then carry out an investigation to minimize their effects through flow control and design.

The experimental study was based on the data obtained using a small (1.67 mm diameter) five-hole probe in the rotating frame of reference. The probe was traversed at 7 radii for 3 axial locations inside the rotor passage near the tip, and at 11 radii for 2 axial locations downstream of the rotor in the near wake. The total and stagnation pressure fields and three orthogonal velocity components were measured. From this data, the axial vorticity and secondary velocity vectors and flow losses were calculated.

The data indicates that the tip leakage vortex originates at the axial location where the blade pressure distribution has its suction peak. The leakage vortex is confined close to the suction surface corner near the blade tip by the relative motion of the blade and the casing and by the secondary flow in the tip region. The tip leakage flow clings to the blade suction surface until the blade suction peaks, and then lifts off of the suction surface to form a vortex in the last 20% of the blade chord. The relative motion between blades and casing leads to the development of a scraping vortex, which along with the secondary flow reduces the propagation of the tip leakage flow into the mainflow.

The structure and behavior of the passage vortex, found close to the tip leakage vortex, has been resolved. The tip leakage vortex was seen to interact with the passage vortex downstream of the rotor. The investigation also compares the decay characteristics of the passage and tip leakage vortices and the decay characteristics of the blade wake. It was seen that the tip leakage vortex is the most dominant feature of the flow field in the tip region. The disturbances and flow losses (**Figure 3**) in the flow due to the tip leakage vortex are more dramatic than the disturbances from the passage vortex and decay more slowly downstream of the rotor. The loss coefficient ζ is defined by

$$\frac{(\text{relative total pressure at inlet}) - (\text{local relative total pressure})}{0.5\ (\text{density}) \times (\text{blade speed at mid-span})^2}$$

The tip leakage vortex produces 55% of the vorticity shed in the last 25% of the blade span. The rotor flow investigation

also shows some difference in the behavior and decay of the tip leakage vortex when compared to the data acquired in cascades.

The unsteadiness in the tip leakage vortex and other features are being investigated using a slanted hot-wire located downstream of the turbine rotor. This effort identifies the unsteadiness in the development of the rotor wake and the leakage vortex due to upstream nozzle. Primary results clearly show frequency distribution due to the turbine rotor and other features.

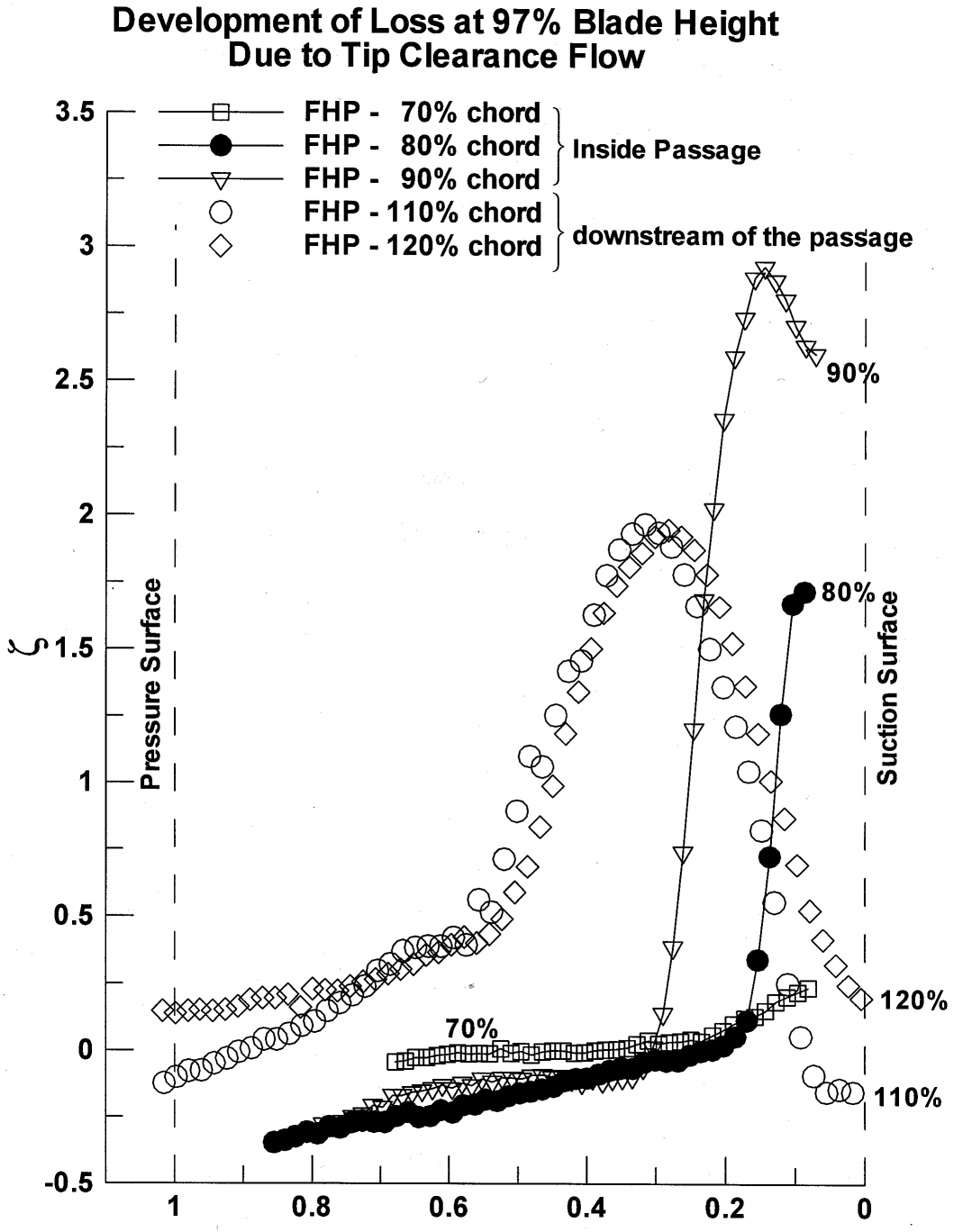

Figure 3 Percent Blade Passage in Tangential Direction

37594-EG "Aerodynamics of Parachute Opening"

H. Johari, Worcester Polytechnic Institute

The objective of this research project is to study the temporal evolution of the flow field in the near wake of a generic, round parachute canopy. The experiments are conducted in a controlled laboratory setting in order to better understand the complex flow physics associated with canopy inflation. The flow field complexity arises from the strong fluid-structure interaction where the fluctuations of fluid dynamic forces alter the geometry of the flexible, porous canopy, and in turn, the canopy geometry sets the boundary conditions for the unsteady, separated flow field. Even under steady state flow conditions, a canopy experiences significant "breathing" motions due to vortex shedding in the wake.

A set of flat circular parachute canopies with diameters of 15, 23, and 30.5 cm were constructed from standard rip-stop nylon used for full-scale fabrication. To minimize the stiffness of these canopies, a single piece of fabric was used, and the suspension lines were thermally fused to the canopy fabric. The suspension lines were attached to a streamlined forebody with a frontal area less than 0.5 % of the inflated canopy area. The parachute system was installed horizontally in a low-speed water tunnel. Quantitative imaging of the canopy geometry during inflation revealed that the canopy inflation was very repeatable. Moreover, the opening times, normalized by the freestream velocity and constructed diameter, appeared to be independent of the range of available Reynolds numbers in the tunnel. The inflation experiments were conducted in a constant freestream velocity simulating the "infinite mass" conditions.

The velocity field measurements were performed utilizing the Digital Particle Image Velocimetry (DPIV) technique. The DPIV system included a 30 Hz progressive scan CCD camera and a dual pulsed Nd:YAG laser. Successive images were interrogated using the cross-correlation method. The flow field in a plane containing the canopy and parallel to the freestream was imaged. The freestream velocity was held at 20 cm/s corresponding to a Reynolds number (based on the constructed diameter) of 3.4×10^4. To maintain satisfactory spatial resolution of the velocity field, the extent of the imaged flow region was reduced as much as possible. This is the primary reason for the small scale of the canopies used in the experiments. The largest imaging area was 18 cm $\times$ 13 cm resulting in a spatial resolution of about 5 % of the canopy diameter. The downstream extent of the imaged flow field was about 1/2 - 2/3rd of the canopy diameter resulting in a few thousand vectors in the region of interest.

During the past year, both inflating and fully inflated canopies were investigated. Scattering of the light sheet by the canopy fabric and presence of shadow regions created difficulties with data extraction in the vicinity of the canopy. Image processing routines were developed to address these issues. Two sets of sample data fields are presented in **Figures 4** and **5**. Instantaneous velocity field data from a fully inflated canopy are shown in **Figure 4** where the "breathing" is clearly visible in terms of the changes in the canopy geometry. The breathing is a result of vortex shedding in the canopy near wake. When the canopy is near its maximum

inflated diameter, a vortex is present very close to the surface of the canopy, as in **Figure 4a**. The low-pressure region associated with the vortex draws the canopy outward into an over-inflated state. Subsequently, the vortex is shed, and the canopy diameter shrinks (**Figure 4b**) until another vortex begins to form behind the canopy that causes the canopy to expand again. The strength of the vortices, canopy geometry, and the drag force will be correlated to ascertain the effect of vortex shedding.

a.

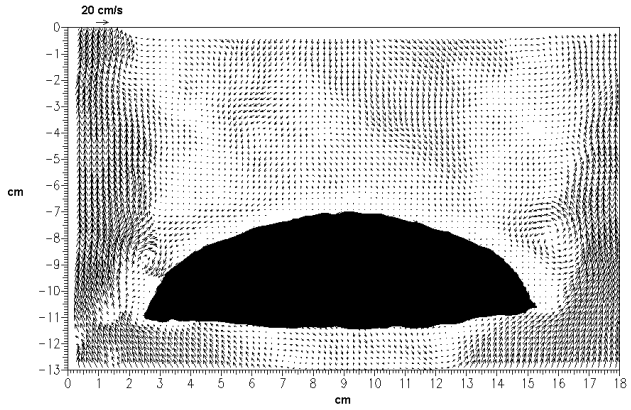

b.

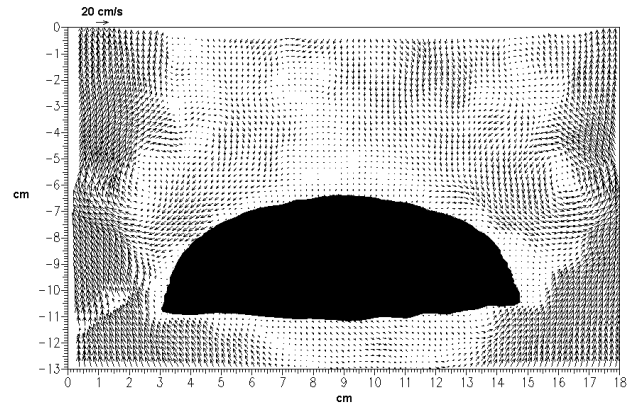

Figure 4 Velocity field at two instants behind a fully inflated canopy. Flow is from the bottom to the top.

Sample velocity field data during the inflation are shown in **Figure 5**. The two images depict the canopy at instants where the canopy is unfolding (**a**), and when the canopy diameter is comparable to that at the fully inflated state (**b**). The canopy diameter continues to grow to a maximum value prior to settling into its steady state. A rolled-up vortex is apparent behind the canopy in (**b**). In the Figures, the canopy images have been superimposed on the velocity field after the data from particle images were processed.

a.

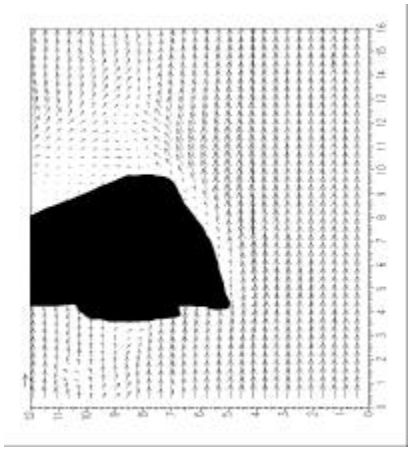

b.

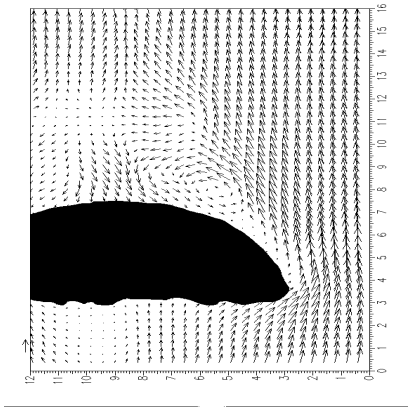

Figure 5 Velocity field at two instants behind an inflating canopy. Flow is from the bottom to the top.

37798-EG "Experimental Study of the Structure of Shock-Induced Turbulent Separated Flow and Its Role in Flowfield Unsteadiness"

D.S. Dolling and N.T. Clemens, The University of Texas at Austin

A flow of particular interest to the U.S. Army is shock-wave induced turbulent boundary layer separation, which occurs on missile fins, base flows and rotor blades. A common feature of these flows is that they are highly unsteady and are characterized by large-scale pulsation at frequencies that are an order of magnitude, or more, below the characteristic frequency of the turbulence. Owing to the complex nature of these flows and the high Reynolds numbers at which they exist, they remain largely beyond the capabilities of current theoretical and computational techniques. This highlights the crucial role that advanced measurements must play if a fundamental understanding of the physics of such complex flowfields is to be attained.

Earlier work in our laboratory using conventional pressure measurements in a shock-induced separated flow has suggested that the large-scale motion is caused by low-frequency variations in the thickness of the incoming boundary layer. Subsequent studies, however, employing planar laser scattering and particle image velocimetry (PIV), were unable to provide any supporting evidence for this mechanism. However, these conclusions were only tentative, because the PIV data set may not have been large enough to achieve statistical convergence.

Over the past year, our primary goal was to acquire a much larger volume of PIV data in the boundary layer just upstream of the interaction. Other improvements in the experiment have yielded velocity measurements closer to the wall and an improved determination of the shock foot motion. To examine the question of whether the boundary layer thickness varies with the shock position, the velocity vectors were conditionally ensemble-averaged and collapsed into velocity profiles for "shock-upstream" and "shock-downstream" positions. No difference in the boundary layer thickness was found, thus showing unequivocally that the thickening/thinning mechanism is not valid.

However, as shown in **Figure 6**, when the velocity fluctuations are conditionally averaged for different types of shock-foot motion, an interesting trend is revealed. Near the wall, negative velocity fluctuations correlate with upstream shock motion and positive velocity fluctuations correlate with downstream shock motion. Interestingly, no correlation is observed in the outer part of the boundary layer. These results are the first to offer direct experimental evidence of a relationship between the velocity fluctuations in the upstream boundary layer and the motion of the separation shock foot. Positive velocity fluctuations produce downstream motions of the separation shock, which, over a sustained period, integrate to a fuller velocity profile for a downstream shock location. Similarly, negative velocity fluctuations produce upstream motions of the shock and integrate to a slimmer velocity profile for an upstream shock location. These observations are consistent with the simple concept of a fuller velocity profile providing increased resistance to separation and thus a downstream shock position. Furthermore, such variations in the shape of the instantaneous velocity profile may yield

changes in the shock position and hence produce the unsteady shock foot behavior.

This past year was also spent developing a DURIP funded multi-camera/laser system that will enable the acquisition of four time-sequenced PIV images. Such time-sequenced velocity fields will be used to investigate the effect of upstream flow acceleration and separated flow structure on the unsteady shock motion of compression ramp and blunt fin interactions.

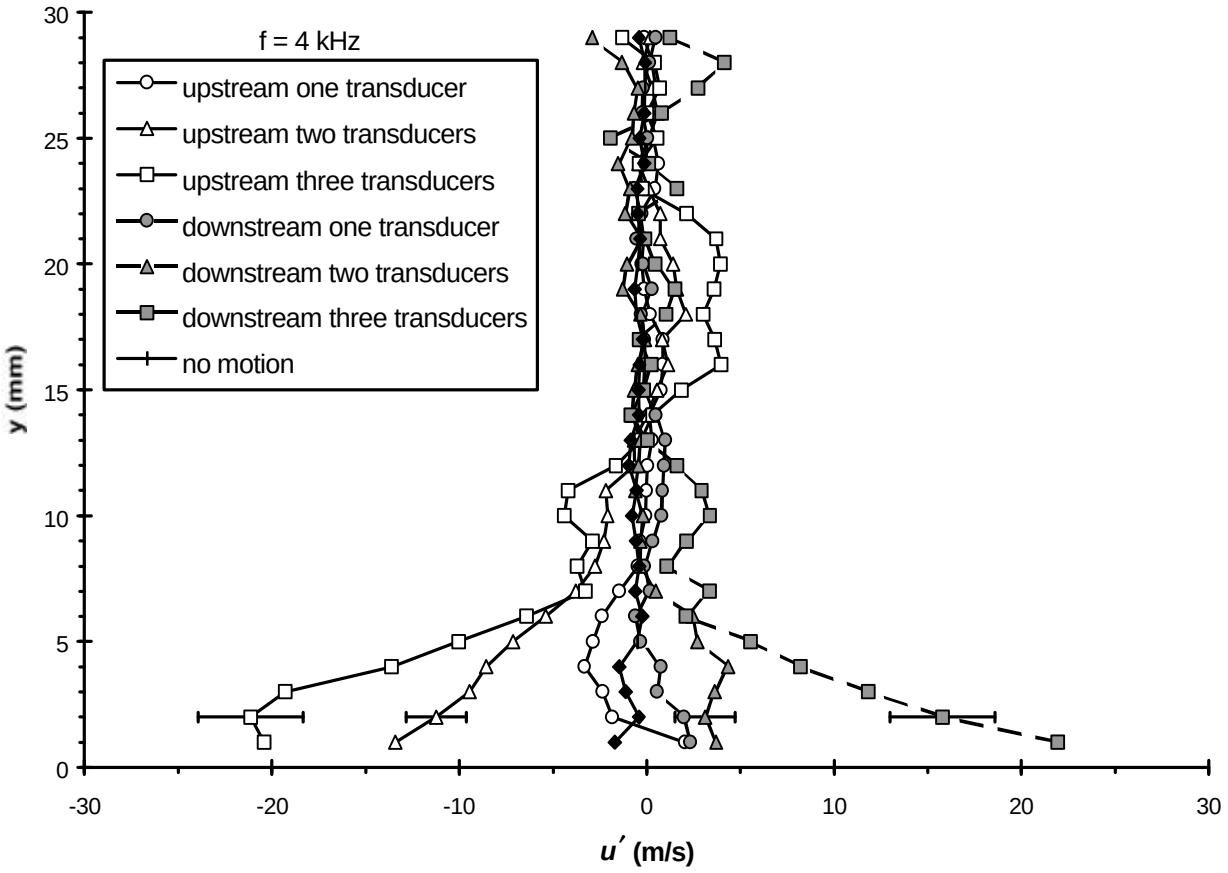

Figure 6 Conditional ensemble-average profiles of the streamwise velocity fluctuations in the incoming boundary layer, conditioned upon the separation shock-foot motion within a time period of 250 s (4 kHz). The profiles are for different types of shock motion. The distance is measured by the number of wall-mounted transducers the shock-foot traverses during the time period. This figure shows that positive (negative) upstream velocity fluctuations near the wall are clearly correlated with downstream (upstream) motion of the shock-foot. Furthermore, this correlation is stronger for larger excursions of the shock.

37822-EG-DPS "Detection and Control of Incipient Stall on Pitching Blades Using a Flexible Wall Transducer Array"

S.K. Sinha, University of Mississippi

Detecting and mitigating incipient separation on rotorcraft blades is important for enhancing their performance and safety. The present effort documents efforts towards achieving this at Reynolds numbers which are high enough to replicate the viscous-inviscid flow interaction physics experienced by prototypical blades. The approach taken is to use a novel active flexible wall transducer array, which can be used for flow condition sensing as well as actuation to defer or delay separation. Based on earlier experiments, this approach seemed to require considerably lower actuation power compared to other currently advocated active flow control techniques, such as those involving periodic blowing/suction. However, the flow transducer-interaction mechanism and its relationship to the unsteady separation process over a rotor blade is not yet clearly understood. Therefore, the focus of the present effort has been to (1) understand the flow-transducer interaction sufficiently and (2) explore the transducers capability in controlling incipient separation over a pitching blade section.

A combination of experiments and simple theoretical reasoning is being used for this study. The experiments are being done on a 300-mm chord NACA-0012 wing section with the transducer array applied to its leading edge. The wing section was mounted in a specially designed test section in a subsonic wind tunnel, which permitted pitching oscillations of the wing about its 1/4-chord point. For the present experiments, a wing section with 55 pressure taps was used. Each pressure tap communicated with its own pressure transducer. The system has been found to able to respond to fluctuations up to 1-kHz. Thus, the pressure measurement system had adequate response to measure the near-instantaneous pressure distribution over the airfoil, even for the highest pitching frequencies of about 12 Hz. The leading edge pressure taps went through the transducer array.

A simplified theoretical analysis indicated that the flexible wall transducer exploited the interaction of the near-wall flow with small-scale geometrical features of the wall. More specifically, the small (~3-mm/s) wall normal actuation velocity of the transducer membrane gets multiplied by the gradient of the streamwise velocity ($\partial u/\partial y$) at the wall in the streamwise momentum equation. The actuation is effective if ($\partial u/\partial y$) is large at the point of actuation. Effective actuation induces fluctuations in streamwise velocity. These fluctuations are eventually convected downstream to any shear-layer-like flow structure which arise in steady and unsteady separating boundary layers. Separation control occurs if velocity fluctuations enhance mixing in these shear-layer-like structures. The above mentioned deductions indicate a possible way to explain earlier experimental results. However, a direct experimental verification has not been possible since it necessitates detailed measurements of the flow within the viscous dominated sub-micron scale wall layer.

Experiments on statically stalled airfoils indicated that pressures in the leading edge region could be lowered by exciting the transducer. The net effect increased the coefficient of lift by about

11% at Re_c = 580,000. The increases come down to about 3% as the Re_c value is increased to 1,000,000. The most effective frequencies (f) for control correspond to a Strouhal number (St = fs/U) of about one (where U represents the velocity at the outer edge of the boundary layer and s the spacing of the transducer strips). This indirectly indicates that the small-scale geometrical features which scale with s directly influence the receptivity of the system to wall actuation. This is in contrast to the established belief that $fc/U_\infty \sim O(1)$ (where c represents the airfoil chord length and U_∞ the upstream velocity) indicates the most effective control frequency. While $fc/U_\infty \sim O(1)$ usually holds for microflaps and pulsed blown jets, for the present studies the value of $fc/U_\infty \approx 230$ for $400{,}000 < Re_c < 1{,}000{,}000$. Earlier flow control experiments on a cylinder indicated that $fd/U_\infty \sim 23$, based on the cylinder diameter d for effective flow separation control with an the active flexible wall transducer. The experiments clearly indicate a different scaling relationship for the active flexible wall as compared to microflaps and pulsed jets.

Next, the transducer was excited while the airfoil was sinusoidally oscillated in pitch between 5 and 20 degrees. **Figure 7** shows the output from a pressure transducer located close to the leading edge (x/c = 0.005). This corresponds to Re_c = 400,000 and a reduced frequency $k = f_{pitch}c/U_\infty$ of 0.039. **Figure 8** shows the same pressure measurement after exciting a leading-edge strip of the transducer at 70-kHz, corresponding to $fc/U_\infty \sim 1000$. Similar effects could be observed as long as the point of actuation ranged between $0<x/c<0.03$. The preliminary results indicated a dramatic (~ 50%) reduction in the leading edge suction peak. We are currently in the process of repeating these tests over a larger range of Re_c and k and reconciling these results with the simplified theory.

37858-EG-YIP "A Computational Investigation of Methods for Active Control of Unsteady Separation"

K.W. Cassel, Illinois Institute of Technology

Unsteady separation is one of the important unsolved theoretical problems of fluid mechanics, and it is also of primary practical importance in a wide variety of applications involving high Reynolds number surface-bounded flows, such as dynamic stall on helicopter rotors. Unsteady separation is characterized by the formation of a recirculation region due to the presence of an adverse pressure gradient and a subsequent local eruption of boundary-layer fluid that moves rapidly away from the surface. This rapidly growing spike induces an interaction between the viscous boundary layer and the inviscid outer flow. Although it involves a small-scale eruption of short time duration, unsteady separation often plays a dominant role in the overall flow evolution of unsteady aerodynamic flows. This investigation addresses both the theoretical issues necessary to increase our fundamental understanding of these important events and the practical issues involved in controlling them in applications.

A computational fluid dynamics (CFD) code based on the vorticity-streamfunction formulation of the unsteady Navier-Stokes equations has been developed and used to compute the flow induced by a thick-core vortex convecting above an infinite plane surface. Calculations have been carried out for a

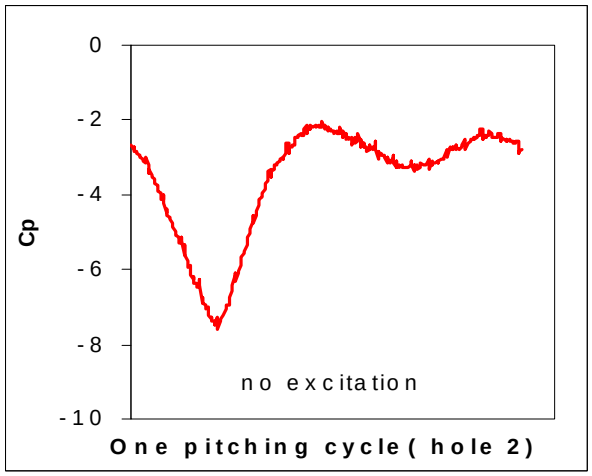

Figure 7 Pressure fluctuation at the leading edge of NACA 0012 airfoil (x/c=0.005, within one pitching cycle, no excitation)

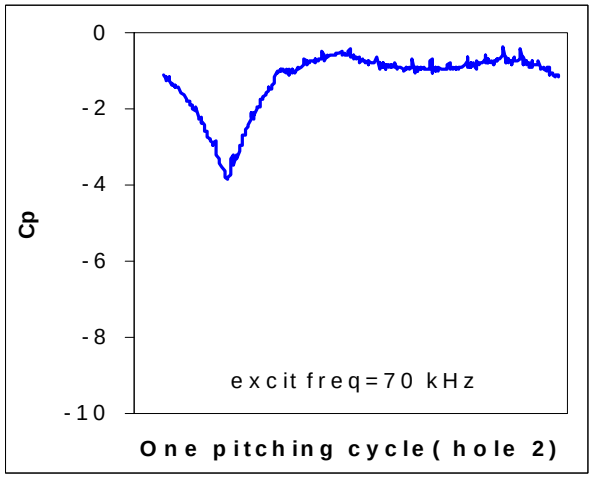

Figure 8 Pressure fluctuation at the leading edge of NACA 0012 airfoil (x/c=0.005, within one pitching cycle, excitation frequency = 70 kHz)

range of Reynolds numbers up to $Re = 10^5$, based on the strength of the vortex and its distance above the surface, to elucidate the unsteady separation process in various Reynolds number regimes in terms of the nature of the viscous-inviscid interaction that takes place. Based on the computational results and the high Reynolds number asymptotic theory, three Reynolds number regimes have been identified as illustrated in **Figure 9**. The low-*Re* regime consists of a large-scale interaction that is on the scale of the re-circulation region, but features no spike formation. The moderate-*Re* regime involves the large-scale interaction, subsequent spike formation and the resulting small-scale interaction. The high-*Re* regime is governed by the current asymptotic theory for unsteady separation, which only involves the small-scale interaction.

Some preliminary work has been done to investigate possible methods for controlling unsteady separation using a heated surface or a moving wall. Computational results for both mechanisms show that they can significantly alter the unsteady separation process. For the heated surface, it has been shown that unsteady separation can be accelerated or delayed, depending upon the direction of the buoyancy force. For the case of a moving wall, unsteady separation is suppressed at a critical value of the wall speed that is slightly less than the maximum magnitude of the external velocity at the outer edge of the boundary layer. This critical wall speed decreases with decreasing Reynolds number.

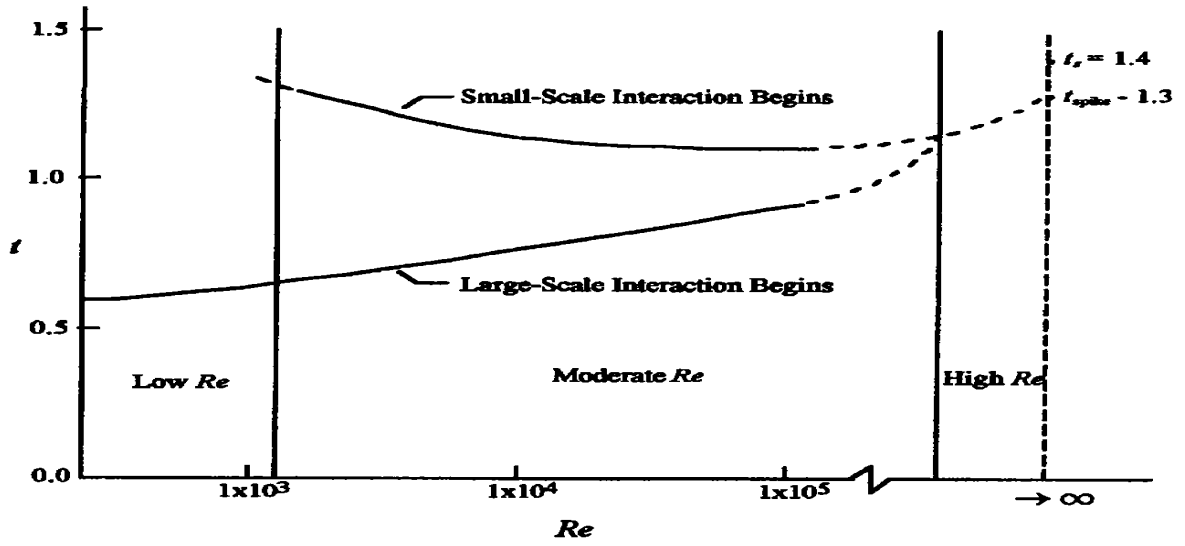

Figure 9 Schematic of the three Reynolds number regimes for viscous-inviscid interaction in unsteady separation. Times, *t*, and Reynolds numbers, *Re*, are representative of results for the thick-core vortex. The times t_s and t_{spike} are from a boundary-layer calculation.

38700-EG "Modeling of Radiation in Plume-Flows"

D.A. Levin, George Washington University

High-quality data on optical radiation that has been recently obtained for space vehicles in-flight stimulate the numerical investigation of rocket motor plume flows. Ground based radiation imagery has been obtained for the Atlas rocket flight from almost lift-off to altitudes of 100 km and more. Numerical modeling of optical radiation is important for imagery analysis, radiation signature prediction, and sensor development. Hypersonic flight has two main features of non-ideal gas flows: significant viscous effects and thermo-chemical nonequilibrium. Chemical reactions and the presence of a wide range of flow length scales make the full simulation of such flows a challenging task. The main goal of this work is to examine the effect of the flow around a complex Atlas vehicle body on the plume structure. To this end, the numerical solution of the viscous formulation of the Navier-Stokes equations for the chemically reacting flow around a three-dimensional model of Atlas moving at the altitude 40 km with the angle of attack 0 degrees is calculated using the GASP Navier-Stokes solver.

The vehicle model used in the computations consists of the axisymmetric part of the body and the three-dimensional aft body. With the origin at the center of symmetry of the multi-nozzle exit plane the computational domain was chosen 46.2 m upstream and 150 m downstream. A multi-zone approach for the computation of viscous chemically reacting problem is to divide the flow domain of interest into three regions. The first one is the region of the flow over axisymmetric part of the vehicle. In the two other regions of computational domain: flow around aft body and Atlas multi-nozzle plume the problem is three-dimensional. The grid for the axi-symmetric part has two zones with 100 by 60 and 130 by 60 cells. The aft body grid has 120 by 140 by 65 cells and the marching zone has 150 by 140 by 65 cells.

There are a total of nine chemical species in fifty finite-rate exchange and dissociation recombination chemical reactions to used to model the reacting LOX/Kerosene - air fuel mixture. The exhaust gases from the Atlas motor consist primarily of H_2O, CO, CO_2, H_2 which are assumed to reacting with the ambient gases N_2, O_2 and CO_2. Due to the high temperature at the nozzle exit and the shear layer, chemical reactions occur in the gaseous mixture and affect the optical radiation.

Figures 10 and **11** below show a comparison of the plume-body flow interactions 1 and 40 meters from the nozzle, respectively. The top and bottom contour plots in each figure represent the calculation with and without the body, respectively.

39086-EG "Projectile Base Flow Analysis"

D.W. Wilcox, DCW Industries, Inc.

To lay the foundation for a study of base flows, we have validated our grid-generation and Navier-Stokes solver for incompressible flow past a backward-facing step. We have duplicated the results of others who, using the old version of the k-ω model, have predicted a reattachment length of 6.4 step heights for a case where the measured value is 6.2 (**Figure 12**). The new version of the k-ω model predicts 6.5 step heights without

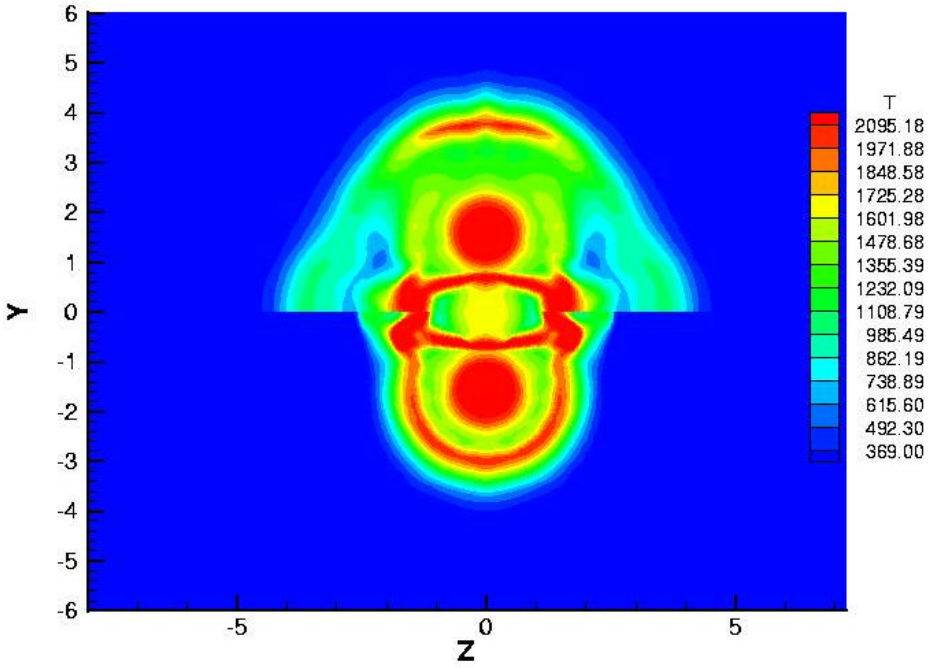

Figure 10 Comparison of the plume-body flow interactions 1 meter from the nozzle

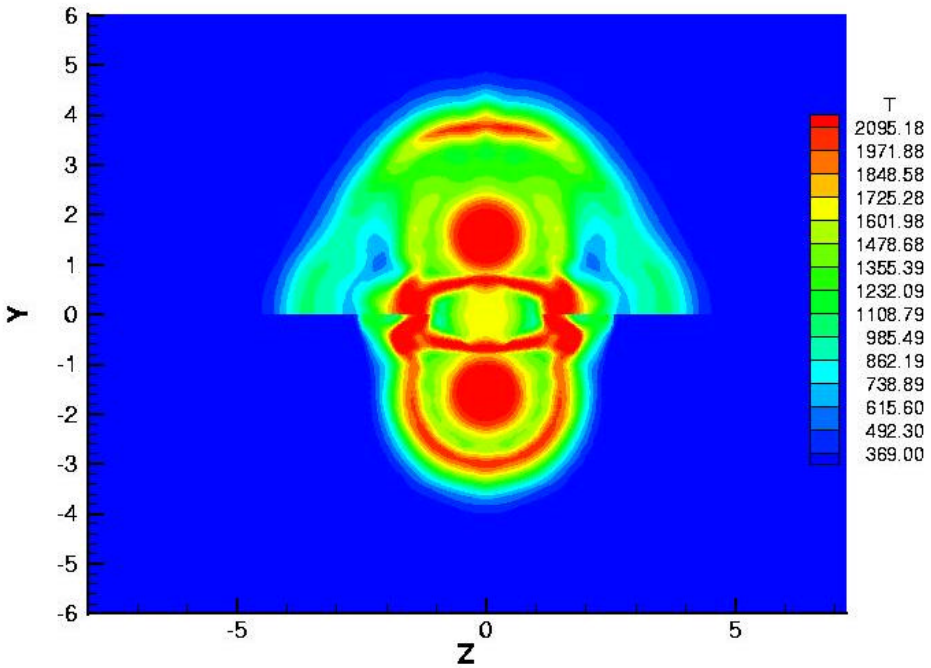

Figure 11 Comparison of the plume-body flow interactions 40 meters from the nozzle

viscous corrections and 6.6 step heights when they are included. The new stress-ω model predicts a reattachment length of 6.7 step heights without viscous corrections and 6.4 step heights with viscous corrections. The four solutions with the new models differ only in minor detail and are far closer to measurements than any other two-equation or stress-transport model reported to date.

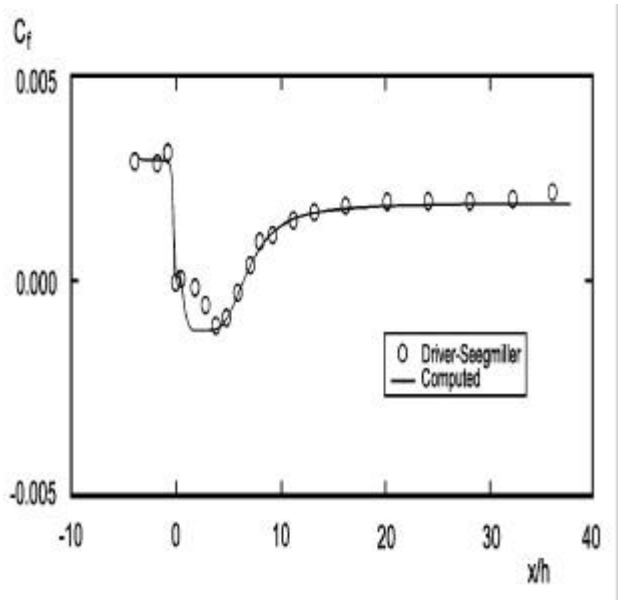

Figure 12

39104-EG "Innovative Solid-State All-Weather Shear Stress Transducers"

D. Pruzan, Nielsen Engineering and Research, Inc.

Nielsen Engineering & Research (NEAR) is currently conducting an SBIR Phase II contract to develop a MEMS-based, all-weather shear stress sensor. During the initial phase of this contract, NEAR evaluated the feasibility of two different shear stress sensor designs. The first transducer uses a solid-state ultrasonic acoustic transmitter and receiver flush-mounted into the skin of the aerodynamic structure being monitored; see **Figure 13a**. Associated electronics determine the time-of-flight of the arriving signal and use this information to infer the shear stress. This concept provides a rugged, nonintrusive sensor with excellent frequency response.

The second sensor design investigated is an environmentally hardened, direct measurement drag balance as shown in **Figure 13b**. This device incorporates a very thin nonconductive silicone rubber membrane mounted flush with the skin of the aerodynamic structure being monitored. As constructed, only the perimeter of the silicone membrane is attached to the sensor body, leaving the central region of the membrane free to deform under the applied shear stress. A rectangular region of conductive silicone rubber, integral to the nonconductive membrane, forms one electrode of a variable surface area, parallel plate capacitor. The other electrode is created within the nonconductive sensor body. A Teflon layer between the membrane and the sensor body provides a solid dielectric gap. Because silicone rubber does not cure to Teflon, the membrane above the Teflon is free to slide. An imposed wall shear stress stretches the central region of the membrane, extending the rubber electrode in the direction of the flow, thus increasing the transducer's capacitance. Simple measurement circuits are used to detect this change in capacitance and determine the applied shear stress.

NEAR has performed low-speed wind tunnel tests on large-scale prototypes of each transducer design. These tests uncovered sensitivity and hysteresis problems with the capacitive transducer which could not be overcome. On the other hand, tests conducted with the

ultrasonic transducer generated very promising results, as shown in Figure 11c. In these experiments, the time for an acoustic signal to travel from the upstream transmitter to the downstream receiver was measured as a function of wall shear stress (as measured with a Selem 351 floating element drag balance). Experimental data were collected for turbulent boundary layers which were "tripped" using a variety of upstream obstacles including 36-grit sandpaper and three sizes of quarter-round wooden molding. The molding strips were placed at different normalized distances, x/h, upstream from the sensor.

As can be seen in this figure, there is a good correlation between the measured time-of-flight and the applied wall shear stress for a variety of turbulent boundary layers. Unfortunately, data collected for laminar boundary layers (not shown) fell on a separate correlation curve. NEAR is currently investigating the feasibility of designing a transducer that will yield a single time-of-flight versus wall shear stress correlation irrespective of the type of boundary layer. To better understand the influence of design variables (e.g., operating frequency, sensor size, and sensor separation distance) on transducer performance, NEAR developed a numerical model based upon the discretized governing equations. Predictions from this CFD analysis are presented in **Figure 13c** for the transducer configuration used in the low-speed wind tunnel tests. The agreement between experiment and CFD analysis is reasonably good. NEAR is currently using the CFD software to investigate design options for the MEMS-scale transducer.

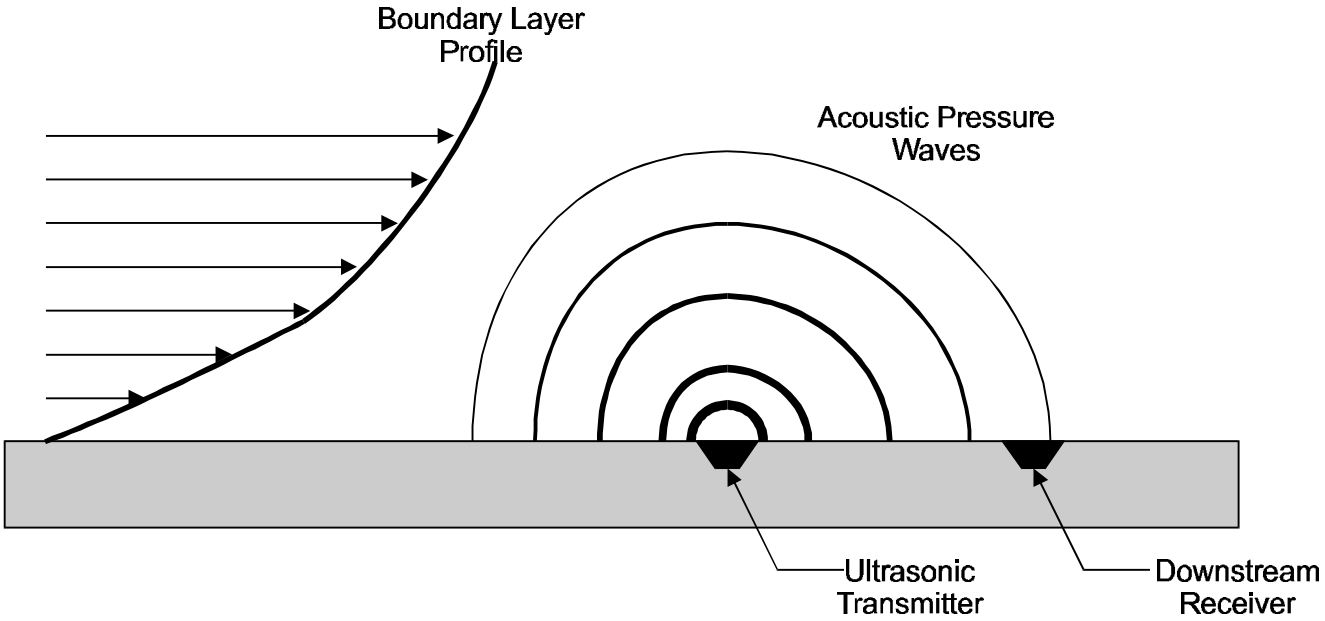

Figure 13a Cross section of the solid-state ultrasonic wall shear stress transducer.

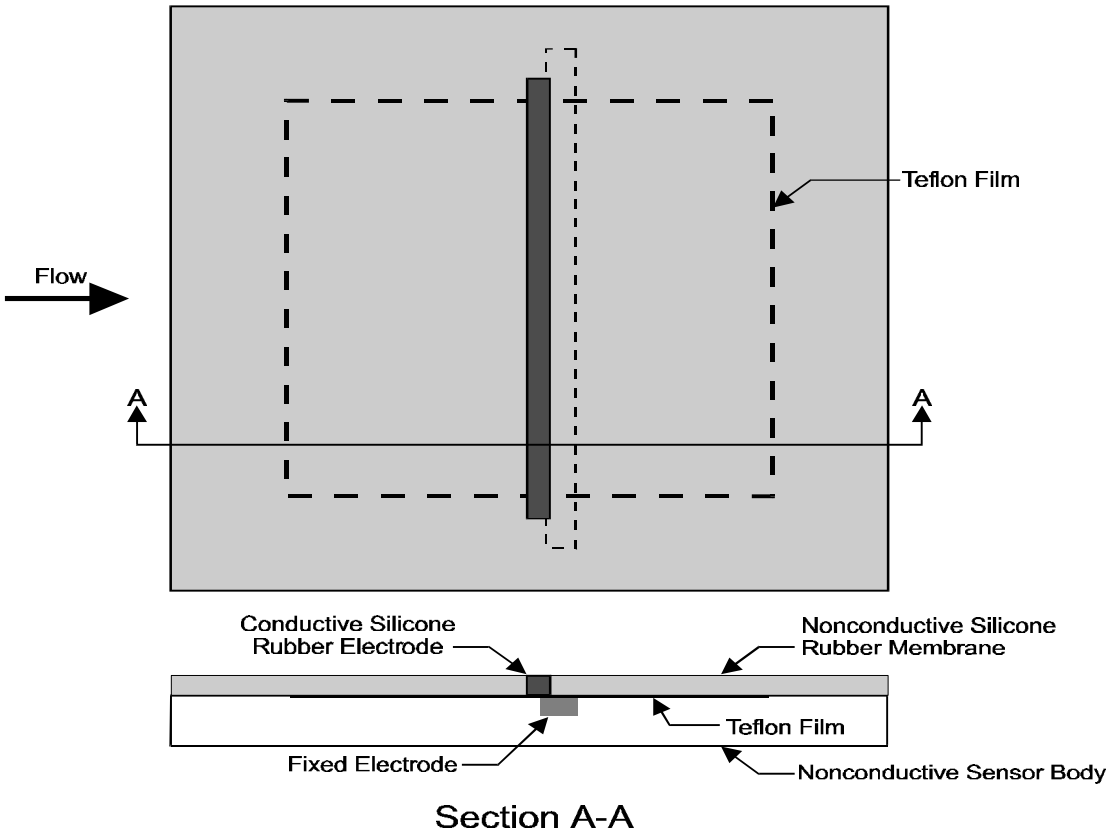

Figure 13b Silicone rubber capacitive wall transducer, top view is shown above, side view is shown below.

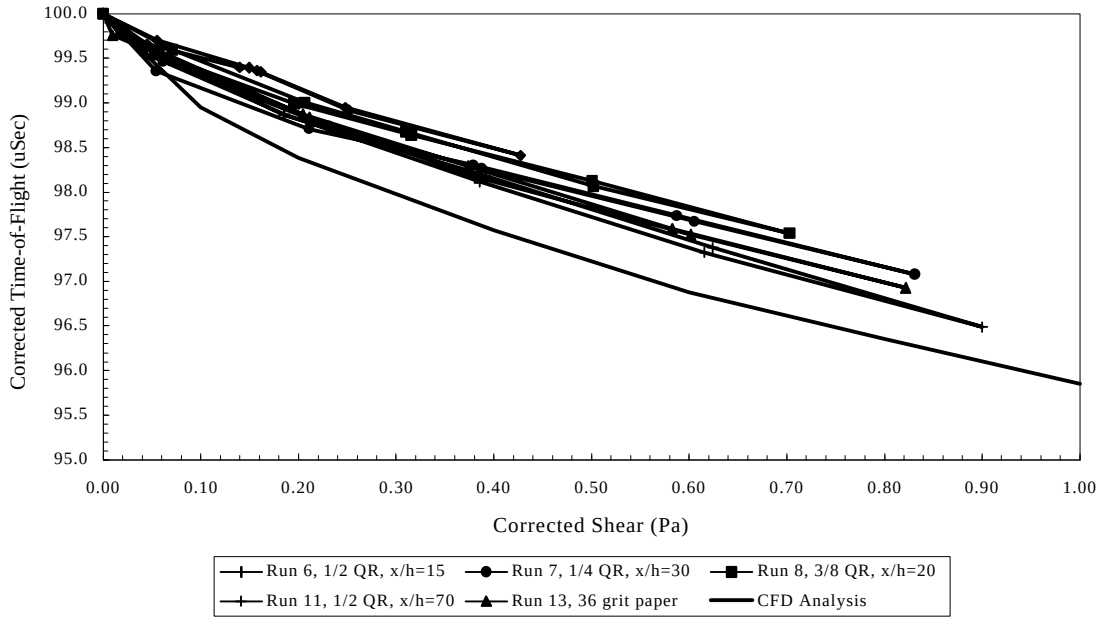

Figure 13c Experimental data showing measured time-of-flight verus measured wall shear stress along with predictions from the CFD analysis. These data are for the Phase I configuration.

39115-EG "Experimental and Numerical Investigation of High-Speed High-Temperature Jet Interaction Flowfields"

R. Bowersox, The University of Alabama

The principal objective of the present research proposal is to improve the understanding and predictability of high-speed high-temperature jet interaction flowfields. A detailed experimental program using advanced laser based flowfield diagnostics is being performed to characterize the flow. The experimental study will provide a detailed and accurate database from which improved understanding and improved physical models can be gleaned. The experimental configuration is designed to simulate realistic jet parameters for the low Mach (~ 3), low altitude (< 20 km) and low jet momentum ratio parameter (~ 0.1) operating condition, which has been documented to be the most sensitive. In addition to temperature ratio affects (1-16), the present study will examine the effects of injection Mach number (1-3), pressure ratio (2-20), the ratio of specific heats (1.3-1.67), injectant gas (air and helium), and jet pulsing. In addition, a companion turbulence model study will be performed. It is anticipated that the combined experimental and numerical research program will yield improved flowfield understanding and useful prediction tools.

The missile model construction for the adiabatic injection was completed on February 12, 1999. Wind tunnel testing of the injector models began on February 15, 1999. Experimental acquisition of the surface oil flow visualizations was completed; the particle image velocimetry data was 70% finished, and measurements of the mean Mach number, static and total pressure contours across the plume were 50% completed. Shown in **Figure 14** is a schematic of the flow field based on the acquired experimental data. Example experimental data (surface oil flow visualization, particle image velocimetry Mie scattering image and a Mach contour at x/D = 0.8) are also included. Preliminary data analyses indicated a minimal plume-surface interaction for the present missiles at a MPR of 0.1. Hence, the test matrix was expanded to include lower MPR values (0.005 and 0.01).

The jet-flow pebble-bed heater, required to produce the high temperature jet interaction, was designed and constructed. Hot gas testing is scheduled to begin June 2000. The numerical solutions will be generated with GASP (a structured flow solver) instead of GUST. GASP was installed on the Cray SV1, Jan 24, 2000. Simulations will begin in September 2000.

39140-EG "Boeing Active Flow Control System (BAFCS)"

D. Jacot, The Boeing Company

The objective of the BAFCS program effort is to show Active Flow Control (AFC) can significantly increase rotorcraft performance. Reducing download effects (rotor downwash on the wings, (**Figure 15a**) on tiltrotor rotorcraft is one such example. BAFCS is developing appropriate AFC technology, and validating its benefits to download reduction on the V-22 aircraft. **Figure 15b** shows how the basic application of AFC to the trailing edge of the V-22 wing can control separation and reduce download. It has been found that by appropriately selecting the location and frequency of these disturbances, a fraction

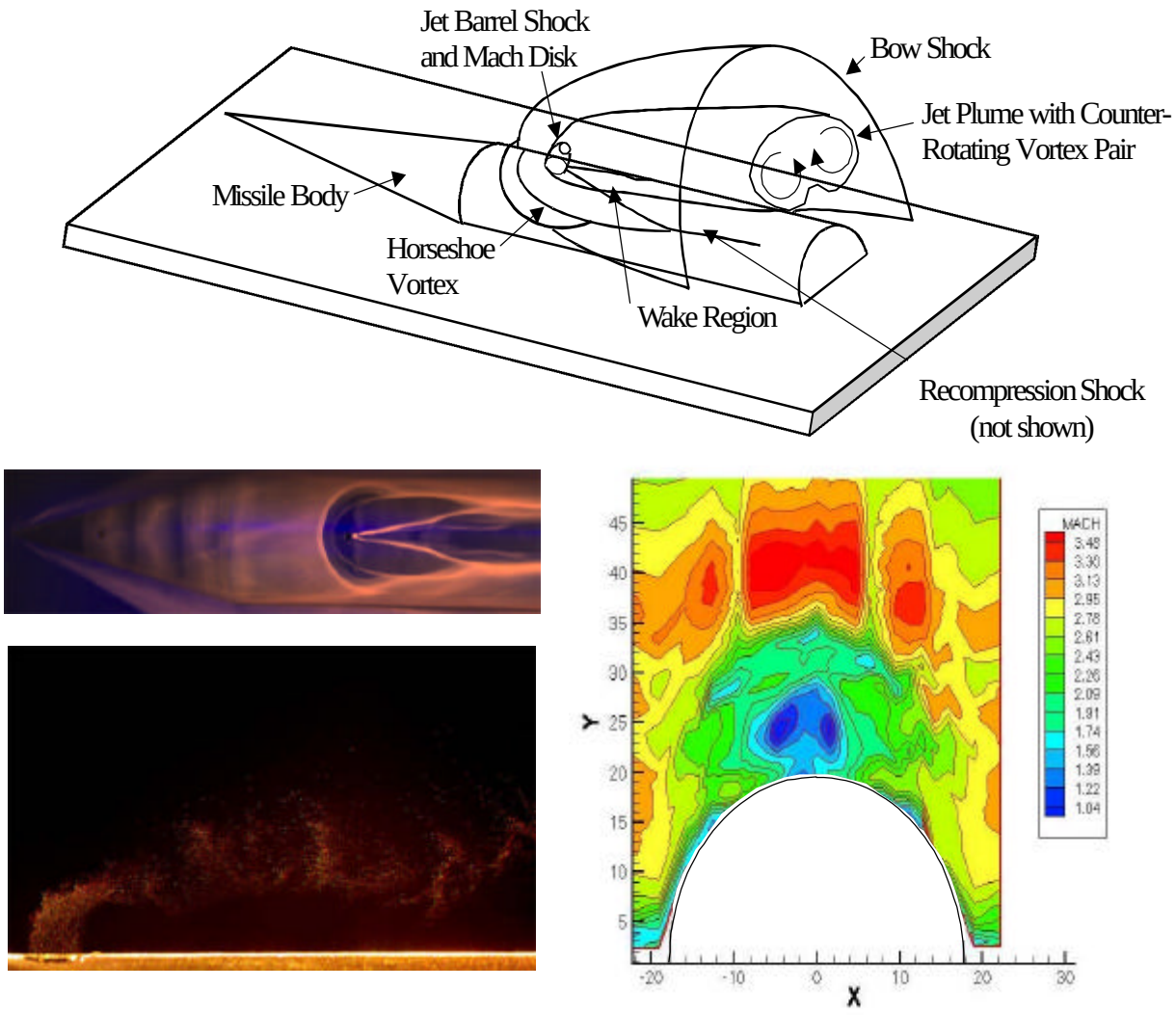

Figure 14 Schematic of the high-speed missile reaction control jet interaction flow field with example experimental data (top left-surface oil flow, bottom left - particle image velocimetry image and right - Mach number contour).

of one percent of the flow being affected is adequate.

BAFCS has shown with two-dimensional wind tunnel testing that payload increases of over 1000 lb are practical as illustrated in **Figure 15c**. This is up to a 20% increase in payload for some missions. Efforts on developing supporting technology are elaborated below.

Two Computational Fluid Dynamics (CFD) approaches (Detached Eddy Simulation and Large Eddy Simulation) are being developed and used to help guide this development as illustrated in **Figure 15d**. CFD is used to understand the flow physics and help in selecting the location, magnitude and frequency of the control perturbations. AFC actuators to generate these perturbations are the key development necessary for the near term application.

BAFCS is developing and evaluating two types of the low frequency actuators necessary, synthetic jets and a vibrating surface called a flipperon. Both are illustrated in **Figure 15e**, and use polymer piezoelectric materials. AFC actuators using newer piezo polymer having an order of magnitude larger strain are also being developed and evaluated. BAFCS is similarly developing testing techniques for proving the performance. The test setup and results from two-dimensional testing are illustrated in **Figure 15f**. The wing is mounted normal to the air flow, and drag is thus a measure of the download. These benefits have been quantified by two-dimensional wind tunnel testing, and the program is now entering into three-dimensional testing to prove such benefits are achievable in the realistic unsteady V-22 flow field. BAFCS has examined the practicality of applying this technology to the V-22, and has found no show-stoppers. Further performance benefits from application of AFC in the cruise mode are expected.

To summarize, AFC offers significant benefits to the V-22, in both payload and range. BAFCS has developed CFD modeling capabilities that agree with wind tunnel tests. Key to near term applicability, actuation and electronics development at these low frequencies has been initiated and approaches found that appear to be successful and scalable to the full scale V-22. The V-22 application is lower speed (lower velocity AFC actuation requirements) and less flight critical than most other real applications. Combined with the large benefits, the V-22 is thus an excellent application for this exciting new technology.

39174-EG "Separation Control For Rotorcraft"

P.F. Lorber, United Technologies Research Center

High performance future rotorcraft will need significant improvements in multiple attributes, including increased range for global self-deployability, increased speed and performance (maneuverability and agility) for demanding combat missions, increased payload, reduced external noise emissions, and reduced cabin noise and vibration. Active flow control technologies may be able to play a significant role in delaying retreating blade stall (RBS). The fluid mechanism involved in RBS is boundary layer separation near the leading edge of the rotor blade during rapid motion to high blade angle of attack. RBS limits the capability to generate lift and can transmit very large impulsive blade pitching

Figure 15 -Boeing Active Flow Control Study (BAFCS)

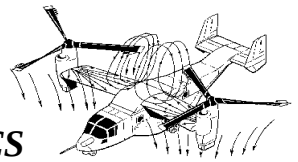

BAFCS

Tiltrotor Download Issue

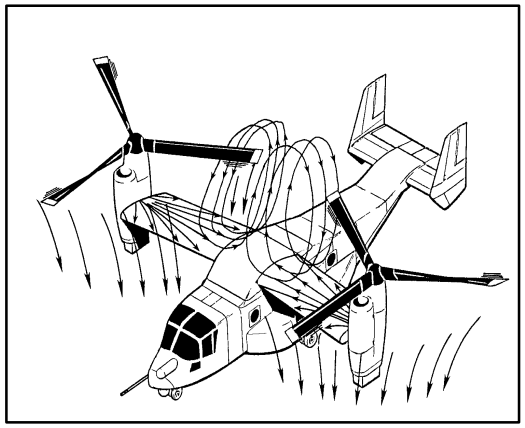

Figure 15A

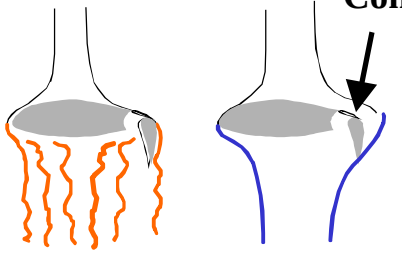

Figure 15B

- Download decrease
  - >5% decrease in
  - WING download
  - (>20% overall
  - download)

- > 1000 lb payload
- increase !!

Figure 15C

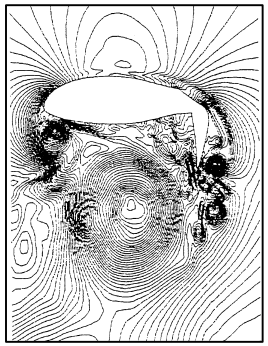

- Developing DES
- & LES CFD
- Capability

Figure 15D

Synthetic Jet

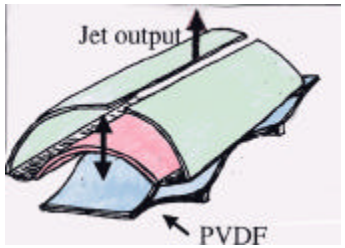

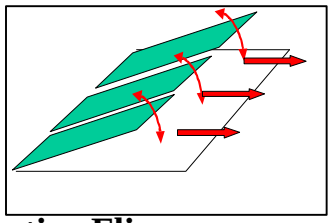

Active Flipperon

Figure 15E

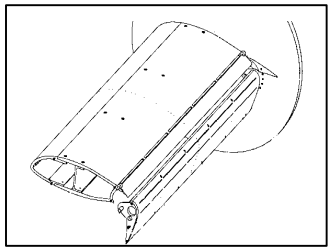

2D Wind Tunnel Model

2D Wind Tunnel Results

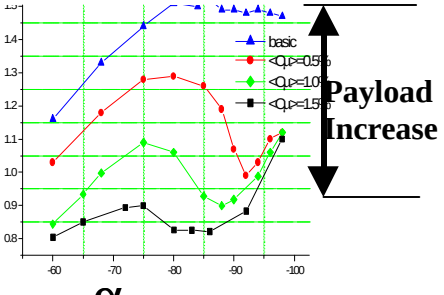

Figure 15F

c:\jacot\afc\aro\Mann\synopsis.pp

moments to the flight control system. Boundaries that must be set to avoid stall reduce maneuverability and agility as well as speed and payload. Any RBS control approach must be effective in an unsteady, compressible, high Reynolds number flow.

Unsteady excitation has frequently been investigated as a way to delay or avoid separation. The primary separation control technique that is applied in the current work is the Directed Synthetic Jet (DSJ). It utilizes the phenomena of acoustic streaming to form a synthetic jet. A typical DSJ configuration is shown in **Figure 16a**. The curved neck allows low momentum fluid to be ingested during the suction phase of the DSJ and high momentum fluid to be ejected during the blowing phase. Both phases energize the boundary layer. Practical DSJ actuation systems are being developed and evaluated using a combination of modeling and prototype construction. Effective actuator designs for the very demanding RBS application must be compact to fit within the limited available space, powerful to provide sufficient authority at the appropriate frequency for the high relative velocities at the blade, robust, and efficient to minimize the power that must be supplied to each blade and the heat that must be rejected.

An analytic electro-acoustic actuator system model was developed and exercised for a wide range of actuator parameters. From this effort, an understanding of the essential parameters for maximizing efficiency was developed. An initial prototype moving-coil actuator was then designed and built to obtain realistic experience and understanding with flexure design, sealing criteria, and internal losses. A benchmark analytical comparison was performed of the three basic electro mechanical actuator configurations (moving coil, variable air-gap, and variable reluctance). The best currently available approach for the RBS application was identified as the moving-coil concept shown in **Figure 16b**.

CFD has been used to study the coupled flow field of the airfoil and DSJ. On-going calculations for pitching airfoils are providing design information on the most effective reduced frequency, momentum coefficient, and slot geometry prior to finalizing the experimental configuration. One example of the flow field is shown in **Figure 16c**.

The effectiveness of the retreating blade stall control approach will be validated using full scale blade section experiments in the wind tunnel. The wind tunnel conditions will duplicate the parameters believed to be most important to the unsteady stall process: Mach number, pitching motion, Reynolds number, and airfoil section. Preliminary design of this experiment is underway. The blade section will be constructed to permit use of both internal electromechanical DSJ actuation and plasma actuation, which is being developed under a parallel DARPA/ARO sponsored effort at the University of Notre Dame.

39806-EG "Improvement of Fast Binary Pressure-Sensitive Paint Technology for Helicopter Rotor Blade Investigations"

V. Koulseh, TsAGI International

Pressure distribution on the surface of the helicopter blades determines the aerodynamic properties of the rotor system and the bending and twisting deformation of the blades. A promising method to solve this problem is the non-contact

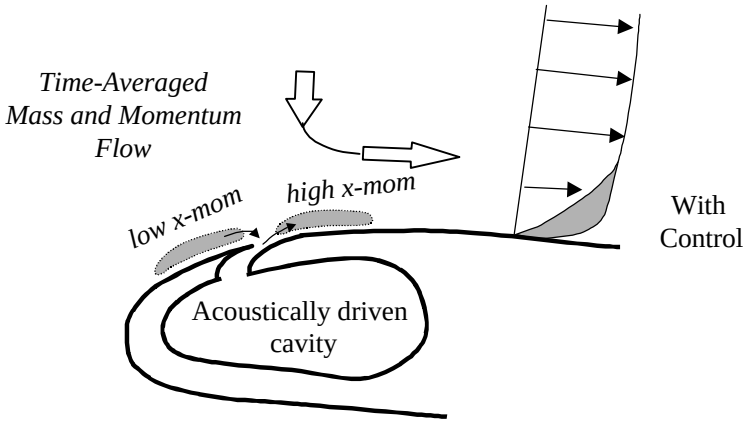

Figure UTRC 16a Directed Synthetic Jet Concept for retreating blade stall control

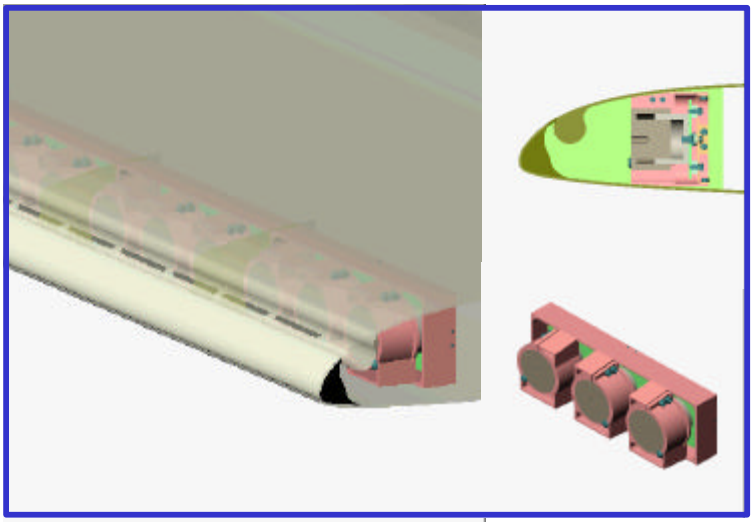

Figure UTRC 16b Preliminary design of moving coil DSJ actuation modules for wind tunnel validation experiment

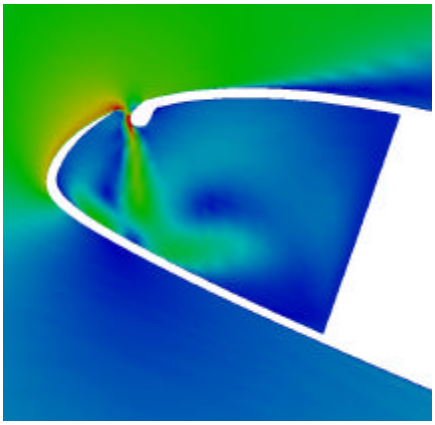

Figure UTRC 16c CFD simulation of airfoil leading edge flow during DSJ instroke.

optical method with using Pressure Sensitive Paint (PSP). PSP is a thin polymeric layer penetrable for oxygen molecules and containing luminophore molecules. This layer is applied on the model surface and luminescence is excited by an appropriate light source. Luminescence output is inversely proportional to the oxygen concentration in the PSP layer, which is a function of the local air pressure on the outer boundary of the PSP layer. Thus digital recording and treatment of luminescent intensity distribution provides the pressure distribution on the surface covered by PSP.

The latest PSP capability to measure the pressure distribution on the helicopter blade surface was demonstrated in TsAGI's T-101 wind tunnel experiment during the tests of the blade of a realistically-scaled rotor of the Russian Kamov-26 helicopter on June 1997. These tests show a basic capability of pressure distribution measurements on realistic-scaled blades of a helicopter rotor. However, realistically scaled tests are very expensive. Besides in realistic-scaled tests it is difficult to realize all regimes necessary for detailed investigations of the flow. For the most part, the current investigations are be conducted in the wind tunnels on the small-scale models, and are focused on pressure distribution measurements on a surface of a model of the blade with help of PSP technology.

Within this investigation the following accomplishments have been completed:

1. The composition of Fast Binary Pressure Sensitive Paint (FBPSP) with low time response has been developed. This paint is intended for pressure distribution measurements on the model of the helicopter rotor blade in wind tunnel tests. The properties of the FBPSP are investigated. The response time of the FBPSP to step pressure change is 2.6 *msec* (**Figure 17**).
2. The investigation of the helicopter rotor model in a wind tunnel by PSP technology has one more problem relative to registration of the image of the blade rotated with large speed. The duration of a pulse of excitation UV-radiation must be small to prevent a smearing of the image. The decay time of active layer luminescent also is rather small-100 *nsec*. However, the decay time of the reference layer luminescent is about 0.5 *msec*. During this time, the end of the blade of 1.25 *m* radius rotated with speed of 700 *rpm* passes a path about 0.08 *m* (corresponding to a turn of approximately 4 degrees). Therefore, the reference image of the blade will appear smeared and completely not suitable for use.

   To obtain a sharp reference image of the blade we apply an optical de-rotator system freezing the view of rotating blade during acquisition of reference component image. This is carried out with the help of a view of the blade through a mirror rotated around of axes of rotation of the helicopter rotor model in a conterminous direction but with twice smaller speed (**Figure 18**).
3. The optical system based on the receiving objective lens with a focal length 80 mm has been designed. Distance to the test blade is about 3m. The prism image splitter is used in this design (**Figure 19a**). The prism image splitters contains two optical filters (red and blue) and a pair of the optical prisms (**Figure 19b**). This splitter is

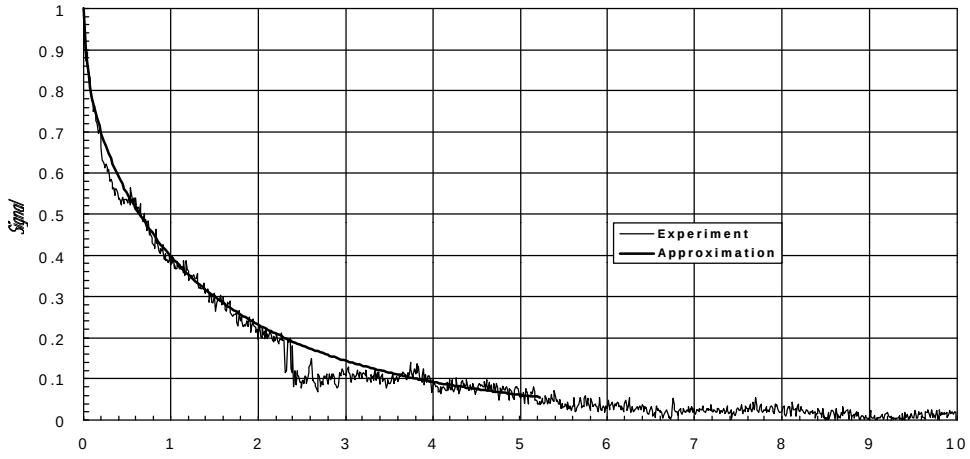

Figure17 Time response of LPS F2 to the step pressure change, t = 2.6*msec*

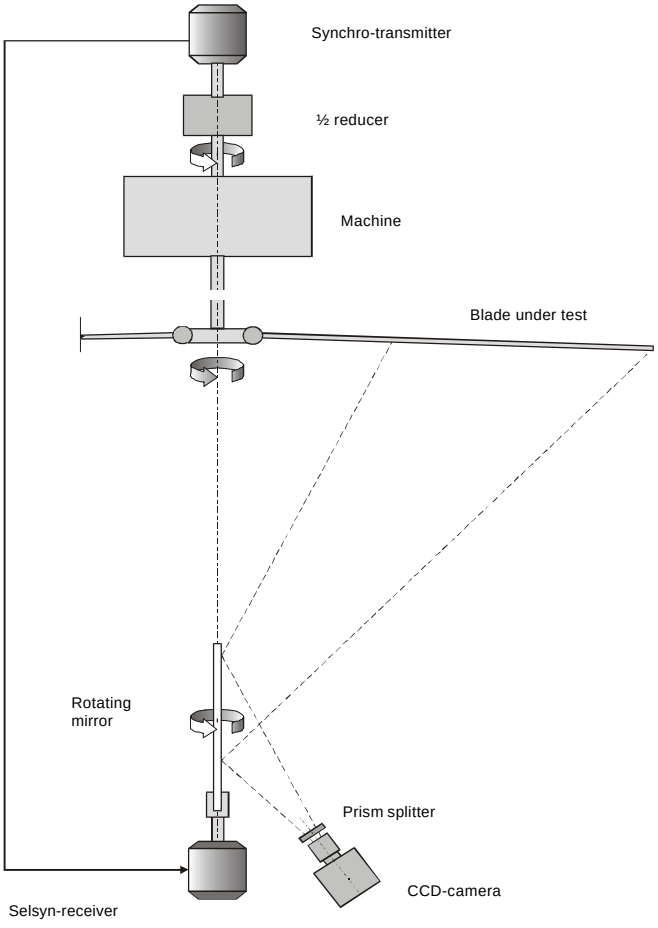

Figure 18 General de-rotator scheme

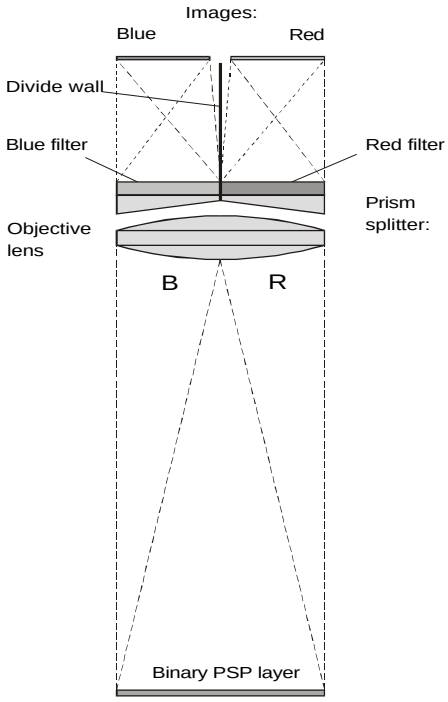

a)

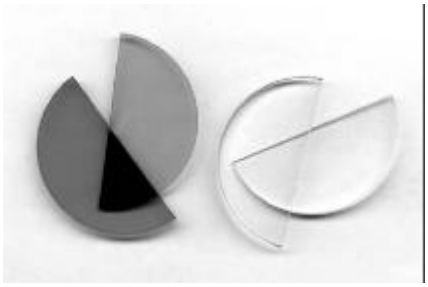

b)

Figure 19 Prism image splitter

needed for simultaneous registration both of the sensitive and reference images on one CCD-array

40019-EG "Fundamental Phenomena Related To Rotorcraft"

J.D.A. Walker, Lehigh University

The research program is a collaboration between Professor J. D. A. Walker at Lehigh University and Professor Anatoly I. Ruban at Manchester University, England. The objective is to study a range of unsteady flow phenomena relevant to the flow process occurring on the blades of rotorcraft. The flow fields in the vicinity of helicopters involve a number of complex unsteady processes that are not well understood but are known to have a substantial impact on performance. The most important of these are typically associated with the flow around the blades on the main rotor. This work is done with a combination of analytical techniques and computational simulations. The research encompasses two- and three-dimensional unsteady processes ranging from low-speed incompressible flow to compressible transonic flow. A central objective is to understand the phenomena that can lead to boundary-layer separation on the blades and can potentially undermine performance; a secondary objective is to determine practical means to control separation and thereby allow for enhanced lift and increased maneuverability.

During the past year, work has proceeded in a number of areas involving three Ph.D. candidates at Lehigh and one at Manchester University. An example of the research is shown in **Figure 20**, where a potential control for dynamic stall is depicted. As a helicopter blade moves, the angle-of-attack is typically increased at certain stages to achieve greater levels of lift. Unfortunately, boundary-layer separation in the leading nose region of the blade can lead to dynamic stall, which in turn may ultimately provoke abrupt degradation in lift and a pitching moment. In **Figure 20a**, calculated instantaneous streamlines are shown near the nose at t = 4.8 for a solid blade whose angle-of-attack (relative to the oncoming flow) is increasing linearly with time. The "hash" in the streamline patterns at this point is indicative that the boundary layer is erupting near the surface in a process leading to dynamic stall. In **Figure 20b**, the blade is modified to include a small suction slot. Now the blade reaches much higher angles-of-attack (with greater levels of lift), and the flow field is still smooth at t = 9. This appears to be a practical means to delay separation through weak suction by taking advantage of the differences in pressure that naturally occur on a pitching blade.

As a blade executes a maneuver, a wake develops at the trailing-edge and influences the external flow around the blade. A model and numerical method has been developed to account for this. Numerical methods and analysis are in progress to consider various flow regimes leading to three-dimensional boundary-layer separation provoked by external vortices or a change in angle-of-attack. An example is shown in **Figure 21**, which illustrates a simulation of separation induced by a moving external vortex; here a cigar-shaped eddy has formed in the boundary layer, which provokes an eruptive tongue of fluid. This is shown in two perspectives in **Figure 21**, where the vortex is outlined, as shown by a sequence of two-dimensional slices. At high Reynolds numbers, three-dimensional

separation typically occurs as a narrow eruptive plume that can only be effectively resolved using a full Lagrangian method of the type developed in this research.

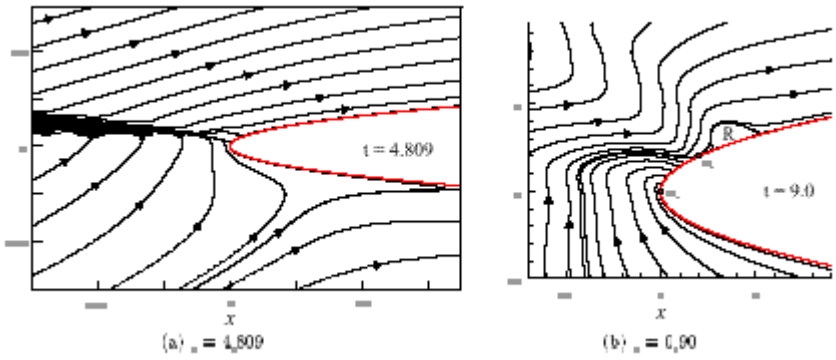

Figure 20 Streamlines near the leading nose: (a) solid blade (b) with suction .

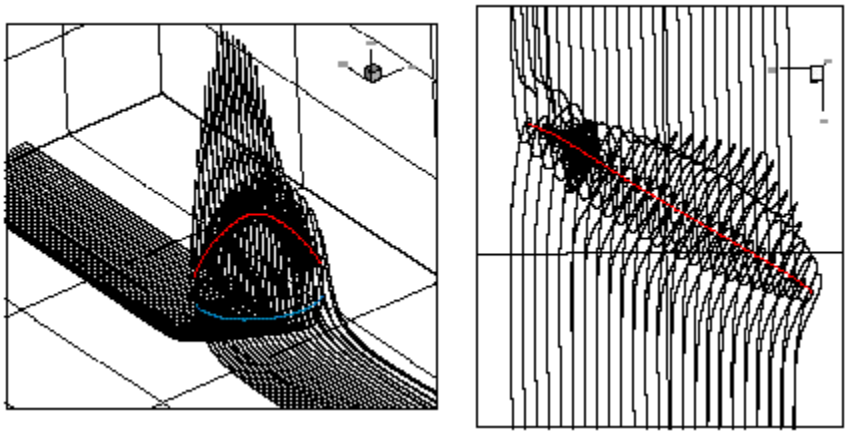

Figure 21 Instantaneous particle traced of a three-dimensional boundary layer separating due to cigar-shaped eddy near the surface

40060-EG "Low Maintenance, Low Energy Water Purification Flow through Capacitor Using Mesoscale Materials"

M. Andelman, Biosource, Inc.

The objective of flow through capacitor development with mesoscale materials is to provide the most energy and weight efficient desalination and water purification technology known to date, for use in truck portable water purification. The principals natural to flow through capacitor design have been identified, understood, incorporated into a model, and experimentally tested. These include use of inductors in energy recovery, hexagonal closed packing for materials design, and the "1/n" charging theory. The "1/n" theory takes advantage of the fact that a capacitor is not a constant voltage device. Charge absorbed during the initial low voltage stage should in theory be absorbed at a lower energy cost. This theory was experimentally proven, and makes use of the equations for charging a capacitor.

$$Q = CV = \sum_{i=1}^{i=n} CV_i, \qquad (1)$$

where Q represents the charge, C the capacitance, and V the voltage. The energy required to charge a capacitor up to V volts is given by:

$$\tfrac{1}{2}\left(\frac{1}{C}\right)Q^2 = \tfrac{1}{2}CV^2, \qquad (2)$$

and the energy to charge a capacitor n times to 1/n volts is then

$$\left(\tfrac{1}{2n}\right)CV^2. \qquad (3)$$

According to (1), a capacitor put through n charge/discharge cycles at 1/n Volts will absorb the same cumulative amount of charge as a capacitor charged up only once to V Volts. Dividing (3) by (2) shows that the energy required to absorb this charge will be reduced by a factor of 1/n. This was experimentally proven by measuring energy usage to purify ions as a function of voltage.

During the course of these experiments, the discovery was made that the ratio of ionic charge absorbed to electronic charge used is greater than unity, and that this ratio increases with concentration. It was postulated that this is due to Debye Huckle effects, which say that ionic charge is electrostatically shielded by clouds of counterions. This data is shown in **Figure 22**. It can be inferred from (2) that this is energetically favorable.

Material needs that are necessary to optimize energy usage were identified. These include linear capacitance with voltage, and with a high surface area to pore volume ratio. Pore volume in particular was identified as a cause of inefficiency, because purified water cannot ordinarily be removed from the pores. Aligned nanotubes were identified as the material of choice due to the fact that hexagonally closest packed cylinders have a surface area/volume ratio of 39/diameter. Experimental verification proved that nanotubes exhibit the required linear capacitance.

It was realized that use of inductors would be required for energy recovery. Experiments proved the concept at 54% energy recovery. It is theoretically possible to achieve close to 100%.

A breakthrough was made that expands the use of the capacitor and which will greatly reduce maintenance. Previously, metals plated onto the capacitor could only be recovered with a cleaning solution, such as an acid. Modifications were made in the capacitor design which allow reversible recovery of metals without added chemicals or cleaning solution.

In addition, it has been discovered that the flow through capacitor sterilizes microorganisms. This is significant, because technologies that remove total dissolved solids typically contribute microbes to the water. As a result of these findings, it will be possible to properly engineer materials, controls, and systems for energy efficient sea water desalination.

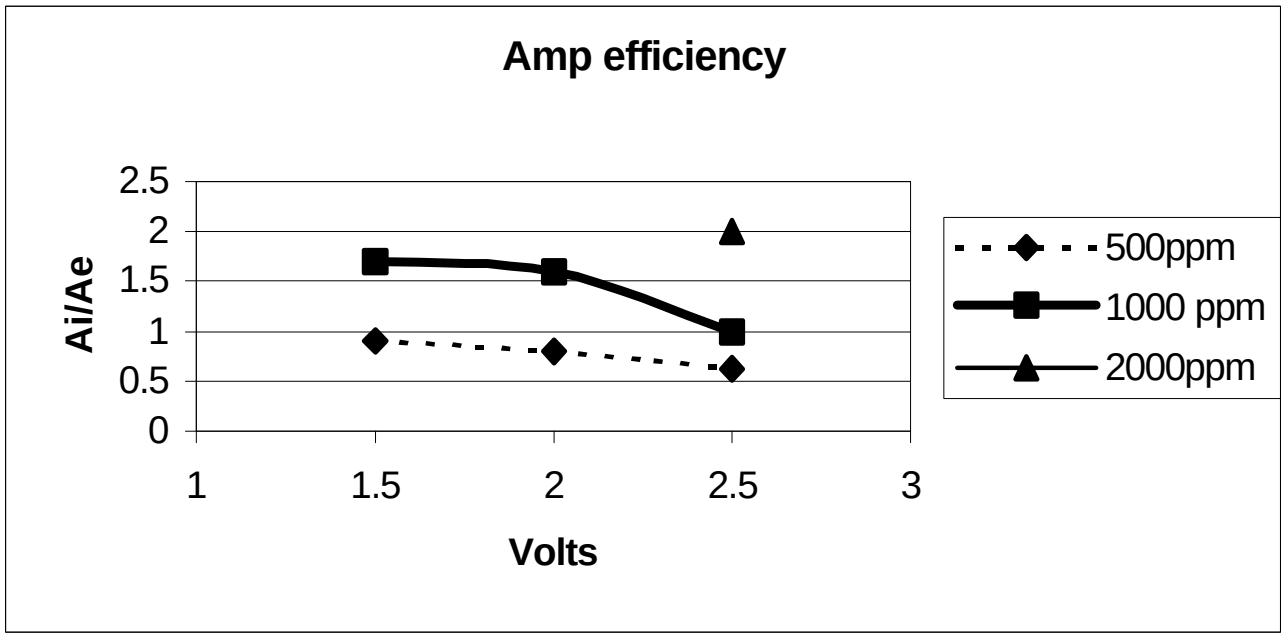

Figure 22 Instantaneous measurements of Coulombs/second ions absorbed = "Ai" (Ionic amps), versus Ae, Coulombs/second electrons used Ae (electronic Amps)

(Intentionally left blank)

PROPULSION & ENERGY CONVERSION

34839-EG "Intrinsic Burning Behavior and Flame Structure Diagnostics of Liquid Propellants"

Kenneth K. Kuo, The Pennsylvania State University

The goal of this research is to study the combustion behavior and flame structure of XM46, a hydroxylammonium nitrate (HAN)-based liquid propellant including triethanol ammonium nitrate (TEAN) as the fuel component and water as diluent. In authors' previous studies, XM46 exhibited unconventional characteristics, such as flashback behavior and non-linear burning rate curve exhibiting negative slope and plateau regions. In order to understand the mechanisms behind the observed phenomena, combustion tests were performed in high pressure testing chamber with liquid propellant strands formed inside quartz tubes or combustible straws. Thermocouples were inserted in the liquid propellant strands to measure the temperature distribution across the reaction zone and the gaseous flame.

The burning rate of XM46 was found to be a highly nonlinear function of pressure due to its dependency on multiple parameters, including: the pressure dependent latent heat of water (ΔHv), the enthalpy increase from initial to surface temperature, the conductive heat flux from the gas phase ($\dot{q}''_{cond}$), the net radiative heat flux absorbed at the surface ($\dot{q}''_{rad}$), and the heat release in the surface layer (Q_s), as shown by the following simplified energy flux balance equation across the gas/liquid interface:

$$r_p r_b \left(\int_{T_i}^{T_s} C_p dT + \Delta H_v \right) = r_p r_b Q_s + \dot{q}''_{cond} + \dot{q}''_{rad} \quad (1)$$

where ρ_p is the propellant density, r_b the burning rate, and C_p the averaged constant-pressure specific heat.

The effect of the latent heat of the water is demonstrated in **Figure 23**. It is seen that the latent heat of water decreases with increase in pressure, while the temperature of the dark-smoke zone increased more than 80 °C with increasing pressure in the range from 7 to 17.5 MPa. The heat released from decomposition of HAN and TEAN has to vaporize the water and to increase the sensible enthalpy of the combustion products. Due to the decrease of the latent heat of water with pressure, the sensible enthalpy of the products is higher at higher pressures, thus increasing the temperature of the product.

In order to examine the role of different fuel components, a HAN-based propellant using glycine instead of TEAN as the fuel component was also tested. As shown in **Figure 24**, the burning rate of HAN/glycine/water mixture is slower than XM46 by two orders of magnitude. A rapid increase of temperature to ~915 °C near the surface followed by the quick drop-off into a uniform gas-phase temperature of 300 °C was observed for test run at 7.2 MPa. Based upon the measured temperature-time trace of the combustion zone, it is evident that surface heat release process dominated the rate of combustion of HAN/glycine/water mixture. Due to the fast surface heat release process, the liquid phase was temporarily in superheated state. Later in the event, these intermediate products gasified, therefore the temperature dropped due to the energy required for the phase change from liquid to gas. It is interesting to note that the gas-

phase temperature after the surface region was very close to the boiling point of the water at testing conditions. This suggested the existence of an extended two-phase region in the post-reaction zone.

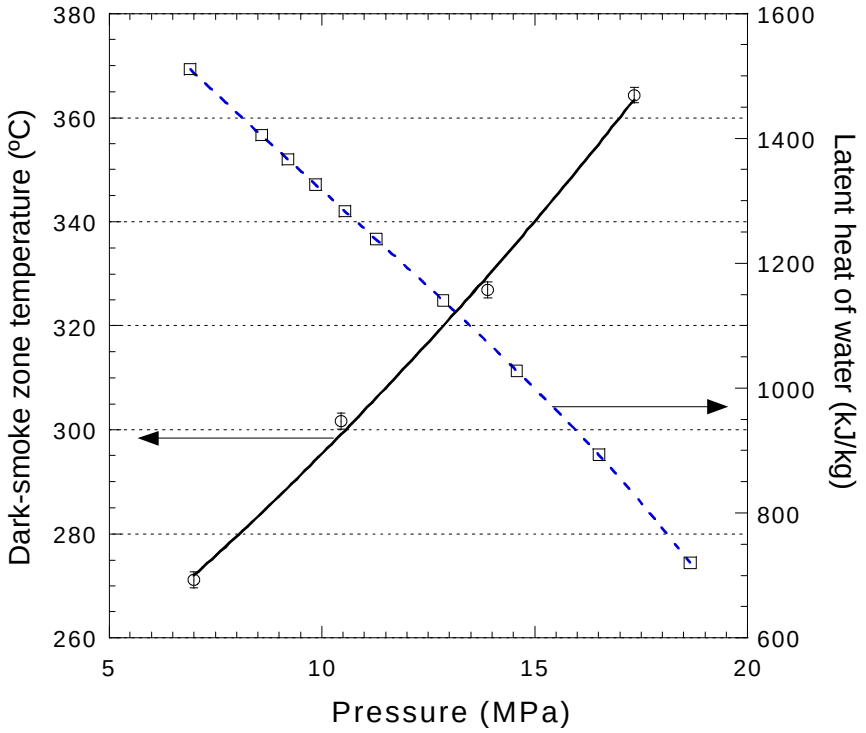

Figure 23 Variation of dark-smoke temperature and latent heat of water with pressure.

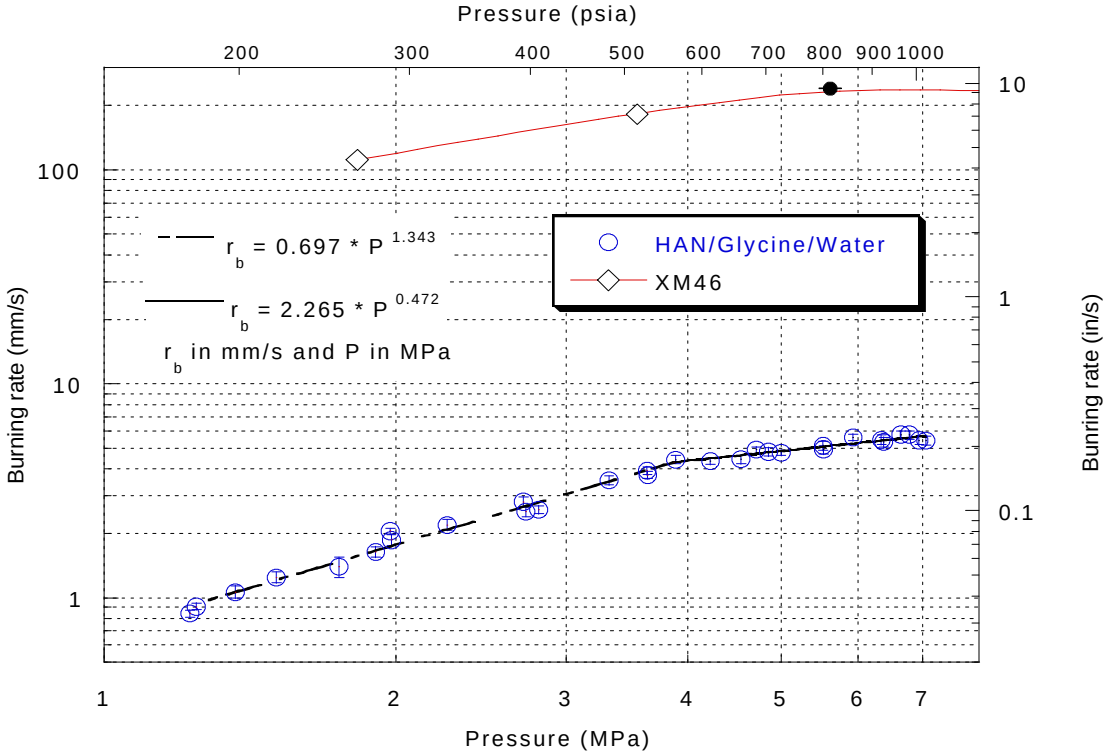

Figure 24 Burning rate comparison between XM46 and HAN/Glycine/Water mixture.

36353-EG "Fluorescent Diagnostics And Fundamental Approaches To Droplet, Spray, Engine, And Aerodynamic Behavior"

Lynn A. Melton, University of Texas at Dallas

Both UT-Dallas (UTD) and United Technologies Research Center (UTRC) have carried out experiments to investigate the shear field in liquid fuel sheets, ligaments and droplets by non-intrusive, optical techniques. The program at UTD emphasizes the development of fluorescent dopants whose fluorescence changes in response to shear within the liquid; these diagnostics should be appropriate for PLIF measurements. The program at UTRC utilizes birefringence, induced by liquid strain rate, on specially seeded fuels. Fringe patterns produced by interference of the light beams enable quantitative measures of the strain rate; these diagnostics should be appropriate for line-of-sight measurements. The data obtained with these shear diagnostics should provide information that is applicable to physics-based modeling efforts of primary atomization processes.

The search for shear sensitive fluorescent molecules has focussed on polymers labeled with fluorescent tags, specifically polyacrylic acid (PAA) with covalently attached pyrene moities. PAA molecules of molecular weight greater than 500,000 are sufficiently large that the modest shear fields available with the shear apparatus (1-1000 sec^{-1}) can induce detectable changes in the polymer conformation. Modest shifts in the pyrene excimer to monomer emission ratio have been observed in pyrene labeled PAA at shear rates of approximately 1000 sec^{-1}.

Shear-induced birefringence is under investigation at a tool for study of the stress/strain rate in spray/break up ligaments. A fluid (hexane) is seeded with optically anisotropic polymer molecules (polyisobutylene), and when the fluid is subjected to flow, ambient stresses orient and/or distort the molecules. The resulting anisotropy of the molecules will impart a bulk birefringence to the fluid. This shear-induced birefringence creates a dependence of index-of-refraction on the polarization orientation of transmitted light, and the effect may be detected using standard polarimetry techniques. UTRC has developed a modified polarimetry apparatus that is based on a 2-D flow cell and which allows time resolved images to be obtained.

The field of view included a region up to 2 nozzle-diameters on either side of the nozzle exit and up to 9 nozzle-diameters downstream. Birefringence was evident throughout this region, following the direction of the jet and maintaining its intensity throughout this region. This free jet should be more susceptible to comparison with analytical models. This comparison is underway and should lead to further understanding of how the observed birefringence corresponds to levels of stress in the flow. (**Figure 25**)

36401-EG "Chemical Kinetics and Aerodynamics of Ignition"

Chung K. Law, Princeton University

The goal of the present program is to investigate the coupled effects of convection, diffusion, chemical kinetics, and turbulence on ignition in a nonpremixed environment simulating those in Diesel engines. The counterflow configuration is used in this work where a cold fuel/inert mixture jet flows against a hot air jet. The temperature of the oxidizer jet is slowly increased until ignition

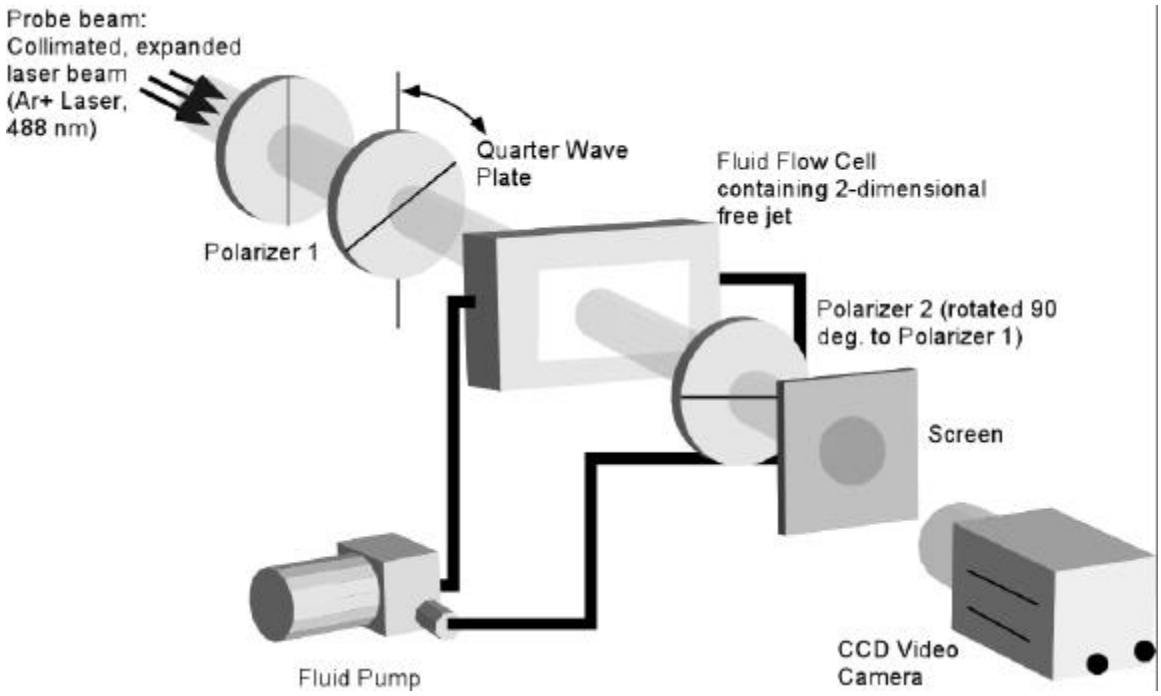

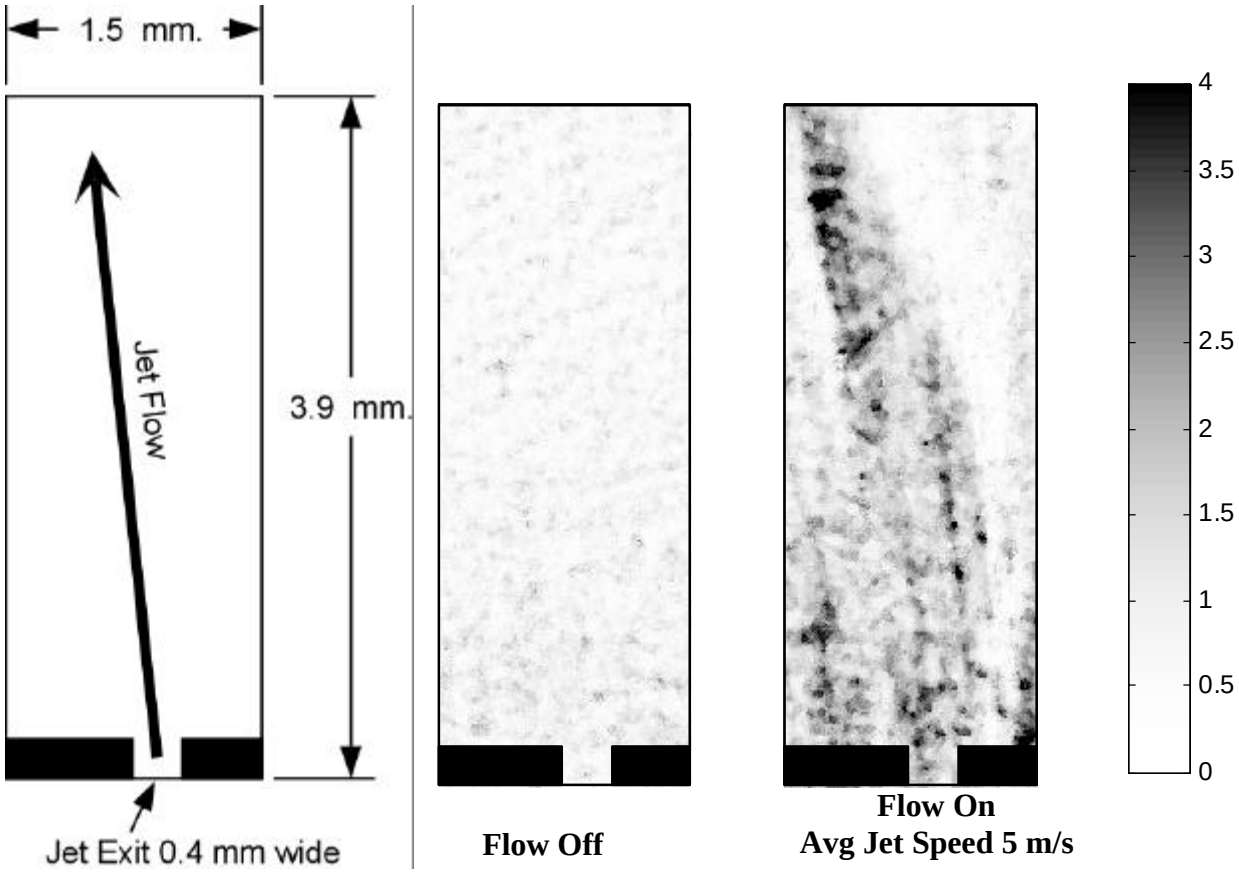

Flow Off **Flow On**
Avg Jet Speed 5 m/s

Figure 25

occurs. This configuration allows for the investigation of the fundamental processes involved in ignition in complex real world systems for improved control and performance. The following aspects were examined during the reporting period:

(1) The ignition of n-heptane and iso-octane in laminar flows was studied experimentally and computationally. The effect of increased strain rate was found to increase the ignition temperature while that of increased pressure was to decrease the ignition temperature. These trends are qualitatively similar to those found for other hydrocarbon fuels studied previously in this program. Evidence was found suggesting that low temperature chemistry does not play a significant role in non-premixed ignition. Calculations were performed with existing semi-empirical high temperature chemistry models and agree with the experiments qualitatively, but overpredict the ignition temperature by about 100K. The system was found to be very sensitive to the fuel diffusivity.

(2) The effect of fuel molecule size was investigated experimentally. The ignition temperature of methane, ethane, propane, n-butane, iso-butane, n-pentane, n-hexane, n-heptane, and iso-octane were measured under similar operating conditions. The results are shown in the figure where a non-monotonic trend can be observed. Fuel molecule structure is important and explains why methane and the branched fuels have significantly higher temperatures. In addition, larger fuels have a lower rate of diffusion, which may explain the increasing ignition temperature between some of the smaller molecules such as ethane and propane. For larger fuels, the effect of finite rate kinetics and the complex coupling between reaction and transport of the intermediate species cause the somewhat uniform ignition temperature.

(3) The turbulent flow field in the counterflow configuration was modeled using a quasi-one dimensional approach. Reasonable correspondence was found between the Reynolds stress model and experiments, but efforts are ongoing to improve the agreement. The results highlight the importance of predicting the mean velocity profile and knowing the turbulent length scale when calculating the evolution of turbulence in a stagnating flow.

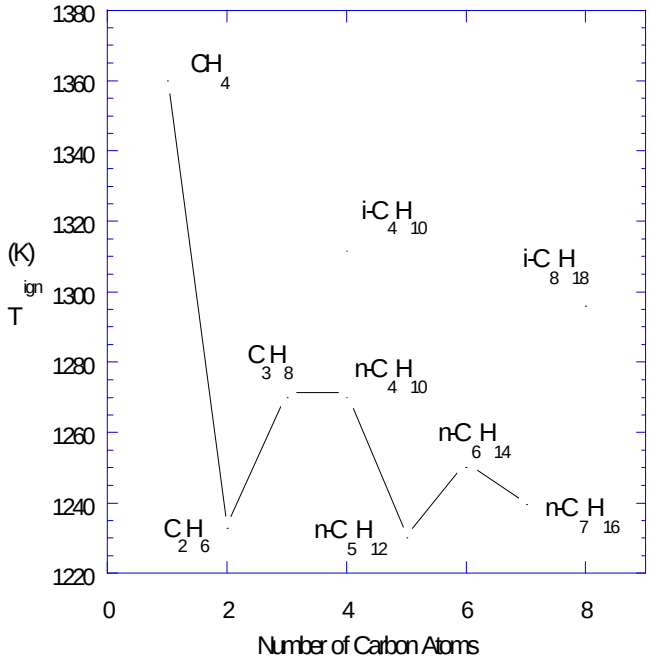

Figure 26

36406-EG "A Three-Dimensional Burnett Solver for Hypersonic Flow at High Altitudes"

Goang-Shin Liaw, Alabama A&M University

The objective of this research is to develop a CFD code to solve the three-dimensional Burnett equations for transitional aerodynamics. The complex, time-dependent, three-dimensional viscous transitional flow over an ellipsoid body with or without a block will be investigated. This will improve the understanding of the low-density hypersonic viscous flows and enable more accurate and confident design for hypersonic flight vehicle maneuvering at altitudes between 70 and 100 kilometers.

Three tasks were completed in 1999:

(1) A 3-D Burnett equations solver was developed. A paper entitled "Implementation of the Burnett Terms into the NPARC Code for Predicting the Low Density Flows" (AIAA paper 99-0746) was presented at the 37th AIAA Aerospace Sciences Meeting and Exhibit, January 11-14, 1999 in Reno, NV. Another paper entitled "Numerical Predictions of the Transitional Flow Over an Elliptic Cylinder by the Burnett Equations and the DSMC Method" (AIAA paper 99-3457) was presented at the 33rd AIAA Thermophysics Conference, June 28 - July 1, 1999 in Norfolk, VA. In addition, two abstracts, "A Modified NPARC code: the Burnett equations Solver for Near-Continuum Flow" and "Application of the Burnett equations to Flow Past a Blunt Body," were submitted to be presented at the 18th AIAA Applied Aerodynamics Conference.

(2) Code validations of the Burnett equations solver were conducted on a CRAY SV1 platform. Tests were conducted for the flows past an ellipsoid and a blunt body at high speeds. Comparisons of the temperature contours obtained by the Burnett equations and the Navier-Stokes equations are displayed in **Figure 27**.

(3) Parametric studies were conducted to obtain better understanding of the characteristics and stability of the Burnett equations. Through development and validation tests of the Burnett equations solver, it was found that:

   (a) The Burnett equations are only valid for Knudsen number less than 1.0, most likely much less than 1.0. None of the Burnett equations, the Augmented Burnett equations, or the BGK-Burnett equations can be used as the governing equations for the transitional flow regime at Knudsen number between 0.1 and 10;

   (b) Presently, the obtained Burnett solution is a perturbation solution of the Navier-Stokes equations. The Burnett equations can improve the accuracy of the Navier-Stokes solutions where the Navier-Stokes equations are still valid, but cannot be used when the Navier-Stokes equations have already failed; and

   (c) The Burnett equations, the Augmented Burnett equations, and the BGK-Burnett equations are sets of nonlinear partial differential equations. Their stability problem cannot be determined by the linear stability theory.

TEMPERATURE CONTOURS

NAVIER-STOKES SOLUTION

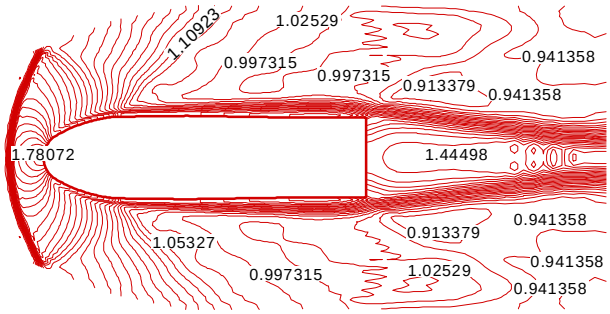

BURNETT SOLUTION

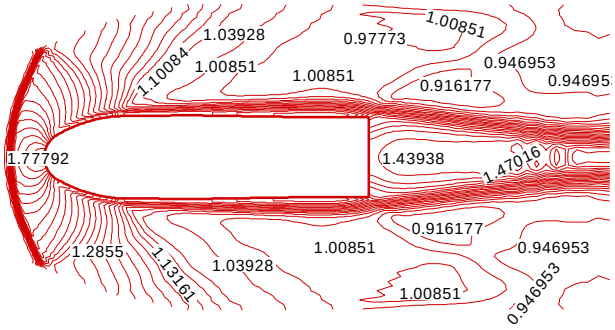

Figure 27 Comparisons of temperature contours obtained by the Burnett equations and Navier-Stokes equations for flow past a blunt body at M = 2.0, Re = 10000.

36750-EG "Shock Tube Studies of Ram Accelerator Phenomena"

Ronald K. Hanson, Stanford University

The objective of this research is to improve understanding of hypersonic, exothermic flows through the application of modern experimental methods and modeling work. The program has three coordinated elements: 1) Imaging and modeling of oblique detonations and shock-induced combustion in high-speed wedge flows. 2) Experimental investigations of fuel jets in supersonic combustion. 3) Measurements and modeling of ignition kinetics in defense-related fuel mixtures.

Oblique detonations, which occur in the limit of fast ignition behind an oblique shock wave, are a phenomenon of significant importance to future high-speed propulsion systems, including ram accelerators. OH PLIF and schlieren imaging have been employed to characterize the flow over the 40° (half-angle) wedge body, and piezo-electric pressure measurements on the wedge surface. The OH PLIF imaging system provides an instantaneous map of the OH distribution (and consequently, the flame front) in the flowfield. The schlieren image, acquired within 2 μs of the PLIF image, provides information on the shock and expansion waves in the flow. Experiments varying the gas mixture composition, pressure, and velocity to alter the ignition delay and energy release have been performed. In parallel, a custom inviscid flow, finite-rate chemistry CFD code for wedge and conical flows has been developed and tested, to validate the numerical model, improve understanding of the experimental results, and aid in future planning.

Hydrogen transverse jet injection into reacting and non-reacting supersonic flow has also been investigated, with a view toward improving understanding of scramjet mixing and flame-holding issues. OH PLIF visualization indicates the autoignition of a hydrogen jet in air cross-flow simulating flight Mach 10 conditions. OH fluorescence appears first in the recirculation region upstream of the jet and extends along the outer edge of the jet plume demarcating the boundary between the fuel and air. Schlieren images, using a new ultra-fast framing camera, reveal large-scale turbulent structures (which persist at least 20 jet diameters downstream of the injector site) and a complex shock wave structure (a bow shock, an upstream separation wave and a downstream reattachment shock). The results showed that the coherent structures tend to travel with velocities that are closer to the free-stream velocity in the far-field ($x/d > 10$). When the images are assembled as a movie, the pulsating nature of the upstream separation region and of the jet causing the bow shock to fluctuate is very apparent, though this unsteady behavior was not anticipated.

Ignition time measurements at high pressures have been made in a high-pressure shock tube facility, employing emission and laser absorption techniques. In particular, we have obtained ignition delay times of a wide range of CH_4/O_2 mixtures of interest to ARL at realistic pre-ignition temperatures (1040 - 1600 K) and pressures (40 - 260 atm). Prior to these studies, no data existed for the extreme, high-pressure conditions found in the ram accelerators. A 279-reaction kinetics mechanism was also developed to predict ram accelerator ignition delay times over this broad range of mixtures and conditions. Reduced kinetics

mechanisms for methane and hydrogen oxidation that faithfully reproduce the experimental ignition data have also been developed for use in ARL CFD codes. Ignition times of larger hydrocarbon fuels, including heptane, decane and JP-10 have also been measured and modeled using these techniques.

37211-EG "Basic and Applied Studies of the Ram Accelerator as a High Performance Launcher"

Adam Bruckner, University of Washington

The acceleration of a projectile in the ram accelerator tube is proportional to the fill pressure, cross-sectional area of the tube bore, and the energy per unit mass of the propellant. In previous work, accelerations of ~30,000 g and muzzle velocities of ~2.7 km/s have been demonstrated in the University of Washington 38-mm-bore ram accelerator using 70 gm projectiles in $CH_4/O_2/N_2/He/H_2$ propellants at fill pressures up to 50 atm. Current experimental efforts are exploring the feasibility of operation at propellant fill pressures up to 200 atm in order to realize a four-fold increase in acceleration. This improvement in performance would permit shortening the accelerator tube by the same ratio. In 1998 the UW ram accelerator facility was upgraded to enable experimentation at fill pressures up to 200 atm. The first 4 m of the test section were replaced with three new thick-walled tubes, in a 1 m-2 m-1 m configuration, designed for static pressure loads of 10,000 atm. A new propellant delivery system using high pressure mass flow rate controllers was installed, which has the capability to pressurize the test section to fill pressures greater than 200 atm from commercially available gas cylinders. Facility shakedown tests were performed at fill pressures of 75 atm and 100 atm, and the experimental results were found to be in good agreement with the theoretical performance predictions based on the Boltzmann equation of state.

Recent experiments have demonstrated that successful starting of the ram accelerator in $CH_4/O_2/N_2$ propellant at 150 atm fill pressure can be accomplished with projectiles having a maximum cross-sectional area that does not occlude the tube by more that 44%. Shown in **Figure 28** are the velocity-distance data from three experiments in which magnesium alloy projectiles were shot at 1.3 km/s entrance velocity into a 1-m-long stage filled with various $CH_4/O_2/N_2$ propellants at 150 atm. It can be seen that ram accelerator operation was initiated in the $3.3CH_4+2O_2+9.7N_2$ propellant; however, too much dilution with excess CH_4 and N_2 resulted in a wave fall-off, and too little dilution resulted in an unstart about midway into the test section. Although suitable for testing the starting characteristics of propellant mixtures and the effects of projectile geometry, the standard magnesium projectiles used in these experiments were found to be inadequate for operation over tube lengths exceeding 2 m. The next phase of the research program is to conduct a series of similar experiments with titanium alloy projectiles, in order to minimize the impact of aerodynamic heating arising from ram accelerator operation at fill pressures of 150 atm or greater.

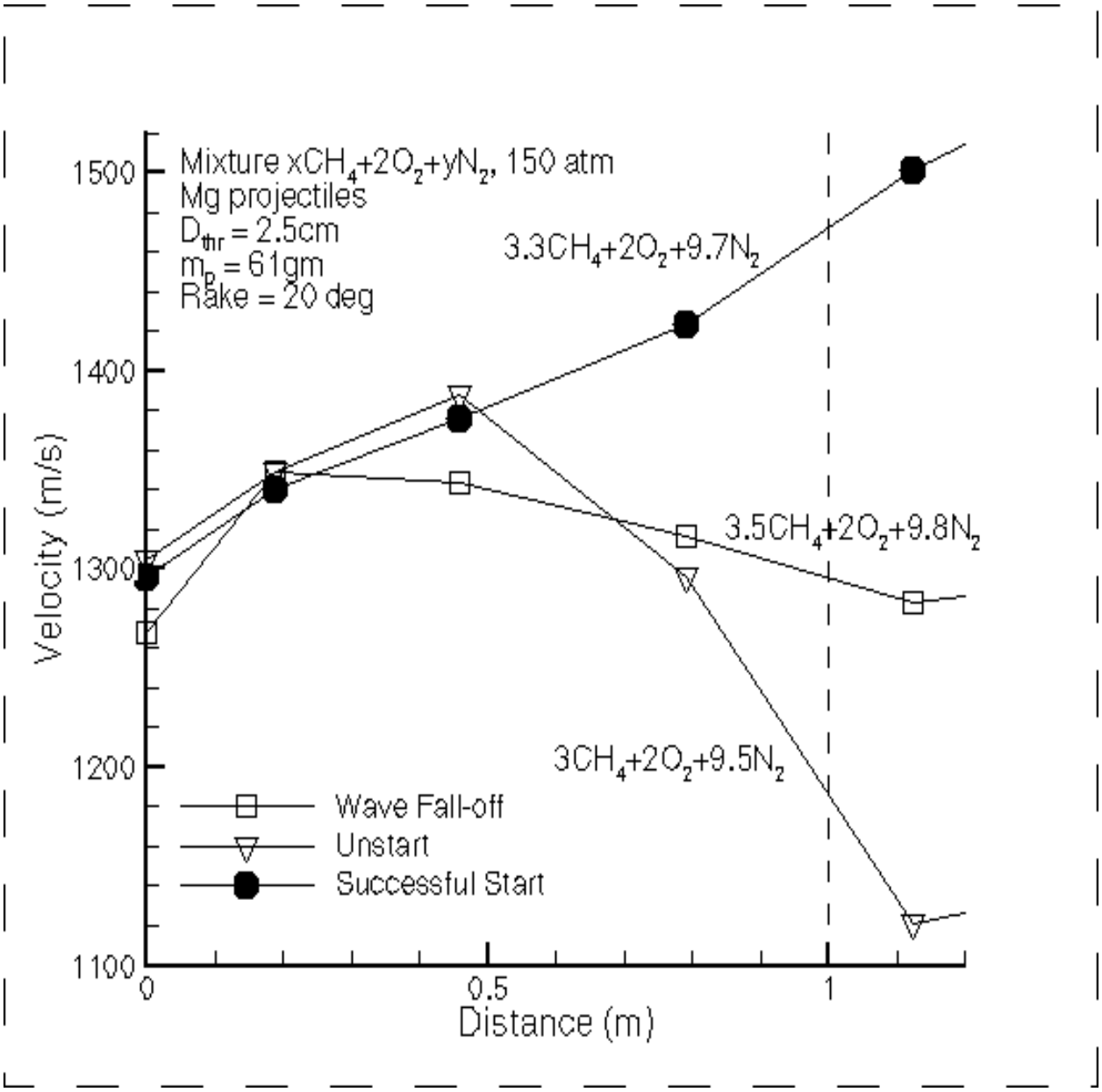

Figure 28 Velocity-distance data from three different ram accelerator experiments using a 1-m-long test stage of 150 atm propellant. The 4-finned magnesium alloy projectile had a 10^{o} conical nose, 2.5 cm diameter throat, 20^{o} rake angle fins with a sharp leading edge, and a 5.1 cm body length.

37304-EG "Modeling Diesel Engine Injector Flows"

S. D. Heister and G. A. Blaisdell, Purdue University

The objective of this research is to obtain a fundamental understanding of the injection flowfield of a high pressure diesel engine fuel injector.

Addressing diesel injector flows is quite challenging because the high injection pressures lead to substantial regions of oscillatory cavitation within the orifice passage. For this reason, a two-phase flow simulation is required. Recently, a new treatment has been developed we have formulated to reflect the dynamics of vapor bubbles in the context of an unsteady, viscous homogeneous fluid (a.k.a. pseudo-fluid) formulation. The methodology is valid for arbitrary void fractions, from pure vapor to pure liquid. Recent efforts have been aimed at understanding three-dimensional and turbulence effects in these flowfields. To this end, a K-Omega turbulence model has been incorporated in the current two-dimensional codes. The implementation has been validated against test data and other computations for a backward-facing step geometry and is at present being validated against cavitating flow experiments of Professor Collicott's research group here at Purdue.

A complex, 3-D calculation involving a mesh containing over 200,000 cells is depicted in the accompanying **Figure 29**. Here, the injection manifold imposes a crossflow (from left to right in the fig.) on the orifice inlet thereby creating the 3-D flowfield. The resulting streamline pattern, which reveals a complex vortex stretched over a portion of the orifice is shown in **Figure 29**. Cavitation regions and velocity exit conditions have also been characterized to aid the designer in understanding the influence of the crossflow on the subsequent flow exiting the orifice.

37555-EG "DI Diesel Performance and Emissions Models and High Power Density Diesel Engines"

A. M. Mellor, Vanderbilt University

Engineering models for DI Diesel power density and emissions of NO_x and soot were the original goals of the present research. Such models are semi-empirical and thus not computationally intensive. In this program they are used to gain insight, but these models can also be employed in engine simulation or CFD codes.

Figure 30 shows the result of an engineering model calculation. An older version of the engineering model for NO_x emissions is used in conjunction with a zero dimensional simulation for which measured cylinder pressure is known. In the graph, measured versus correlated emissions for four DI Diesel engines are shown to have excellent statistics. Direct prediction of the measurements by this version of the model leads to an overestimate by a factor of 2.4, which is removed for the correlation in the figure. Other model concepts have also been tested against the available data, and these comparisons allow model validation.

Another method of model validation was provided by engine tests in which pure NO was injected into the intake air of a 2.4L high speed DI Diesel engine. Results were analyzed via a stand-alone NO_x model based on the same two-zone representation of the DI Diesel spray plume, and mixing times in the stoichiometric contours of the spray

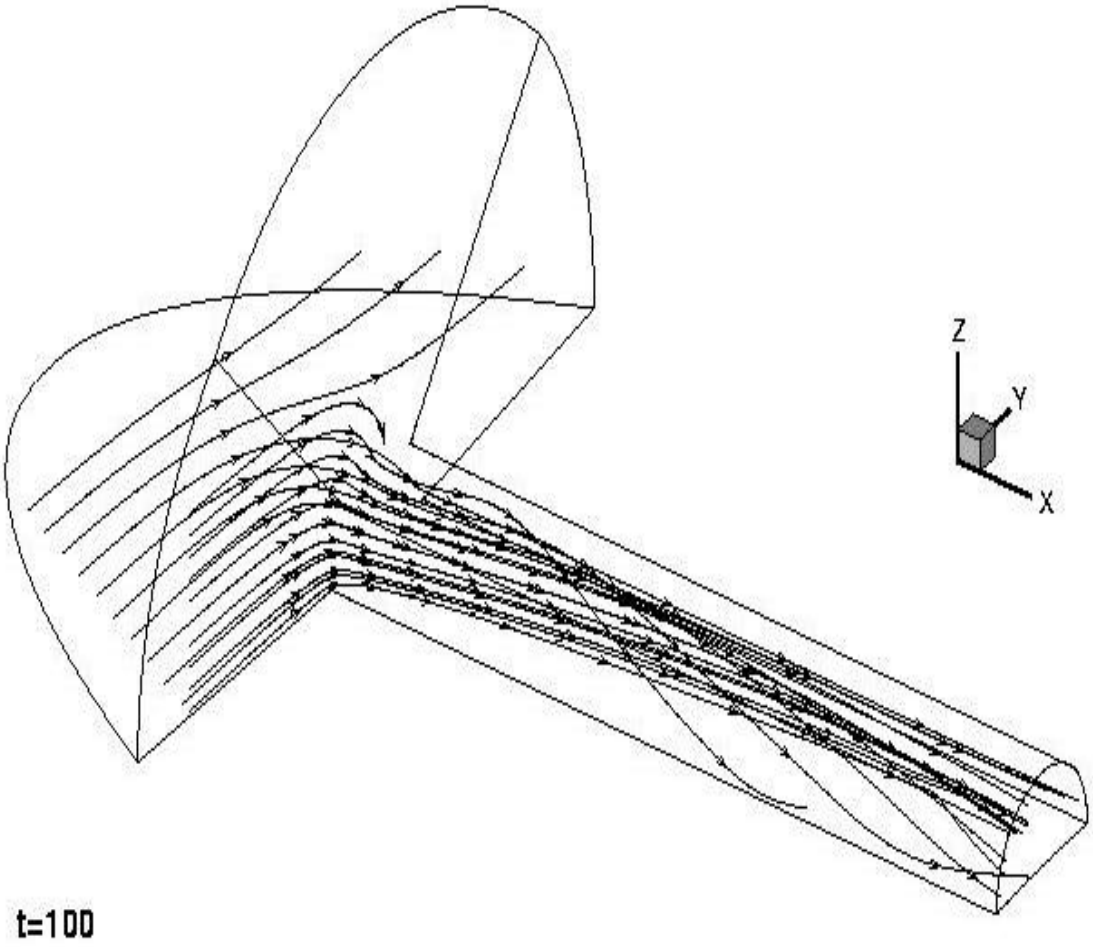

Figure 29 Instantaneous Streamline Pattern in a Diesel Engine Atomizer Design Subjected to a Crossflow. A Cavitation Region forms at the Upstream Portion of the Inlet Lip (not visible in this plot). Complex Vorticity Patterns are Convected to the Outflow Boundary Thereby Affecting Subsequent Spray Formation Processes.

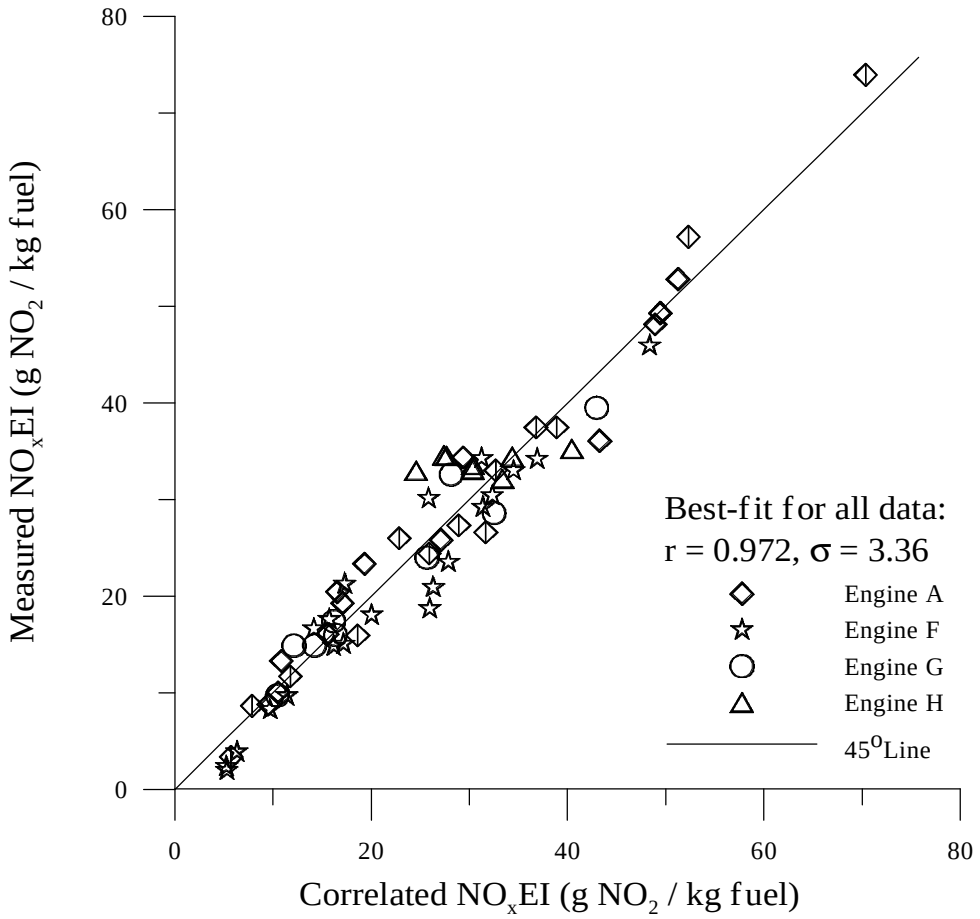

Figure 30. Correlated Engine-Out No_x Emissions Index

- Correlation of engine-out NO_x emissions using a two-zone flame model incorporated in a zero dimensional engine simulation code.
- Measured data are from 4 different DI Diesel engines ranging in size from 0.98 – 2.5 L/cyl.
- Operating conditions include significant variations of engine speed and load, SOC timing, EGR, and injection pressure.

plumes have been quantified for several different fuel injectors.

Development of a power density model is still in its preliminary stages. As a first step, measured engine brake mean effective pressure (BMEP) has been correlated with fundamental engine parameters using full load sweeps, speed sweeps, EGR variations, injection pressure variations, and various fuels, from two engines. Since BMEP is approximately proportional to NO_x emissions, the foundation for the power density model is established.

Analysis of the effect of alternative Diesel fuels on emissions is also underway using data taken on a 1.2L high speed DI Diesel operated with four fuels. A California Air Resources Board (CARB) fuel was used as baseline, and low sulfur/hydro-cracked (LSHC), Fischer-Tropsch, and LSHC blended with 15% dimethoxy methane fuels were also tested. Engineering models have been used to analyze these data in order to aid in explaining the experimental results.

Efforts to model soot emissions have been de-emphasized in order to address (1) the effects of advanced injectors (split injections, injection rate shaping) and (2) the homogeneous charge compression ignition (HCCI) engine as a propulsion system with low NO_x and soot emissions and perhaps high power density. Tests with advanced injectors and with an optically accessible HCCI engine are planned for summer 2000 at Ford in collaboration with the ARO program.

37699-EG "The Chemistry Controlling Ignition of Hydrocarbons and Their Mixtures at High Pressure"

N.P. Cernansky and D.L. Miller, Drexel University

This is the second year of an experimental program to investigate the chemistry controlling ignition of hydrocarbons and their mixtures at elevated pressures. The objective of this program is the development of kinetic and mechanistic information in the low and intermediate temperature regime (600-1000 K) over a range of pressures (up to 20 atm). Significant progress has been made in all facets of the program, with the most significant progress this year focusing around the oxidation of JP-8, identification of individual species using multi-component Fourier Transform Infrared (FT-IR) spectra, and the development of in situ (laser) techniques for the spectral separation of radicals from non-radical species using Magneto-Optic Rotation (MOR).

Continuing our work with industry standard fuels (ISF), JP-8 was oxidized in our Pressurized Flow Reactor (PFR) to identify the existence of a Negative Temperature Coefficient (NTC) region. Utilizing the CO reactivity mapping technique, a clear NTC behavior was observed for JP-8 at two different experimental conditions. The JP-8 experiment was conducted at conditions similar to previous ISF work; pressure of 8 atm, equivalence ratio of 0.3, nitrogen dilution of 75%, and residence time of 180 ms. During the controlled cool down experiment, a clear NTC behavior was observed (**Figure 31)**. The temperature where the reactivity peaked, referred to as the start of NTC, occurred at 700 K.

The second research area involved the development and testing of methods for the analysis of complex multi-component FT-IR spectra. Chemometrics offers a

statistical approach to species identification and concentration measurements. Two chemometric techniques, factor analysis and target testing, have been applied thus far. Factor analysis is a method by which the number of chemical species affecting the FT-IR absorption spectra of a multi-component mixture can be determined. Target testing is a chemometric method that tests whether the spectra of a single chemical species has affected the measured multi-component spectra. Utilizing our chemometric algorithms, neopentane PFR data was analyzed correctly determining both the proper number and identity of the major oxidation products.

We have been developing advanced laser diagnostics techniques for measuring radicals in flame environments. We have recently separated radical (paramagnetic) species from stable (non-paramagnetic) species in a flame environment. A Magneto-Optic Rotation (MOR) experiment was performed in an acetylene/air flame that was doped with Zn atoms (which are only weakly paramagnetic). A small nitrogen-pumped dye laser was used as the probe and scanned from 305 to 312 nm. The Zn line at 307.59 nm overwhelmed the 25 to 30 much weaker lines due to OH radical. A 4 kilogauss external magnetic field was applied axially with respect to the laser propagation direction to produce the MOR effect. With MOR, the strongly absorbing Zn atoms show a very weak line at 307.59 nm and the OH absorption was predominant (**Figure 32**). This technique will greatly improve our ability to detect the HO_2 radical at 1430 nm, which is a region congested with strong water, CO, and CO_2 lines.

Overall, the ongoing experimental studies are providing new diagnostic techniques and important information into the behavior of JP-8. These efforts are expected to culminate in a better understanding of hydrocarbon preignition chemistry for single and multi-component blends.

37730-EG "Effect of nitric oxide and other diluents on cold starting, combustion instability, and white smoke emissions in diesel engines"

N. A. Henein, Wayne State University

The primary objective of this research is reducing the cold starting problems in military and commercial diesel engines including hesitation, the emission of large amounts of unburned hydrocarbons in the form of white smoke, or the complete failure of the engine to start. Failure of the autoignition process is one of the main contributors to the cold starting problems.

Autoignition failure can be attributed to two factors. The first is the low compressed air temperature caused by the low ambient air temperatures, in addition to the high rates of heat losses to the cool engine walls. This results in long cranking periods, accumulation of the liquid fuel in the combustion chamber, and the emission of large amounts of fuel vapor when the engine fires. The second is the dilution of the charge by residual gases remaining from the previous firing cycle. This results in misfiring after the engine fires and accelerates. In both cases autoignition reactions are slow causing combustion to occur very late in the expansion stroke. There is a point in the expansion stroke beyond which combustion would fail. Consequently, there is an injection timing later than which combustion would fail.

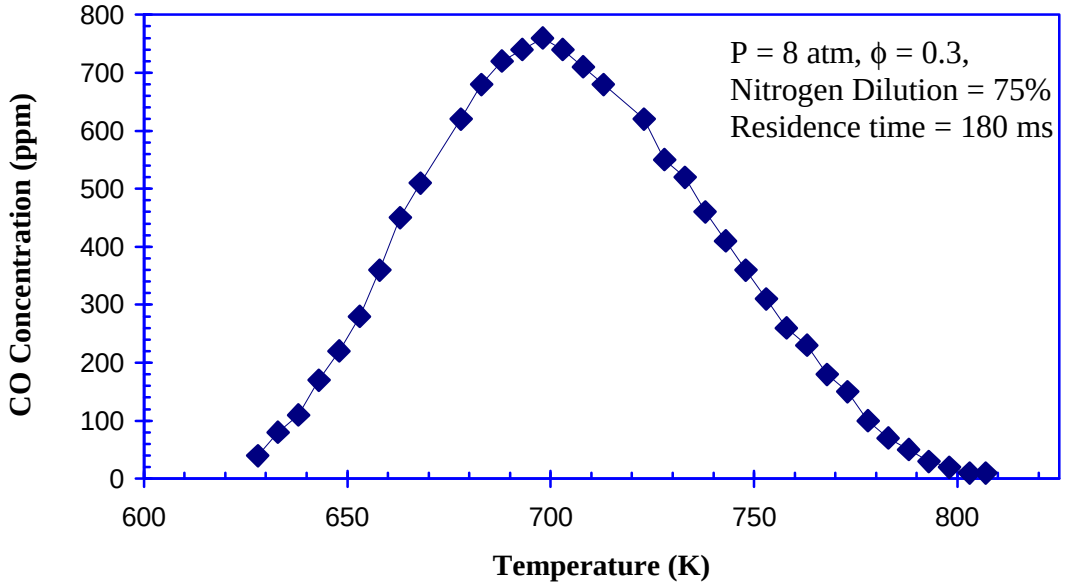

Figure 31 Controlled cool down PFR experiment for JP-8, showing a strong NTC behavior.

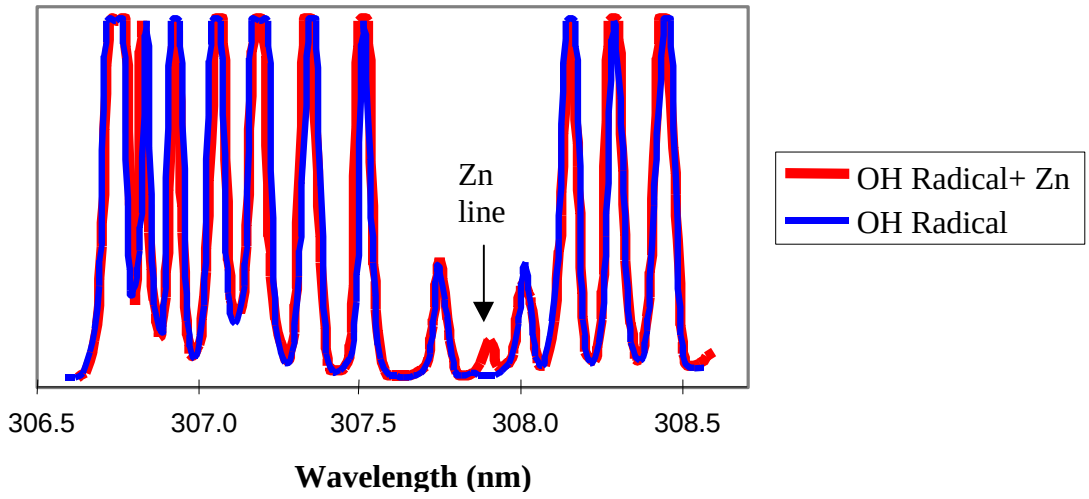

Figure 32 Effect of doping an acetylene/air flame with the strongly absorbing Zn atoms while using the Magneto-Optic Rotation technique.

The ignition delay (ID) is considered to be an indicator of the global rate of the autoignition reactions. Most of the previous investigations on ID_v were conducted in constant volume vessels where the gas temperature and pressure remain almost constant. This is not the case in engines because of the piston motion. During the compression stroke the piston motion adds energy to the reacting mixture. Meanwhile, during the expansion stroke the drop in the gas temperature slows down the autoignition and combustion reactions.

As a first step in this program, a new formulation is developed for the ID_e to account for the piston motion in engines. The formulation is derived theoretically by considering the ID_e to end when the chain carriers reach a critical concentration. In the experimental part of this program the ID_e is considered to end when a rise in the cylinder pressure due to combustion is detected. The model is applied to predict the boundary of the stable combustion zone. Experimental results showed a good agreement with the model predictions.

A 4-cylinder, direct injection, heavy-duty diesel engine was used in this investigation. The experiments were conducted in a cold room after the engine was soaked with its fuel tank and battery for more than eight hours before starting. The data was collected during the first few minutes of the starting process. The experiments covered a wide range of ambient temperatures, from 21^o C to -10^o C. The pressure history and injection events of all the four cylinders were measured during the starting transients. The model is applied to predict the boundary of the stable combustion zone. Experimental results showed a good agreement with the model predictions.

Tests are conducted on a single-cylinder, air-cooled, naturally aspirated, direct injection, diesel engine. The engine exhaust was modified to allow the introduction of EGR at different ratios. The engine was instrumented to measure the cylinder gas pressure, fuel line pressure, needle lift, air mass flow rate, intake and exhaust gas temperatures, intake and exhaust absolute pressures, crank-case pressure and instantaneous engine speed. The emissions were measured with a Horiba Gas Analyzer, a FFID for the measurement for the instantaneous cycle resolved unburned hydrocarbons, and a two channel fNO_x analyzer for the measurement of instantaneous cycle resolved concentrations of NO_x in both the exhaust and intake manifolds. The tests were conducted at steady state at no load, room temperature of 28 ^oC and different speeds. The EGR ratios were varied from 0 with a step equal to 5% up to 65% for engine speeds of 1500 and 2000 rpm, and up to 45% for 900 rpm. The data is analyzed to determine the ignition delay, the rate of heat release and its peak value and location, the premixed combustion fraction and its duration.

Work is in progress to determine the effect of EGR on the global rate of the autoignition reactions for DF-2, Amoco Premium fuel, and JP-8. The effect of EGR ratio on the overall activation energy of the different fuels will be determined. Such information is needed to develop engine controls to reduce the cranking periods of diesel engines at low ambient temperatures. Further more, electronic controls can be developed to reduce engine hesitation and improve engine startabilty with military as well as commercial fuels.

37761-EG "Improved Modeling of Drop Vaporization and Combustion in Diesel Sprays"

John Abraham, Purdue University

Understanding the penetration of the liquid fuel in a Diesel engine is important under cold start conditions. In the context of computational modeling of Diesel engines, the ability of spray models to predict this penetration is important when employing such models for Diesel cold-start conditions. Optimum engine deigns would avoid the impingement of the liquid on the piston and cylinder walls. The vaporization of the droplets is an important process that would affect this penetration. Hence, the need to predict the vaporization with adequate accuracy. Prior work by the P.I. had shown that simplified models for vaporization that are employed in multidimensional codes overpredict the vaporization rate by 25-50% relative to detailed models. This would imply that all other parameters being the same, the computed liquid penetration would be underpredicted. To further clarify these effects, comparisons of computed and measured liquid-phase penetration in Diesel sprays were carried out under a wide range of operating conditions including Diesel cold-start conditions. The measurements are those reported by Siebers (Liquid-Phase Fuel Penetration in Diesel Sprays, SAE Paper 980809). Figure 33 shows one example of such a comparison where computed and measured liquid penetration are shown as a function of ambient density for a fixed ambient temperature of 700 K. Significant differences may be observed. However, subsequent study of these differences have shown that the differences do not arise so much from inaccuracies in vaporization models as from numerical inaccuracies of the Lagrangian-Drop-Eulerian-Fluid approach.

Effect of ambient density on liquid penetration. d_0=0.246 mm, T_a=700 K, T_f=438 K, U_0=463 m/s

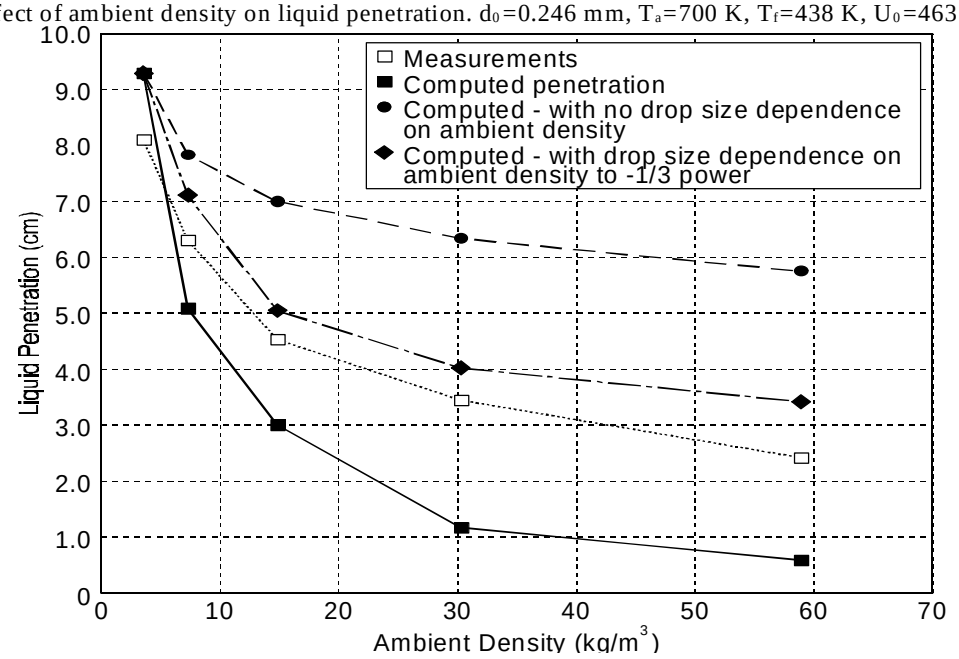

Figure 33 Improved Modeling of Drop Vaporization and Combustion in Diesel Sprays

37768-EG "Simultaneous Measurement of Species Concentration, Temperature, and Flow Velocity in a Flame"

R. Gupta, University of Arkansas

It has been demonstrated that the photo-thermal deflection spectroscopy (PTDS) has the potential of yielding three important combustion parameters, minority species concentration, temperature, and flow velocity simultaneously in a single laser pulse. The current work focuses on developing the technique fully for a simultaneous measurement of these three parameters. This work represents a radically different idea than that pursued by many other investigators, such as laser-induced fluorescence (LIF) or coherent anti-Stokes Raman spectroscopy (CARS).

The idea is simple. A pulsed dye laser beam (pump beam), tuned to the absorption frequency of the species to be measured, propagates through the medium. Absorption of the beam heats the irradiated region slightly, and thus, changes the refractive index of this region. The refractive index change is detected by the deflection of a weak probe beam passing through this region. The amplitude of the deflection signal is proportional to the concentration of the species. Moreover, the temporal evolution of the signal yields the value of the thermal diffusivity, which, in turn, yields the local temperature of the medium. If the probe beam is placed downstream from the pump beam, then the time-of-flight of the heat pulse from the pump to the probe beam yields the flow velocity of the medium. Thus, an analysis of the amplitude, width, and the arrival time of the PTDS signal can yield the species concentration, temperature, and flow velocity, respectively. The technique is suitable for in-situ measurements, is non-perturbing, has high temporal and spatial resolutions, and can yield absolute values.

The initial experiments have been performed in a cold flow (a room temperature jet of N_2 seeded with 0.5% NO_2 to make it absorb visible radiation), where all the parameters are precisely known. These experiments have given a valuable insight into effects that can lead to significant errors if not corrected for. For example, it has been found that the optical saturation of the signal (which can become significant even for quite-low laser powers) not only reduces the observed absorption coefficient, but also broadens the width of the PTDS signal. Therefore, unless the saturation effects are taken into account, one gets anomalously low values of species concentration and anomalously high values of the temperature. A very thorough investigation of these effects has been made. Another effect which leads to anomalous signal widths is the existence of velocity gradients. Schemes have been devised to minimize the effect of velocity gradients. Accurate values of the three parameters have been obtained in the cold flow.

PTDS signals from OH in a methane-air flame have been observed but an analysis of the signals has not yet been started.

38352-EG-CCE "Cold Climate Energy Program"

Arthur B. Lewis and Scott D. Stouffer-University of Dayton Research Institute

The objective of the program is to develop and demonstrate the use of thermal energy storage systems to improve the starting characteristics of Army Diesel

engines that are exposed to cold temperatures overnight. Improvement in cold starting allows the reduction or elimination of idling overnight, which reduces wasted fuel and the wear on the engine during idling.

The most critical factor in starting a Diesel engine is attaining sufficient cranking speed to allow autoignition of the fuel. Two of the most important factors governing the cranking speed at startup are the battery strength and oil viscosity. Both the oil viscosity and battery resistance increase as temperature drops, lowering the cranking speed and probability of starting.

A passive Energy Storage Device (ESD) thermal protection system was designed for the oil system that used Phase Change Materials (PCM) for thermal storage. The PCM-ESD system was designed to fit on the outside of the oil pan and oil filter. During operation of the engine, waste heat from the engine is conducted through the outside of the oil pan and oil filter and is stored in the PCM as it melts. After engine shutdown, the thermal energy stored in the PCM-ESD is released back to the oil system as the PCM freezes. Insulation was applied to the outside of the PCM to decrease the energy lost to the surroundings. Both conventional polyisocyanurate and Vacuum insulation (R- 40 per inch) were used as the outer layer of the PCM-ESD in separate tests.

The goal was to maintain the temperature of the oil above 0°C under exposure to ambient temperatures as low as –18°C overnight. To promote heat transfer from the PCM-ESD to the oil system, the hydrocarbon gel PCM was designed to freeze at 14°C.

A proof of concept thermal protection system using PCM-ESD was designed, built and applied to the oil pan and oil filter of a US Army M925 (5-ton) Truck equipped with a Cummins 6CTA8.3 Diesel engine. Finite Element thermal analysis was used to guide the development of the design of the PCM-ESD.

Experimental tests of the thermal protection system were conducted over the past winter with the truck exposed to the environment in Dayton Ohio. At the lowest average air temperature that the truck was exposed to overnight (-10°C) the oil temperature measured near the bottom of the pan was +10°C after 12 hours exposure to the cold. During all of the tests conducted the thermal protection system was able to maintain the temperature oil in both the oil filter and oil pan more than 12°C above ambient air temperatures for periods over 14 hrs. During cold start tests conducted after overnight exposure to the cold, the engine with the PCM-ESD applied to the oil system started faster and required much less time and cranking energy from the batteries to start than the baseline engine exposed to similar conditions.

While the primary interest in the PCM-ESD system is improved starting, a secondary benefit of the PCM-ESD system is the improved oil flow for lubrication of engine parts at startup, which may reduce engine wear. (See **Figure 34**)

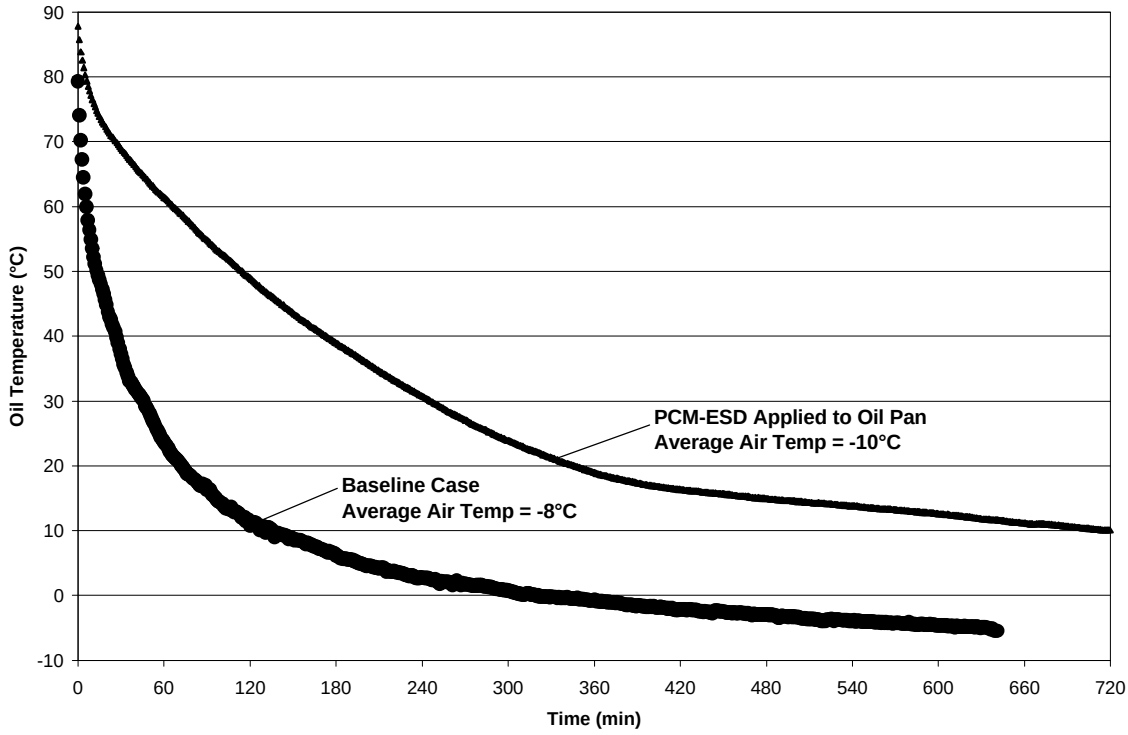

Figure 34 Comparison of the Oil Temperature Measured Near the Bottom of the Oil Pan With and Without the Phase Change Material-Energy Storage Device (PCM-ESD) Thermal Protection System. The PCM-ESD System Passively Maintains the Temperature of the Oil above the Ambient Air Temperature for Extended Time Periods after Shutoff Reducing or Eliminating Idling in Cold Weather.

38364-EG "Investigation of Preflame Reactions and Flame Propagation in Direct-injection Diesel Engines"

K. T. Rhee, Rutgers, The State University of New Jersey

Research conducted during the present reporting period was directed to characterization of spatial and temporal nature of preflame reactions (PFR) in the engine cylinder.

Fuel-air mixtures under compression in the engine cylinder undergo chemical reactions prior to being consumed via the propagation of flame fronts. In Diesel or compression ignition (CI) engines during the ignition delay period and mixtures in the end gas of spark ignition (SI) engines produce new intermediate species widely suggested as being the precursors of self-ignition. When such PFR are not properly controlled, engines undergo knock causing degraded behavior and increased emissions, which are affected by various engine design, operation and fuel factors.

Better understanding is needed of where and what chemical species are produced in the PFR period. In addition, determination is needed of the relationship of the PFR to the onset of self-ignition at the end of ignition delay period.

The Rutgers developed high-speed multi-spectra infrared (IR) imaging system (called Super Imaging System, SIS), enables visualization of PFR and combustion reactions in the cylinder. Briefly, in this system, four units of high-speed IR digital cameras are connected to a single optical train containing three spectral beam splitters so that four sets of images in respective spectral bands can be simultaneously captured at high rates. One of the spectral bands employed in the SIS is 3.42μm to exhibit images of progressively changing radiation produced by PFR species during the ignition delay period of a direct-injection Diesel or compression-ignition (DI-CI) engine.

Extensive experiments were conducted for several engine-fuel combinations, including: (a) DI-CI using D-2 fuel; (b) DI-CI with fumigation by propane; (c) DI-CI self-ignition as fueled by homogeneous propane-air mixtures. Also the same was performed for reactions in a spark-ignition (SI) engine when operated by different fuels, e.g. gasoline and propane in order to compare their results with the findings from DI-CI combustion.

Some of findings from this work are: (1) the fuel injected into the cylinder immediately starts chemical reactions in a CI-DI engine; (2) the PFR observed the early cycles, are comparable those under the warm condition; (3) images taken of at identical spatial and temporal locations (e.g. DI-CI reactions) are different in each spectral region, in some cases even the direction of reaction propagation; (4) the PFR species seem to be rapidly consumed as soon as high-temperature kinetics take over the in-cylinder reactions (i.e., after the onset of premixed combustion stage); (5) when the pilot injection was used to ignite the fumigated mixture, the initiation of combustion seemed to be delayed compared to when the pilot injection is used alone.

38736-EG "Lattice Boltzmann Simulation of MEMS Controlled Fuel Injectors"

Suresh Menon, Georgia Institute of Technology

Significant improvement in the performance of next generation gas turbine engines is currently being sought in order to develop lightweight, compact, fuel-efficient propulsion systems for helicopters and tanks for the Army After Next. Reduction in size and weight would go a long way towards reducing the logistic burden for rapidly deployable forces. Reduction in fuel consumption is considered especially critical since fuel is majority of the logistic burden. To reduce fuel consumption without sacrificing performance, advance, fuel efficient combustion systems are being developed. However, experimental investigation of such systems is complicated by the difficulty in obtaining non-intrusive access to the hot, turbulent reacting region in the combustor. Numerical tools that can predict the unsteady combustion processes may be able to provide a new, hitherto unavailable capability to investigate mixing enhancement process thereby, advancing the design process.

In this study, a numerical simulation model has been developed to evaluate the

performance of "smart" fuel injectors. Innovative techniques based on micro-electromechanical systems (MEMS) technology are being studied, whereby, the fuel jet is actively forced using synthetic *micro-jets* that are embedded *inside* the fuel injector nozzle. The numerical tool solves the Lattice Boltzmann equation (LBE) in order to simulate efficiently, flows generated by micro-scale MEMS devices (conventional finite-volume schemes are prohibitively expensive due to the very small time-step required to resolve these very micro-scale flows). Results clearly identify the various physical features of the synthetic jets, their sensitivity to various design parameters and the process of interaction between the MEMS jets and the fuel injector. Simulations have identified that the synthetic jet cavity dimensions, the forcing frequency and amplitude have to be properly optimized in order to achieve enhancement in mixing. Some design criteria were developed based on these simulations. It is also shown that forcing the fuel jet from inside the fuel nozzle can result in significant fuel-air mixing enhancement. This result provides first-principle proof of the potential benefit of using such "smart" injectors in future combustion systems in order to reduce fuel consumption without sacrificing required performance. Currently, this model is being extended to study combustion and heat release effects in order to demonstrate the superior capability of these "smart" fuel injection systems in actual engines. Optimization of the design of injectors will help in the development of next generation, fuel efficient, compact engines. The simulation tool can also be used to study the physics of many fundamental problems known to impact the design of engines: stability of lean premixed flames, active control of combustion instability, suppression of flame extinction, etc. (**See Figures 35 - 36 - and 37)**

38966-EG "Crossed-Plane Laser Imaging of Premixed Turbulent Combustion Processes"

F. C. Gouldin, Cornell University

The primary objective of this research is two fold: 1) develop a better understanding of the structure of premixed turbulent combustion processes and 2) provide a data based for validation of combustion models and design codes. Important applications of premixed turbulent combustion systems include spark ignition engines and natural gas fired gas turbines. SI engines are widely used in Army vehicles, while gas turbines can provide clean power for a variety of applications.

For a broad range of conditions appropriate to premixed combustion systems, chemical reactions are confined to thin sheets separating reactants from products -- flamelets -- that fluctuate in space and time. For this flamelet regime, the mean rate of chemical reaction per unit volume is equal to the product of the mean flamelet surface area per unit volume or surface density and of the mean rate of chemical reaction per unit flamelet surface area. Hence, the ability to predict both the topography of wrinkled flamelet surfaces and the local structure of the flamelet sheet is of great value. The structure is given by the distribution of temperature and composition within the thin sheet, which, to first approximation, is similar to the laminar flame structure of a Bunsen burner flame. To predict these features we must first measure them.

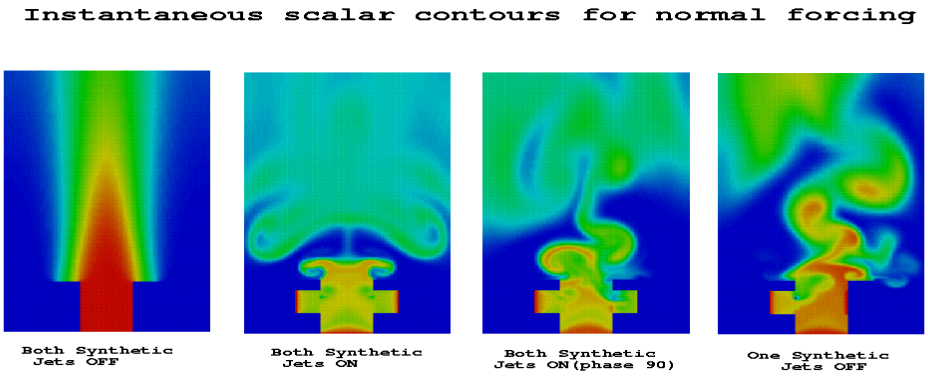

Figure 35. Effect of synthetic micro-jet on mixing enhancement. Red indicates pure fuel and blue indicates pure air. All intermediate colors indicate a mixed state. Clearly, significant enhancement occurs with synthetic jets (small cavities inside the fuel jet). By pulsing and/or turning one or both injectors, it is also possible to "vector" the fuel jet that allows another avenue for mixing control.

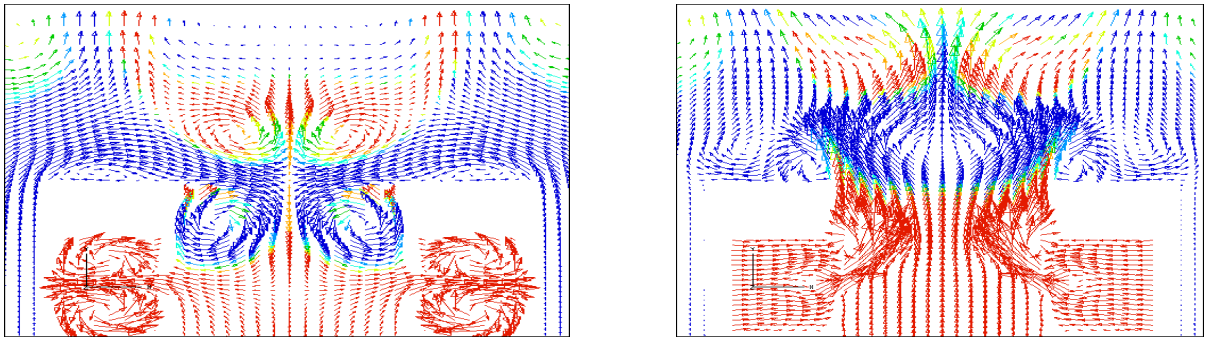

Figure 36. Velocity vector field in the vicinity of the synthetic jet during the forcing cycle. (**a**) Suction phase when the fuel (red vectors) is sucked into the cavity, (**b**) Blowing phase when the fuel is forced out. Blue vectors show the air that is entrained during the synthetic jet operation. This entrainment of air results in the increased mixing.

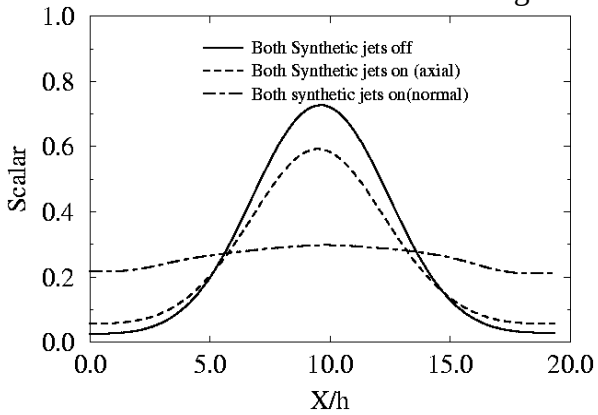

Figure 37: Fuel species mass fraction profiles across the fuel jet at a downstream axial location. Larger spread of the profile implies increased mixing. Thus, normal forcing (**Figures 35 and 36**) results in improved mixing than axial forcing at the fuel injector lip.

In previous work sponsored by ARO, a method, crossed-plane laser imaging, was developed for measuring an important aspect of the flamelet surface topography, namely, the instantaneous normal vector to the surface. The method has been validated in measurements at Cornell and been applied to study both laboratory flames and, at Sandia National Laboratory, SI engine flames. An important finding of this work is that the statistical distribution of measured surface normals in both systems can be represented by the same, one-parameter, functional form. An important consequence of this finding is that the flamelet surface density is a simple function of the parameter and the easily measured flamelet-surface crossing density -- the ensemble mean number of times flamelet elements cross a unit length of a line spanning the turbulent flame brush.

During 1999, analyses of data from the SI engine measurements were completed, and the results were presented at an SAE meeting. Statistical distribution data for flamelet normal and crossing density data were used to estimate the heat release rate within the cylinder, and the results were compared to estimates based on cylinder pressure measurements. The two estimates do not agree raising significant questions about current engine combustion models. Additional engine measurements are called for and under discussion with researchers at Sandia. Measurements on laboratory flames designed to test the hypothesis that certain fuel-air mixtures support flamelets that are unstable to perturbation and hence are more highly wrinkled by turbulence than other flames were made. The results, which will be reported this summer at the Combustion Symposium, show no evidence for this effect. Further measurements in different flame configurations and for different conditions are planned to further test the hypothesis.

In the future we will make additional normal measurements concentrating on different flame configurations, pursue SI engine measurements, and extend the crossed-plane imaging method to study flamelet structure via planar Rayleigh scattering for temperature.

39074-EG "Experimental Study of Plasma/Propellant Interactions"

Stefan T. Thynell and Thomas A. Litzinger, The Pennsylvania State University

Plasmas are being investigated as an ignition source for solid propellants, particularly for application in the electro-thermal-chemical gun propulsion system. Tests have shown the plasma to provide more reliable ignition and compensation for low temperature performance. As a result of these attractive benefits of ETC, investigations based on experiments and numerical simulations have been performed for the purpose of improving the understanding of the plasma/propellant interaction (PPI).

The overall objective of the experimental study is to gain insights from parametric studies that will contribute to the formulation of a more complete understanding of the various chemical and physical processes that occur during ignition by the plasma igniter. To meet the objectives of this research program, a new test rig has been designed and its construction has been completed. The test rig has several major components: 1) a plasma generation chamber, 2) a sample holder interfaced to a triple-quadrupole mass spectrometer, 3) an electrical circuit for discharging up to 10 kJ of electrical

energy in a few milliseconds, and 4) various diagnostic components such as pressure transducers, thermocouples, IR-detectors, heat flux gages, and high-speed film camera.

An initial check-out of the mass spectrometer was performed to detect any problems caused by the RF signal generated by the plasma discharge. The mass spectrometer was fully powered up prior to the plasma discharge, but the sampling probe was blocked-off during this initial test. No adverse effects of the RF signals were detected on the control signals nor on the output signals. Next, tests were performed by sampling from room air, rather than the plasma, and signals looked fine once again. At this point, a test was set-up with the sample probe placed in the first sampling port from the centerline of the plasma jet. An off-center position was selected as a precaution to avoid damage to the probe, because the pressure and temperatures at the stagnation point of the plasma jet were not well known. In this test, the mass spectrometer was set to detect a mass-to-charge ratio of 14, corresponding to CH_2, expected to be an major fragment from hydrocarbon species in the plasma. The results showed a peak of approximately 200 microseconds duration, matching the expected duration of the plasma discharge from the plasma power curves. After this, a series of tests were performed at different mass-to-charge ratios including 28, which could correspond to CO and C_2H_4. All tests yielded reasonable results. Finally, daughter mode tests were performed to confirm the presence of C_2H_4 in the sample. In this case a peak at a mass-to-charge ratio of 13 was used as a marker for C_2H_4. These tests were successful, but did point to the need to increase the A/D sampling rate to improve temporal resolution.

The design and optimization of the molecular beam sampling system is now complete, and the components are being ordered. One of the greatest challenges in the design is the limited space that is available within the test cell walls, which requires a very compact design. The perpendicular configuration of the quadrupole filters and the molecular beam will enhance sensitivity as well as decrease the total length of the system.

A Cordin 350 high-speed film camera has been acquired and utilized for capturing a portion of the plasma evolution. This camera utilizes 35 mm film and is capable of acquiring up to 35,000 pictures per second. Each image measures 7 by 10 mm on the film, and a total of 224 images can be acquired. The negative on the film is scanned directly into the computer using a Nikon 2000 35 mm film scanner. Simultaneous to acquiring pictures, the current is measured and voltage drop deduced across the plasma chamber. A diode captures the emergence of the plasma from the chamber and its evolution. Up to eight pressure transducers are utilized to capture the pressure at equally spaced locations along a flat surface.

At the bottom of **Figure 38** is shown the various configurations that have been utilized. The left configuration yields data on the plasma evolution itself and will be useful for Dr. Nusca of ARL and his modeling effort, as well as sampling using the mass spectrometer. However, in this configuration, a significant amount of the hot plasma never reaches the opposing surface as can be seen in the image above the sample configuration. Due to its rapid

Figure 38. From left to right, the second image from Test 90, 92, and 124 is shown. The image is acquired about 50±17 μs from the first emergence of the plasma. Below are given the various sample configurations for comparison purposes with respective images. A polyethylene capillary was used.

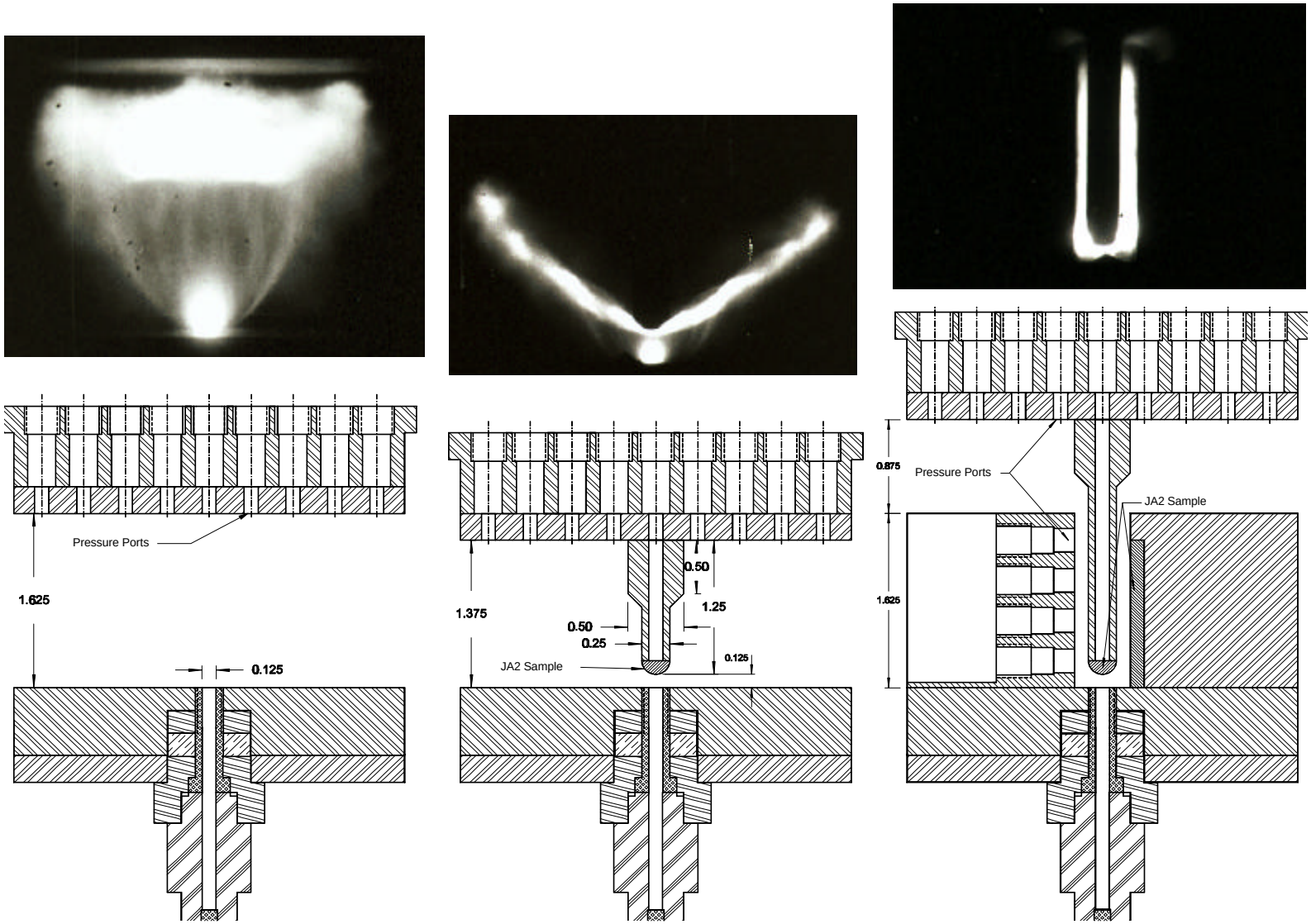

radial expansion, the plasma simply pushes and compresses the air which effectively shields the surface where the transducers and propellant sample are located. Since the shutter speed is only about 0.9 μs and the plasma travels at about 1,200 m/s, the image is somewhat fuzzy.

To yield configurations in which the plasma interacts with the plasma, two other configurations have been designed and utilized. In the middle portion of **Figure 38**, the propellant sample is located about 3 mm from the plasma port. This configuration essentially represents flow of a plasma across a cylinder. As seen in the image above the configuration, the plasma is deflected significantly in the radial direction. Strongly luminous zones are seen several inches away from the plasma port. Since the JA2 propellant is eroded significantly, it is possible that these luminous zones are caused by mixing and reactions with the surrounding air. Experiments with a brass sample have also been conducted, but no images were obtained for reasons that are unclear; these experiments will be repeated. The inert brass sample eroded significantly, however.

To yield plasma flow in a flat channel, a third configuration was designed and utilized and shown to the right in **Figure 38**. In this case, a additional piece of JA2 sample was embedded on one of the flat walls and pressure transducers installed on the opposite wall. The image above the configuration shows slightly more emission from the right channel, suggesting that the eroded propellant from the cylindrical piece of propellant sample reacts/interacts with the embedded JA2 sample. The JA2 sample embedded in the right wall showed very limited surface ablation, however.

In any of the experiments conducted so far, a sustained ignition and burning of the propellant sample has not been obtained. That is, self-sustained burning of the propellant sample was not achieved after complete discharge of the electrical energy in the capacitors. For the two configurations with significant erosion of the sample, which occurs for the sample subjected to direct plasma impingement, (see center configuration in **Figure 38),** it is likely that the plasma flow in the latter portion of the event extinguishes the flame. That is, the flow is too strong yet too weak to sustain pyrolysis, and blows away a flame that might be present. This effect can be mitigated by adding recirculation zones. In addition, the recovered samples shows evidence of a discoloration and/or surface erosion.

39092-EG-SB2 "Diesel Engine Efficiency Improvements Through Closed Loop Air-Fuel Ratio Optimization"

Kresimir Gebert, BKM, Inc.

The project objective is to demonstrate closed loop air fuel ratio control (AFR) of a diesel engine using cylinder pressure ratio method. Ultimate goal is to develop technology to enable engine efficiency and emission optimization using boost air pressure as a control variable.

A hydraulically driven supercharger and boost-air bypass valve are additional air-management hardware components used to increase and decrease AFR from the baseline setting. Engine cycle simulation and CFD (KIVA) are used to optimize engine-supercharge-turbocharger

match and better understand the effect of combustion stoichiometry on engine performance and emission.

During 1999, the following tasks were accomplished:

a. The quality of in-cylinder pressure signal from the fiber optic sensor, built into the injector, was thoroughly evaluated for the purpose of the closed loop AFR control. As a result, the optical sensor was replaced with a standard piezoelectric unit and moved from the injector to the cylinder head for the remainder of project.

b. The algorithm and software for open and closed loop air fuel ratio control, based on cylinder pressure ratio method were developed and electronic control hardware (LMM - Lambda - Management Module) was designed, developed and tested. A hydraulically driven super-charger was selected, matched to the engine and bench tested and new components of engine air management hardware (hydraulic super-charger and intake-air electronic by-pass valve) were installed on a heavy duty, turbo-charged, inter-cooled diesel engine (Caterpillar C12). Testing is in progress.

Preliminary test results show consistent increase of engine thermal efficiency with increasing AFR. However, at some test points, a gain from improved combustion is offset by parasitic loss of driving supercharger hydraulic system. Future research will focus on control algorithm and software refinements.

39509-EG "Nonlinear Distortion and Disintegration of Conical Liquid Sheets at High Pressure"

William A. Sirignano, University of California, Irvine

Our current research effort has focused on theoretical and numerical analyses of the nonlinear distortion and break-up of liquid films generated by injection through annular slit-nozzles or swirl-atomizers. As for the previous analysis of planar sheets, the approach was based on a reduction of the problem-dimensionality by considering thin films only. Linear analysis of the dimensionally reduced problem (e.g., with respect to wave properties on annular and conical sheets) and numerical prediction of nonlinearly distorting sheets modulated at the nozzle exit provides greater insight into the nonlinear dynamics and break-up process of thin sheets or films than can be currently expected by higher-dimensional, multi-purpose, two-phase models. The prescribed analyses were primarily directed towards a better understanding of the primary atomization process, which significantly influences the subsequent spray formation and the resulting spray characteristics.

Three-dimensional temporal and spatial nonlinear wave distortions of the planar sheet were analyzed by the reduced-dimension approach. Symmetric dilational distortions and antisymmetric sinuous distortions were identified. When wavelengths in both streamwise and lateral direction were comparable, some interesting exchange of energy between modes was identified. The formation of droplet arrays was predicted. In the non-swirling annular case, again, the nonlinear temporal and spatial, dilational and sinuous modes were predicted and analyzed by the reduced-dimension

approach. In the axisymmetric geometry, some important couplings between dilational and sinuous oscillations appeared to lower order in amplitude than found for the planar geometry. Sufficiently strong swirl caused the formation of a conical sheet with subsequent thinning of the sheet as it flowed. In all configurations, the first point of stream disintegration was predicted over a range Weber numbers and modulating frequency. Preliminary results have been obtained for assymmetric nonlinear wave distortions on a conical liquid sheet. These result from the modulations of all three-velocity components on the swirling sheet. A spiraling or "corkscrewing" instability has been predicted.

In a first effort to analyze the combined effect of capillary and aerodynamic forces on the sheet distortion and disintegration process, the analysis of inviscid planar two dimensionally distorting sheets, considered in an earlier study, has been extended to include the effect of gas-phase inertia by using a discrete boundary-element method to model the co-flowing potential gas streams surrounding the liquid film. Coupling between gas and liquid streams occurs through pressure forces at the phase interfaces and included the solution of the unsteady Bernoulli equation on the gas side along the interface. The prescribed method allows the study of sheet or film distortion and rupture under the influence of complex surrounding gas-flow fields, such as those encountered in practical fuel atomization and injection systems. These techniques will be extended to the conical configuration.

39758-EG "Sub- and Super-Critical Evaporation and Combustion of a Moving Droplet"

George Gogos, University of Nebraska-Lincoln

A comprehensive computational study of fuel droplet evaporation and combustion in sub- and super-critical ambient conditions under forced convection is being conducted. The aim is to provide basic understanding and prediction of evaporation and combustion of moving droplets at elevated pressures. Results obtained are of great interest for major industrial applications (such as diesel engines, high-output combustors for aircraft jet engines and liquid-fueled rocket engines).

Two aspects of droplet evaporation/ combustion have been studied during the past 12-month period. First, an experimentally validated model for a moving spherical droplet that undergoes evaporation has been developed. The model is used to predict evaporation constants and droplet lifetimes over a wide range of ambient pressures. Future work will allow for droplet deformation, which becomes important due to reduction in surface tension at elevated pressures. Second, a low pressure experimentally validated model for a moving spherical droplet that undergoes combustion has been developed. This model employs a one-step overall reaction and is used to predict extinction velocities for different size droplets. In future work, semi-detailed chemical kinetics will be incorporated in the present model.

Results presented in **Figure 39** were calculated for a moving n-heptane droplet evaporating within a nitrogen environment. The initial diameter is 100 μm and the initial temperature is 300 K.

Figure 39a shows the droplet average evaporation constant as a function of ambient pressure for different initial droplet velocities. Here, the droplet average evaporation constant is defined as the average evaporation constant when the dimensionless droplet diameter squared is less than 0.5. The average evaporation constant increases almost linearly with ambient pressure. At an ambient pressure which is a few times the thermodynamic critical pressure of the fuel, the slope of the average evaporation constant changes sharply, leading to a weak linear variation with further increase in the ambient pressure. With increasing initial droplet velocity, the above change in slope occurs at higher ambient pressures. Simulations with initial velocities of 5.0 m/s were obtained for ambient pressures smaller than 4 MPa. For higher pressures the criterion for droplet sphericity is not valid and droplet deformation needs to be considered. The velocities considered in Fig. 1a are relatively small compared to actual velocities in a typical spray. It can then be concluded that in an actual spray, especially at elevated pressures, droplets experience significant deformation that can not be neglected. The decrease in surface tension with increasing ambient pressure leads to significant droplet deformation. **Figure 39b** shows the droplet lifetime as a function of ambient reduced pressure for four different initial droplet velocities. The droplet lifetime decreases with increasing ambient pressure or increasing initial droplet velocity.

Results are presented in **Figure 40** for extinction velocities for n-heptane droplets burning in air at room temperature and a pressure of 1 atm. Droplet diameter (d) is varied to determine its effect on extinction velocity ($U_{\infty,e}$). Spalding (1953) and Agoston et al. (1957) conducted porous sphere experiments employing kerosene and n-butyl alcohol, respectively. Both studies show that the extinction velocity varies linearly with diameter. The present numerical model (solid line) predicts this linear dependence for approximately d > 2 mm. Large activation temperature asymptotics by Wu et al. (1982) also predict this linear dependence. The magnitudes of the measured extinction velocities by Spalding and Agoston et al., however, differ from the present model predictions possibly because the fuels are different. Buoyancy effects are negligible for the size of porous spheres employed by Spalding and Agoston et al. due to the small Richardson number (~ 0.05). Gollahalli and Brzustowski (1975) employed the same fuel (n-heptane) as in the present simulations. The buoyancy-induced flow in their experiment aids the forced convection flow. Fig. 2 shows that the extinction velocity corrected for the presence of natural convection lies very close to the numerical prediction for the same fuel. In addition, Fig. 2 shows that for diameters in the range of 180 μm – 1000 μm, the present numerical model predicts that the extinction velocity exhibits a nonlinear dependence. Extrapolating the linear curve predicted for larger droplets may provide an erroneous value for extinction velocities of droplets of, say, 100 μm, which are encountered in a typical spray.

39886-EG "Chemical-Kinetic Characterization of Autoignition and Combustion of Diesel and JP-8"

K. Seshadri, University of California, San Diego

The principal objective of the research is to obtain a fundamental understanding of the physical and chemical mechanisms

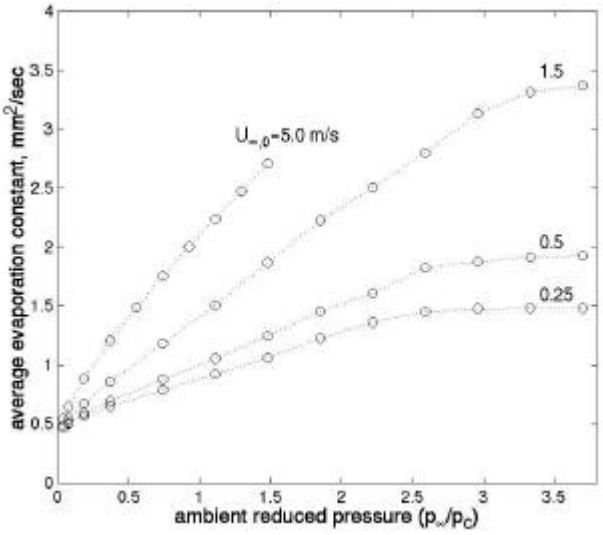

Figure 39a Average evaporation constant with ambient pressure for different initial droplet velocities (p_c =2.74 MPa).

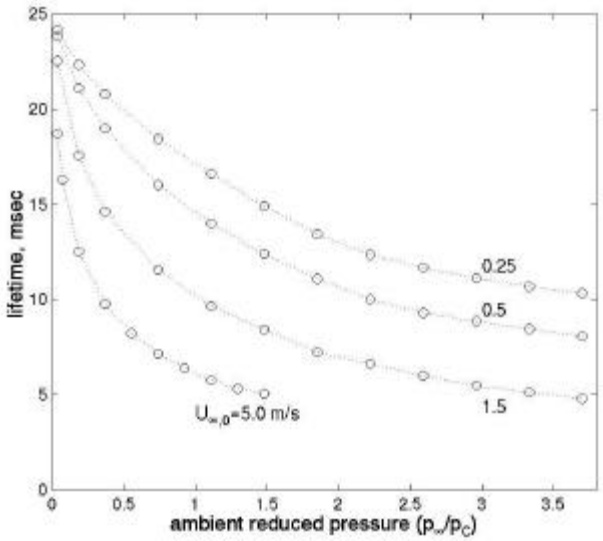

Figure 39b Droplet lifetime with ambient pressure for different initial droplet velocities (p_c =2.74 MPa).

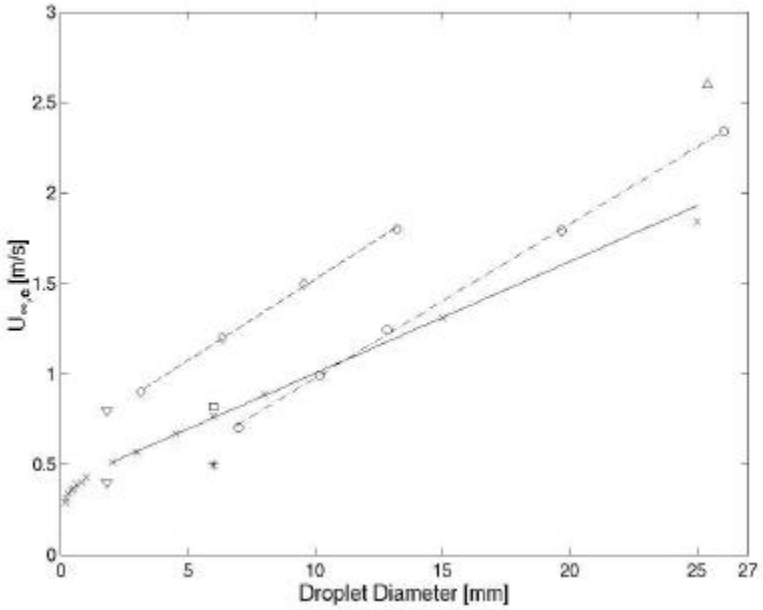

Figure 40 Extinction velocity vs. droplet diameter: (x) - numerical predictions for n-heptane under zero-gravity ($T_¥$= 300 K and $p_¥$= 1 atm). Experimental data under normal-gravity for various fuels in air at "room" temperature and atmospheric pressure; (o) - kerosene (Spalding, 1953), (♀) - n-butyl alcohol (Agoston et al., 1952), (*) - n-heptane (Gollahalli and Brzustowski, 1975), ( ) - previous point corrected for natural convection, (∇) - gasoline (Agafonova et al. 1960, lower: aiding natural convection, upper: opposing natural convection), (Δ) - n-heptane (Gore et al., 1990)

of autoignition and combustion of diesel and JP-8 in non-premixed systems. The knowledge gained from this research can be used to compute the dynamics of the combustion process in engines. To compute the dynamics of combustion, it is necessary to have an improved understanding of chemical-kinetic mechanisms of autoignition and combustion of diesel and JP-8. These fuels are made up of numerous different hydrocarbon compounds. Detailed chemical-kinetic mechanisms describing autoignition and combustion of a number of these hydrocarbon compounds are not available. Therefore, simulated diesel and simulated JP-8 each preferably made up of three hydrocarbon compounds will be developed. The hydrocarbon compounds in the simulated fuels will be chosen from *n*-heptane, *n*-dodecane, cyclohexane, methylchexane, toluene, and ethylbenzene and 1-methylnaphthalene.

Experimental, numerical, and analytical studies are in progress. Experiments were carried out in the counterflow configuration. In this configuration, two counterflowing streams flow toward a stagnation plane. One stream comprises fuel and the other oxygen. A burner was built to carry out experiments on autoignition using prevaporized liquid fuels. The fuels tested were *n*-heptane, *n*-decane, JP-10, and toluene. Experimental data obtained were the velocities and temperatures of counterflowing streams at autoignition. The strain rates, which are a measure of the characteristic residence times, at autoignition were calculated using the measured velocities of the counterflowing streams.

A detailed study was performed to elucidate the mechanisms of extinction and autoignition of *n*-heptane in strained laminar flows under non-premixed conditions. A previously developed detailed mechanism made up of 2540 reversible elementary reactions among 557 species was the starting point for the study. An intermediate mechanism made up of 1282 reversible elementary reactions among 282 species and a short mechanism made up of 770 reversible elementary reactions among 160 species were assembled from this detailed mechanism. Ignition delay times in an isochoric homogeneous reactor calculated using the intermediate and the short mechanism were found to agree well with those calculated using the detailed mechanism. The intermediate and the short mechanism were used to calculate extinction and autoignition of *n*-heptane in strained laminar flows. The results were found to agree well with experiments. Sensitivity analyses were carried out to evaluate the influence of various elementary reactions on autoignition. At all values of the strain rate investigated here, high temperature chemical processes were found to control auto-ignition. In general, the influence of low temperature chemistry was found to increase with decreasing strain. A key finding of the present study is that strain has more influence on low temperature chemistry than the temperature of the reactants**.**

40513-EG-SB1 "Planar Image Particle Analyzer For Whole Field Spray Applications"

Cecil F. Hess, MetroLaser, Inc.

The objective of this work is to develop a whole-field measurement technique that is capable of simultaneously sizing multiple transparent droplets on a plane from scattered light features that are

independent of laser beam intensity and obscuration. Light scattered by reflection and refraction from droplets immersed in a laser sheet will be recorded with digital holography and subsequently analyzed to produce the droplet size distribution as a function of position anywhere and everywhere on the sheet. One of the major challenges is transitioning from optical holography to digital holography. The small size of the CCD and large pixel size limit the size of the measurement region and the smallest measurable particle.

The technique is called Planar Image Particle Analyzer (PIPA). The general configuration of PIPA is given in **Figure 41**. A laser sheet illuminates the particles and their scattered light (object beam) and is collected by a receiver of finite f-number (f/#) placed at a collection angle θ. A beamsplitter mixes the reference beam with the object beam on the hologram.

Each particle will scatter a fringe pattern that results from the interference of the refracted and reflected light. The number of fringes corresponding to each particle is given by:

$$\#\text{fringes} = \frac{R_E L'}{f\#\, l}, \quad (1)$$

where $R_E L'$ represents the separation between the refraction and reflection spots of each droplet. This is related to the droplet diameter by simple trigonometric relationships. Note that the number of fringes anywhere in the reconstruction is only a function of the receiver f/# and the separation between the refraction and reflection spots from which the droplet size is obtained.

Phase I research at the time this synopsis was written (three months into the program) has consisted of the following major elements:

a. Numerical analysis of PIPA using optical holography and digital holography.

b. Design and construction of optical holography breadboard**.**

c. Photographic and holographic spray droplet data acquisition and analysis

d. Identification of digital holography strategies and their compatibility with the convolution theorem.

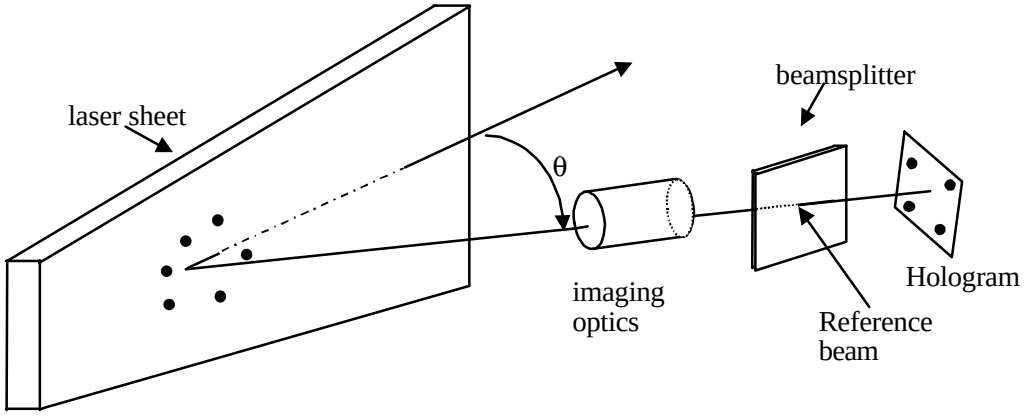

Figure 41 Schematic of PIPA

41116-EG "Large Eddy Simulations Of Supercritical Multicomponent Mixing Layers"

Josette Bellan, Jet Propulsion Laboratory

The objective of this study is the fundamental understanding of fuel disintegration and mixing in a supercritical environment (relative to the fuel) in order to determine parameter regimes advantageous to mixing. The approach is based on developing a model of a supercritical, turbulent jet mixing with surrounding fluid. The method is one that combines the modeling of supercritical fluids with a systematic development based on the Large Eddy Simulation (LES) approach. This systematic development includes a consistent protocol based upon Direct Numerical Simulations (DNS) for developing a Subgrid Scale Model (SGS) appropriate to supercritical fluids, rather than choosing in an ad hoc manner an existing SGS model developed under assumptions inconsistent with supercritical fluid behavior. This SGS model will be used in the LES of a supercritical turbulent jet.

The first step in this effort consists in the development of a DNS and associated code for a supercritical shear layer. The shear layer is chosen as the simplest configuration from which one may obtain results that will establish, through DNS, a framework for understanding mixing of supercritical fluids at small scales. Since the turbulent behavior at the Kolmogorov scales is universal (i.e. geometric-configuration independent), once this behavior is determined (e.g. in a shear layer geometric configuration), it can be utilized to model a variety of geometric configurations (for the same fluids) having the same physics. Since the interest of AFOSR is in hydrocarbons, the chosen shear layer is that of heptane (lower stream) in nitrogen.

The model of supercritical behavior is based upon fluctuation theory (Keizer, 1987). The advantage of this theory is that it inherently accounts for non-equilibrium processes and naturally leads to the most general fluid equations by relating the partial molar fluxes and the heat flux to thermodynamic quantities. Thus, Soret and Dufour effects (which are potentially important at supercritical conditions) are taken into account from first principles through the transport matrix where they complement the traditional Fick's mass diffusion and Fourier thermal diffusion terms. Results from the recent supercritical simulations of Harstad and Bellan, 2000, using heptane drops in nitrogen have been validated with the microgravity data of Nomura, 1996, within an average of 15%, thereby showing that the fluid model is correct. It is precisely this model that is here adapted to the shear layer configuration. However, there are specific issues that must be considered in the DNS of a three-dimensional (3D) shear layer that were not relevant to the drop model:

(a) In contrast to the drop study, the treatment of the transport coefficients cannot be exact in the context of DNS since the Reynolds number, *Re*, would be far too large to make the computations feasible. Since it is required that the Batchelor scales (the smallest scales associated with scalar mixing, $h_B \sim h_K / Sc$ where h_K is the Kolmogorov scale and *Sc* is the Schmidt number) be resolved, this dictates the maximum *Sc* which can be used in the particular calculation. For example, for heptane/nitrogen, *Sc* is too large for any domain size if heptane has a liquid-like density. The strategy is then to calculate these numbers based upon the

observations that the viscosity is primarily a function of *T*, whereas *Sc* and *Pr* are primarily functions of the mass fractions, and to find approximate fits for these quantities in the range of parametric interest.

(b) It is here unpractical to use the very accurate and computationally efficient non-ideal EOS's employed in Harstad and Bellan, 2000, because these might still be too computationally intensive when performing 3D simulations. Instead, we used the Peng-Robinson EOS based on pure species reference states accurate to better than 1% relative error (on pure reference states) through comparisons with highly accurate EOS's (Harstad et al., 1997) over the range of variables used in this study.

Results were first obtained for a 2D shear layer in order to study an issue of general interest which is the identity and value of the thermal diffusion coefficient appearing in the Soret and Dufour contributions to the molar and heat flux. The results showed that indeed the model is sensitive to both the identity and value of the thermal diffusion factors. In fact, combined with the effect of the mass diffusion factor (a quantity calculated entirely from the EOS), constant positive large BK thermal diffusion factors retard diffusional mixing; whereas constant moderate IK factors tend to promote mixing. Constant positive BK thermal diffusion factors also tend to maintain density gradients, with resulting greater shear and vorticity. These conclusions about IK and BK thermal diffusion factors are species pair dependent, and therefore are not universal, pointing out to the difficulties associated with the lack of thermal diffusion factor values for most species.

Results from the 3D shear layer showed that the density stratification is stabilizing the layer and preventing it from achieving the transitional regime at a non-dimensional time at which a transitional state had been reached by a layer whose lower stream was initially laden with drops. This lack of transition is due both to the initial strong density stratification and to the formation of regions of strong density gradient magnitude both in the braid and in between the braid plane. In fact, a density interface is very effective at damping turbulent eddies, being qualitatively similar to a rigid flat plate. The appearance and geometry of these regions of high density gradient magnitude is intriguing because it corresponds to the wispy threads of fluid emanating from a supercritical nitrogen jet in gaseous nitrogen as observed by Chehroudi et al., 1999. These features do not exist at subcritical conditions either in the experiment or in atmospheric air DNS simulations, indicating that they may be specific to the supercritical situation.

(Intentionally left blank)

SOLID MECHANICS

34432-EG "Layering Concepts for Wave Shaping and Lateral Distribution of Stresses During Impact Loading"

J. L. Ding, Y. M. Gupta, and Josh Robbins, Washington State University

The main thrust of this research program is to demonstrate a potential new approach to enhance the survivability of an armor system. The basic concept is to employ a high wave speed layer to rapidly spread (μs time scales) the impact load and thus reduce the damage imparted to the armor system. In particular, the potential use of thick diamond films for lateral distribution of stresses is an important element of the research effort.

To explore the layering concept, we first used idealized numerical simulations to demonstrate the feasibility of load spreading and wave shaping by layered structures. After the proof of concept, we then devised a measure, based on normalized dissipative energy density (NDE), to quantitatively characterize load spreading. Using this measure, we were able to gain considerable insight regarding the mechanisms governing load spreading and the behavior of layered structures to impacts. In addition, we also developed a new energy approach to correlate load spreading with penetration and to study the time dependence of the penetration process. Some qualitative experiments have also been initiated.

The current year's effort focused on the study of the effects of layer fracture and interfacial failure on load spreading and project defeat and the possible correlation between load spreading and penetration. The numerical code used was EPIC. Representative examples are shown in **Figures 42 and 43**. **Figure 42** shows the effect of layer fracture on the NDE distribution in targets layered with SiC of various thicknesses. **Figure 43** shows the time dependence of the penetration process as indicated by the histories of the dissipative energy of the projectile and layer energy fraction (normalized with respect to the total energy imparted to the target).

Significant results obtained from the current research efforts are:

- Effective load spreading requires high wave speed to spread the load rapidly and high impedance and strength to transmit the load from the layer to the substrate effectively.
- To defeat the projectile, the strength and fracture resistance of the layer appears to be the dominant factor. Effective load spreading, which requires both strength and high wave speed, plays more significant role in enhancing the integrity of the target. Since projectile can penetrate only if it can move away the target material ahead of it, increased integrity also leads to enhanced penetration resistance. However, the extent of load spreading on overall penetration resistance remains to be investigated.
- Under ideal condition, i.e. no layer fracture or interfacial failure, a single thick high wave speed layered target has the best load spreading and projectile defeat capability. Because of the high strength and stiffness of the layer, more impact energy is dissipated

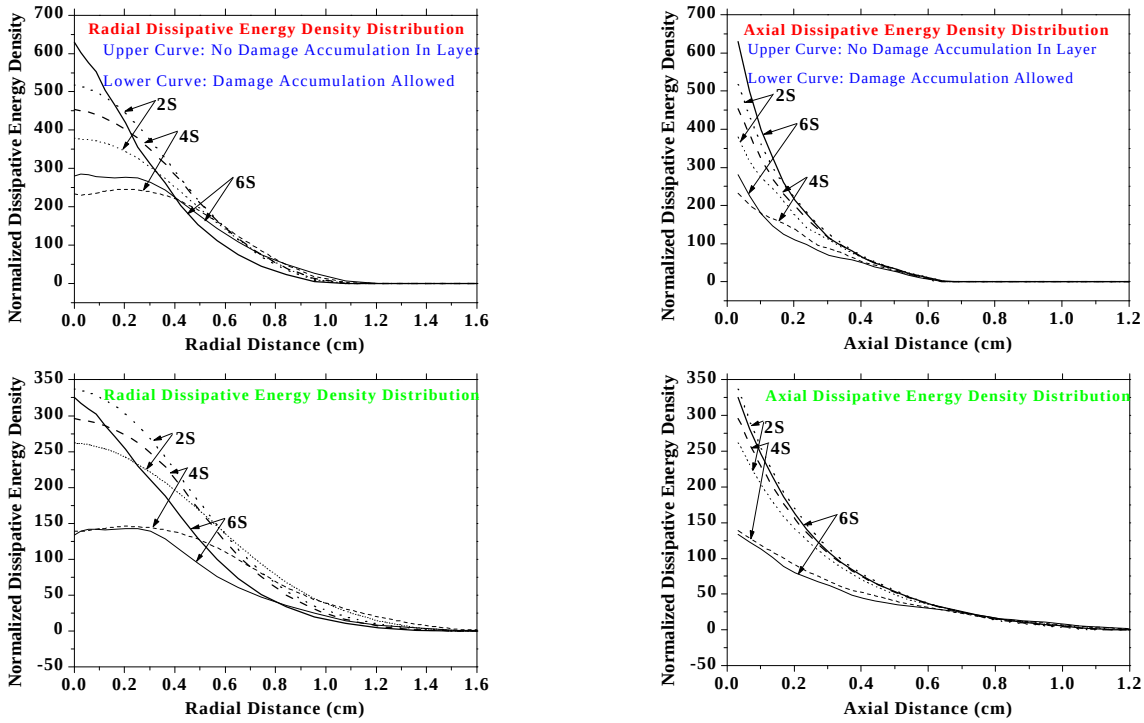

Figure 42: Effect of layer thickness and fracture on NDE distributions for an aluminum substrate layered with SiC of various thickness (2S: 2mm; 4S: 4mm; 6S: 6mm). The shock front is at 1cm and 2 cm into the substrate for the top and bottom figures respectively. Note that layer fracture leads to steeper gradient in NDE distribution, indicating more localized damage in the substrate. The target is impacted by a hard steel ball at 750 m/s.

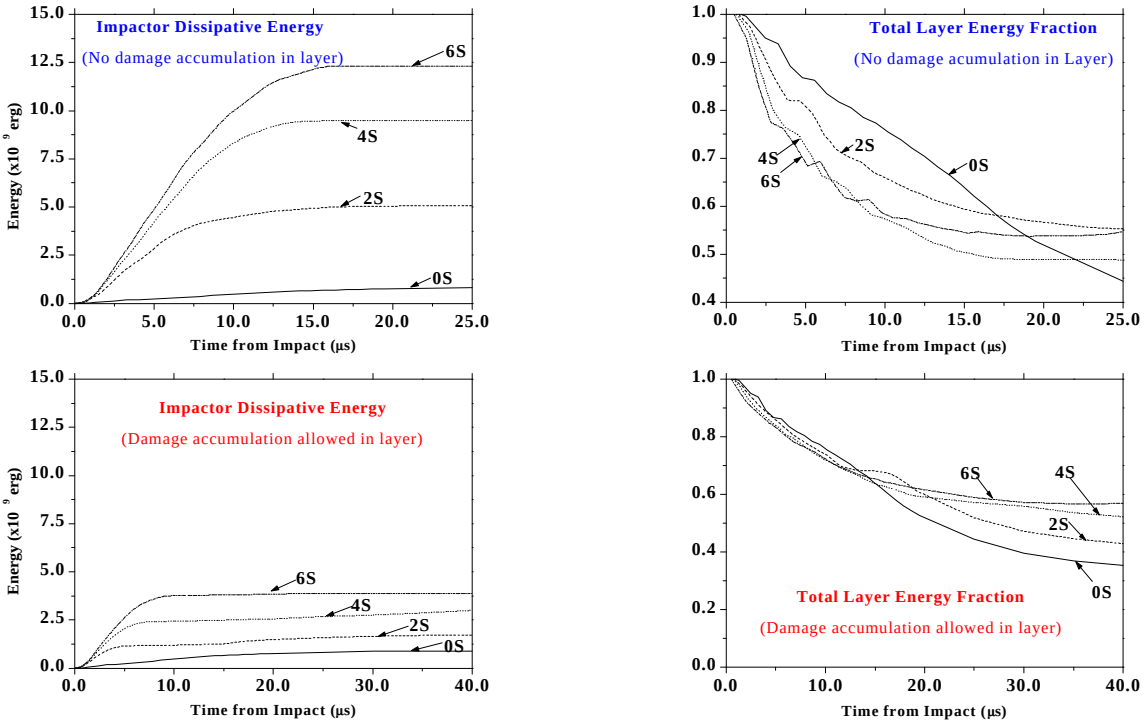

Figure 43: The time dependence of the penetration process as indicated by various energy histories. The dissipative energy in the projectile and layer energy fraction (the ratio of the energy in the layer to the total energy imparted to the target) are used here as examples. Note that both the projectile defeat capability as indicated by the dissipative energy in the projectile and load-spreading capability as indicated by the initial slope of the layer energy history increase with the layer thickness. Also note that layer fracture leads to both degraded projectile defeat and load spreading.

in defeating the projectile and less impact energy is delivered to the target. Furthermore, since the energy imparted to the target is more widely distributed due to the load spreading, less localized damage is introduced in the target.

- Layer fracture degrades significantly the capability of the target to defeat the projectile and spread the load.
- Interface failure appears to have a more pronounced effect on load spreading than projectile defeat.

34908-EG: "Crack Tip Fields Mapping and Failure Characterization of Functionally Graded Material Compositions"

H.V. Tippur, Auburn University, Alabama

The dynamic crack growth in Functionally Graded Materials (FGMs) subjected to low velocity impact is investigated. The case where the crack is located on the compliant side of the FGM, parallel to the direction of the gradient, is studied and compared to the behavior of a homogeneous composition of identical geometry subjected to the same loading conditions.

The FGM and homogeneous materials used in this study are particulate composites, with solid A-glass spheres (mean diameter 42 μm) suspended in an epoxy matrix. Gravity casting methods are used to produce FGM samples with pure epoxy at the top of the mold and a composite with ~ 50% volume fraction (V_f) of glass beads in the matrix at the bottom. The compositional gradient produces nearly linear Young's modulus variation over the height of the beam samples (37 mm), varying from 4.5 GPa to 11.5 GPa. Also associated with these are increasing longitudinal and shear velocities, and density, while the Poisson's ratio decreases with V_f. An edge crack is introduced on the compliant side of the beam with a high-speed diamond saw such that the crack tip modulus is 6.5 GPa. The homogeneous beam has a uniform elastic modulus of 7.5 GPa.

The optical method of Coherent Gradient Sensing (CGS) is used to measure surface slope $\partial w/\partial x$, where w is the out-of-plane displacement and x denotes the coordinates along the crack orientation. Both samples are impacted at 5.3 m/s along the crack line, on the edge opposite the crack. The event is recorded by a high-speed camera at a rate of 200,000 frames per second. Selected frames illustrating the crack propagation for both the homogeneous material and the FGM are shown in **Figure 44**. These frames correspond to times close to crack initiation, and approximately 40 μs following initiation in each case. Of interest in both cases are the familiar three lobe patterns present in homogeneous material under quasi-static loading which suggest mode-I deformations. However, the fringe patterns in the FGM ahead of the crack tip are visibly enlarged laterally (normal to the elastic gradient) due to the monotonically increasing Young's modulus when compared to the homogeneous counterpart. Also due to the distinctly different elastic characteristics of the FGM and the homogeneous sample, the deformation fields far away from the crack tip are noticeably different implying distinctly different stress-wave propagation behaviors between the two cases.

Experimental measurements of crack velocities consist of a period of sharp acceleration followed by deceleration. Peak velocities are similar for both

materials. Recently developed asymptotic expressions for out-of-plane deformation of FGM beams experiencing steady-state crack growth are used in evaluating stress intensity factor history ($K_I^d(t)$) from the CGS fringes as the crack propagates. Finite element simulations were also undertaken up to crack initiation. These results show excellent agreement with optical measurements. Prior to initiation, there is a monotonic increase in the stress intensity factor of both materials. Beyond initiation, the energy required to extend the crack remains constant in the homogeneous material. However, it increases continuously for the FGM, a behavior due to the increased concentration of glass beads in the epoxy matrix, which results in rising dynamic fracture toughness as the crack extends.

FGM

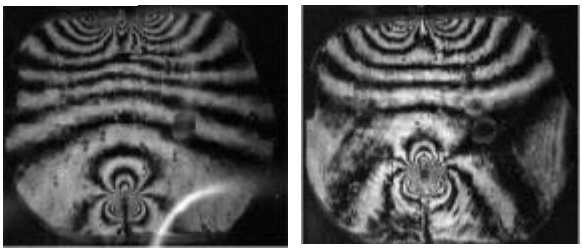

Homogeneous

Figure 44. CGS fringes for homogeneous and FGM beams near crack initiation and at 40 μs following initiation.

35045-EG "Three Dimensional Modeling and Simulation of Shear Banding and Fracture Mechanisms in KE Penetrator & Armor Materials"

M. Ortiz, California Institute of Technology

The overarching theme of the work under this grant concerns the development of three-dimensional computational capability enabling the lagrangian simulation of armor penetration. The principal objectives of the work are:
i) The development of three-dimensional computational capability including adaptive meshing, direct simulation of fracture and fragmentation by cohesive elements, nonsmooth contact and friction;
ii) Verification and validation of the unit algorithms;
iii) The demonstration of the predictive ability of the integrated facility in problems of ballistic penetration of interest to the Army.

All the unit algorithms required to carry out the simulations of interest in three dimensions have been developed and successfully tested. The degree of difficulty involved in the development of these algorithms varies from low (e. g., the extension of the constitutive updates to three dimensions) to exceptionally high (most notably, the development of automatic 3D meshing capability for arbitrary domains). The focus of most of the recent work has been to improve the robustness and reliability of the remeshing algorithm. We have found that a remeshing procedure based on element subdivision and edge collapse to be the superior approach among those evaluated. These techniques have been extensively validated against impact experiments. These experiments pertain to surface erosion in metals by spherical projectiles as shown in **Figure 45**.

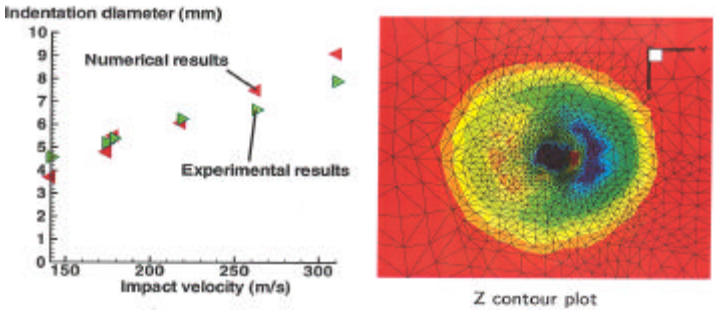

Figure 45 3D simulation of surface erosion

36349-EG: "A Synergistic Damage Mechanics Approach to Durability of Composite Structures"

R. Talreja, Georgia Institute of Technology

The overall technical goal of this research is to develop a methodology for assessment of durability of composite structures operating under extreme environments typical of Army vehicles. The scientific goal is to develop an approach that combines the conventional micromechanics and continuum damage mechanics approaches into a synergistic approach that maximizes advantages of the two approaches while minimizing their inherent deficiencies. Having completed the mathematical formulation of the synergistic approach and derived the stiffness property changes with damage in previous years the specific objective of work in this twelve-month period has been to develop a life prediction methodology.

In order to develop a life prediction methodology one must first describe the evolution of damage as well as the critical damage states associated with failure. The mechanisms of damage evolution under fatigue of woven fabric composites have been studied in this project. Optical microscopy in conjunction with edge replication and X-ray radiography has been used to observe cracking within the fiber bundles and disbonding of the bundles from the neighboring bundles. The progression of the intrabundle cracking in cyclic loading was explained by a model that conducted a detailed stress analysis of the woven fabric composite by simplifying it as a cross ply laminate. The analysis indicated that the redistribution of stresses was caused by the growth of interbundle separation. It was possible to predict the increase in the number of cracks per unit length of a given fiber bundle. This result when used in the stiffness-damage relationships provides the stiffness degradation with fatigue.

The ongoing work is developing a fatigue life prediction method that will use the damage evolution model and a criterion of critical damage states associated with failure. The upper left picture (**Figure 46a**) shows the cracks observed within the fiber bundles in a woven fabric composite. The upper right picture (**Figure 46b**) shows the separation of two bundles at their interface close to the tip of a crack. The plot shows the increase in the normal stress between the cracks as the inter-bundle separation distance grows.

a.

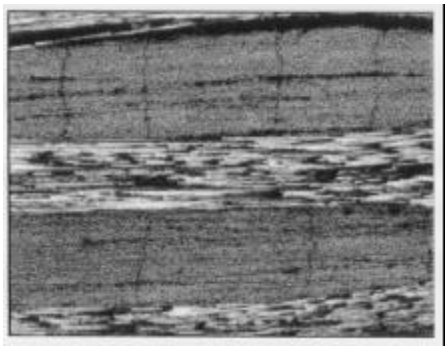

b.

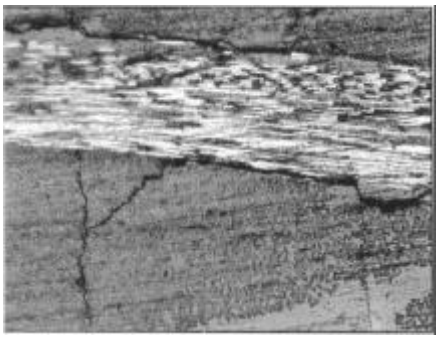

Figure 46 Damage and crack propagation in woven composites

36356-EG: "A Progressive Damage Model for Laminated Composites Subjected to Impact Loading"

D.H. Allen, Texas A&M University

Impact induced damage in laminated composite structures is in general not brittle in nature, containing significant energy dissipation other than that caused by crack growth. This energy dissipation can be traced to material inelasticity, chiefly viscoelastic in nature, at points of high stress concentrations. Therefore, traditional linear elastic fracture mechanics approaches cannot accurately model this problem. In addition, the development of hundreds and perhaps in some cases even thousands of cracks during the impact event precludes the development of analytical techniques for predicting component response during impact. Furthermore, the response is so complicated that even currently available computational approaches will require significant advancement.

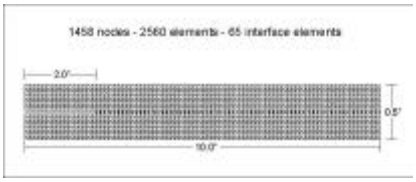

Figure 47 Impact composite damage zones

The objective of the research effort is to develop a model capable of predicting the evolution of matrix cracking, delamination, and fiber cracking in laminated composite plates subjected to ballistic impact. The research methodology is based in continuum mechanics and utilizes advanced damage, fracture, and computational mechanics to obtain accurate predictions of damage evolution in composite structures during ballistic impact. The underlying concept is to utilize the concept of cohesive zones ahead of all crack tips to model the physics of the fracture process.

During the past year, the author has developed a physically and micro-mechanically based model for a cohesive zone that includes the effect of microscale wave propagation in the cohesive zone. The cohesive zone model is both rate and history dependent, thus producing rate dependent fracture in composite media.

The development of a model for predicting impact resistance in laminated composites is far more important than in metallic media, wherein the design variables are essentially limited to a few parameters such as armor thickness and fracture toughness. Because of this, it is possible to choose metallic armor by experimentation, even though it is expensive. In the case of laminated composites, there are far too many design variables to optimize to solve the problem experimentally. Development budgets would quickly be exhausted because of the excessive number of design variables, including thickness of each ply, number of plies, orientation of each ply, fracture toughness of each ply, fracture toughness of each ply interface, and viscoelastic properties of each ply. Thus, the development of models can help reduce the number of experiments required to choose acceptable composite armor, thereby meeting budgetary constraints while at the same time saving lives on the battlefield.

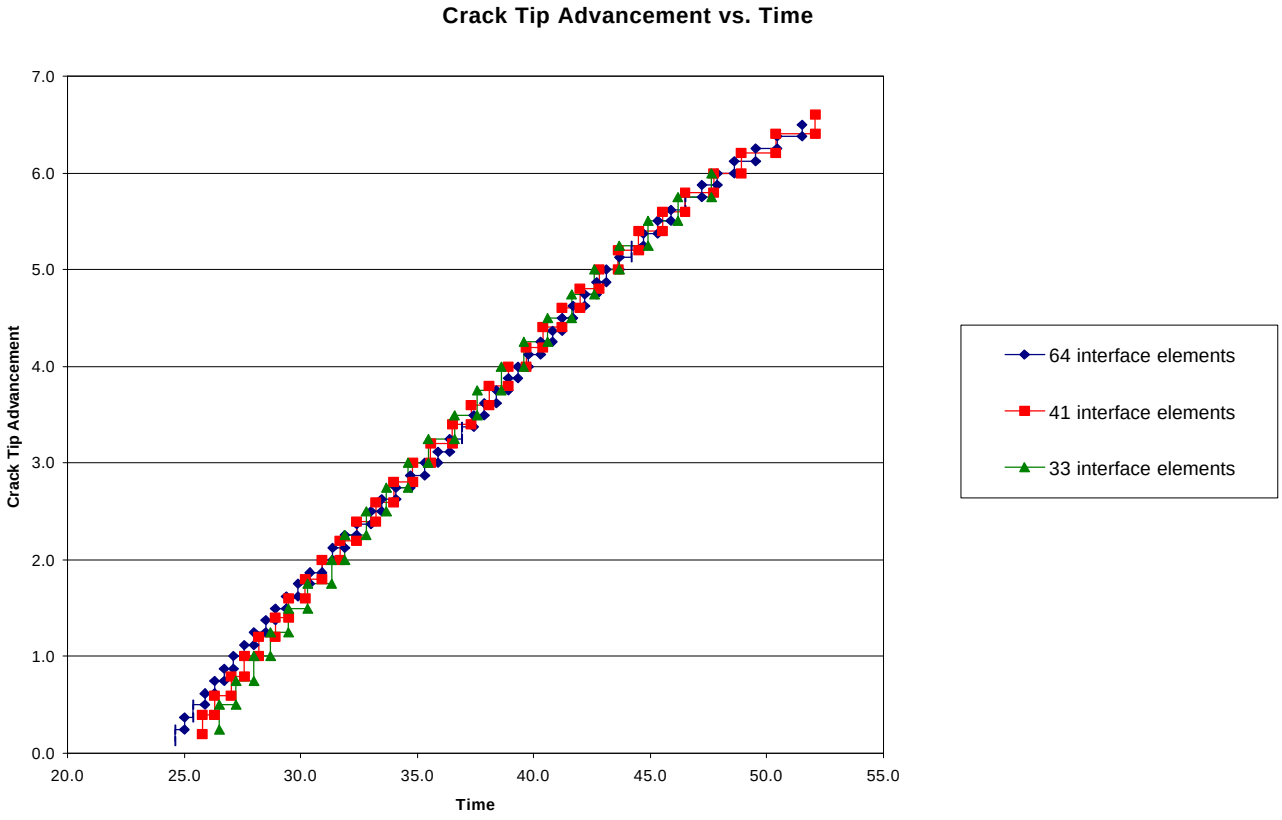

Figure 48 Crack Growth Predictions for Three Different Finite Element Meshes Showing Convergence with Relatively Coarse Mesh

37777-EG "Self-Consistent Polycrystal Plasticity and Anisotropic Yield Surfaces for Hydrocodes"

S. Ahzi, Clemson University

The objective for this project is to develop an understanding, through modeling and simulations, of the plastic deformation and failure in ductile metals under high deformation rates. For this, one needs to develop physically-based models for dynamic plasticity and for dynamic failure that would be coupled and implemented in a finite element hydrocode to simulate and predict elastic-plastic behavior as well as ductile failure under high velocity impact conditions.

Based on the physical mechanisms of ductile dynamic failure involving crack/ void nucleation and growth, a model was developed for failure in ductile metals under high strain rates. The mechanical threshold stress (MTS) as well as the Zerilli-Armstrong (ZA) models were suggested for the modeling of dynamic plasticity. During the last twelve months, the developed model was implemented into the finite element code Abaqus. The recent efforts were focused on testing and validation the model by simulating planar impact test of OFHC copper. To test the validity of our modeling under multi-axial strain states, the planar impact test was used with two different geometries: a cylindrical and a conical target. Our results were confronted to the experimental results and good agreement was found. The experimental tests' results were found in the literature for OFHC copper, particularly those of Rajendran and co-workers (from ARL). In this modeling effort, a comparison of the results from two different dynamic plasticity models (MTS and ZA) was conducted.

The major accomplishments can be summarized as follows:

1- The proposed dynamic failure criterion is physically based and accounts for ductile failure to occur by the process of nucleation and growth.
2- The constitutive equations of the criterion are simple to comprehend and are logical in construction. This will facilitate the application of this criterion to simulate other impact tests.
3- Our results show that the choice of either the MTS or the Zerilli-Armastrong model for dynamic plasticity is valid as long as the model parameters are well defined for the considered material.
4- The failure criterion predicts failure with considerable accuracy for both cylindrical and conical targets.
5- In comparison with the widely accepted Tuler-Butcher criterion for dynamic failure, the proposed failure criterion not only is more physical in philosophy but also predicts the experimental results accurately.

38081-EG "Stress Wave Propagation Through Heterogeneous Media"

G. Ravichandran, California Institute of Technology

The primary objective of this research is to experimentally investigate attenuation and dispersion of shock waves in heterogeneous solids (layered media, composites) as a function of loading rate, length scales associated with hetero-geneities (fiber diameter) and material properties. Other goals of the research include developing robust computational simulations to delineate the role of interfaces and non-periodic geometries on energy transport and dissipation in heterogeneous materials and the development of physics-based models for

shock wave propagation in heterogeneous solids that can be implemented in numerical codes for simulations of impact phenomena in heterogeneous systems. Initial experimental and computational studies are focused on investigating the attenuation and dispersion of shock waves in model periodic heterogeneous media consisting of alternate layers of hard and soft materials.

The experimental geometry for one-dimensional shock wave propagation studies is shown in the figure in which a periodic array of two materials exhibiting markedly different compliance properties is impacted by a flyer plate. Polymethyl-methacrylate (PMMA) is used as the softer media while either metal or glass is used as the harder media. The in-material particle velocity or the interface velocity is measured using high-resolution (VISAR) diagnostics. Powder gun technology provides planar-impact shock wave loading over the impact-velocity range of 0.5 to 2.0 km/s. Axisymmetric numerical simulations are performed with the DYNA finite element wavecode. Grüneisen equation-of-state and elastic-plastic constitutive strength properties model material response within the wave code.

Experiments were conducted to investigate dispersion due to scattering (interfaces), dissipation due to material nonlinearities (viscosity) and the effect of impedance mismatch on shock wave propagation in layered solids. Also, computational simulations have been used to identify the characteristic features of shock wave attenuation in periodic layered media and compared with experimental measurements. Typical experimental results for PMMA-steel and PMMA-aluminum layered composites are shown at two different impact velocities of 450 m/s and 150 m/s are shown in **Figure 49**. Following initial shock compression the velocity profile exhibits resonance vibrational motion dependent on both the impact amplitude and the nature of the composite periodic heterogeneity. At low impact velocities, shock wave propagation is dominated by dispersion and at high impact velocities by dissipation. The results of the investigation have been used to validate effective medium theories for nonlinear scattering and to identify the role of material properties and dominant length scales in heterogeneous solids under impact shock wave loading.

38324-EG "Models for Damage-Resistant Design of Composite Structures"

G. J. Dvorak, Rensselaer Polytechnic Institute

Prestressing of fibers prior to matrix solidification and releasing it afterwards induces residual stresses that can retard damage in composite laminates. Initial damage envelopes of laminated plates can be translated into the tension/tension region of the in-plane loading plane, so that transverse matrix cracking is delayed or suppressed. Free edge stresses due to either uniform hygro-thermal changes or through-the thickness gradients can be cancelled by specific prestress distributions in individual plies. Free edge stresses due to mechanical loading can be altered by optimized distributions of fiber prestress in individual plies. Both symmetric laminates loaded by symmetric or non-symmetric distributions, and non-symmetric laminates have been investigated. Applications have been developed for typical glass-epoxy laminate layups, loaded by mechanical loads and by both uniform thermal changes and gradients.

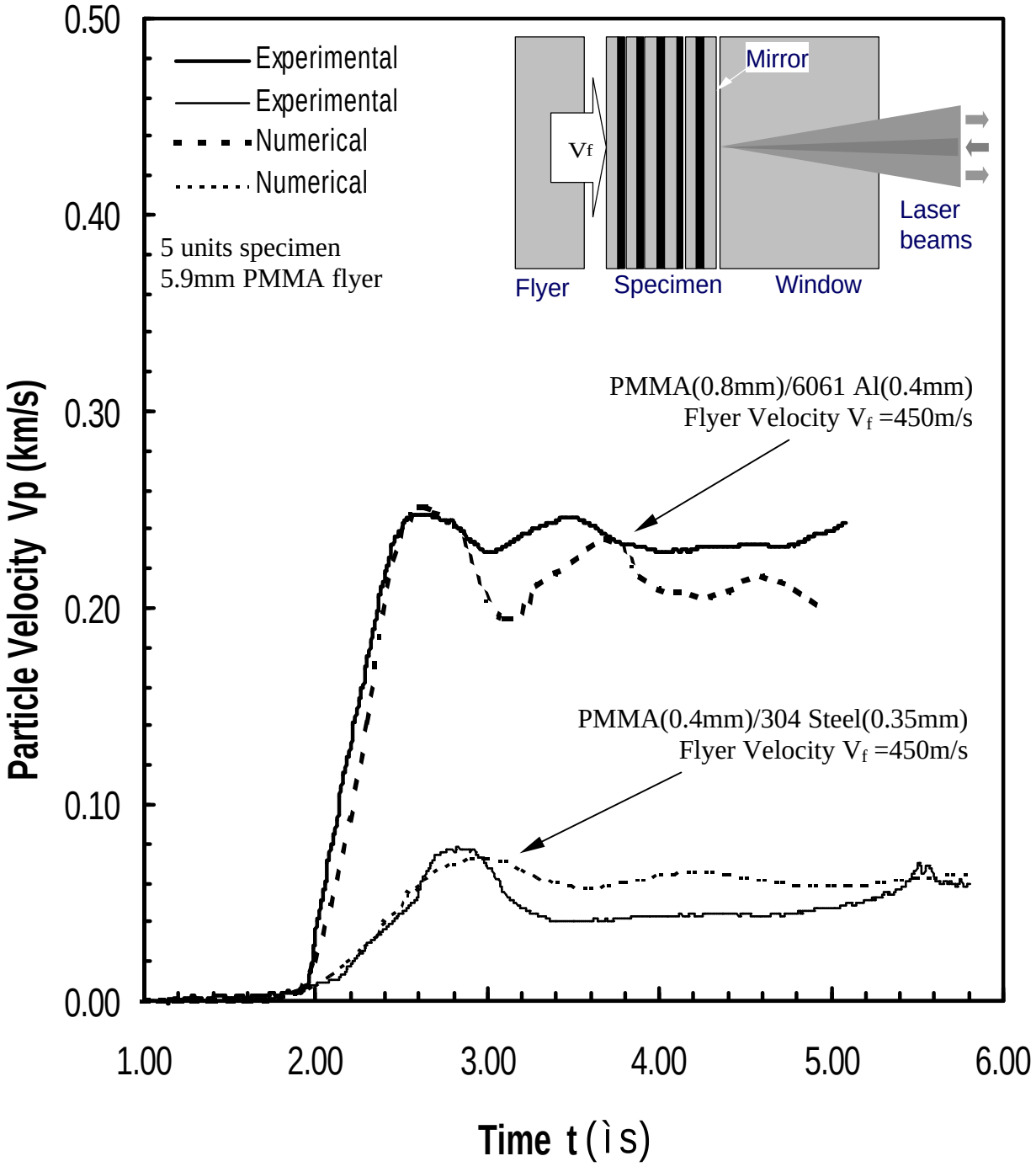

Figure 49 Comparison of Interface Particle Velocity Profiles between Experiments and Simulations

An application of fiber prestress has been identified in the upper hull structure of the composite armored vehicle. Embedded in this structure is a ceramic armor tile plate, supported by a laminated plate. Related ARO-supported research has shown that projectile penetration resistance of ceramics can be substantially elevated by confining pressure. In the composite vehicle armor, such improvement of penetration resistance can be achieved by wrapping the ceramic tiles in a 0/90 laminate with prestressed fibers. High-strength S-glass, aramid or carbon fibers with long-term creep resistance appear most suitable for this application. Modeling of the fabrication process shows that large compressive residual stresses can be induced in an 0.75 in. thick alumina armor plate by few over-wrap layers of a AS4/3501-6 carbon epoxy 0/90 laminate; for example, six 0.1 in. thick plies can generate 1500 MPa of biaxial compression. This may improve penetration resistance by several orders of magnitude.

A new part of the research will address the role of prestress on retardation of creep deformation in laminated composite cylinders subjected to internal heating. This may have potential applications in composite over-wraps of pressure vessels and gun barrels.

Transformation analysis is used to derive the overall response of a progressively damaging heterogeneous solid, in terms of several interacting damage and deformation mechanisms, and also with the effect of fiber prestress. Interface decohesion of reinforcing fibers or particles, inelastic matrix deformation, and thermal and transformation strains are among the local mechanisms considered. The approach is based on converting all local mechanisms into equivalent eigenstrains and on analyzing the interactions of these eigenstrains under incremental overall loading.

39511-EG "Evolving Multiscale Deformation and Damage in Polycrystals"

D. L. McDowell, Georgia Institute of Technology

Polycrystalline metals are complex heterogeneous materials that exhibit inelastic deformation and material damage. Models for failure at the scale of individual grains (crystals) differ significantly from those for polycrystals. This research is pursuing both computational micromechanics and large strain experiments which examine lattice orientation fields and surface displacement fields over mesoscales of collective grains. Program objectives focus on:

- measuring and modeling de-composition of rotation and stretch fields over ensembles of grains with subgrain resolution,
- developing an improved, physi-cally based description of length-scale dependent decomposition of stretch and rotation in the presence of multiscale heterogeneity of inelastic deformation and damage,

- using experiments and computational micro-mechanics to explore simplified forms of constitutive laws for coupled plasticity and damage based on incompatibility fields, and
- incorporating microscopic or mesoscopic material attributes (e.g. crystallographic orientation) into constitutive models along with macroscopic attributes (e.g. hardening and plastic deformation in high symmetry crystals) to develop hybrid multi-scale plasticity models that are accurate yet much more computationally efficient.

This research is relevant to applications such as advanced penetrators that employ texture control, optimizing resistance to break-up of shaped charge jets, low velocity impact damage, and manufacturing and dual use technology for large strain problems (machining, metal forming, etc.).

Large-strain compression and torsion experiments on Cu with and without grain boundary segregates will be conducted. Measurements of texture and surface displacement fields will provide necessary information to compare with finite element simulations of the large strain elastic-plastic deformation distributed through the microstructure. These comparisons will be used to establish the limitations of existing phenomenology of crystal plasticity and the manner in which elastic and plastic deformation is decomposed over sets of grains. Similarly, the combined effects of large plastic strain and material damage (voids, grain boundary or triple point cracks) will be examined as a function of the length scale over which failure criteria are written, ostensibly leading to the macroscopic scale of relevance to structural analysis and design.

Key accomplishments in the first seven months of this grant include: completed internal state variable model for grain subdivision processes and formation of microtextures within grains, including effects on slip system hardening; developed of simplified grain interaction models for polycrystal behavior; development of an approximate, extremely efficient time integration scheme for stress-strain relations of rate-dependent crystals; conducted preliminary finite element studies of the average incompatibility tensors for grains in polycrystals subjected to different states of deformation; and obtained initial Laue diffraction and electron backscattering diffraction pattern (EBSP) measurements of lattice misorientation distributions in fine and coarse polycrystals.

39760-EG "The Role of Fracture Surface Topography & Friction in Dynamic Response of Armor Ceramics"

R. Feng, University of Nebraska-Lincoln

One of the primary failure mechanisms in ceramics subjected to ballistic impact is shear microcracking. Because of the very large inertia confinement associated with the impact-induced shock wave compression, micro cracks in this process are believed to be *closed*. However, many damage models developed for armor ceramics are based the fracture mechanics theory for *open* cracks. A good understanding of the dynamic friction between the crack surfaces and its role in the damage evolution in armor ceramics is therefore very important for developing better ballistic performance predictions

and design strategies for ceramic armor structures.

To this end, an experimental investigation on the topography and dynamic friction of ceramic fracture surfaces has been undertaken. The objectives of their work are: 1) to establish an experimental capability for characterizing the transient frictional response of fractured ceramic interface under dynamic loading, and 2) to develop a material model that takes into account the effects of the surface topography and dynamic friction of closed micro cracks on the damage process in armor ceramics.

This work so far has been focused on a novel technique for dynamic tribometry of fracture surfaces and a new facility for optical surface characterization. Utilizing the split-Hopkinson *torsion* bar technique, they have developed a dynamic tribometer that is capable of delivering rapid rotational sliding (with a rise time within 100 μs and angular velocities up to 1200 rad/s) under compressive forces up to 60 kN. To address the need for fracture surface characterization, they have set up a surface mechanics and tribology laboratory equipped with a Proscan 1000 surface profilometer that enables laser-based, high-precision, three-dimensional surface profiling as well as a full range of statistical surface analyses.

As a proof of the concept, several experiments have been carried out on 7075-T6 aluminum specimens (which are much less expensive to machine). Each specimen has as-fractured surfaces with an arithmetic mean roughness of about 30 μm. The results of this series of dynamic tribometry experiments are summarized in **Figure 50**. The ratio of the friction over the compression is seen to increase sensitively with the applied compressive stress. At the largest compressive stress examined (287 MPa), the peak frictional stress reached 241 MPa. This value approaches the yield strength of the material.

Although the material tested is significantly more ductile than ceramics, the results clearly demonstrate that the load bearing capacity of closed fracture surfaces under large confinement can be very substantial. Work is currently underway to carry out the dynamic tribometry of as-fractured ceramic samples and to develop a ceramic model that incorporates the experimental results on the topography and dynamic friction of ceramic fracture surfaces.

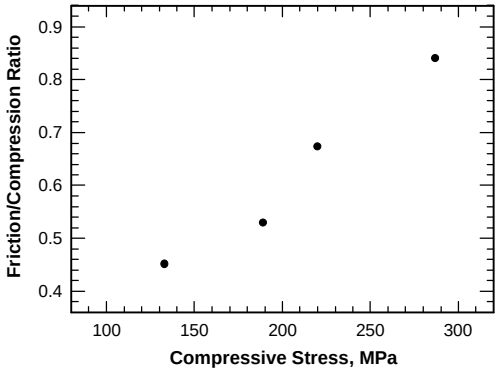

Figure 50 Dynamic friction data on 7075-T6 A1

39794-EG A Fundamental Investigation into the Deformation and Failure Behavior of Heterogeneous Materials with the Aim of Developing Design Guidelines

K. Ravi-Chandar, University of Houston

In traditional materials design, material properties are affected by processing induced microstructural changes; the structural analysis and design use these properties as inputs. For composite materials, this approach has lead to a

number of *ad hoc* definitions of "strengths". We believe that through an understanding of the micromechanical deformation and load transfer, design with composites can be approached by coupling the microstructural design and macrostructural design. This approach will eliminate the need for *ad hoc* strengths and provide for design using the fundamental material properties of the constituents. In order to develop this methodology, it is necessary to understand the deformation and failure behavior of composites at the level of the heterogeneity. This is the objective of the present work. This is approached through fully instrumented experiments, where all the boundary conditions are measured, regardless of whether they are controlled or left free. This makes the interpretation of the experimental results straight-forward. We are examining multiaxial loading conditions in graphite-epoxy specimens. While most experiments in the past have focused on measurements at the global level, we combine these global measurements with measurements of the local variations of the deformation through a digital image correlation technique. Local mechanical properties are also necessary to implement these ideas. Once the mechanical response at multiple scales is obtained, the ideas can then be transferred to design new micro and macrostructures for composites. The program is in its first year and significant results are not yet available for distribution.

40191-EG "A Novel Approach to Large Electrostriction in Ferroelectrics"

K. Bhattacharya, G. Ravichandran, California Institute of Technology

Ferroelectric materials are currently used in a variety of sensor and actuator applications. Conventional materials offer a high frequency, linear response with useful strains of up to 0.1%. Additional applications can be imagined for actuators that generate a greater degree of strain. The current investigation is an experimental study of single crystal ferroelectrics aimed at offering increased actuator performance over conventional materials. In addition, the study offers insight into the underlying principles of behavior of those materials currently in use.

A set of experiments were designed and performed to investigate the possibility of achieving large strains in ferroelectrics using combined electro-mechanical loading of a single crystal. The experiments were carried out with crystals of barium titanate ($BaTiO_3$). The basic principle of operation, illustrated in **Figure 51**, is the following: a thin single crystal plate, is subjected to a constant, uniaxial compressive stress (P) and a variable electric field. At zero applied voltage, the applied stress forces the polarization to be in-plane, as illustrated in the figure. As the voltage is increased, the electric field tries to align the polarization in the out-of-plane direction, but this is resisted by the stress. There is an exchange of stability at a critical voltage and the polarization switches with an accompanied strain that can be as large as 1.1%. Finally as the voltage is decreased, the polarization reverts back to an in-plane direction, recovering the strain. Thus, as the load is held fixed and the voltage cycled, domain switching provides an electrostriction as large as 1.1%. Strains as large as 6% are predicted for other materials of the same class.

An experimental setup has been

designed to provide a constant stress and variable electric field to a ferroelectric crystal and measure the induced electrostrictive strain. The experimental setup consists of a loading mechanism, displacement measurement transducer, electrodes and CCD camera. The loading mechanism uses dead weight and a lever to deliver a force to a loading frame. The force is transmitted to a pair of optically flat, glass plates that sandwich the specimen (**Figure 51**). Glass plates are used so that the entire load axis is transparent, allowing direct observation of the specimen during the test. Semi-transparent electrodes deposited on the surface of the glass plates are connected to a high voltage power amplifier to generate an oscillating electric field across the crystal. The crystal strain is measured by recording the load frame displacement during the course of the experiment, which corresponds to the change in thickness of the specimen. The displacement is measured using a high-resolution LVDT.

Experiments have been performed at different levels of applied stress. Data are shown in **Figure 52** for a compressive stress of 3.6 MPa. In the figure, the measured strain is plotted as a function of electric field. A maximum strain of about 0.8% is measured in this experiment with a response which is nearly the same for positive and negative values of electric field, hence it is electrostrictive, not piezoelectric.

Experiments are being continued to gain further understanding on the strain-electric field response at different levels of compressive stress. Experiments will also investigate the frequency response and time dependence to understand its influence on accumulation of damage in the material. Theoretical studies will be conducted to understand the effect of texture on electrostriction.

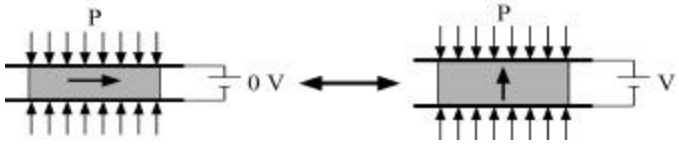

Figure 51. – Mode of operation for large strain electrostriction in a ferroelectric single crystal

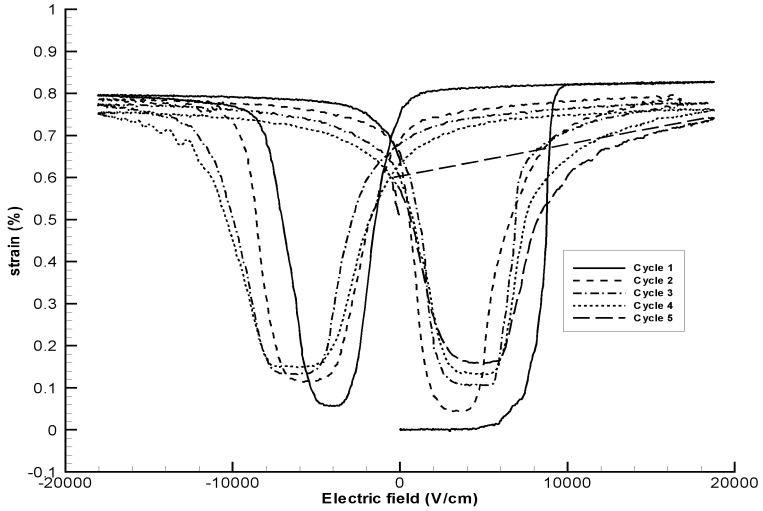

Figure 52. – Strain response as a function of electric field for a barium titanate crystal under a constant compressive stress of 3.6 MPa with a 1/20 Hz. sinusoidal input signal.

40192-EG "Optimizing Functionally Graded Materials to Resist Failure under Dynamic Loading"

T. Nakamura, State University of New York at Stony Brook

This research is focused on optimizing FGM/layered materials performance through characterizing of their dynamic deformation and failure resistance behavior. The aim is to develop an effective computational tool to simulate crack propagation in graded, multi-layered and functional materials (i.e., spatially varying properties) and to establish the phenomenological link between micro-scale cracking/damages and structural level fracturing in functionally graded materials (FGMs).

In order to investigate the dynamic failure phenomenon, fracture models based on graded/layered ceramic-metal using critical energy criterion were considered as the initial approach. Here, streamlined crack propagation scheme (e.g., cohesive model) was developed for finite element codes. Important micro-structural features such as voids and cracks are also modeled to investigate the evolution of crack initiation, growth, and coalescence in non-homogeneous media.

During the first year, several computational analyses were performed. First, the crack propagation through porous medium was simulated to determine the critical temperature/load, which leads to the coating failure. Second, dynamic deformation and failure resistance of functionally graded materials (FGMs) were characterized through numerous computational studies. Third, the energy absorption within the FGMs by the impact load was closely monitored under dynamic conditions (**Figure 53**). The last analysis led to the quantification of relative energy release/absorption by different mechanisms in the protective layer. The important observation was that cracking and plastic dissipation absorbed significant parts in the impact energy. Such phenomena may offer a means to control and maximize the protective capability of functional coatings. In addition some issues related to the stability and accuracy of the crack propagation schemes were elucidated.

40296-EG "High Temperature Field Processing of Engineering Materials"

H. Garmestani, Florida State University

The primary objective of this proposal is to investigate the effect of high field/temperature in the development of texture in magnetic materials. The process of crystal reorientation under high field will be studied both experimentally and analytically to find a framework to synthesize materials with specific texture and microstructure. We will focus on two important ferromagnetic materials in the form of bulk (ferrites) and thin film (magneto-strictive) materials. Both these materials require a highly ordered microstructure specifically in the easy axis of magnetization. This is presently only possible through mechanical forming and heat treatment. Such Ferrites are the main components of motors and electronic devises to convert energy. A new generation of ferromagnetic shape memory alloys with *a large stroke, a high force and a superior dynamical response*, have attracted increasing attention in recent years. It has been shown that highest strain properties can be obtained for the single crystal or highly textured form and only in specific orientations. The successful production of field induced shape memory alloys can provide new

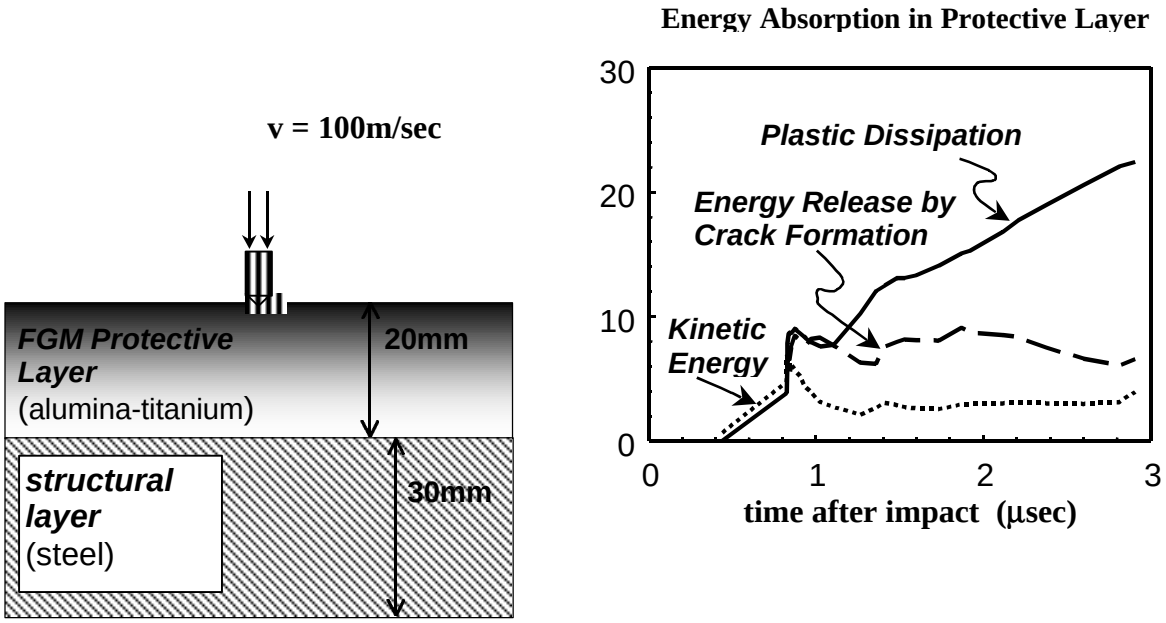

Figure 53 Impact of FGM system

smart structures, devices, microactuators and micromachines with smaller dimensions and simpler configurations. A high temperature furnace has been constructed in the bore of a high field magnet (20 Tesla). Initial texturing of superconducting materials showed promising results. A new set-up is presently being constructed to measure magnetic susceptibility at a variety of temperatures up to 1300 degrees C **(Figure 54**).

Magnetic annealing is a method of high temperature processing of materials under an applied field. It is known that materials with preferred crystallographic orientation can be produced by solidification while cooling under an applied field. Interesting structural properties are produced as a result of this process. In addition, some materials such as Sm_2Co_{17} have a huge difference in the anisotropy of the paramagnetic susceptibility at high temperatures. Engineering of new materials with the control of properties is an area of great practical interest. The research proposed here is still in its infancy and most of the results have been obtained in the field of high temperature superconductivity. It has been shown that at certain temperatures the anisotropy energy associated with the paramagnetic state of Y-Ba-Cu-O is strong enough to induce alignment of particles in a magnetic material (the c axis aligns parallel with the applied field). As yttrium is non-magnetic, this anisotropy energy is attributed to the paramagnetic susceptibility associated with the Cu-O planes.

This energy has been used to produce aligned sintered ceramics from particles suspended in a liquid and oriented at room temperature.

This approach has been extended to solidification from a melt; because it was postulated that sufficient anisotropy would remain at temperatures high enough to induce partial melting of YBa2CU3O (T>1000 ^{0}). The effect of magnetization has also been studied in other materials of Ho-Ba-Cu-O (3). All these studies are in their initial stages but they suggest that it is possible to develop highly ordered microstructures in a magnetic field at high temperatures. The major success in the reorientation has been processing through the melting temperature (Melt Texturing) under large magnetic fields (20 Tesla). It is however not very clear as to the nature of recrystallization and reorientation (texturing) during this process. One reason maybe that the recrystallization and grain growth is a complex process and a fundamental understanding of texturing during recrystallization is still in its infancy in materials science.

The major success in the reorientation has been processing through the melting temperature (Melt Texturing) under large magnetic fields (20 Tesla). It is however not very clear as to the nature of recrystallization and reorientation (texturing) during this process. One reason maybe that the recrystallization and grain growth is a complex process and a fundamental understanding of texturing during recrystallization is still in its infancy in materials science. In general, four regions can be identified through the magnetization process: Region I: Solid state Region II: Solid liquid phase, Region II: Melt texturing region, Region IV: Solidification region.

To apply this technique, a high temperature furnace has been constructed to be compatible in the bore of a high field magnet (**Figure 54**). The furnace has been tested four times in ambient environment up to 1200°C. The furnace temperature was monitored with an "R" type thermocouple. The outside temperature of the furnace was relatively low. The furnace was tested up to 850°C at 20 Tesla in the 195 mm resistive bore magnet in cell 4. No unexpected abnormalities were observed. The furnace was stable throughout the entire test. It took about 1 hour to heat up the furnace and was cooled overnight.

40344-EG "Cohesive Formulations for Delamination in Polymer Layered Composites"

S. Saigal, Carnegie Mellon University

Polymer layered composite materials are used in several critical applications like aircraft and automotive structures, containers for hazardous and sensitive materials, and micro-electromechanical devices. Design of these constructions requires the knowledge of the failure behavior of the composite materials. Since obtaining design data through experiments is prohibitively expensive, numerical simulations employing finite element methods are extensively used for the analyses of such design problems. The objective of this STIR project is to build a tool that can reliably predict the interfacial delamination response in practical engineering applications and to validate this tool with experimental data.

Cohesive surface formulations have emerged as an attractive strategy for interfacial mechanics as they incorporate the constitutive behavior at a micro-scale.

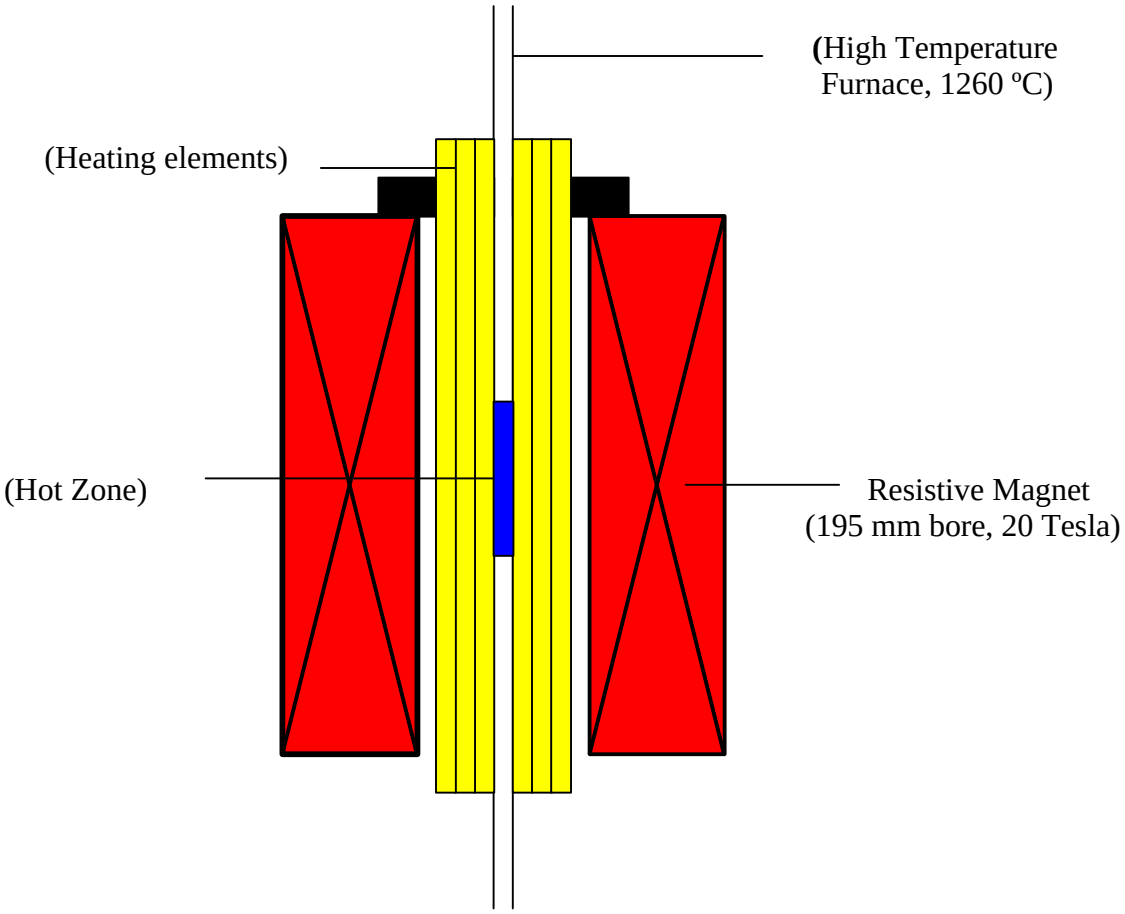

Figure 54. High Temperature High Magnetic Field Processing of Highly Textured Materials

in a model of macro length scales. Further, they allow delamination to occur along arbitrary paths without the imposition of any additional failure criteria, and are formulated independent of the bulk material kinematics. The present study follows an integrated experimental/ analytical approach in developing cohesive formulations that build towards a numerical tool for the prediction of the delamination in composites.

The Through-Crack-Tension (TCT) configurations were employed in the present study. It consists of a glass-polymer glass laminate system with a through crack opening in the glass sheets. This model provides a fundamental understanding of the delamination process, may be used to estimate interfacial properties, as well as to define constitutive models that govern failure of polymer ligaments connecting glass fragments in post shatter behavior of architectural and automotive glass structures.

Polymers exhibit a non-linear time-dependent behavior. The effect of non-linear behavior of the polymer in the TCT was investigated. The polymer was

modeled as a hyperelastic material and a potential based rate-independent interface was assumed. The force-displacement response was obtained and compared against experimental data to obtain a good agreement. These results serve as an expeditious way to characterize the interfaces as hard and soft interfaces. Such characterizations serve as useful tools in the design of interfaces.

The effect of rate on the force-displacement -displacement response was obtained by modeling the polymer as linear viscoelastic material. These results indicate the range of velocities where rate effects are important. These effects are negligible at very high and very low velocities and the limiting values approached at these velocities are consistent with scaling laws.

Intentionally left blank

STRUCTURAL DYNAMICS & VIBRATIONS

34765-EG "Active-Passive Hybrid Adaptive Structures For Vibration Controls -- An Integrated Approach"

K. W. Wang, Pennsylvania State University

Objectives: The objective of this research is to develop, validate and evaluate novel *active-passive hybrid* adaptive structures for real-time vibration controls. These types of structures normally require less power than the purely active systems. Also, since energy is almost always being dissipated, this method is more stable than the active approach. In other words, it has the advantages of both the passive (stable, low power requirement, fail-safe) and active (high performance, feedback actions) systems.

Approach: The major research tasks include (a) actuator concept development, (b) actuator structure modeling and characterization, (c) control law development and system integration, (d) adaptive structure concurrent design methodology development, and (e) experimental validations.

Accomplishments: The recent achievements are described in the following paragraphs:

(1) *Hybrid constrained layer* (HCL) configuration development -- To further advance the state of the art in active constrained layer (ACL) and enhanced active constrained layer (EACL) research, the Penn State researchers recently explored the feasibility of the hybrid constraining layer (HCL) configuration (see **Figure 55**). That is, they combined both the active and passive materials into the constraining layer (coversheet). Combining the overall active and passive actions, the EACL with sufficiently stiff edge elements not only could achieve better performance (smaller vibration amplitude) with less control effort (lower voltage or power) compared to the ACL systems, but also will outperform the purely active system. Analysis also showed that the EACL treatment is a more robust design.

In both the ACL and EACL treatments, the constraining layer (coversheet) is completely made of piezoelectric materials (e.g., PZT ceramics or PVDF polymer) because of their active action capabilities. PZT materials are in general much better than PVDF polymers for this purpose. Nevertheless, having a density similar to steel (relatively heavy) and a modulus close to aluminum (moderate stiffness), PZTs are not ideal as constraining materials. Because of the limited selections of active materials, it is difficult to find one with both features - good material property for constraining purpose and strong active action.

(2) *Active-passive hybrid piezoelectric network* (APPN) enhancement and high-authority non-linear action utilization -- The APPN hybrid networks consist of piezoelectric materials in series with an active voltage source and passive shunt circuits (**Figure 56a**). A comprehensive analysis has been performed to provide more insights and understandings to the system. A systematic *concurrent* design method is developed to ensure that the passive and active actions are optimally synthesized. Through these investigations, it is shown that compared to a purely active arrangement, the shunt circuit not

only can provide passive damping, they can also enhance the active action authority around the tuned frequency. Therefore, the integrated APPN design will be more effective than a system with separated active and passive elements, and will achieve more vibration reduction with less control effort. It is also demonstrated that the efficiency of the actuator can be further enhanced through on-line varying the resistant element. A parametric control law is derived to minimize the control voltage and power by appropriately adjusting the resistor. To increase the control bandwidth and achieve *dual-functional* (narrow-band and broad-band controls) effects, the Penn State researchers have also explored the feasibility of combining the EACL (enhanced active constrained layer) and APPN configurations. Analysis results show that the integrated EACL-APPN approach can outperform the individual EACL or APPN configurations throughout a wide frequency range.

It is recognized that the APPN enhanced active authority is due to the voltage amplification characteristics of the circuit around the tuned frequency. During some operating conditions, this high voltage (electric field) across the piezoelectric material will cause significant non-linear effects. To further advance the technology and utilize the high authority APPN actions, a robust sliding mode controller was recently developed for the APPN configuration, which can take care of the piezoelectric non-linearity that deviates from the usual linear assumption at high electrical fields. In this research, the non-linear behavior of the piezoelectric material is investigated experimentally and analytically. Non-linear constitutive laws are developed and a robust sliding mode control algorithm is synthesized. Part of the non-linearity is treated as uncertainty in the controller design, and the uncertainty bound is extracted from the experimental observations. Analysis results are given to demonstrate the validity of the proposed controller design. It is shown that the performance of a linear optimal controller will be seriously degraded by the non-linearity. On the other hand, when compared to the linear control approach, the proposed sliding mode scheme can achieve more vibration reduction with the same control effort (**Figure 56b**). That is, with this non-linear robust controller, one can fully utilize the high authority characteristics of the APPN system.

34766-EG "Computational Approaches for Smart Materials and Structural Systems Including Non-Linearities"

J. N. Reddy, Texas A&M University

Objectives: Develop (1) models of ferroelectric and electrostrictive behavior of single crystals and ceramics to include non-linearity between strain and electric field (electro-strictive), and non-linearity and dissipation between polarization and electric field (ferroelectrics); (2) constitutive models for martensitic phase transformations in shape memory alloys; (3) computational strategies to study material behavior using coupled electrothermomechanical analysis; (4) theoretical models for the piezo-thermoelastic behavior of plate/shell systems; and (5) computational strategies for vibration control of structural systems using magnetostrictive layers. Use the developed global-local tools to study plate/shell configurations of smart structural systems.

Impact: The research will aid in the design and development of smart materials

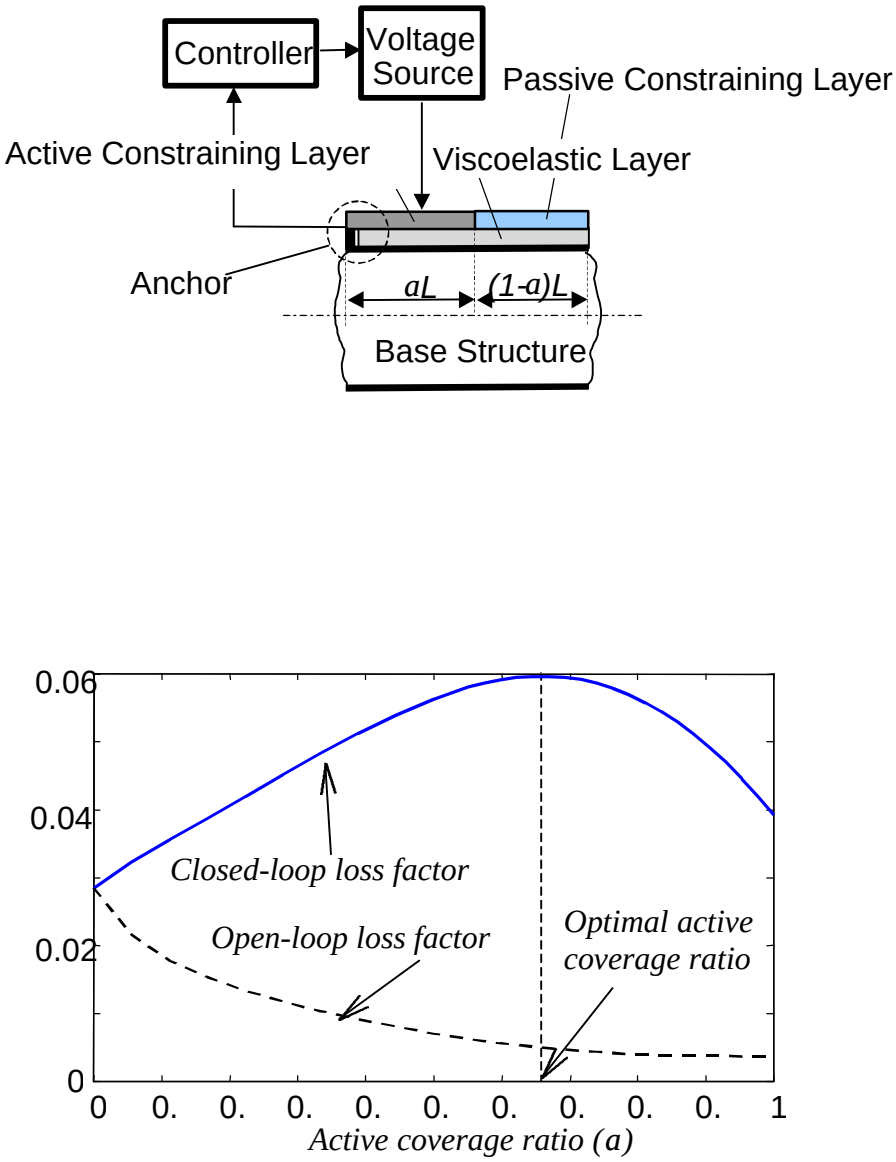

Figure 55. Upper figure: Hybrid Constrained Layer (HCL) damping treatment. Lower figure: Loss factor plot showing with proper selection of the constraining layer materials and active-to-passive length ratio, the HCL treatment could provide better (larger loss factor) open-loop damping (no active action, fail-safe ability) and closed-loop damping (total damping under control) than a system with purely active coversheet. Here, α=1 means purely active coversheet, and α=0 means purely passive coversheet.

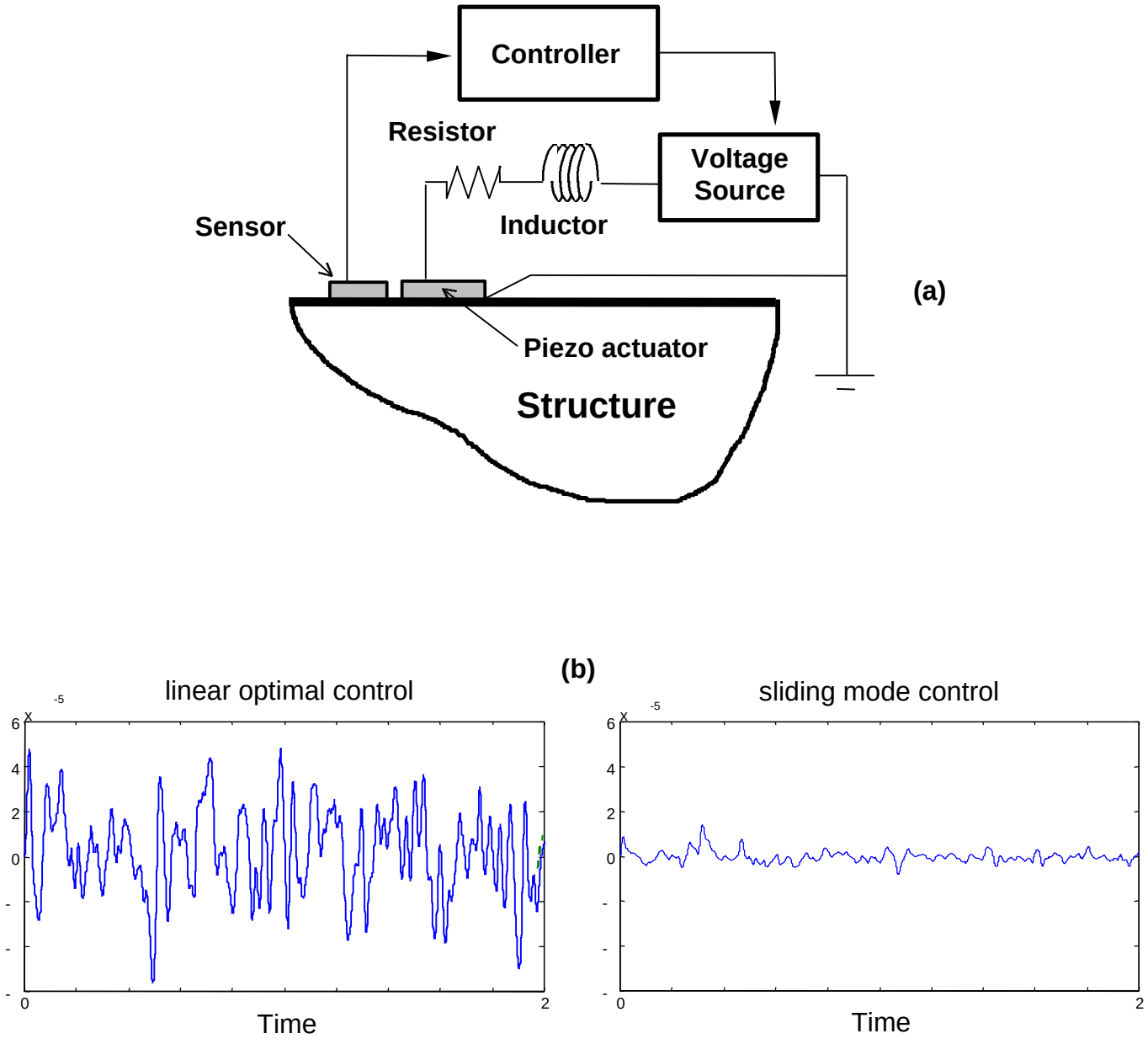

Figure 56. (**a**) Upper plot: the Active-Passive Hybrid Piezoelectric Network (APPN) damping treatment. (**b**) Lower plots: Comparing vibration control results (non-dimensionalized structural vibration amplitudes) between linear (optimal control) and non-linear (sliding mode control) controllers for APPN under high electric field operations. For a fair comparison, the two controllers are so designed that they have the same RMS value of control power input.

and structural systems related to Army's needs, such as advanced rotorcraft, weapon platforms, weapon/ordinance systems, etc. Some of the possible applications of the developed methodology are:

- Coupled analysis of smart structures under varying conditions (numerical simulations).
- Study of structures with embedded or mounted sensors and actuators at different locations, with minimal restrictions on the geometry of the structure.
- The use of the methodologies developed to build software to aid the design process, eventually leading to a complete numerical simulation of the operating conditions of a smart structural system.
- Application of the developed tool to design smart material systems as related to the Army's needs in weapon systems, rotorcraft, land vehicles among others.

Accomplishments: During the course of this research project, the following milestones have been achieved:

- Development of global-local computational tools for efficient analysis of field concentration regions.
- Analysis of smart structural systems with piezoelectric sensors and actuators.
- Development of a general constitutive model for ferroelectrics and electrostrictives.
- Development of a constitutive model for shape memory behavior.
- Computational analysis of shape memory behavior.
- Computational analysis of ferro-electric and electrostricitve behavior.
- Development of theoretical models for deformation of multi-electrode laminates and smart FGM systems.
- Development of computational models for vibration control of laminated structural systems with layers of magnetostrictive material.

The research performed in this area by the principal investigator is already finding interest and application among researchers and analysts in other universities (e.g., University of Maryland, Georgia Institute of Technology, and Virginia Polytechnic Institute) and government laboratories (Sandia National Laboratories). It is believed that the results of this research will be of considerable use to the Army and its allied groups, universities, and industries.

34775-EG "Development of a Balanced Active Rotor Blade Flap System Using Piezoceramic C-block Actuators"

Diann Brei, University of Michigan and Ronald Barrett, Auburn University

Objectives: The primary goal of this research project is to develop an active rotor blade flap system which will be less sensitive to gust loads and will experience little to no degradation in performance with increasing rotor speed. This will lead to a rotorcraft with lower vibration levels, better handling, and better overall performance. To accomplish this goal, the present study takes a new approach to active flap actuation. The University of Michigan researchers have designed a new actuator technology, called C-blocks, that eliminates the need for external mechanical amplification. The emphasis in this research is to exploit the C-block actuator design to develop an internally

amplified piezoceramic actuator that will allow for very large flap deflections while maintaining an adequate frequency response of at least 4/rev. This active rotor blade flap system will be designed to be both mass and aerodynamically balanced, and will be used for both higher harmonic control (HHC) and individual blade control (IBC) systems.

Approach: Several current flap actuation schemes use piezoceramic stacks or bimorphs. Neither stacks nor bimorphs alone, however, can simultaneously produce both the necessary deflections and forces required for rotor blade applications; thus, mechanical amplification devices, which tend to be inefficient, are needed in these applications. Previous efforts to implement HHC and IBC systems have incorporated unbalanced active flaps. Because they are not balanced, the flap deflections are considerably degraded at nominal rotational speeds by aerodynamic and frictional hinge moments and are highly sensitive to gust loads. In addition, they have the potential danger of aerodynamic control surface lock. In this research effort, the C-block based active rotor blade flaps are both aerodynamically balanced and mass balanced to eliminate the problems that have plagued earlier active flaps.

Accomplishments: A high authority piezoceramic C-block actuator system has been designed and fabricated (**Figure 57a**). The performance output of a generic serial C-block actuator has been analytically modeled and the models have been experimentally validated, both quasi-statically and dynamically utilizing a variety of ceramic and polymeric piezoelectric prototypes (**Figure 57b**). A 12-inch chord model of a rotor blade section has been designed and fabricated. The NACA 0012 carbon fiber blade section incorporated a mass and aerodynamically balanced trailing edge flap. The C-block wind tunnel test specimen was tested in the 4ft x 3ft subsonic wind tunnel at Auburn University. Flap deflections were observed to be highly insensitive to airspeed for deflections under 15° peak-to-peak for airspeeds up to tunnel limit of 130 ft/s (**Figure 57c**). At 28 Hz, the frequency associated with the predominant vibration loads on a helicopter (corresponding to the number of blades / revolution), flap deflections in excess of 17° peak-to-peak were obtained at 400 V/mm for all airspeeds tested. Flap deflections as high as 20° peak-to-peak were achieved at 40 Hz (130 ft/s). The ability of the flap to induce a pitching moment about the blade section's ¼ chord was examined. Low frequency testing at airspeeds from 0 to 130 ft/s resulted in a maximum blade pitch of 33° peak-to-peak (**Figure 57d**).

35711-EG "Non-Linear Coupling between Control and Dynamic Parameters in Flexible Multi-Body Dynamics"

Ahmed A. Shabana, University of Illinois at Chicago

Objectives: The objective of this research project is to develop new computational methodologies in the area of mechanics and control of constrained deformable bodies as applied to large scale flexible mechanical systems. The main objectives of the project can be summarized as follows:

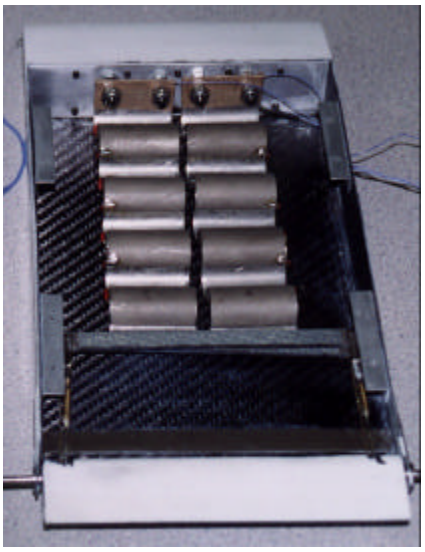

a) Wind Tunnel Test Article

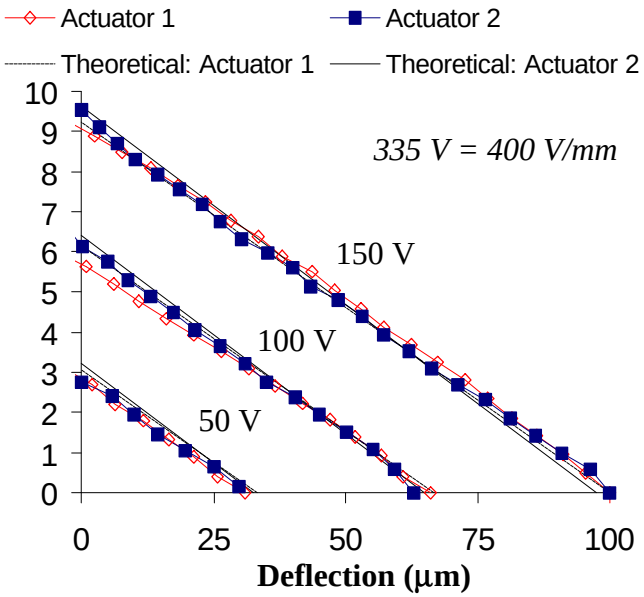

b) Force-Deflection Response of the Rotor Blade Actuators (43% Max Power)

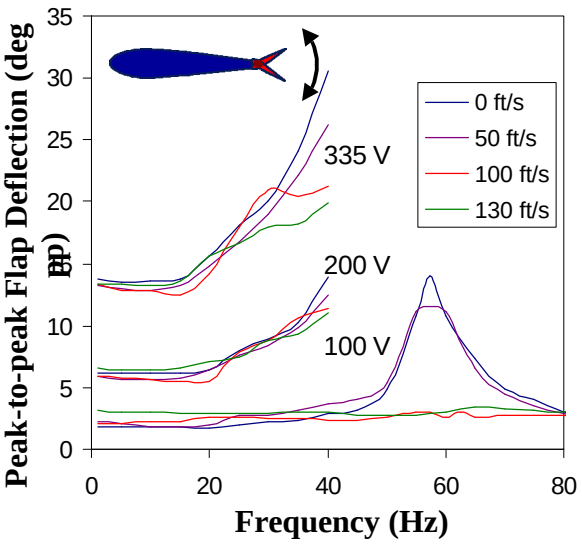

c) Flap Deflection

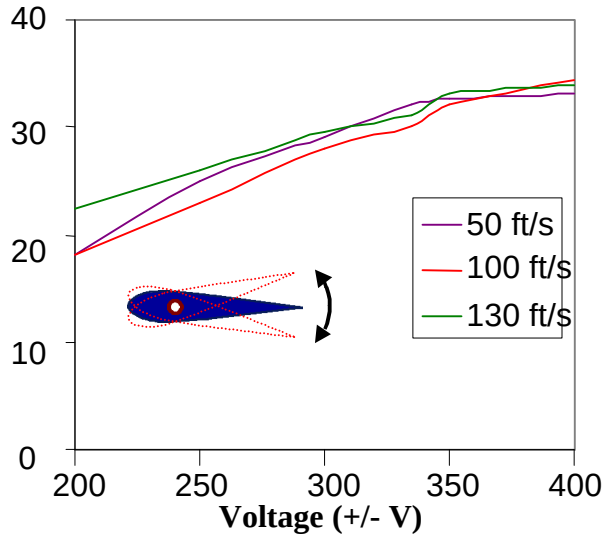

d) Blade Pitch

Figure 57: **(a)** The Wind Tunnel Test Article consists of two serial PZT-5H C-block actuators connected in parallel driving a mass and aerodynamically balanced carbon fiber trailing edge flap. **(b)** A maximum blocking force of 10.1 N and a maximum deflection of 101 µm were obtained for the rotor blade actuators at 43% of the maximum allowable voltage. **(c)** At 28 Hz, the frequency associated with the predominant vibration loads on a helicopter, flap deflections in excess of 17° peak-to-peak were obtained at 400 V/mm for all airspeeds tested. **(d)** Low frequency testing at airspeeds from 0 to 130 ft/s resulted in a maximum blade pitch of 33° peak-to-peak.

1. Develop a classification of the methodologies used in the dynamics and control of flexible multi-body systems in order to define the basic assumptions underlying each method.

2. Use the new classification to define for the first time the relationship between different methods used in flexible multi-body dynamics, and examine the effect of the linearization resulting from the use of the incremental finite element formulations on the definition of forces in flexible multi-body dynamics.

3. Develop new and efficient computational finite element procedures for the non-linear dynamic analysis of constrained flexible multi-body systems.

4. Examine the fundamental relationship between the deformable body coordinate system, the boundary conditions, the resonance conditions, and control forces in the dynamics of constrained deformable bodies, and demonstrate the use of the new procedures and formulations developed in this research project using flexible multi-body applications.

Approach: The approach employed is the new finite element *absolute nodal coordinate formulation*. This new computational method leads to accurate representation of the large displacements and can be used to circumvent the limitations of existing methods used in the non-linear dynamic simulation of constrained flexible multi-body systems.

Accomplishments: Some of the important results obtained during the last year can be summarized as follows:

1. The performance of the new absolute nodal coordinate formulation developed in this investigation was compared to the incremental finite element methods using several structural and mechanical system applications. Several large rotation and deformation multi-body problems showed that the absolute nodal coordinate formulation is more efficient and leads to a better accuracy.

2. New and simple elastic force models were developed using the absolute nodal coordinate formulation. These new force models were used to develop a general purpose flexible multi-body computer algorithm.

3. The problem of the geometric centrifugal stiffening in rotating beams was examined in details. It was shown that the absolute nodal coordinate formulation-automatically accounts for the geometric centrifugal stiffening.

4. It was demonstrated that the absolute nodal coordinate formulation can lead to a constant mass matrix for three-dimensional elements by increasing the number of nodal coordinates. Using this important property of the new formulation, an efficient procedure for the solution of the large deformation in spatial flexible multi-body systems can be developed.

RESULTS

Convergence of the New Method

- A simple example is used to examine the convergence of the proposed absolute nodal coordinate formulation.

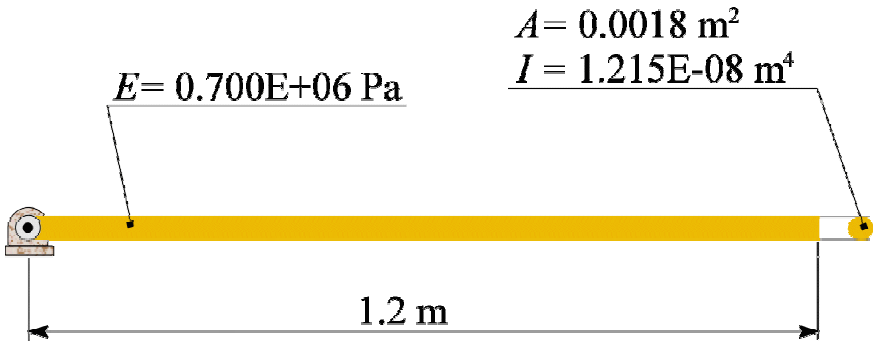

Figure 58 Flexible pendulum.

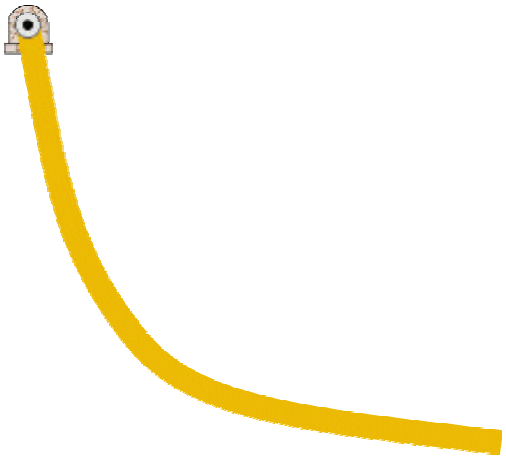

Figure 59 Deformed configuration.

- The results obtained in this project show that the incremental finite element formulations as the one implemented in ANSYS do not converge unless a large number of elements is used.

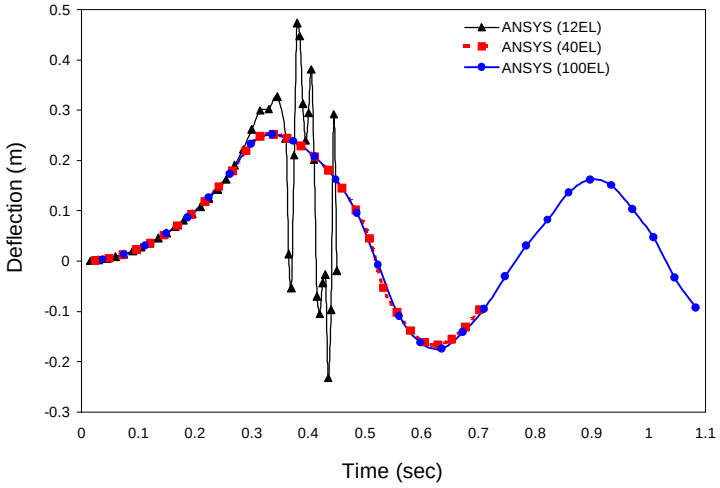

Figure 60 Midpoint deflection predicted using ANSYS with 12, 40, and 100 elements.

- The same simple example demonstrates that the absolute nodal coordinate formulation converges with a small number of elements.

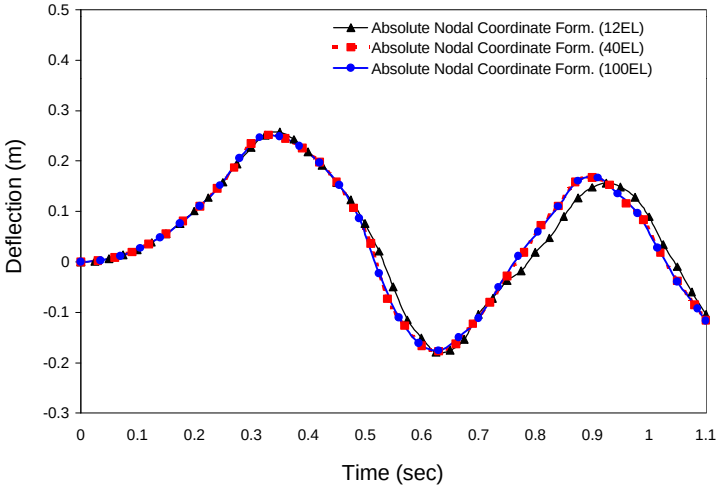

Figure 61 Midpoint deflection predicted using the absolute nodal coordinate formulation with 12, 40, and 100 elements.

Energy Principles

- The results obtained in this research project showed that the absolute nodal coordinate formulation yields better accuracy as compared to the incremental methods when flexible multi-body systems are considered.

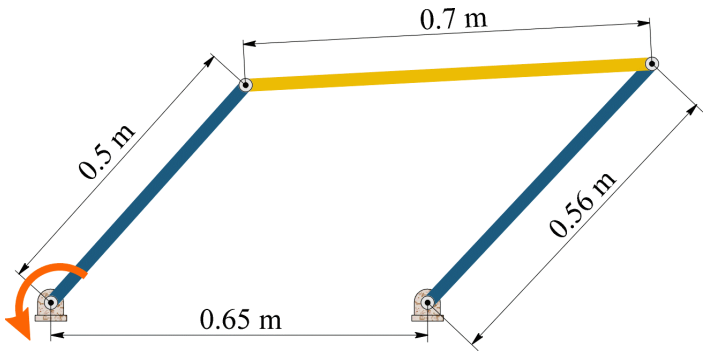

Figure 62 The four-bar mechanism driven by an applied moment.

- Using flexible multi-body applications, it can be shown that the energy principles are satisfied when the absolute nodal coordinate formulation is used, while some of the existing incremental methods violate these principles.

Figure 63 Energy balance for the four-bar mechanism

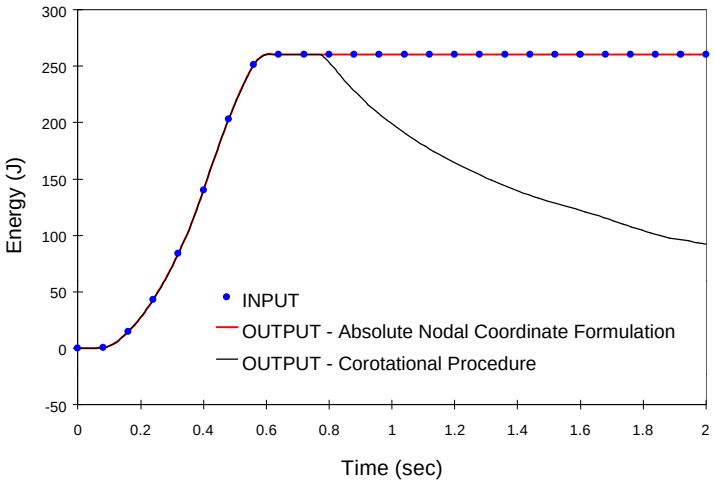

Figure 64 Energy evaluated using the absolute nodal coordinate formulation and the incremental methods.

35800-RT-RSP "Active and Passive Control Of Smart Structures"

Mario Casarella, The Catholic University, and Amr M. Baz, University of Maryland

Objectives: (a) Develop theoretical equations describing the vibration and acoustics of SMART structural systems (stationary and rotating beams, plates, and cylinders) treated with the Piezoelectric-Magnetic Constrained Layer Damping (PMCLD) Treatments. (b) Develop robust control strategies and boundary control laws for SMART structural systems treated with PMCLD Treatments. (c) Evaluate experimentally the performance of the PMCLD treatments in controlling the vibration and sound radiation of the SMART structural systems.

Approach: (a) Development of a Distributed-Parameter Finite Element Method (DPFEM) to analyze efficiently the static and dynamic characteristics of structures. (b) Development of DPFEM to describe the dynamic interaction between the viscoelastic damping layer, magnets, the piezoelectric sensor, the piezoelectric constraining layer and the base structure (beam, plate, or cylinder) that are treated with the PMCLD treatments. (c) Experimental SMART structures (beams, plates, and cylinders) will be built with the various PMCLD configurations. The effect of varying the properties of the viscoelastic cores as well as the magnetic and the piezoelectric actuators on the overall performance of the SMART structures will be investigated. Comparisons will be made with conventional PASSIVE constrained layer damping and active constrained layer damping (ACLD) in order to define the merits and limitations of the proposed PMCLD.

Significance: The proposed concepts have numerous potential military and commercial applications. In the military field, the active and passive smart structures can be utilized in manufacturing stable platforms for observation, communications, and military applications such as vehicles, automobiles, aircraft, high rise buildings as well as home and office equipment. The developed concepts are now being considered to manufacture quiet passenger aircraft (Cessna Citation II), stable target recognition system (BMDO/JPL) as well as torpedo shells with controlled wave propagation from the propeller to the torpedo nose where all the electronic sensors are located. (**Figures 65-67**)

PUBLICATIONS

1. Baz, A. " Vibration Control with Shape Memory Alloys," Encyclopedia of Vibration, Ed. by Simmons, Ewins and Rao, Academic Press, 2000. (in press)
2. Baz, A., "Shape Control of Flexible Structures," in Smart Composites, ed. by K. Uchino, Elsevier Pub. Co., 2000. (in press).
3. Park, C. and A. Baz, "Vibration Damping & Control Using Active Constrained Layer Damping: A Survey," *J. of Shock & Vibration*, Vol. 31, No.5, pp.355-364, 1999.
4. Park, C. and A. Baz, "Comparison between Finite Element Formulations of Active Constrained Layer Damping using Classical & Layer-wise Laminate Theory," accepted in *Intl. J. of Finite Elements*, 2000.
5. Park, C. and A. Baz, "Vibration Control of Bending Modes of Plates using Active Constrained Layer Damping", *J. of Sound & Vibration*, Vol. 227, No.4, pp.711-734, 1999.
6. Omer, A., and A. Baz, **"**Vibration Control of Plates using Electro-magnetic Compressional Damping Treatment", ASME 17th Biennial Conference On Vibration & Noise, Las Vegas, Nevada, Sept. 1999. And submitted to the journal *Smart Materials and Structures*.

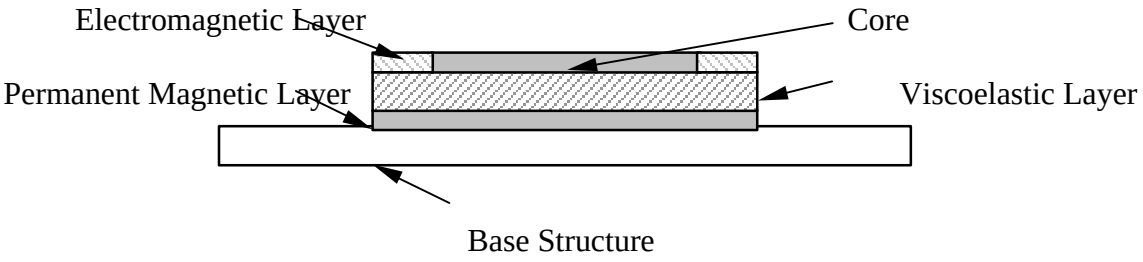

Figure 65 – Electromagnetic Compressional Damping Treatment (ECDT)

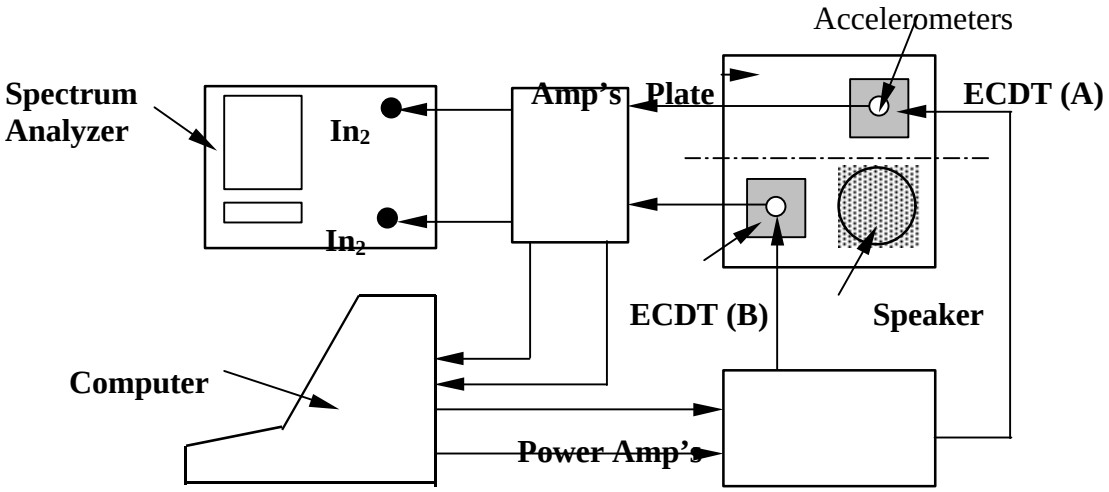

Figure 66 – Schematic drawing of the experimental set-up

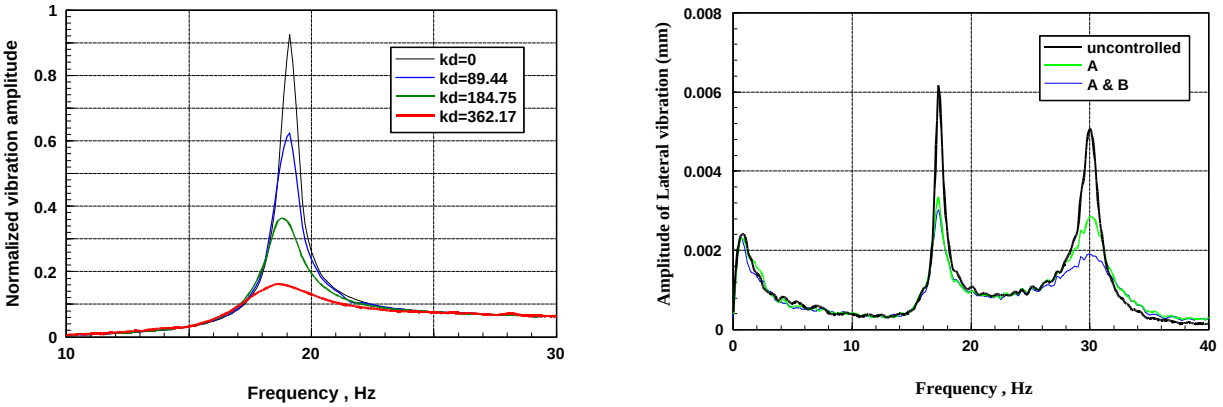

(a) Single mode control (b) two mode control

Figure 67 – Control with single and multiple patches

35828-EG "Use of Aeroelastic Couplings & Multi-Point Optimization to Design Damperless Aeromechanically Stable Helicopters"

Farhan Gandhi, Pennsylvania State University

Objective - This project seeks to determine optimized aeroelastic couplings for helicopter main rotors (couplings of blade pitch and flap motions, pitch and lag motions, and flap and lag motions) that will improve rotor lag mode damping over a broad spectrum of variations in configuration and operational conditions. This would enable the elimination of auxiliary lead-lag dampers from helicopter rotors, while maintaining required aeromechanical stability margins.

Army Relevance - Army helicopters can be susceptible to catastrophic aero-mechanical instabilities such as ground resonance due to poor damping in the lead-lag mode. While auxiliary lag dampers are currently used to alleviate instabilities, they increase hub complexity, weight, aerodynamic drag, and maintenance requirements. Further, their behavior is complex, non-linear, and depends strongly on temperature, oscillation amplitude, and frequency. At extreme temperatures, there can be significant loss in damping, and helicopters with these auxiliary lag dampers have often displayed limit cycle oscillations. The fatigue characteristics of elastomeric dampers are of concern, and raise the issue of reliability. In order to further simplify the rotor hub, reduce cost, and improve reliability of Army helicopters, it is proposed that these auxiliary lag dampers be eliminated - and the rotor be designed with appropriate aeroelastic couplings to ensure adequate damping in the lag mode.

Accomplishments - A coupled rotor-fuselage aeromechanical stability analysis was developed and validated with experimental results obtained by researchers at the US Army Aeroflightdynamics Directorate. A highly specialized, robust and numerically efficient (*two-stage, moving point*) optimization procedure was developed and integrated with the aeromechanical stability analysis. Optimal aero-elastic coupling parameters are determined that produce *improved lag mode stability characteristics over a wide range of variations in configuration and operating conditions*. This is a particularly challenging problem since previous researchers have reported (based on their parametric studies) that aero-elastic couplings, beneficial in one condition, are often destabilizing in another. It was shown that further improvement in stability margin was possible using a *concurrent optimization procedure* (fundamental flap and lag stiffness simultaneously introduced as design parameters in addition to aero-elastic couplings), rather than a sequential optimization procedure (optimal aero-elastic couplings evaluated *after* the rotor stiffness parameters were fixed). It was verified that the optimal design was beneficial in hover and forward flight conditions, and for variations in body inertia. Even rotor configurations that were not *completely* stabilized using optimized aero-elastic couplings displayed a *much milder instability over the entire range of operating conditions*. This could then be alleviated through landing gear design. In summary, the results obtained demonstrate that if optimal aero-elastic couplings, and rotor and landing gear stiffness parameters are concurrently evaluated, adequate lag damping can be introduced without violating any

constraints on system frequencies or design parameters; for ground contact, hover, as well as forward flight conditions (and for variations in thrust, rotational speed, and body inertia). Results of the current research have been reported in the following papers - (1) Optimized Aeroelastic Couplings for Alleviation of Helicopter Ground Resonance, *AIAA Journal of Aircraft*, Vol. 35, No. 4, July-Aug. 1998, pp. 582-590; (2) Individual Blade Control for Alleviation of Helicopter Ground Resonance, *Proceedings of the 39th AIAA/ASME/ASCE/AHS/ASC Structures, Structural Dynamics and Materials Conference*, Long Beach, California, April 1998; and (3) Concurrent Optimization of Aeroelastic Couplings and Blade Root Stiffness for Aeromechanical Stability Augmentation, *Proceedings of the 55th American Helicopter Society Forum*, Montreal, Canada, May 1999 (also presented at the Army Research Office Rotorcraft Aeroelasticity Workshop, October 1999, University Park, Pennsylvania; and accepted for publication in *AIAA Journal of Aircraft*).

35912-EG "Non-linear Modal Analysis and Component Mode Synthesis of Large-Scale Structural Systems"

Christophe Pierre, University of Michigan and Steven W. Shaw, Michigan State University

Objectives: Following are the main objectives of this research project:

- To systematically generate optimal reduced-order models for large scale, non-linear structures through the development of non-linear modal analysis methodologies.
- To implement these models computationally and to utilize the computer codes generated to predict effectively the non-linear vibrations of structural components, joints, and assemblies, and to assess attendant durability.
- To ultimately enable fast, high fidelity simulation of the structural and acoustical responses of rotorcraft and ground vehicle structures.

Approach: Reduced-order models of non-linear structures are traditionally obtained using the modes of the associated linearized structure as trial functions. This *linear modal analysis* of non-linear systems yields undesirably large models, because of the two-way exchange of energy between the sets of modeled and unmodeled modes. The non-removable coupling of the linear modes through the non-linearities causes this contamination, and it results in deteriorated modal convergence. In the *non-linear modal analysis* developed in this project, the contamination between modeled and unmodeled modes is automatically eliminated, thereby allowing one to construct the smallest possible, uncontaminated reduced-order model to characterize the complex dynamic behavior of non-linear structures to a prescribed accuracy. Removal of modal contamination is achieved by choosing the trial functions to be the *non-linear normal modes* of the structure, rather than the linear ones. A novel methodology is formulated, in which non-linear normal modes are defined as globally invariant motions for the non-linear system. This approach systematically embeds the non-linear effects in the non-linear normal modes, thereby eliminating contamination to a given order.

Accomplishments: The major accomplishments of the research team are listed below:

- *Multi-non-linear mode reduced-order models* have been constructed for general non-linear structural systems. They represent the minimal set of equations necessary to describe completely the motion of the system. They also automatically indicate dangerous internal resonances, without requiring *a priori* knowledge of them. Models based on non-linear modal analysis have been found to require many fewer modes than those using standard linear modal analysis do.

Non-linear modal analysis has been successfully implemented and demonstrated using *finite element models* for beams, plates, and rotorblades, for both discrete and distributed non-linearities. This is crucial, since the majority of practical vibration problems are cast in finite element form. It is also unique, since most analytical techniques developed for non-linear vibrations are incompatible with finite element formulations.

Computer codes have been developed that *automatically* produce reduced-order models for a large class of non-linear dynamical systems, given the system model and the non-linear modes of interest. The availability of these codes, together with their ability to interface with standard finite element packages, allow for the application of the methodology to general structural systems.

- A novel, *non-linear Galerkin technique* has been developed, in which the invariant manifold equations are discretized via a Galerkin expansion in amplitude and phase coordinates and subsequent projection, yielding a set of non-linear algebraic equations that is solved using the Hybrid Powell method. This approach replaces the asymptotic series solution and avoids its inherent shortcomings. Key features of this new method are: the vibration amplitude range is specified by the user, and the accuracy over that range can be controlled by the user as well, by simply varying the number of terms in the Galerkin expansion. Critical benefits of the method are that it eliminates all guesswork concerning the accuracy of the reduced-order model generated and its range of validity, and that it is extremely accurate over a large amplitude range. This approach allows for implementation for a wide variety of non-linearities, including harsh non-linearities such as those arising from backlash, as well as those that may involve additional state models, for example, from hydraulic dampers. This breakthrough significantly extends the reliability and applicability of invariant manifold-based non-linear modal analysis to the realm of strongly non-linear systems and/or large amplitude motions.

Non-linear modal analysis has been applied to the non-linear coupled axial and transverse vibrations of a uniform *rotor blade*. Both asymptotic and the new non-linear Galerkin methods were used, and both assumed-mode and finite element representations of the blade were considered. The result is that the non-linear Galerkin approach significantly out-performs all other methods. The large-amplitude reliability of this reduced order model and the versatility of the approach are the essential driving forces behind the current research program.
(**See Figures 68 & 69**)

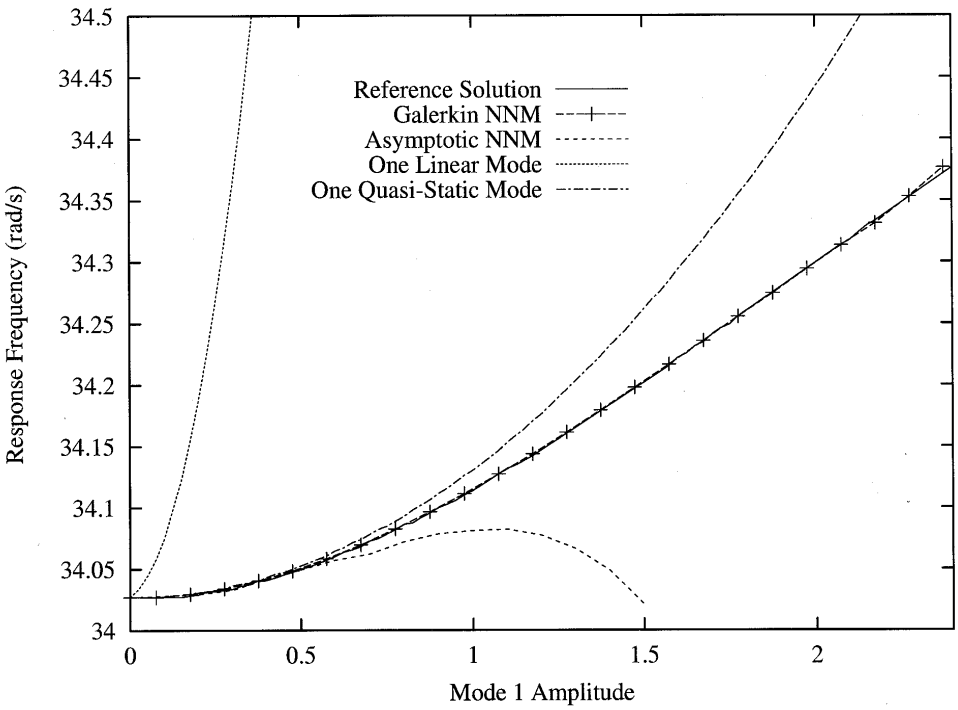

The frequency of the first non-linear flapping mode of a rotating beam (shown above) as a function of vibration amplitude, developed by a variety of approaches. Note how well the non-linear Galerkin method performs, for "peak-to peak" blade tip amplitudes greater than 10% of beam length, and how it outperforms all other methods.

Figure 68 Comparison of variations of the frequency response with amplitude as computed from different approximation schemes.

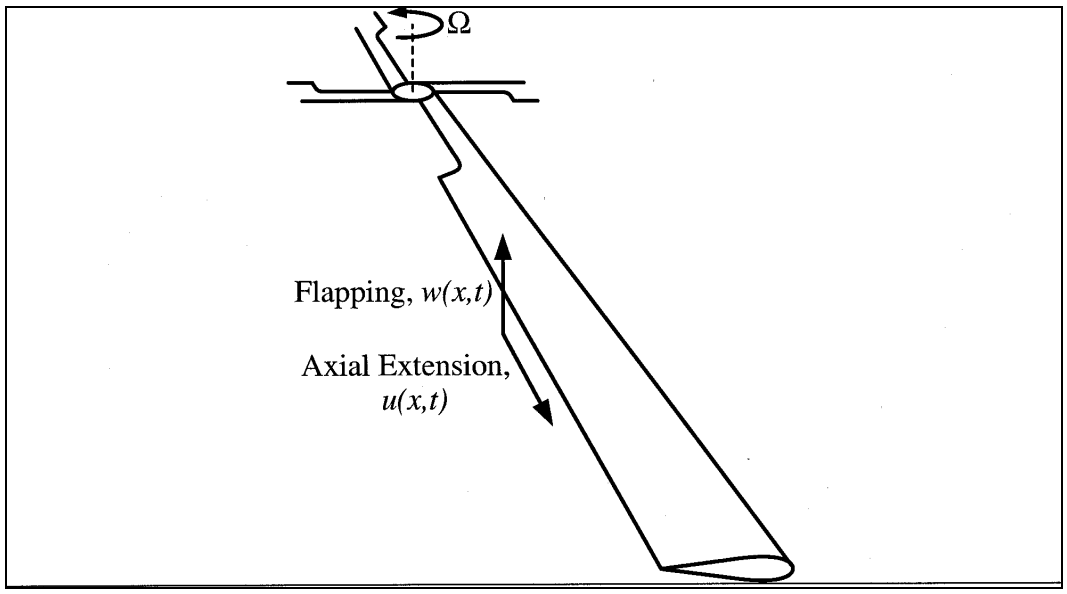

Figure 69 A helicopter rotor blade rotating at angular speed Ω that undergoes transverse flapping and axial extension deformations**.**

37370-EG "Surface Damping Treatments: Innovation, Design, and Analysis"

I. Y. (Steve) Shen and Per G. Reinhall, University of Washington

Objectives: The primary objective of this research project is to develop two innovative surface damping treatments: collapsed bubble constrained layer treatments and active standoff constrained layer treatments. Another objective is to conduct fundamental studies on surface damping treatments for beams, plates, and shells.

Approach: For collapsed bubble constrained layer treatments, a feasibility study is being carried out to ensure that the loss factor of the new treatment can increase by at least a factor of five. Simultaneously, a mathematical model is being developed to predict the increase of loss factor. For active standoff constrained layer (ASCL) treatments, calibrated experiments are performed to show that the passive and active components of ASCL have superior damping performance characteristics for wide-band and narrow-band excitations, respectively. In addition, a mathematical model is developed to predict the damping performance. Finally, the geometry of ASCL treatment is arrived at to maximize damping performance. For fundamental studies on beams, the current focus of the research project is to develop an experimental technique to directly measure thickness deformation of constrained layer treatments. An existing mathematical model verifies the laboratory measurements. Another fundamental study being carried out is directed toward investigating the situations under which the boundary conditions of Mead-Markus theory will fail. For fundamental studies on plates, the current focus is to develop novel dampers to control nonlinear vibration of flat plates subjected to high acoustic loading (>170 dB) and high temperature (400° F). For fundamental studies on shell damping treatments, the current focus is to develop an isoparametric finite element formulation for plates and shells subjected to constrained layer treatments.

Accomplishments: For collapsed bubble damping treatments, a thermal cycling process has been developed to manufacture microcelluar foams with collapsed bubbles (see the scanning electron microscope (SEM) photo in **Fig. 70**. For active standoff constrained layer (ASCL) treatments, an accurate mathematical model has been developed to predict the response from the passive component of ASCL treatments (**Fig. 71**). For fundamental studies on beam treatments, an experimental technique has been developed that directly measures thickness deformation of the viscoelastic layer with great accuracy. The direct measurements agree well with the proposed mathematical model (**Fig. 72**). In addition, various numerical simulations have shown that the boundary conditions proposed by Mead-Markus theory may yield inaccurate theoretical predictions. This phenomenon has also been verified by calibrated experiments (**Fig. 73**). For fundamental studies of shell damping treatments, an 18-node degenerate constrained layer element has been developed for plate and shell structures. For thin plate structures, numerical results show that the isoparametric element can predict the natural frequencies, loss factors, and mechanical impedance almost as accurately as NASTRAN with substantially fewer elements (**Fig. 74**).

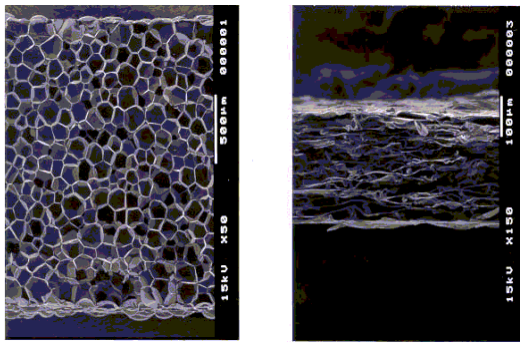

(a) (b)

Figure 70 SEM photo of thin microcelluar foams with collapsed bubbles: (a) uncompressed foam, (b) compressed foam

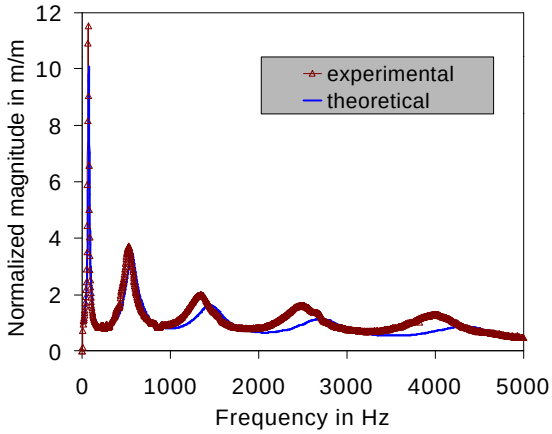

Figure 71 Theoretical and experimental frequency response function of passive stand-off layer treatment

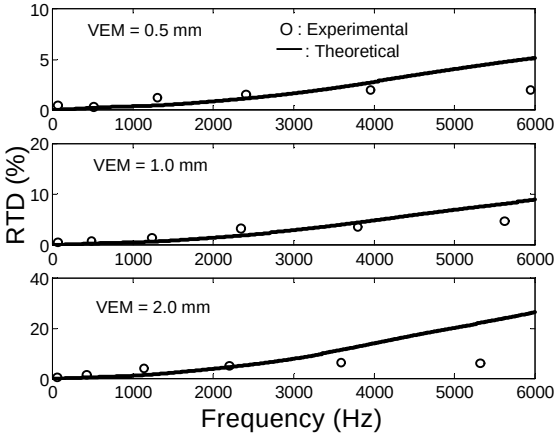

Figure 72 Theoretical predictions and experimental measurements of thickness deformation of constrained layer treatments

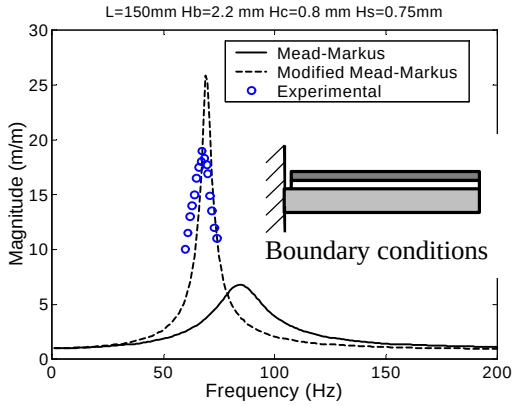

Figure 73 Deviation of Mead-Markus formulation for constrained layer treatments

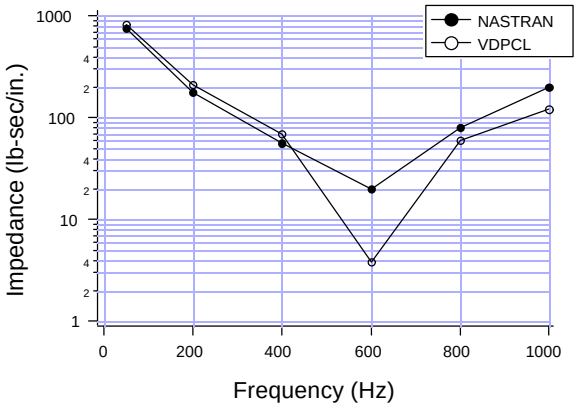

Figure 74 Mechanical impedance predicted by NASTRAN and isoparametric constrained layer plate element VDPCL

37394-EG "Design, Modeling and Testing of Smart Electromagnetic Structures (SEMS)"

Gregory Washington and Roberto Rojas,
Ohio State University

Objectives: The primary objective of this research project includes a utilization of active materials in the design of the next generation of antennas and electromagnetic devices. Inherent in this objective is the development of alternative uses of active materials. The type of devices that will be developed are electrically active (oscillator) integrated conformal/planar antennas, mechanically and electrically active microstrip patch antennas, and mechanically active reflector antennas. In addition, algorithms for control of these active elements and advanced electromagnetic field simulations will be developed. Advanced simulation techniques for smart electromagnetic antennas will also be devised.

Approach: In order to accomplish thoroughly the stated objectives, the following five mini- projects have been developed: Piezoceramic Active Aperture

Antenna Modeling and Testing, Ferroelectric Patch Design, Design of Electrically Active (Oscillating) Integrated Conformal Antennas, Advanced Simulation Techniques, and Electromagnetic Field Testing. The projects will be handled collaboratively by Dr. Gregory Washington of the Mechanical Engineering Department and Dr. Roberto G. Rojas of the Electrical Engineering Department.

Accomplishments: In the areas of Piezoceramic Active Aperture Antenna Modeling and testing and Active Patch Design, three major milestones have been achieved. The first lies in the completion of analytical models that predict aperture antenna shape from piezoelectric bias voltages to the actuators. The singly curved (cylindrically shaped) and doubly curved (bowl shaped) antenna models, with attached actuators have been completed and experimentally verified (**Figure 75**). They were tested this past summer at NASA Johnson aboard the KC135-09 micro-gravity aircraft and are now in the construction and the electromagnetic field testing stage. The second milestone lies in electromagnetic field testing of the mechanically active microstrip patch antenna. This antenna has the ability to vary its (operating) or resonant frequency and vary its bandwidth. Tests were conducted in the far-field range at NASA Glenn research center in Cleveland, OH. The final accomplishment is in the area of advanced simulations. An efficient technique for calculating the electromagnetic fields emanating from a large dielectric coated conducting cylinder has been developed. This technique will be used to model electromagnetic fields emanating from antennas mounted on the shell of a helicopter.

In the areas of Design of Electrically Active (Oscillating) Integrated Conformal Antennas and Advanced Simulation Techniques three milestones have been achieved (a) The development of an advanced field simulator to calculate the fields propagating on the surface of a dielectric coated cylinder. This simulator can calculate the mutual coupling between two antennas. It complements the field simulator developed last year, which calculates the fields radiated by an antenna. It can handle electrically large as well as small cylinders. Most available methods can only handle electrically small cylinders. It will be used in the study of coupled oscillators (two transmitting antenna elements), (b) the design of a single active integrated patch antenna mounted on a dielectric coated circular cylinder has started (once the design is completed, it will be built and tested), and (c) literature search and review completed for analysis and design of coupled oscillators. Mutual injection locking concepts as well as phase locked loops will be considered to synchronize two transmitting antenna elements.

37565-EG "Modeling Damping in High Performance Vehicle Systems"

Daniel J. Inman and Romesh C. Batra, Virginia Polytechnic Institute and State University

Objective: The main objective of this research is to improve the modeling of passive and active damping mechanisms and render these models more useful in finite element codes, and to increase an understanding of finite element modeling of rubber and viscoelastic components for advanced applications with complex states of deformation. This research is laying the

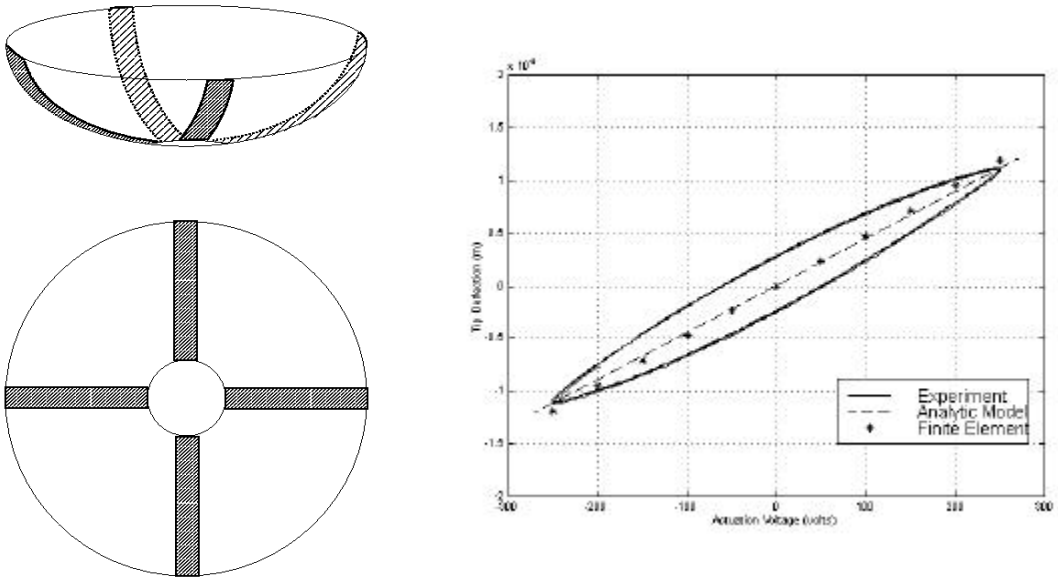

Figure 75 . Aperture Reflector Modeling and Design

groundwork for non-traditional uses of viscoelastic materials in both active and passive vibration suppression technologies. In addition, active control techniques are being used to improve analyses of structures using viscoelastic materials represented by internal variable methods.

Approach: The approach used in this research project is to investigate issues of basic mechanics modeling techniques for structures that include thermo-electro-mechanical properties of piezoelectric and viscoelastic materials. In addition, new ways to include internal variable representations of viscoelasticity into finite element codes are being investigated. Accurate modeling of physical phenomena is always relevant, particularly for next-generation Army structures. An accurate modeling of viscoelastic materials involves the selection of an appropriate and simple constitutive relation for modeling their finite deformations.

Accomplishments: Three-dimensional analytical solutions for thick laminated plates with piezoelectric layers have been developed. The method has been used to study the quasi-static deformation and steady-state vibration of plates with surface-bonded and embedded actuators. The displacements, stresses, natural frequencies, and mode shapes from the three-dimensional solution have been compared with those obtained from plate theories. Analysis of finite deformations in simple shearing, steady state oscillations of a cylinder, and slow finite shearing deformations of a constrained viscoelastic layer have been performed. The studies reveal that a linear relationship between the second Piola-Kirchhoff stress tensor and the history of the rate of change of the Green-St. Venant strain tensor does not predict results in agreement with the test

findings. However, predictions from the linear relation between the Cauchy stress tensor and the history of the rate of change of the relative Green-St. Venant strain tensor agree with experimental observations. It is therefore recommended that the latter constitutive relation be used. Responses of internal variables have been reconstructed from measured outputs using standard controls techniques for some preliminary cases. This facilitates full-state feedback, and the current research is seeking other options that will both model active control in the presence of viscoelasticity more accurately and affect how viscoelasticity is modeled in standard finite element codes. The attached plot demonstrates reconstruction of an internal variable from measured output (See **Figure 76**).

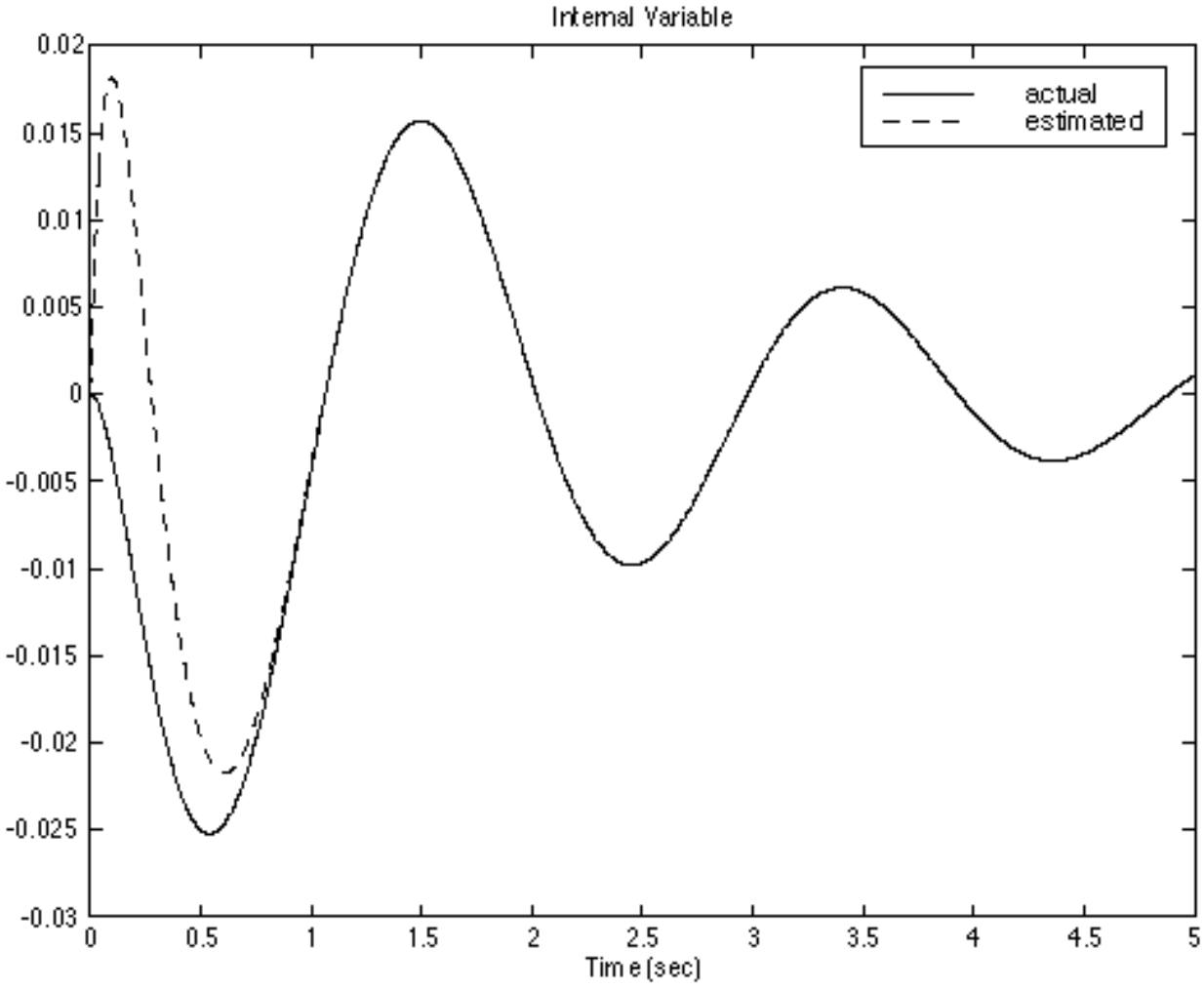

Figure 76

37705-EG "Optimal Design of Smart Actuators and Structures"

Jahangir S. Rastegar, State University of New York at Stony Brook

Objectives: The main objective of this research is to develop novel systematic methods for relating the effects of structural flexibility and nonlinear characteristics to the dynamic behavior of mechanical systems. The methods are particularly suitable for optimally tailoring smart material based actuation devices for integrating them into the structure of machines for the purpose of significantly reducing vibration and increasing the system performance and precision. Another objective is to develop an integrated structure and task-specific optimal design methodology for high speed and precision machines with integrated smart materials. Modeling and developing design methodology for a number of novel hybrid smart materials based actuators for large displacement and fast dynamic response is an additional objective of this research effort.

Approach: The methods being formulated are based on "tracing" the propagation of the high frequency component of motion along the structural elements of machines and determining the effects of structural flexibility; kinematics constraints (e.g., closed-loop chains); and dynamic non-linearity on the response characteristics of a system. The methods clearly identify the mechanisms with which structural flexibility and non-linear dynamics of a mechanical system affect the dynamic response. The primary advantage of these novel methods is that they naturally lead to a systematic methodology for designing high speed and precision mechanical systems with integrated smart materials by tailoring them to the inherent requirements of the system to achieve optimal performance, i.e., providing minimal internally generated vibrational excitation, maximum vibration damping and high precision.

Accomplishments: The following results have been generated under this research effort. Theoretical foundation of the proposed methods has been laid by proving that the effect of flexibility of a structural element of a nonlinear dynamic system is to "filter" the higher harmonic components of its input motion. For systems with kinematics constraints, (i.e., with closed-loops), the result of the filtered high harmonic component of motion is an increase in the amplitude of the higher harmonics of the system output. The effect of structural flexibility of a nonlinear dynamic system is to increase the demand on the dynamic response ("bandwidth") of the system drives (actuators). It was shown that the (undesirable and vibration inducing) high harmonic motions of the structural elements and the system output may be eliminated by using appropriately sized (in terms of force, displacement and "bandwidth") and positioned smart materials based actuation devices. Furthermore, by increasing the operating speed of a non-linear dynamics system, a speed is reached above which the dynamic response of the system becomes non-periodic. Also, the proper integration of smart materials based actuators into the structure of a machine can significantly increase the range of operating speed within which periodic dynamic response can be obtained. An experimental testbed is being designed for the purpose of validating the obtained results and the developed optimal smart materials integration methodology.

37747-EG-DPS "A Novel Magneto-Rheological Shock Absorber for Vibration Control"

Faramarz Gordaninejad, University of Nevada at Reno

Objectives: The primary goal of this research project is to develop a basic understanding of the non-linear force-displacement and force-velocity behavior of a new magneto-rheological fluid (MRF) damper. The major research issues and the specific objectives of the project are: (1) to develop a theoretical model which predicts non-linear behavior of the new MRF damper; and (2) to conduct a comprehensive experimental study on the proposed MRF damper to validate all theoretical findings. Particularly, the focus of the research is on the specifications required for the U.S. Army's high mobility multi-purpose wheeled vehicle's (HMMWV) suspension system.

Approach: Both theoretical and experimental studies are performed to evaluate the University of Nevada, Reno (UNR) MRF shock absorber. The Bingham Plastic and Herschel-Bulkley non-Newtonian fluid theories are employed to analyze the non-linear behavior of the MR fluid. Because the MRF damper uses an incorporated electromagnet for controlling the fluid shear yield stress (and ultimately the damping), a three-dimensional magnetic finite element analysis was performed on the device to determine material types, magnetic wire size, magnetic saturation of fluid, power requirements and optimal geometry for the best MR-effect (the method of changing shear yield stress). This effort began with creation of a three-dimensional solid model, which can be directly ported into different finite element software packages.

Accomplishments: Several prototype UNR MRF dampers have been developed and tested which explore the design parameters. These dampers were tested for a wide range of frequencies, displacements and input currents. Test results show that the new MRF fluid shock absorbers can provide three to four times the amount of damping force than provided by the original equipment manufacture (OEM) units. In addition, without electrical current applied, the UNR MRF damper acts as a passive shock absorber, providing the same performance as the OEM unit. This new design of MRF damper has also addressed the issue of fluid sealing by adopting a seal pack that does not leak fluid. This prototype MRF fluid damper has undergone over more than 1000 different tests without any fluid leakage. As shown in **Figures 77 and 78**, the theoretical and experimental results for force-displacement and force-velocity are demonstrated to be in excellent agreements. Since MRF fluid dampers are energy dissipating devices, the issues of heat generation and dissipation are important. The UNR MRF damper is also experimentally evaluated for temperature changes that results from various types of sinusoidal input motions. In addition a theoretical model is developed which predicts the temperature increase of the MRF dampers. This model is solved numerically, and is compared with experimental results. It has demonstrated that the temperature effect on the damping force is significant and must be considered in modeling and development of the control system for MRF dampers.

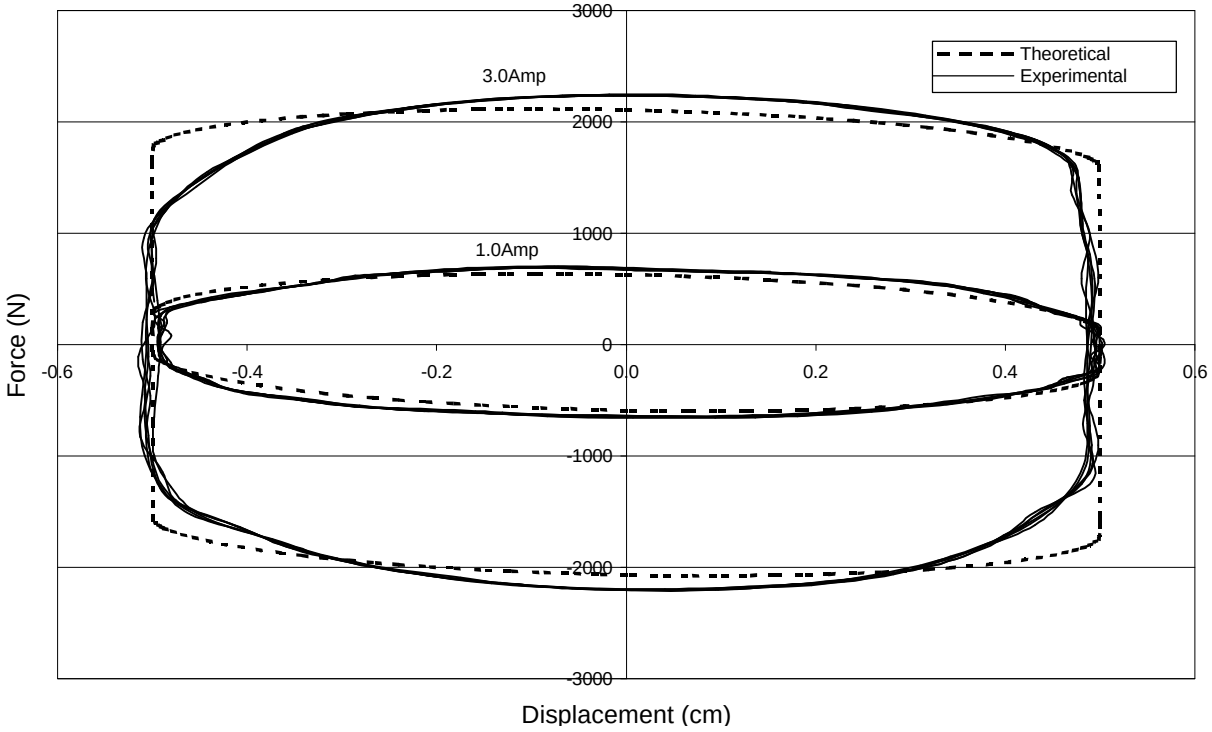

Figure 77 . Comparisons between theoretical and experimental force-displacement results of the MRF HMMWV damper for zero-field and 3.0 Amp input electric current.

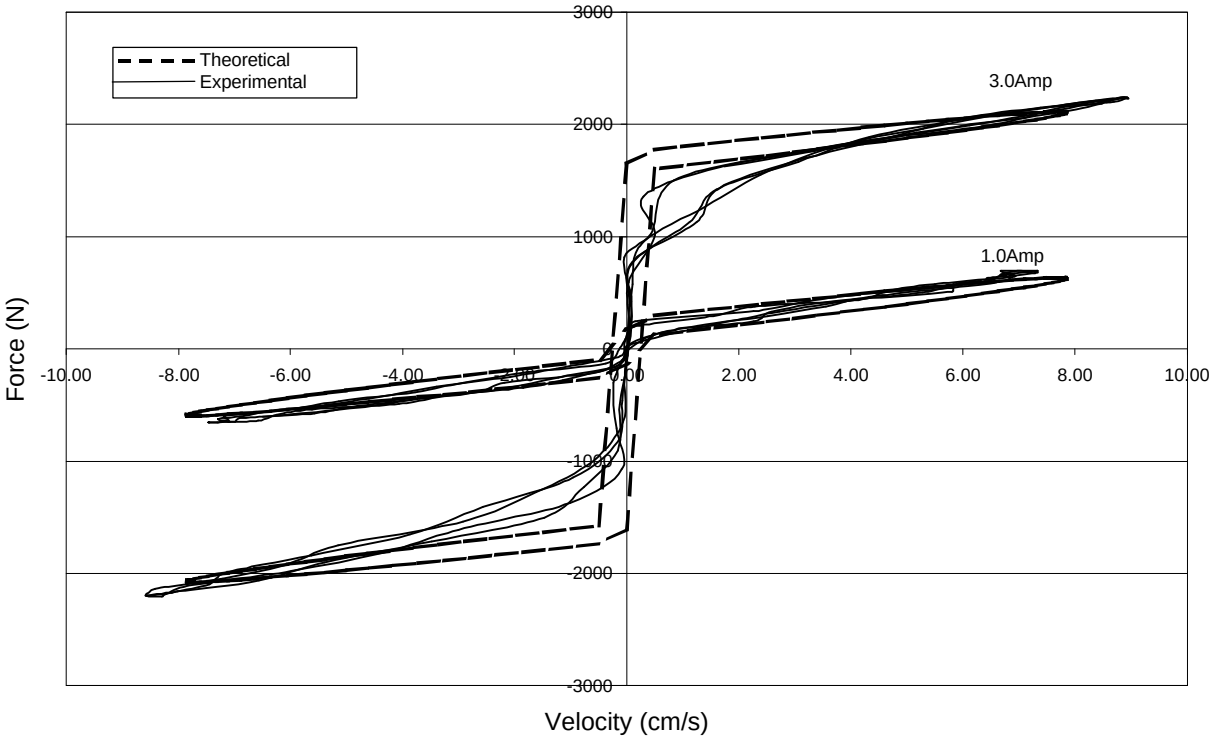

Figure 78 Comparisons between theoretical and experimental force-velocity results of the MRF HMMWV damper for zero-field and 3.0 Amp input electric current.

37803-EG "Research in Damper Free Rotor Design Based on MAPLE® Generated Non-Linear Simulation"

E. Roberts Wood, Naval Postgraduate School

Objectives: The objective of this research project is to develop a general rotor stability and analysis tool by applying concepts from modern dynamics, control theory and enhanced computer graphics. This tool takes advantage of symbolic processing to derive the full error-free non-linear equations of motion for the helicopter rotor/fuselage system. The resulting analysis tool is no longer hampered by the usual limitations that would restrict the method to small amplitudes and angles, linear springs, linear dampers and prescribed ordering schemes for variables. This work has the potential for generating a new rotor design methodology that eliminates the need for lead/lag dampers.

Approach: The method is based on using MAPLE® software for dynamic non-linear simulation. This simulation tool permits detailed studies of rotors with non-linear material properties instead of expensive dynamic model testing. The simulation work has generated a non-linear design parameter that may be used to design a damperless rotor. A damperless rotor would benefit all military services, since Army, Navy, Marines and the Air Force employ helicopters extensively. Blade dampers lead to costly maintenance and corrosion problems. Blade lead-lag instability, when it occurs, can build up to destructive proportions in a matter of seconds.

Accomplishments: Numerical simulations of hub and blade lag motion were carried out in Simulink®. In place of auxiliary lag dampers, the analysis introduced non-linear flexbeam stiffness properties at the blade root to limit in-plane motion of the blade. For the initial analysis, flexbeam stiffness properties were modeled in the manner of a classic Duffing-type, cubic stiffness, spring (**Figure 80**). The effect of interconnecting the blades was also investigated for rotor stability control using a four-bladed rotor simulation developed specifically for this project. Efforts have also been successful in "streamlining" the analysis to simplify running it and to accelerate its run time. Initially in the "derivation approach", the MAPLE®-derived equations of motion (EOM) were "cut and pasted" by hand into a Matlab-format file for use by the Simulink® simulation package. A derivation and checkout of an "automated cut and paste" approach from Matlab has been completed. A study on how to best "automate" the "cut and paste" process from MAPLE® has been in progress. Such automation will eliminate labor in running the problem as well as avoid any potential errors introduced due to editing by hand. One Ph.D. dissertation, two Master of Science in Aeronautical Engineering (MS/AE) theses, two journal papers, and four conference papers have been authored describing the result obtained during this project, including the 1999 American Helicopter Society (AHS) Lichten Award paper.

37828-EG-DPS "Femtosecond Laser Assisted Manufacturing of High Speed Quartz Oscillators

Dennis R. Alexander and **Dana E. Poulain**, **University of Nebraska–Lincoln**

Objective: To use new femtosecond laser nano-machining manufacturing techniques to develop higher speed electronic devices; to develop techniques for producing quartz crystal oscillators that have selected

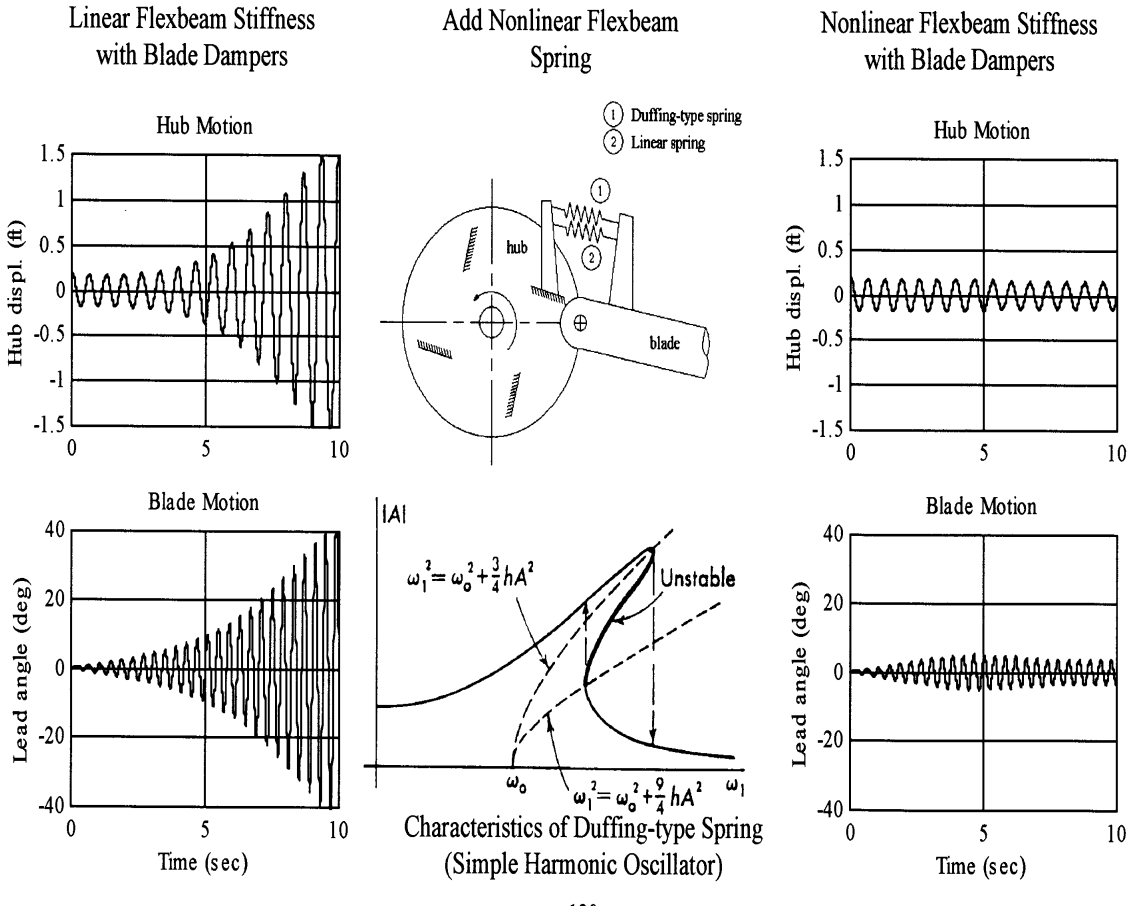

Figure 80 Comparisons of Hub and Individual Blade Responses Show Significant Attenuation with Duffing-Type Nonlinear Characteristics in Flexbeam.

overtones; to understand the basics of femtosecond laser nano-machining of quartz, semiconductor materials, and other brittle materials.

Approach: The new approach is to use femtosecond laser pulses to remove nano-layers of materials and to drill high aspect ratio holes, ~1 mm in diameter, in electronic chip materials. This new manufacturing method has the potential to have higher precision than chemical etching techniques and the material removal processes can be monitored and controlled in real time. Furthermore, the new femtosecond laser machining process is superior to longer pulsed laser machining. This process eliminates small crack formations since micron-sized holes can be drilled with aspect ratios greater than 20-to-1. These high aspect ratio holes can provide integrated chip manufacturers a method to access electronic conducting paths and thus perform failure analysis on electronic chips. Because femtosecond laser/material interaction breakdown thresholds are very sharp, diffraction limited optical processes can be defeated. As a result, sub-surface channels are possible as well as holes smaller than the diffraction limit. These channels offer the possibility of 3-D interconnects and subsurface data storage.

Modern electronic devices used by the U.S. Army require greater processing speeds with smaller and smaller physical size. It is important for the U.S. Army to maintain superior computer, electronic and telecommunications systems that have the highest data transfer rates possible. This is especially true when one looks at the need to transmit and process the ever-increasing volume of video data. New manufacturing techniques must be developed to produce quartz crystal oscillators, micro-electro-mechanical systems (MEMS), surface acoustic wave (SAW) devices, and other new electronic devices with long term durability. In addition to manufacturing techniques, the ability to perform failure analysis on integrated circuit devices is of great importance to the U. S. Army. The investigators' current research is leading to new manufacturing techniques for brittle materials, such as quartz crystal oscillators, and the ability to drill 1 mm diameter holes in semiconductor devices for failure analysis studies, in Kovar metal alloys (e.g., neutron generator getters for nuclear weapons applications), and in other DoD applications.

Accomplishments: A unique femtosecond laser machining facility has been established at the University of Nebraska-Lincoln (UNL). Melles Griot x-y-z nano-movers and associated software (developed under this contract) and controllers allow the researchers to machine materials in a discontinuous manner which eliminates micro cracking in brittle materials. In addition to the removal of nano-layers of brittle quartz materials, high aspect ratio holes are being drilled in metals (e.g., aluminum and Kovar) and semiconductors. The UNL team is currently drilling small holes in Kovar, which will be used in the getter part needed for nuclear weapon maintenance. These new manufacturing techniques are being used by M-Tron to generate next generation quartz crystal oscillators. Advanced Micro Devices (AMD) is using the new manufacturing technique to drill 1mm holes in SiO_2 and silicon for failure analysis studies of integrated circuits. Research has also shown that it is possible to fill these holes with gallium to produce micron-sized conducting paths. The manufacturing technique developed under this ARO

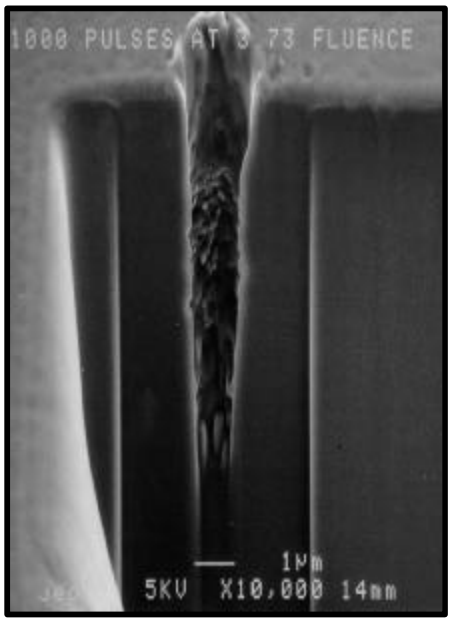

←TOP LEFT

High aspect ratio hole drilled in silicon by femtosecond laser nanomachining. Diameter is ~1 mm.

RIGHT →

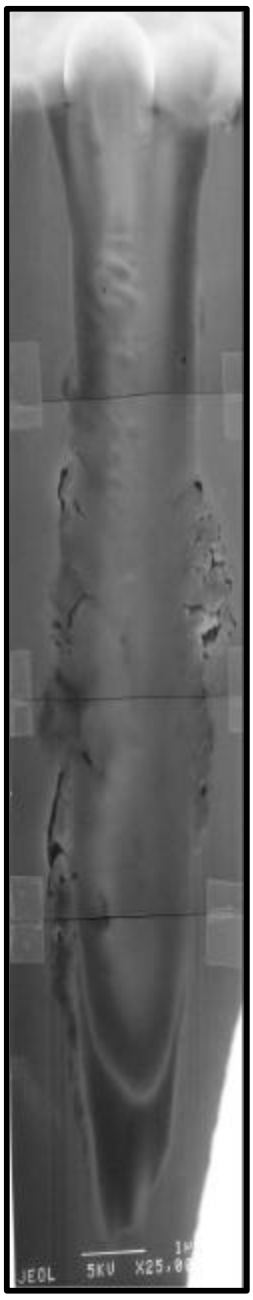

High aspect ratio hole back-filled with gallium.

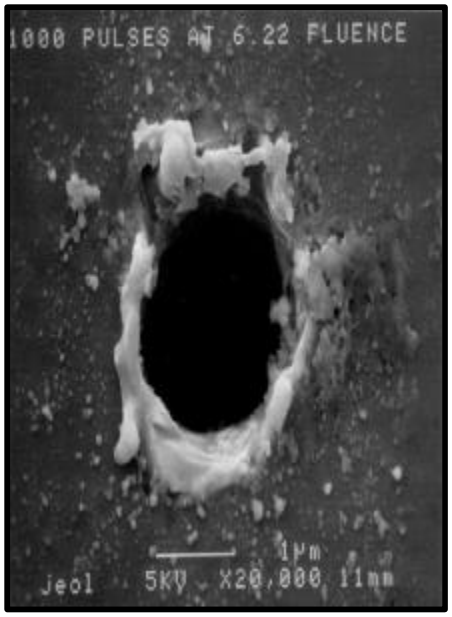

←BOTTOM LEFT

Top view of a hole drilled in silicon by femtosecond laser nanomachining. Note the nano-sized silicon particles around the hole.

Figure 81

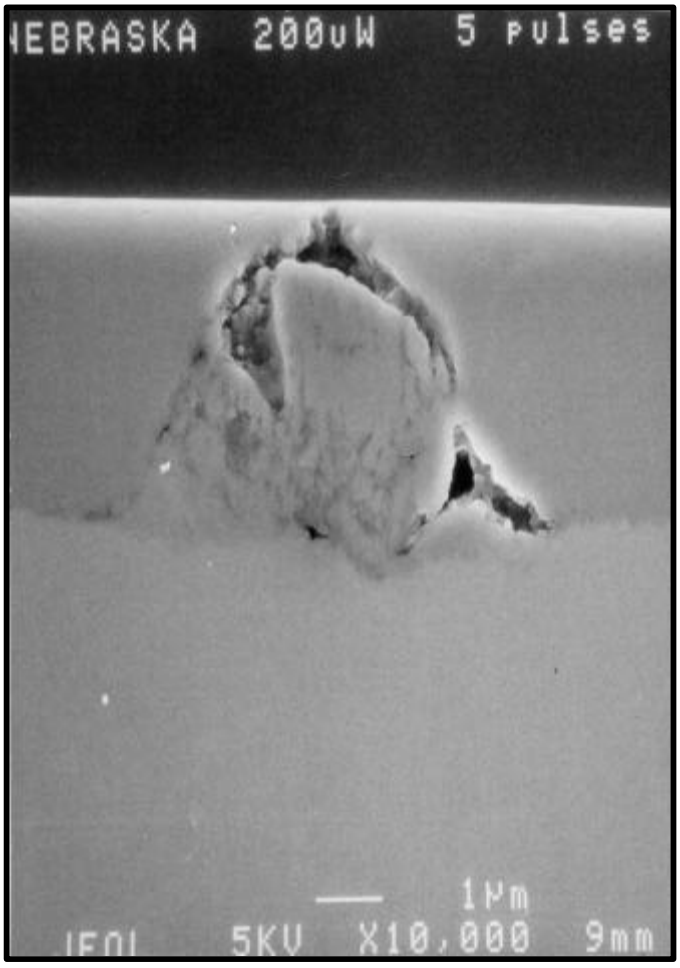

SEM cross-section image of a subsurface channel formed in a silicon substrate with a 3 µm oxide coating. Such channels offer great potential for 3-D interconnects and subsurface data storage.

Figure 82

contract is being used by NASA Johnson Space Flight Center to cut and process aerogel samples containing comet particulates returned from space missions.

Engineers at the Sandia National Laboratories are interested in duplicating the UNL femtosecond laser nano-machining manufacturing facility. Having Sandia National Laboratories become interested in the manufacturing capabilities developed under this ARO contract is indeed an accomplishment.

37856-EG-DPS "Space-Based, Long - Distance Laser Pointing and Tracking"

John E. McInroy and Jerry C. Hamann, University of Wyoming

Objectives: The following three main objectives are being pursued in this research project for rapidly and reliably acquiring and maintaining a laser on a long-distance, space-based target (or receiver):

1. A pointing system capable of locking onto the position of a target (or receiver) over a wide field-of-view is being developed. The lock will be maintained despite vibrations aboard the transmitting and receiving platforms, relative motion between the platforms, and some component failures.

2. A test-bed capable of physically simulating space-based pointing and tracking systems is being established. Six degree-of-freedom satellite vibrations will be induced in the transmitting and receiving platforms. Relative motion between the platforms will be created. Sensing time delays will be included.

3. The pointing/tracking system and test-bed are being combined to test operation under a variety of scenarios. Different distances, pointing accuracies, relative motions, etc. will be evaluated.

The hexapod platform, developed at the University of Wyoming to provide (a) high precision pointing, (b) vibration isolation, and (c) programmable/repeatable disturbances in six axes, is a six-legged parallel kinematic machine.

Approach: This project is developing the technology necessary to incorporate within a hexapod structure the attributes of the most advanced pointing and tracking systems (including inertial stabilization, active pointing, and fault tolerance). This will allow the laser mount to consolidate several functions, with the resulting cost and weight advantages. Note that laser weapons are but one application of this very general pointing and tracking approach. For example, space-borne laser communications, where both a transmitter and an active receiver are utilized, constitute an additional promising application area. High power laser weapons provide a striking example of the hexapod's utility in pointing and tracking applications. Most high power lasers bear some relationship to jet engines because flowing gases are combusted to produce light energy. This process generates significant unwanted vibrations. A hexapod, in some ways, is similar to the structural designs used for decades to mount aircraft engines. That is, six members are designed to carry predominantly axial loads so that the engine is rigidly constrained in all six degrees-of-freedom by a lightweight structure. The hexapod replaces the rigid axial members with active devices capable of absorbing vibrations and precisely pointing.

Accomplishments: A test-bed has been constructed with two custom designed hexapods (**Figure 83**). Pointing and vibration isolation algorithms have been developed and verified on the physical system. Analytical efforts to better model the interaction of the vibration disturbance platform and the precision pointing system are currently under investigation. Pointing precision has been demonstrated to within tolerances required for long-distance laser communication even in the presence of significant vibrational disturbances and limited actuator faults.

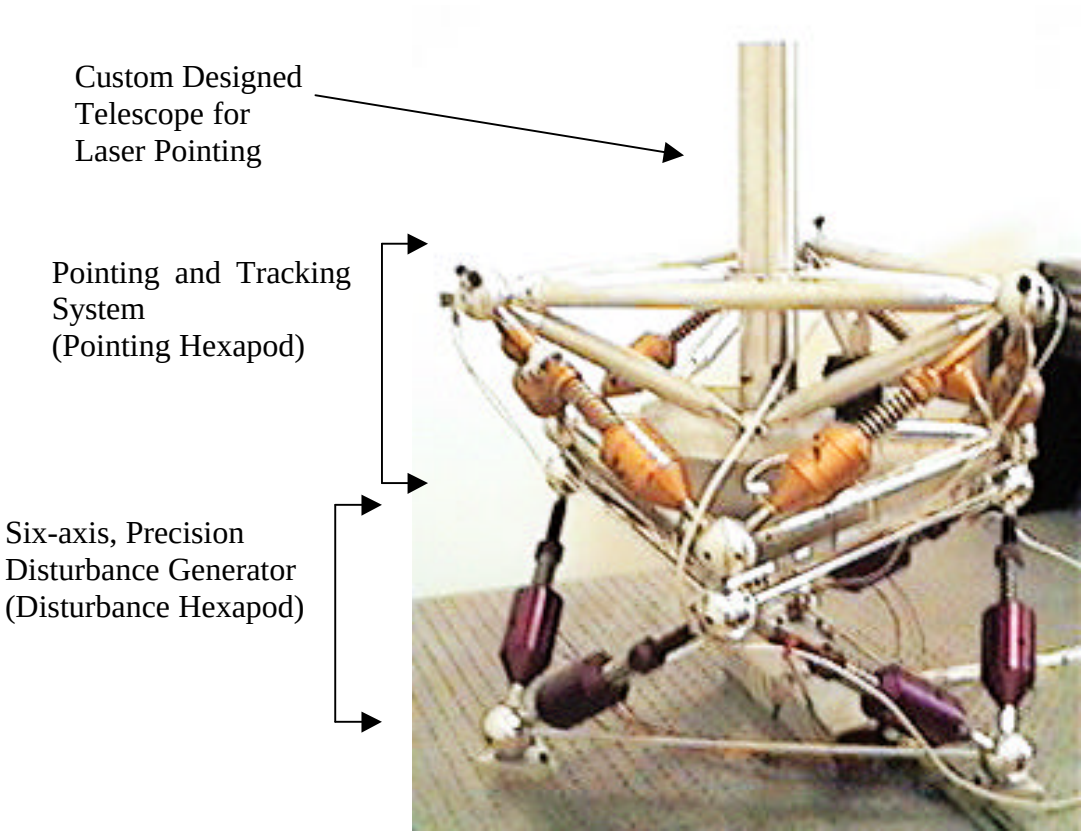

Figure 83

38714-EG-AAS "Active and Passive Magnetic Composites"

A. Baz, University of Maryland

Objectives: The major objectives of this research project are as follows:

1. Develop finite element models (FEM) to describe the static and dynamic characteristics of the Magnetic Composites (MC).

2. Validate the predictions of the FEM models of the Magnetic Composites against the predictions of commercially available software packages (COSMOS).

3. Experimentally evaluate the effectiveness of the Magnetic Composites in controlling the vibration of flat plates in comparison with nonmagnetic damping composites.

Approach: In order to meet the above three objectives, the following approach is utilized.

1. A finite element model (FEM) is developed to describe the interaction between the visco-elastic damping layer, the base structure and the magnetic strips. Particular emphasis is placed on structures that are either fully or partially-covered with MC.

2. The predictions of the static and dynamic FEM are validated using the currently available software package of COSMOS/M. The validation process involves the effect of the different lay-up and stacking configurations of the magnetic strips. The effect of the magnetic parameters of the strips and the structural boundary conditions are also to be investigated.

3. Experimental plates will be built and treated with optimally placed patches of the MC. The performance of the plates will be monitored under various types of external excitations (tonal and random vibrations) to evaluate the effectiveness of the MC in attenuating the resulting vibrations.

Comparisons will be made between MC and unmagnetized strips in order to define the merits and limitations of the proposed MC. (See **Figures 84 - 86**) Emphasis will be placed on orientation of the magnetic strips with respect to the plates' sides in order to demonstrate the capabilities of damping several modes simultaneously.

Accomplishments: Several journal papers have been published that describe the results obtained during the course of this research project. In addition, a doctoral dissertation has been completed. The Magnetic Composites, which are manufactured from magnetic strips and/or magnetic fibers, woven in a braided fashion to form intricate fabric, are suitable for making base isolators, cushions, passenger seats and other flexible mounts. Such a new class of magnetic composite can provide multi-axis damping and support for critical instruments and structures. It can also be used as a self-damped acoustic coating for various types of enclosures such as power tools, passenger cars, helicopter cabins, and aircraft fuselages.

Active and Passive Magnetic Composites

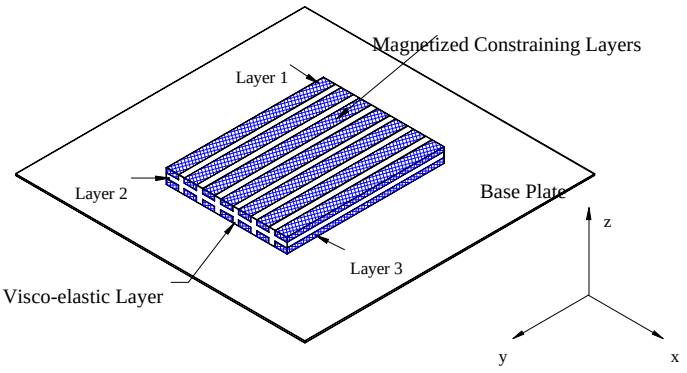

Figure 84 Schematic drawing of the **P**assive **M**agnetic **C**omposite (**PMC**) treatments of a plate

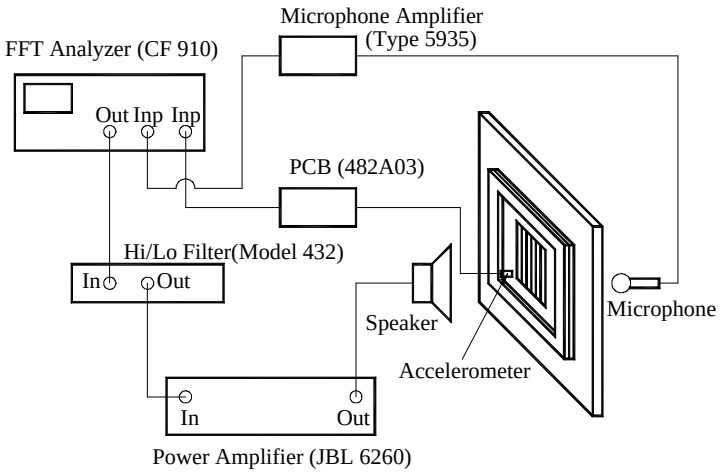

Figure 85 Experimental set-up for dynamic measurements

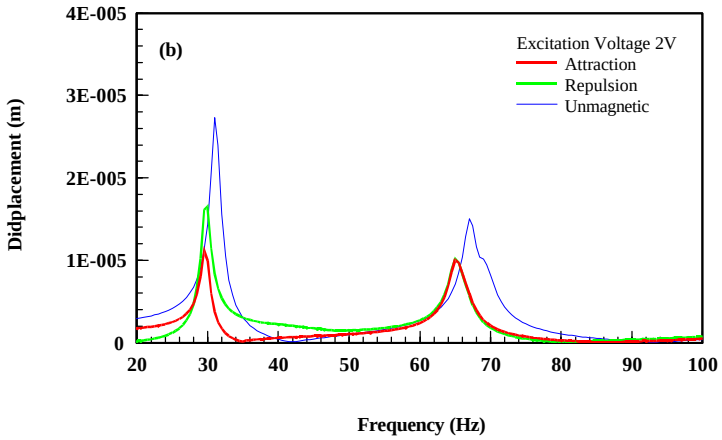

Figure 86 Comparison between attraction and repulsion configurations for **PMC** with plate

38768-EG "Non-linear Dynamic Simulation and Control of Military Ground Vehicles"

Andrew J. Kurdila, University of Florida

Objectives: This research program seeks to derive, develop, implement and validate formulations for non-linear, multi-body dynamics for military ground vehicles. The objectives of the research program include:

1) The derivation of a general theory for constraint stabilization methods designed to improve the accuracy and stability of simulations for non-linear, flexible vehicle dynamics with a large number of degrees of freedom

2) The derivation and development of robust non-linear multi-body simulation methods that accommodate and compensate for known, intrinsic instabilities corresponding to configuration dependent singularities associated with closed kinematic loops in vehicle suspension systems.

3) The derivation and development of virtual prototyping capabilities that facilitate the simulation of coupled vehicle dynamics and weapon subsystem dynamics.

4) The derivation and development of low dimensional reduced order models for the simulation of flexible components within multi-body models of vehicle dynamics.

Approach: A theory for utilizing Lie algebraic formulations to enable constraint stabilization, and thereby enable, inherently parallelizable formulations of multi-body dynamics has been derived and validated on prototypical simulations. The stabilization techniques have been verified and validated on multi-body models including the HMMWV (High Mobility Multipurpose Wheeled Vehicle) models developed at the Redstone Arsenal. Further refinements of the vehicle models include a weapon sub-system developed in collaboration with Picatinny Arsenal researchers.

Accomplishments: The technical aspect of these formulations has been accepted for publication in peer reviewed journals *Philosophical Transactions, Royal Society of London A*, and *Nonlinear Dynamics*. In addition to the derivation of stabilization techniques, the researchers have derived and developed mode scheduling methods that yield reduced order structural mechanics models for flexible sub-assemblies and components. The modal scheduling models are based on hybrid system dynamics and switched system representations. Effective error indicators that are based on the residual measures of modal participation are used to drive switching dynamics within the multi-body formulation. The stability of the switching strategy is established using the method of multiple Lyapunov functions. Stability is reduced to the solution of a linear matrix inequality corresponding to quadratic stability of the switching system. The theoretical aspects of switching stability as it pertains to modal scheduling has been presented at the *41st Structures, Structural Dynamics and Materials Conference, April, 2000.*

38770-EG-ST2 "Fatigue Reliability Prediction of Tapered Composites"

Robert Tryon and Animesh Dey, PerSyst Development Group, Inc.

Objectives: The primary objective of this project is to predict the reliability of composite structures subject to fatigue delamination, buckling, and several other failure modes through integration of a probabilistic analysis framework with current laminate design methodologies. The end product of this project will yield a software enabling the design engineer the capability to predict component reliability, identify and prioritize the reliability, and optimize the structural design of aerospace components (**Figure 87**). This project was focused at design development of a composite helicopter rotor hub.

Significance: The material and geometric properties of composites, and applied loads typically have significant variability. Variability can come from manufacturing methods, raw material batches, environmental conditions, or other sources. Traditional design methods normally rely on testing for variability analysis. This is both time consuming and costly. Seldom are test data available soon enough to cost effectively streamline the design process. According to research partner, Bell Helicopter, typical certification test requirements for the rotor hub design model will cost approximately $1 million. It is estimated that use of software being developed under this Army project has the potential to reduce certification cost by at least a third. Additionally, the design development (cycle) time could be shortened by months.

Accomplishments: This project has successfully demonstrated that the analysis software developed under this Army SBIR accurately predicts failure probability for composite aerospace components. **Figure 88** compares the prediction results against data obtained from traditional flexbeam testing of a composite helicopter rotor hub.

Bell Helicopter is currently beta testing the software developed under this SBIR program. This project will yield methodology and software with potential to improve development of new rotorcraft using modern composite materials and technologies, and is especially relevant to damage tolerance and crash-worthiness analyses. More information on this project is available by contacting the investigators at 1-877-776-2878.

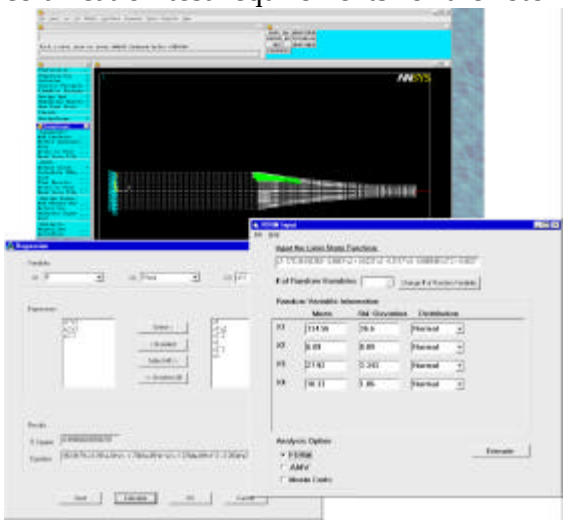

Figure 87 Analysis software developed under Army SBIR

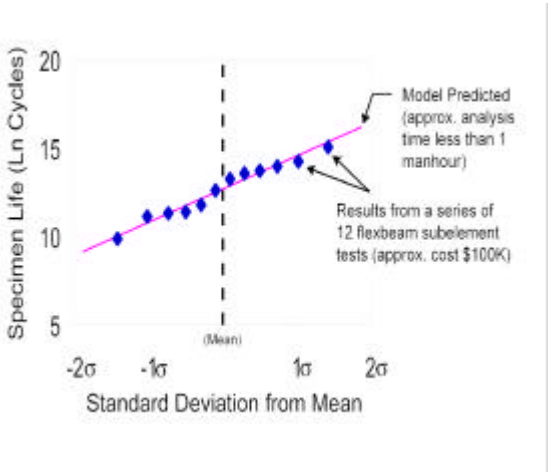

Figure 88 Comparison of software predicted results against Bell Helicopter test data.

38852-EG "Computerized Design, Generation, and Simulation of Meshing and Contact of Gear Drives with Modified Gear Tooth Surfaces"

Faydor L. Litvin, University of Illinois at Chicago

Objectives: The major objectives of this research project are as follows:

(1) An analytical and computational investigation of the influence of errors of alignment on transmission errors and contact of gear tooth surfaces; and

(2) Development of computerized design of low noise and stable bearing contact of gear drives.

The proposed principles are general and may be applied to a variety of gear drive types and configurations; for instance, to spiral bevel gears used in helicopter transmissions. Typical examples of application in the project are new types of face worm gear drives that might be used in Army tank and helicopter transmissions.

Approach: The novelty of the developed approach lies in the proposed modification of the gear geometry. The modification requires double crowning of the driving member of the gear drive that enables to provide a localized bearing contact, avoid edge contact, amend the shape of error function and the magnitude of transmission errors, and reduce vibration and noise levels. A new approach has been developed for computerized simulation of meshing and contact of gear drives. The computer programs are written in Visual Basic language. Use of this software yields a combination of numerical computations and graphical illustrations of resulting bearing contact and transmission errors (see **Figure 89**).

Accomplishments: New types of face worm gear drives with cylindrical and conical worms and substantially improved versions of conventional worm gear drives have been developed, and design and simulation of meshing and their contact geometry have been computerized. The output from the computer programs has confirmed the validity of the developed ideas. These new concepts have been extended for modification of helical and spur gears. A patent on modified helical and spur gears has been claimed by Visteon/Ford on the basis of license from UIC (University of Illinois at Chicago). Also, the developed ideas of designing low-noise, stable bearing contact gear drives have been successfully implemented in the case of spiral bevel gears at the Bell Helicopter Company.

38856-EG-YIP "Active/Passive Damping Control of Rotor Systems"

Norman M. Wereley, University of Maryland

Objectives: The primary objective of this research project is to augment helicopter lag mode damping by at least 50% by the year 2000 with an ultimate increase of 100% by 2005. This is based on the DoD Rotary Wing Technology Development Approach (RVW-TDA) goals. Advanced rotor designs (e.g., RAH-66 Comanche) tend towards hingeless and bearingless rotors to reduce life cycle costs (fewer parts) and improve handling qualities. Due to stress and weight considerations, advanced rotors are soft-inplane, and are susceptible to aeromechanical instabilities. However, lag damper effectiveness is reduced for advanced rotors due to small displacements near blade roots. This reduced effectiveness, coupled with high

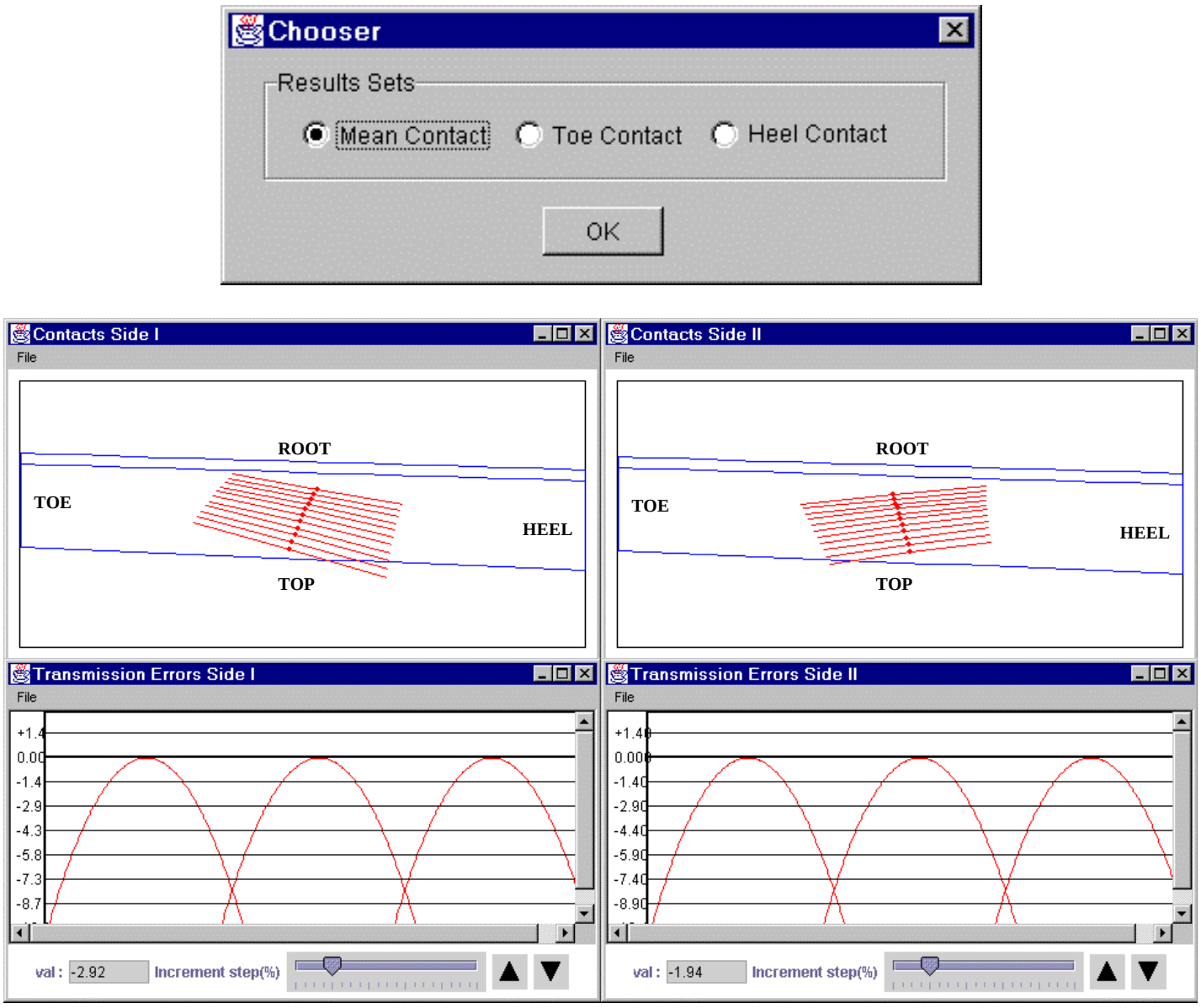

Figure 89 Example of output from the simulation program

maintenance cost, and weight/drag of mechanical dampers, and high cost of existing elastomeric dampers, makes alternative rotor stability augmentation schemes attractive. Analytical and experimental studies of lag mode dampers and damping augmentation strategies using magnetorheological (MR) fluids are the main focus of this research effort.

Approach: The research approach used under this program was to design, fabricate and test a linear stroke magnetorheological damper (**Figure 90**). This damper has several features that are important for its performance. The magnetic circuit consists of a magnetic coil wrapped around a bobbin, which is inserted concentric to a tubular magnetic flux return that forms the outer wall of the damper piston. The bobbin and flux return forming an annular MR valve through which the MR fluid flows. This design of the magnetic circuit ensures that the magnetic flux lines are perpendicular to the direction of flow (axial flow is along the piston/rod axis). A nitrogen gas accumulator is used to account for thermal expansion of the fluid, changing rod volume, and to prevent cavitation. A leakage valve is used in parallel with the MR valve to smoothen the force response. The damper was tested using a scotch-yoke type mechanical damper dynamometer that induces sinusoidal motion of the piston in the damper. The force is measured via a load cell, and the displacement and velocity via LVDTs. These force versus displacement and force versus velocity hysteresis cycle data are shown as symbols in **Figure 91** for the damper with leakage. As the magnetic field increases, the area within the force versus displacement hysteresis cycle increases, indicating that the damper is dissipating more energy. The yield force of the damper is the intercept of the high-speed asymptote of the force versus velocity diagram with the force axis. As the magnetic field increases, the yield force also increases, indicating that the yield stress of the fluid is increasing.

Accomplishments: The damper was designed using a non-linear fluid mechanics analysis, based on a Bingham plastic constitutive shear flow relationship. The analysis (solid lines in **Figure 91**) predicts the force response, which agrees very well with experimental data. For control purposes, a damping coefficient, C_{eq}/C, assesses damper performance. This is a ratio of the non-linear or magnetic field controllable damping, $C_{eq,}$ to the zero-field or passive damping, C (**Figure 92**). Ideally, for controllable damping, such a ratio should be much greater than 1. For this damper, the damping coefficient can be as high as $C_{eq}/C = 20$. A key advantage in control design is that the MR damper only extracts, and does not inject, energy into the rotor, which guarantees that the MR damper will be a stabilizing influence. By exploiting this controllable damping capability, the DoD goals of 50-100% increase in inherent lag damping can be realized. Studies are ongoing under this research program to assess the performance of non-linear adaptive control algorithms for augmenting rotor stability.

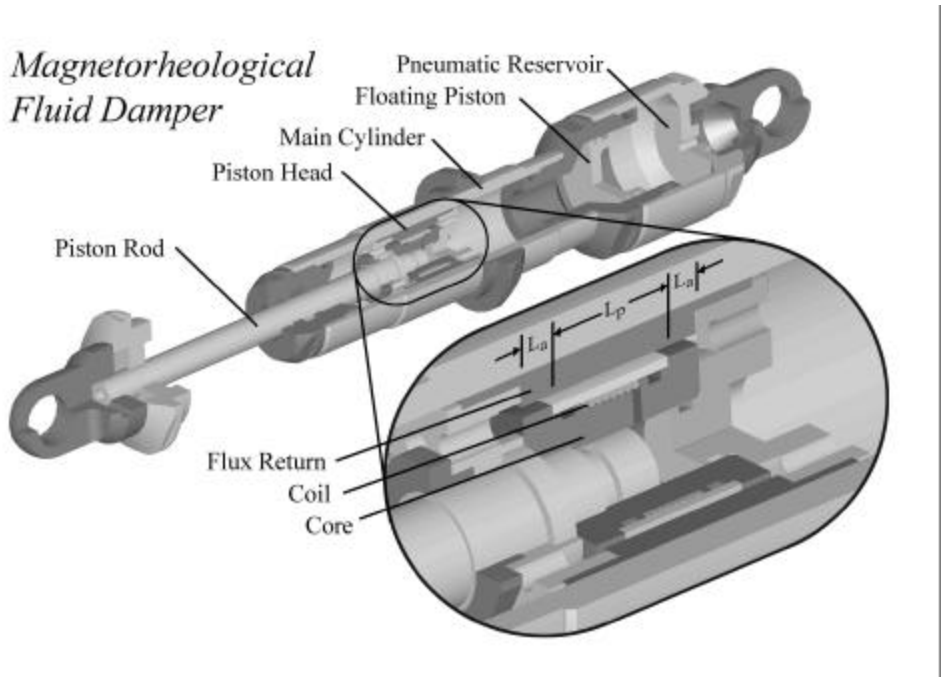

Figure 90: Prototype magnetorheological (MR) damper with magnetic circuit embedded in the piston head, and a gas accumulator to account for thermal expansion of fluid, changing rod volume, and to prevent cavitation. A leakage valve is used in parallel with the MR valve to smoothen the force response.

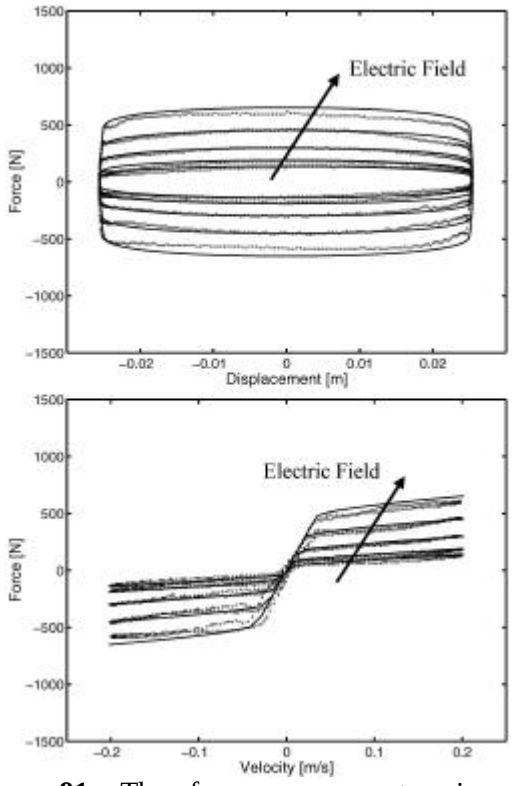

Figure 91: The force response to sinusoidal displacement and velocity inputs had been successfully modeled under this program.

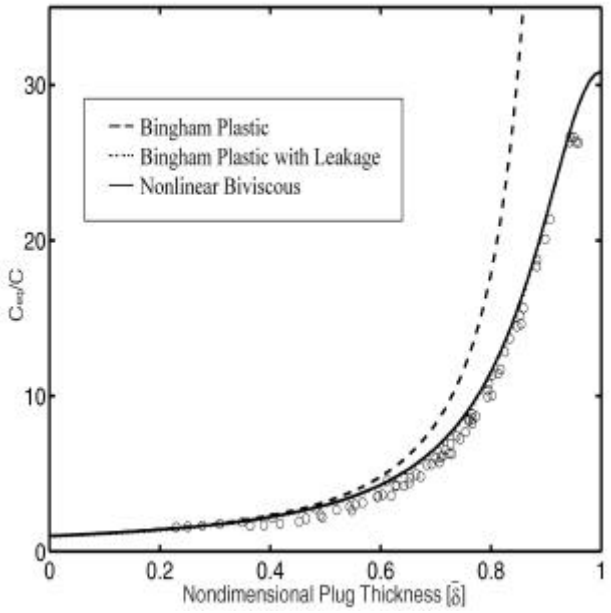

Figure 92: The performance of the damper is represented by the ratio of the magnetic field controlled damping, C_{eq} to the passive or zero field damping, C. Bingham plastic models are used for dampers with no leakage dampers, and biviscous models are for leakage.

38891-EG "Advanced Structural Modeling for Fully-Coupled Parachute Dynamics"

Michael L. Accorsi and John W. Leonard, University of Connecticut

Objectives: The dynamic behavior of parachute systems is extremely complex. To date, most parachute designs have been based on semi-empirical methods supplemented with extensive testing. This approach to design is time consuming and expensive. The goal of this project is to develop a structural model that can be used to perform computer simulations of parachute dynamics and provide a "virtual" testing ground to evaluate candidate parachute system behavior. This capability will allow the Army to reduce the time and cost of (1) developing new and reliable airdrop systems, (2) retrofitting existing systems for new applications, (3) developing new control strategies for airdrop systems, and (4) testing the feasibility of innovative air drop designs.

Approach: The parachute structural model is based on the Finite Element Method (FEM) and accounts for the large displacements and highly dynamic behavior that occur during typical parachute operations. The model has been highly tailored for parachute simulations by including specific features that are unique to parachute systems. New developments are implemented in a source code that is owned and maintained at the U.S. Army Soldier Systems Center. Through the use of this approach, the model is continuously developed to address evolving Army needs in airdrop systems. (**Figure 93**)

Accomplishments: During the last twelve months, the following accomplishments were achieved:

- Formulated and implemented a model for orthotropic and anisotropic materials that undergo large displacements and rotations. This is necessary since most parachute fabrics are not isotropic.
- Improved a basic parallel code by adding wrinkling mechanics and drag forces and by enhancing the time integration scheme.
- Enhanced the environmental load models by adding options for user-defined flow or pressure fields.
- Formulated and implemented an efficient contact search algorithm.
- Formulated and implemented an improved method for imposing static constraints on a model.
- Developed user-friendly programs to generate automatically the fluid surface meshes needed for coupled simulations using general mesh generation software developed by the Army High Performance Computing Research Center (AHPCRC) at Rice University.

38955-EG "State-Switched Absorber/ Damper for Active Structural Control"

Kenneth A. Cunefare, Christopher H. Lynch, and Gregg Larson, The Georgia Institute of Technology

Objectives: The fundamental objective of this project is to improve the control and suppression of vibration through the modeling, analysis and development of state-switchable vibration absorbers. Classical passive vibration absorbers comprise an inertial mass on a spring, with some damping incorporated for motion limitation. Such a passive absorber has but a single tuned frequency of most effective operation. In contrast, a state-

Highly Folded Initial Configuration

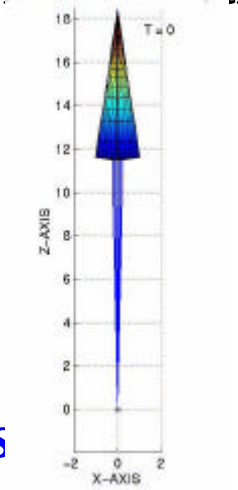

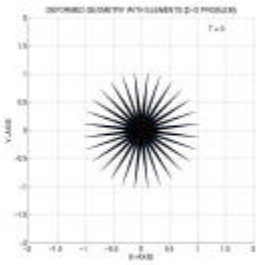

Top View

Side View

Inflation of Round Parachute with and without Wrinkling Mechanics

With Wrinkling

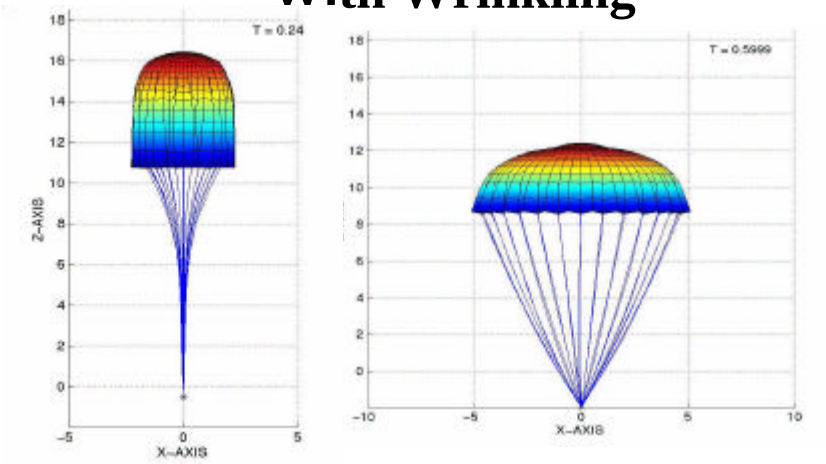

Without Wrinkling

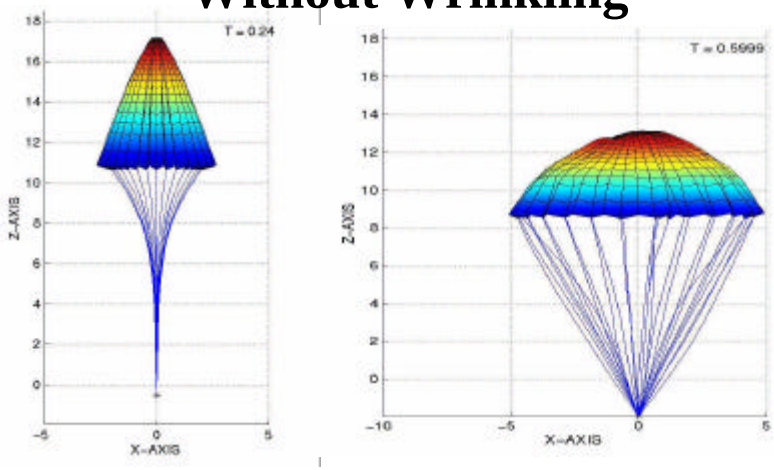

Figure 93 Inflation of Round Parachute with and without Wrinkling Mechanics: A special algorithm was developed to allow membranes to "wrinkle" at the onset of compressive stress to model parachute fabrics more realistically. This figure shows two configurations of a round parachute during inflation as predicted with and without he wrinkling algorithm. The results are dramatically different. Qualitatively, the shapes obtained with the wrinkling algorithm agree significantly better with experimental observations than those obtained without wrinkling.

switched vibration absorber (SSA), depicted in conceptual form in the sketch below, has the capability to instantaneously alter its stiffness state. This change in stiffness instantly retunes the absorber to a new operating frequency. This permits the device to be effective against multiple disturbance frequencies, over a broader bandwidth than strictly passive devices. The state-switch is accomplished through either electrically switching a stiffness element, such as a piezoelectric spring, or by mechanically engaging and disengaging parallel mechanical springs.

Classical passive vibration absorbers are not capable of adapting to changing operating conditions, nor is a single such device generally effective against multiple frequencies. With state-switching, a single absorber may be made effective against both of these limitations of current technology. State-switching may be capable of yielding enhanced performance at reduced weight as compared to current technology (fewer devices required). A state-switchable device, especially one with many possible tuning states, can be made to be highly adaptive and frequency-agile.

In terms of Army issues, a state-switched absorber may find application in reduced vibration transmitted into electronics and avionics, reduction of vibration levels on helicopter fuselage structures, and enhanced damping of gun barrels.

Time-domain simulations of state-switched absorbers attached to lumped element single degree of freedom systems, and to beam and plate systems, have been developed and tested (See **Figure 94**). Detailed performance optimization for the single degree of freedom system has clearly demonstrated that the state-switching concept has the potential for significant performance gains over classical technology. The performance of the stated-switched device has been shown to be consistently better than the performance of classical passive devices. Development of hardware for experimental validation of the predictions is in progress.

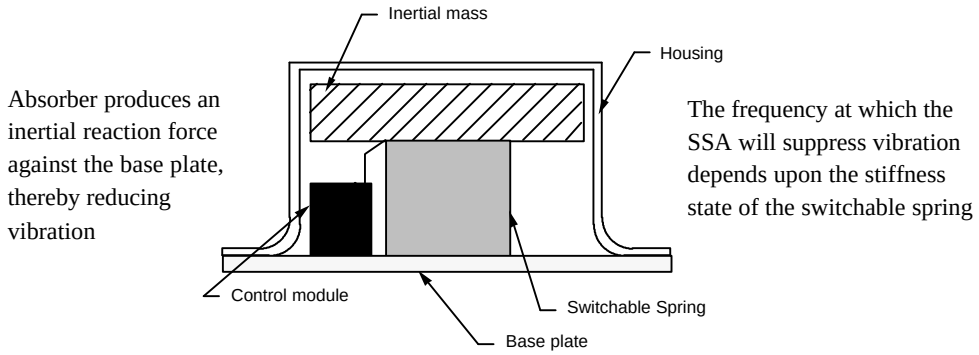

Figure 94 Components of a state-switchable vibration absorber

39126-EG "Active and Reactive Shells"

Amr M. Baz, University of Maryland

Objectives: This study aims primarily at demonstrating the feasibility of utilizing a new class of Active and Reactive Shells (AS/RS) in impeding the propagation of waves as they travel from one end of the shells to the other. The shells consist of tubes that have optimal passive or active sources of mechanical impedance mismatch in an attempt to control the wave propagation along the shells. Such passive/active control capabilities aim ultimately at enhancing the dynamics and the critical velocities of the new generation of high-speed guns.

Approach: (a) Development of a finite element model to describe the propagation of waves in variable-impedance shells with passive and active capabilities. The model will be used to select the optimal configurations of these shells to maximize their critical velocities. (b) Experimental evaluation of the effectiveness of the active/reactive shells in suppressing the transmission of vibrations and maximizing the critical velocities. The experiments will be conducted at the University of Maryland and the Bènet Laboratory at the Watervliet Arsenal.

Significance: The proposed concepts have numerous potential military and commercial applications. In the military field, the active and reactive shells can be utilized in manufacturing stable guns with high firing speeds. In the commercial field, drive shafts of cars and helicopters can be configured as active or reactive struts. Space platforms, large robotic manipulators, and massive cranes are also among the candidate applications. In another situation, the developed concepts are now being considered for application to the manufacture of quiet torpedo shells with controlled wave propagation from the propeller to the torpedo nose, where all the electronic sensors are located.

Progress & Accomplishments: The following is a summary of the accomplishments to date (See **Figure 95**):

1. A finite element model is developed using 3-D elasticity equations of thin reactive shells.
2. A finite element model is developed using axi-symmetric thin reactive shells.
3. The time response of the radial and transverse deflections of a shell are computed during the propagation of a pressure wave along the shell.
4. An experimental set-up is now under construction to monitor the radial strains and the transverse deflection of different shell configurations due to the propagation of a pressure wave along the shell. The set up will be used to verify the predictions of the finite element models and monitor the elastic stability problems associated with high wave propagation speeds.

MANUSCRIPTS

1. A. Hassan, M. Ruzzene, S. Poh and A. Baz, "Wave Propagation in Rods Treated With Active Constrained Layer Damping: Spectral Finite Element Modeling and Experiments", submitted to J. of Experimental Mechanics, 2000.
2. M. Ruzzene, J. Oh, A. Hassan, and A. Baz, "Control of Wave Propagation in Shells Treated With Active Constrained Layer Damping: Spectral Finite Element Modeling and Experiments", submitted to J. of Sound and Vibration, 2000.

DYNAMIC RESPONSE OF PLAIN SHELLS TO PROPAGATION OF PRESSURE WAVES

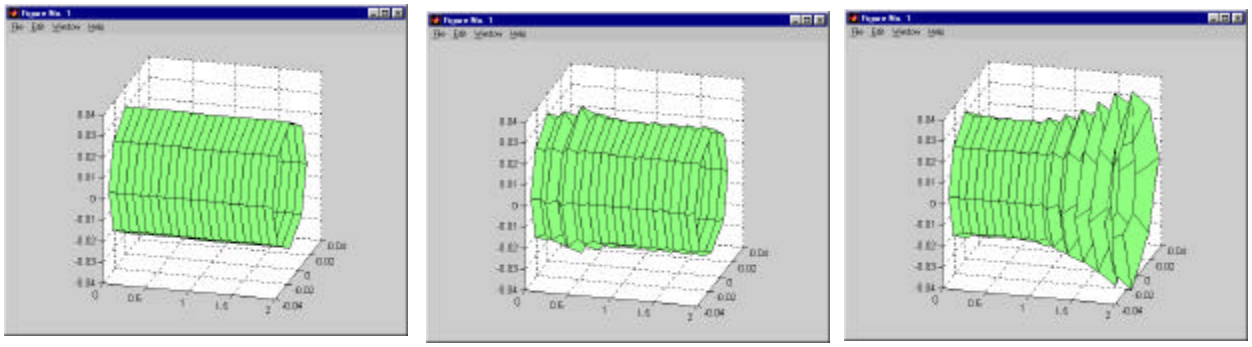

a. Start of wave propagation b.End of wave propagation

Undeformed Shell **Radial Deflection of shell**

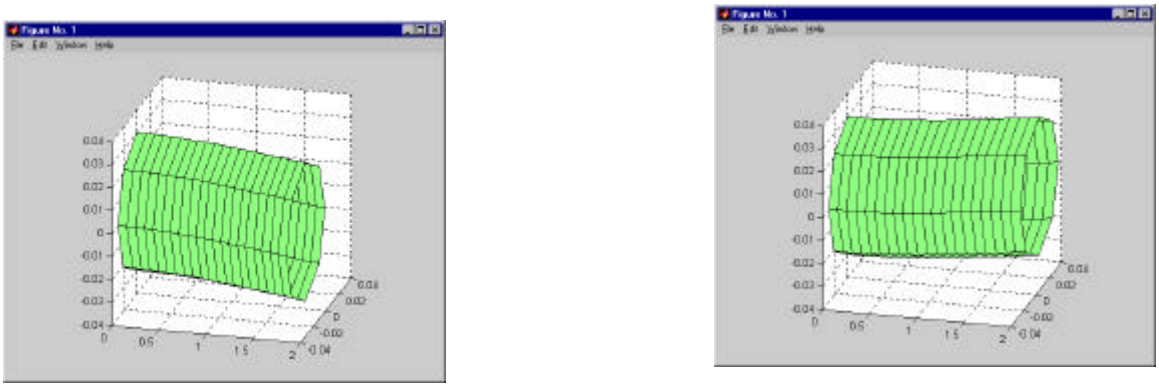

(a) – downward deflection (b) – Upward deflection

Figure 95 Transverse Deflection Following the Release of the Pressure Wave Propagation

40056-EG-YIP "Planetary Gear Dynamics in Military Helicopters"

Robert G. Parker, Ohio State University

Objectives: This research is a comprehensive analytical and computational investigation of the dynamic response of planetary gears. In military helicopters, planetary gears are typically the last stage gear reduction whose output drives the main rotor. Their dynamics dominate the cabin noise, which can exceed 100 dB. In the Apache helicopter, for example, all dominant peaks in the helicopter noise spectrum are at the planetary gear mesh frequency and its harmonics. Furthermore, the frequency of the noise is in the range most audible by humans. With deeper understanding of planetary gear dynamics, the goals are to reduce the noise, vibration, and weight of helicopter planetary gears. In this project we will develop two unique analysis tools: (1) a validated computational tool uniquely suited to gear dynamics, and (2) an analytical model required for early design use by helicopter contractors and fundamental research (**Figure 96**). These tools are notably lacking despite the importance of planetary gears in helicopters, cars, heavy machinery, marine vehicle, and other applications.

Approach: The most difficult aspect of gear dynamics is modeling the tooth contact. This study uses specialized finite element modeling to capture the tooth mesh forces and contact mechanics. A unique semi-analytical formulation combining analytical and finite element solutions with advanced contact modeling is used. The remarkable advantages are that one can define the tooth surface geometry with arbitrary precision, model the contact more realistically, and obtain excellent results with a relatively coarse mesh.

In a parallel effort, a lumped parameter model that represents the gears as rigid bodies interconnected by springs modeling the tooth meshes is employed (**Figure 96b**). The intent is to develop this simpler model in conjunction with the computational model to capture the critical dynamic phenomena and provide a tool suitable for practical design/analysis as well as basic research.

Accomplishments: The finite element approach has been validated against single-mesh gear dynamics experiments. Complex, non-linear experimental phenomena were predicted with strong correlation. **Figure 97** compares the dynamic response amplitude of a gear pair from experiments and finite element analysis. The obvious non-linear jump phenomena and dangerous secondary resonances at speeds 1/2 and 1/3 of the primary resonance speed near 2700 Hz are accurately predicted by finite element. The root cause of the non-linearity is contact loss at the tooth mesh.

A finite element model of the Army OH-58 Kiowa planetary gear (**Figure 96a**) has been developed and verified with a collection of test cases. The study is the most comprehensive dynamic analysis of a planetary gear system available and provides a benchmark that has been notably lacking in the literature. **Figure 98** shows a sample result of the planet gear deflection spectra for a range of operating speeds (i.e., mesh frequencies). Dynamic response analyses across a wide range of operating speeds and torques reveal unique behavior caused by the constantly changing number of teeth in contact at

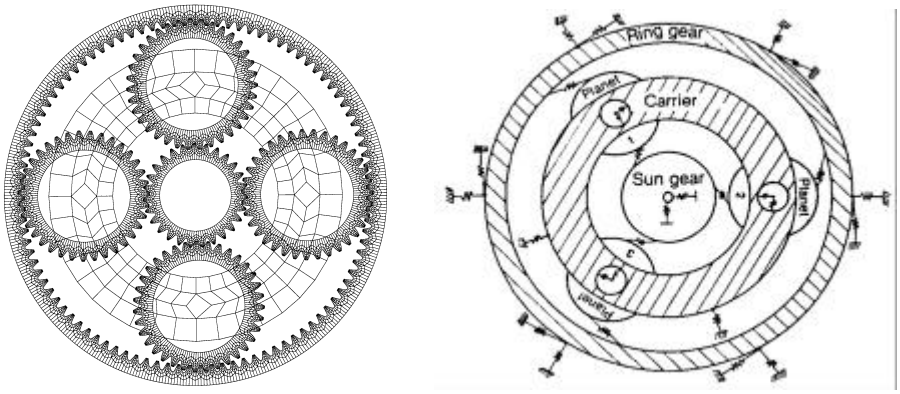

Figure 96 (**a**) Finite element model. (**b**) Lumped parameter model.

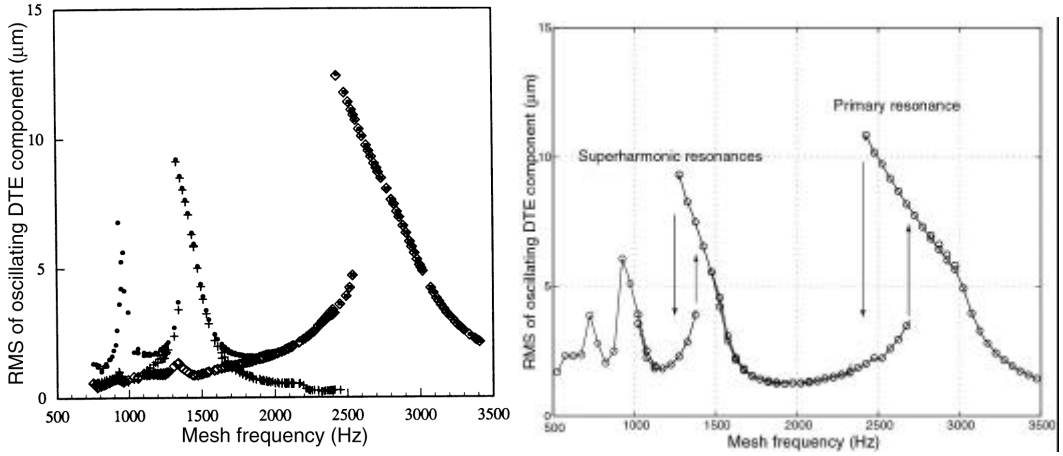

Figure 97 Dynamic response amplitude of a single-mesh gear pair for changing speed (i.e., mesh frequency). (a) Experimental and (b) Finite element.

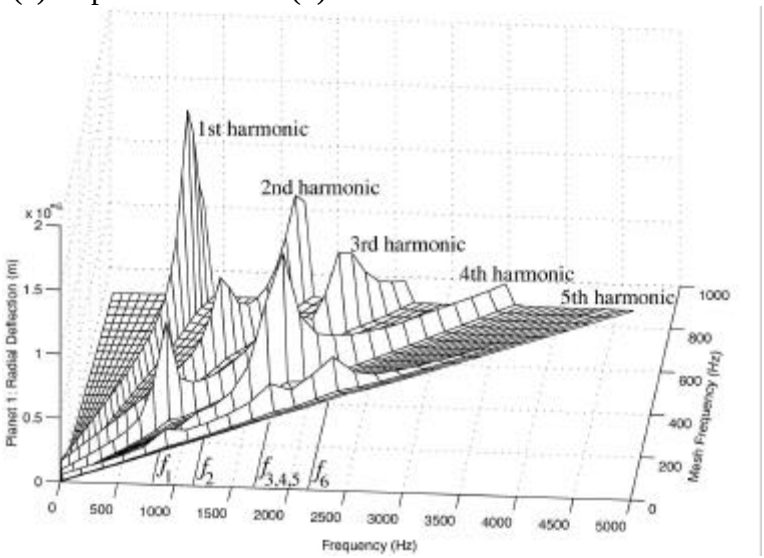

Figure 98 Spectrum of the dynamic response of a planet gear for a range of operating speeds (i.e., mesh frequencies).

each mesh. These have been explained physically.

A rigorous examination of the sensitivity of planetary gear natural frequencies and vibration modes using the lumped parameter model has been conducted. Using the highly structured natural frequency spectrum and vibration mode properties developed under this project, we derived simple expressions for how the free vibration properties change with model parameters. These results have immediate design use. A computer code to determine and plot the natural frequencies, vibration modes, and sensitivities to design changes has been developed and will ultimately be available to the Army Research Laboratory (ARL) and Army contractors.

40169-EG "Design, Modeling, and Development of Precision Apertures"

Gregory N. Washington, The Ohio State University

Objectives: The overall goal of this study is the development of high precision reflector surfaces for large radio frequency antenna systems. The surface will be deformed by large deflection (0.50" – 2.00"), high resolution (~1.0 micrometer), piezoelectric actuators. The specific objectives of the proposed work are:

1. The use of adaptive structures in the development of aperture antenna concepts for large aperture structures.
2. To develop algorithms for shape prediction and control with smart materials.
3. The development of an understanding of the effect that large changes in reflector shape have on the resulting radiation patterns and to create mechanisms for predicting these changes.
4. The development of novel measurement techniques for active apertures.

Approach: To complete the stated objectives thoroughly, the following four mini- projects have been developed: Piezoceramic Active Aperture Antenna Modeling and testing utilizing point actuators: The models will be developed using composite shell theory coupled with piezoelectric material modeling. Advanced models employing fewer assumptions (than previous studies) and a finite element code will constitute a significant part of the future work. Advanced Surface Measurement techniques: The technique that will be used is an in-situ stereoscopic measurement technique, in which multiple cameras will be used to obtain a three-dimensional image from two-dimensional data. This measurement technique will be used to verify the models and to implement control algorithms. Aperture Antenna Shape Control: The control algorithms will use data from the actual surface measurements and model predictive based controls to maintain aperture shape. Structural construction and testing: An actual working prototype will be built and field tested. The main issue involves the protection of information disseminated to ground troops. In this aspect aperture antennas are needed that have the ability to shape the radiation pattern in the same manner that ground troops are spread on the ground. They also must have the ability to scan as troops move from one place to another. The work being conducted in this study will lay the groundwork for the next generation of multi-functional antennas. These antennas are capable of varying their beam width, resonant frequency, or radiation pattern. The ultimate goal of this research is to develop antennas that have

Point Actuated Aperture

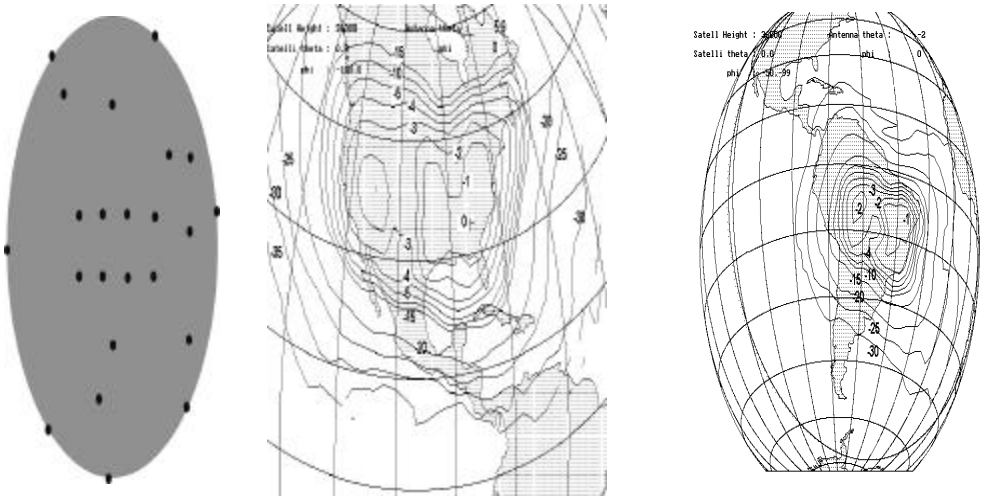

Figure 99 Radiation patterns of undeformed antenna (US) and of Deformed

Smart Aperture Antenna Program (SAAP)

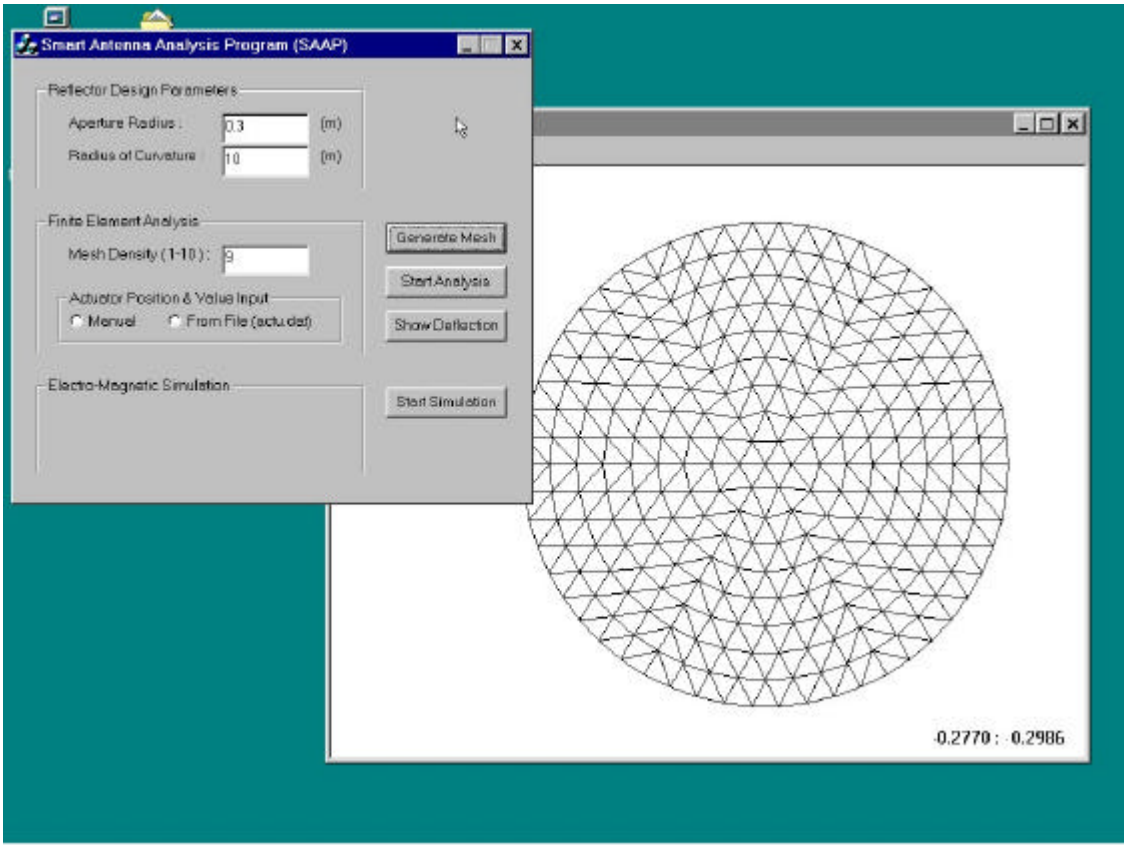

Figure 100 This plot shows the front window of the GUI based code and the FEM mesh that is generated

SAAP -Continued

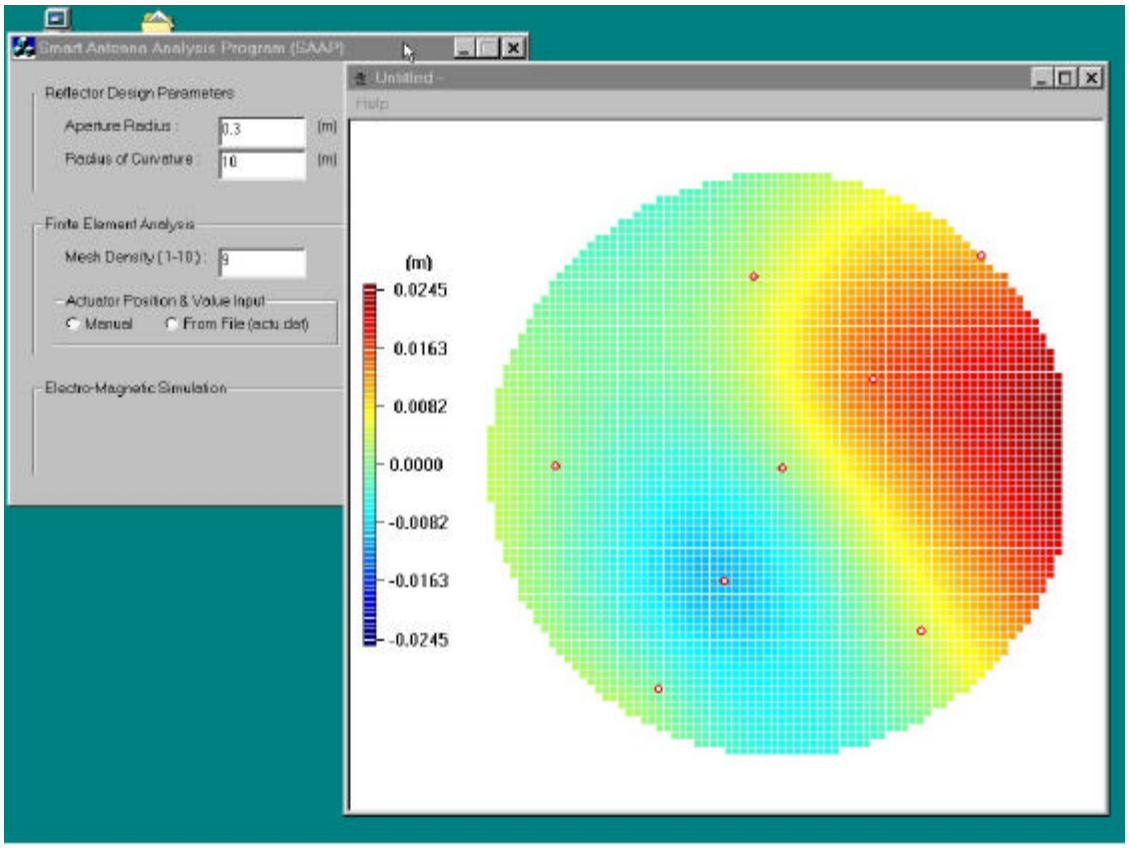

Figure 101 This plot shows the output from the GUI based code

the ability to replace several antennas either on aircraft or satellites.

Accomplishments: The work in this project is only 6 months old. In that time, we have accomplished the following tasks: The initial models of the structure have been completed (**Figure 99**). Finite element modeling has also been completed and incorporated in a object oriented computer code that allows the user to place point actuators anywhere on the surface. The code then generates the surface deformations and plots them in a manner in which the user can visualize the deflections (**Figures 100 and 101**). Equipment for the measurement system has been ordered.

40326-EG-SB2 "Microdrive Actuator Technology"

Gareth J Knowles, QorTek, Inc.

Objectives: The objective of this research project is to develop technology for long-range target acquisition systems for military engagement. Specifically, the application is to advanced helicopter InfraRed/Forward Looking InfraRed (IR/FLIR) systems. A primary goal of this research is to develop and demonstrate a full 3-axis vibration isolation system suitable for integration with the Boeing/Lockheed Night Vision Position Sensor (NVPS).

Approach: The vibration isolation system incorporates three new patent-applied-for concepts -- that of multi-cellular actuators themselves; the novel concept of zero net charge power electronics; and the concept of compression wave piezoelectric transformers. The research develops and integrates advances made by Morgan Matroc Corporation (Unilator Division) in multi-laminar active ceramic materials, processing and fabrication; QorTek Industries' regenerative electronics developed for monolithic and multi-layer electronic ceramics; and recent advances made by the Pennsylvania State University-IMRL in piezoelectric trans-former design, actuator geometry, and construction. The research provides new integrated design capability that imparts high strain-low bandwidth and low strain-high bandwidth. This innovation represents a necessary technology for improved control of fluid-structure interaction, acoustic loads, and mechanical vibration. The goal will be to achieve a 12-dB transmission reduction at 200 Hz sloping down to 2 dB at quasi-static condition. This will be achieved by a 4-point isolation system, chosen to decouple the x-axis and y-axis. Each isolator will be a totally new QorTek integrated design that features flextensional multi-cellular actuators, advanced power electronics and novel co-located sensing. Each unit will weigh about 4 lb and will be approximately 3 inches in height. Due to full integration, these units would be made weatherproof for operational conditions (e.g. hermetically sealed).

Accomplishments: The mechanical design developed has the piezomechanical isolation system consisting of the isolator assembly; actuation transducers; unique co-located sensing to eliminate phase lag and improve stability at high frequency; and shear isolating coupling and fixturing. Optimized titanium materials and force/strain flextensional geometries have been developed. Initial non-optimized prototypes have been tested with excellent results. Radical new designs for drive/power of piezoelectric devices have been devised. These include simulation, hardware implementation, and testing of

the new concepts of zero net charge (ZNC) electronic drives and high-power piezoelectric transformer design. A new revolutionary direct driverless piezo-electronics system has been designed and simulated with extremely promising results. Currently, one Master's degree student and one post-doctoral fellow are being supported by the research funds.